

NGT-21-⁻⁰⁰²⁻~~111~~-080
NGT-80001

UTAH STATE UNIVERSITY

LUNAR ORBETING PROSPECTOR

(NASA-CR-184755) LUNAR ORBITING PROSPECTOR
Final Report (Utah State Univ.) 310 p
CSCI 22B

N89-18510

Unclas
G3/18 0189636

FOREWORD

This final report describes the design of the "Lunar Orbital Prospector" (LOP), a Lunar orbiting satellite designed by students at Utah State University. This design project has been completed under the sponsorship of NASA/OAST through the Universities Space Research Association (USRA).

We at Utah State are very pleased with the results of this design effort. We are proud of the product, the LOP design, and we are excited about the achievement of all our learning objectives. The systems design process is one that cannot be taught, it must be experienced. The opportunity to use our maturing engineering and scientific skills in producing the LOP has been both challenging and rewarding. We are proud of the final design, but, equally important, we are grateful for the skills we have developed in identifying system requirements, spreading them into subsystems specifications, communicating with each other in all sorts of technical environments, conducting parametric and trade-off studies, and learning to compromise for the good of the system.

Elements of this design project have migrated into other forums. In late April, class members presented the final results to the monthly meeting of the Utah Section of the AIAA. Also in April, Dr. Frank Redd and Mr. James Cantrell presented a paper on the LOP at the Lunar Bases and Space Activities in the 21st Century conference in Houston. A revised copy of that paper has been submitted for publication in a book to be published from the output of that conference.

We wish to gratefully acknowledge the support of NASA/OAST and USRA, without which this experience could never happen. Mr. James Burke, our mentor from JPL, has provided mountains of technical data and a priceless reservoir of mature technical experience. It's been a great year.

Frank J. Redd, PhD
Professor, ME

James N. Cantrell
Student Manager

CLASS PARTICIPANTS

James Cantrell
Kyle Adams
Robert Schmid
John Atkinson
Craig Christensen

Perry Voyer
Oscar Monje
Kimberly Anderson
Lorraine Barnum
Steve Brown
Ali Siahpush
Greg McCurdy
Bennett Keller
Allison Goodworth
Blake Crowther
Pete Krull
Roger Meline
James Singer
Shelly Wegener
Raymond LeVesque

Systems Engineering
Structures
Structures and Thermal Control
Structures
Orbits, Structures, and
Thermal Control
Propulsion
Propulsion
Power, Structures
Radar Mapping
Instrument Systems
Attitude Control
Raman Spectroscopy
Raman Spectroscopy
Instruments
Power
Power
Communications
Communications
Technical Writer
Advisement

TABLE OF CONTENTS

Executive Summary

- 1.0 Background
 - 1.1 Lunar Prospecting
 - 1.2 Lunar Geoscience Orbit
 - 1.3 The Lunar Orbital Prospector
 - 1.4 GTV
 - 1.5 Mission Description
 - 1.6 System Description
- 2.0 Remote Sensing the Moon
 - 2.1 Reflectance Spectroscopy
 - 2.2 Gamma Ray and X-Ray Spectroscopy
 - 2.3 Subsurface Sensing
 - 2.4 Conclusion
- 3.0 Environment
 - 3.1 Environmental Parameters
 - 3.1.1 History
 - 3.1.2 Diversity
 - 3.1.3 Lifeless
 - 3.1.4 Dryness
 - 3.1.5 Lunar Chemistry
 - 3.1.6 Gravity
 - 3.1.7 Radiation and Particles from Space
 - 3.1.8 Lunar Atmosphere and Surface Pressure
 - 3.1.9 Lunar Surface Temperature
 - 3.1.10 Moon Magnetism
 - 3.1.11 Center of Mass
 - 3.1.12 Moonquakes
 - 3.2 Prospecting Parameters
 - 3.2.1 Regolith Thickness
 - 3.2.2 Regolith Composition
 - 3.2.3 Lunar Rocks
 - 3.2.4 Surface "Weathering"
 - 3.2.5 Possible Sources for Mineral Concentration
- 4.0 Instrument Groups
 - 4.1 LOP Mission Packages
 - 4.2 Instrument Descriptions and Functions
 - 4.2.1 Radar Altimeter
 - 4.2.2 Gamma Ray Spectrometer (GRS)
 - 4.2.3 Thermal Infrared Mapping Spectrometer (TIMS)
 - 4.2.4 Visible and Infrared Mapping Spectrometer (VIMS)
 - 4.2.5 Visible High Resolution Solid State Imager (VHRSSI)
 - 4.2.6 Magnetometer and Electron Reflectometer
 - 4.2.7 X-Ray Spectrometer
 - 4.2.8 Ultraviolet Spectrometer
 - 4.2.10 Microwave Radiometer
 - 4.2.11 Laser Altimeter

- 5.0 Passive Packages
 - 5.1 Metals and Radioactive Element Package
 - 5.2 Thermal, Silicates and Water Package
- 6.0 Active Sensing Packages
 - 6.1 Topographic Mapping Package
 - 6.2 Raman Spectroscopy
- 7.0 Application of Raman Spectroscopy in Lunar Remote Sensing
 - 7.1 Current Applications
 - 7.2 Principles of Raman Spectroscopy
 - 7.3 Lunar Orbiting Platform Application of Raman Spectroscopy
 - 7.4 Laser Sources
 - 7.5 Differences and Similarities to Infrared Spectroscopy
 - 7.5.1 Surface Resolution Difference
 - 7.5.2 Bandwidths
 - 7.5.3 Spectra Difference
 - 7.5.4 Intensity of Spectral Lines Difference
 - 7.6 Mission Scenario
- 8.0 Radar SURface and Subsurface Mapping
 - 8.1 Mission Objectives
 - 8.1.1 Surface Mapper
 - 8.1.2 Subsurface Mapper
 - 8.2 General System Operation
 - 8.3 The Instrument
 - 8.3.1 Introduction
 - 8.3.2 Introduction Hardware Components
 - 8.3.3 Fixed Parameters
 - 8.3.4 Experimental Parameters
 - 8.4 Conclusion
- 9.0 Orbital Analysis
 - 9.1 Constraints
 - 9.1.1 Topography and Center of Mass
 - 9.2 Gravity Field
 - 9.3 Orbital Strategies
 - 9.3.1 Orbital Considerations
 - 9.3.2 High Resolution Strategies
 - 9.3.3 SPECific Missions
 - 9.4 Fuel Consumption
 - 9.4.1 Coplanar Orbital Maneuvers
 - 9.4.2 Plane Changes
 - 9.5 Conclusions
- 10.0 Propulsion System
 - 10.1 Mineral and Element Concentrations
 - 10.2 Lunar Production Processes
 - 10.3 Lunar Oxygen Production
 - 10.4 Lunar Hydrogen Production
 - 10.5 Vacuum Reduction of Minerals
 - 10.6 Lunar Derived Fuels from Human Wastes
 - 10.7 Fuels Derived from Agricultural Wastes
 - 10.8 Other Production Elements

- 10.9 Production Constraints
- 10.10 Production Rates
- 10.11 Processing Plant Sizing
- 10.12 Lunar-Derived Propellant Possibilities
- 10.13 Propellant System Quantities
- 10.14 Production Costs
- 10.15 Propellant System Decision
- 10.16 Effect of Rate of Fuel Production on LOP Mission
- 10.17 Establishing a Lunar Materials Processing Plant and Base
- 10.18 Propulsion System Analysis
- 10.19 Thrust Chamber
- 10.20 Liquid Oxygen System
- 10.21 Starting Problems
- 10.22 Future Considerations
- 10.23 Conclusion

11.0 Communications System

- 11.1 Introduction
 - 11.1.1 Control and Maintenance
 - 11.1.2 Data Transmission
- 11.2 Internal System Schematic
 - 11.2.1 Optical Fiber System
 - 11.2.2 Communication Computers
 - 11.2.3 Antenna Modules
- 11.3 External Design
 - 11.3.1 Antenna/Transceiver Units
 - 11.3.2 Central Computer Module
 - 11.3.3 Optical Storage Module
- 11.4 Data Format
 - 11.4.1 Pulse Coded Modulation
 - 11.4.2 Data Bit Rates
- 11.5 Power Budget
 - 11.5.1 Transmitter/Receiver Power Requirements
 - 11.5.2 Communication Computer/Storage Power Requirements
- 11.6 Size and Mass Budget
 - 11.6.1 Transceiver/Antenna Size and Mass Budgets
 - 11.6.2 Communications Computers Size and Mass Budget
- 11.7 Communication System Backup
 - 11.7.1 Antenna Failure
 - 11.7.2 Transmitter/Receiver Failure
 - 11.7.3 Communications Computer Failure
 - 11.7.4 Optical Data Bus Failure
- 11.8 Relay Sites
 - 11.8.1 Ground Based Relay Stations
 - 11.8.2 Satellite Relay Stations

12.0 Power System

- 12.1 Options and Considerations
- 12.2 Solar Array, Secondary Batteries
- 12.3 Thermal Power
- 12.4 Solar Array/Batteries/RTG's
 - 12.4.1 Power Needs
 - 12.4.2 Component Size
- 12.5 Solar Array Sizing

12.6 Design Parameters

13.0 Configuration and Structure

13.1 Configuration

13.1.1 Propulsion System

13.1.2 Altitude Thrust

13.1.3 Attitude Thrust

13.1.4 Module Support

13.1.5 Science Packages

13.1.6 Modularity

13.1.7 Other Modules

13.2 Sizing the Structure

13.3 Materials

13.3.1 Lunar Materials

13.3.2 Earth Materials

13.3.2.1 Lightweight

13.3.2.2 Low Coefficient of Thermal Expansion

13.3.2.3 Stiff

13.3.2.4 Vibration Resistant

13.3.2.5 Fatigue Resistant

13.3.2.6 Creep Resistant

13.3.2.7 Impact Resistant

13.4 Space Environment

13.4.1 Outgassing

13.4.2 Thermal Cycling

13.4.3 Radiation

13.5 Thermal Control

13.5.1 LOX Tank

13.5.2 Scientific Instruments

13.6 Conclusion

14.0 Thermal Considerations

14.1 Sources of Heat

14.1.1 Solar Radiation

14.1.2 Reflected Solar Radiation

14.1.3 Thermal Radiation from the Moon

14.1.4 Internally Generated Heat Loads

14.2 Radiation Out

14.3 Equilibrium Skin Temperature

14.4 Recommendations for Surface Coating

14.5 Special Problems

14.6 Conclusion

15.0 Design of a Bias Momentum Wheel

15.1 Theoretical Analysis and Equations of Motion

15.2 The Pitch Loop

15.2.1 Root Locus of the Pitch Loop

15.3 The Roll/Yaw Loop

15.3.1 Root Locus of the Roll/Yaw Loop

15.3.2 Computer Simulation of the Roll/Yaw Loop

15.4 Momentum Wheel Desaturation

15.5 Conclusion

LUNAR ORBITAL PROSPECTOR
Utah State University
Executive Summary

One of the primary rationales for establishing a manned lunar presence is the possibility of exploiting the Moon's resources. The Moon is known to be abundant in oxygen and various metals. Given the known resource potential of only a few explored lunar sites, the possibility of large deposits of these resources and other undiscovered resources elsewhere on the Moon seems highly likely. A continued search for lunar resources and exploration on a global scale in conjunction with a manned lunar base will aid in fully exploiting the Moon's resource potential.

A remote sensing orbital mission, such as the planned Lunar Geoscience Orbiter (LGO), is a necessary precursor to the development of a manned lunar base. The need for a mission of this nature, however, does not end with the establishment of the base. Long term observation of the Moon, a continued search for lunar resources with new techniques, and continued lunar science studies are paramount to understanding the Moon and fully benefitting from its total resource potential. While there is much discussion of human and robotic exploration of the lunar surface, such exploration is necessarily limited to some proximate distance from the support colony. However, remote sensing the lunar surface from orbit can be a more versatile prospecting method providing large scale coverage.

The Lunar Orbital Prospector Concept

The Lunar Orbital Prospector (LOP) is a lunar orbiting platform whose primary mission is to prospect and explore the Moon from orbit in support of early lunar colonization and exploitation efforts. Using LGO as a baseline, the LOP is designed to direct the next generation of lunar exploration in conjunction with an early manned base.

The LOP concept is divided into two distinct parts; an orbiting platform carrying the remote sensing instruments and a servicing vehicle that is lunar launched and landed. The orbiting platform contains its own propulsion system for orbital maneuvering and remains in lunar orbit indefinitely. The platform mounts modular remote sensing instruments packages, communications modules, and power systems. The servicing vehicle, called the Generic Transfer Vehicle (GTV), launches from a base site, rendezvous with the platform for servicing, and returns to the base site. The GTV serves as a "lunar truck" to fly up replacement instrument modules and refueled propulsion modules, and services the platform in the event of failure.

The primary purpose of the orbiting platform is to map the chemical and mineralogical composition of the Moon. Remote sensing instruments mounted on the platform probe the lunar surface and subsurface with electromagnetic energy. The data returned from the instruments will give an indication of the mineral and chemical species present and an indication of the subsurface geological structure of the Moon. Through careful processing and examination of this data, lunar resource distribution on a global scale can be determined.

The ability to replace, repair, and upgrade remote sensing instruments is a critical attribute. The concept of modularity permits the orbiting platform to be upgraded and modified as needed. The spacecraft can be repaired, refueled, and its instrument packages upgraded to perform nearly any required remote sensing task. Highly specialized lunar remote sensing missions can be performed and/or small lunar experiments flown without tailoring and deploying an entire space-craft for each application. The value of this concept has been proven in Earth applications by shuttle based experiments.

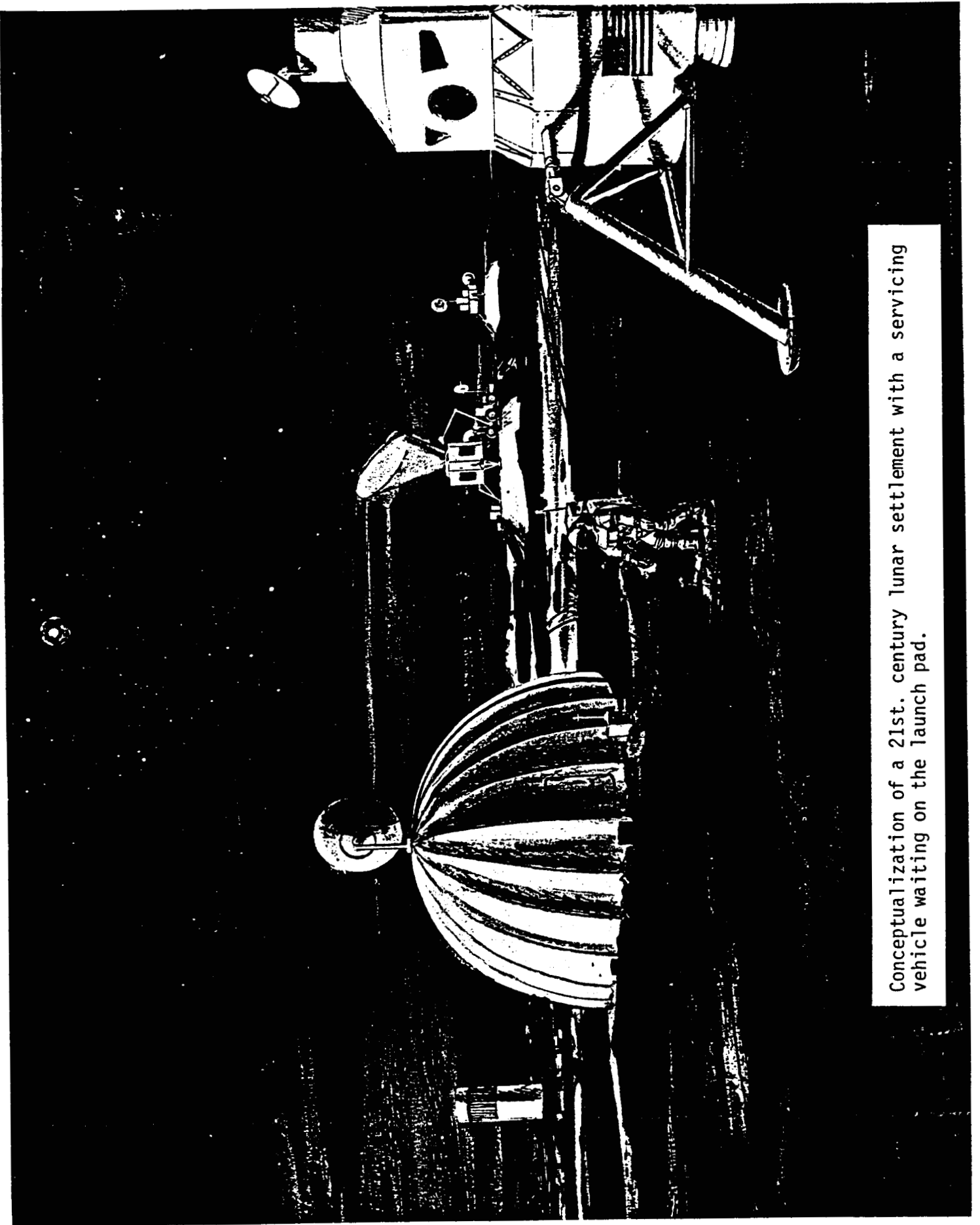
Mission Description

The LOP mission is divided into three primary phases: transport from Earth to low lunar orbit (LLO), operation in lunar orbit, and platform servicing in lunar orbit. Transport of the platform from Earth can be accomplished by a vehicle with a 1000 Kg Earth escape payload capability. This is within the capabilities of the Titan 34D rocket or a Space Shuttle/IUS upper stage combination.

After delivery to low lunar orbit, normal orbital operation commences. Here the platform alters its orbit to obtain the desired surface viewing, and the orbit can be changed periodically as needed. After completion of the initial remote sensing mission, more ambitious and/or complicated prospecting and exploration missions can be contemplated. A refueled propulsion module, updated instruments, or additional remote sensing packages can be flown up from the lunar base up to the platform by the GTV.

System Description

Figure 1 shows the platform configuration. The overall goal of the configuration is to allow the platform to grow and adapt to new and different science and exploration needs. The base structure of the spacecraft houses the propulsion module and supports the required power, control, and communications subsystems. The sides of the spacecraft provide 24 instrument drawers for mounting required subsystems and sensor payloads. These instrument drawers provide the opportunity for replacing, adding, and upgrading any compatible instrument system.



Conceptualization of a 21st. century lunar settlement with a servicing vehicle waiting on the launch pad.

ORIGINAL PAGE IS
OF POOR QUALITY

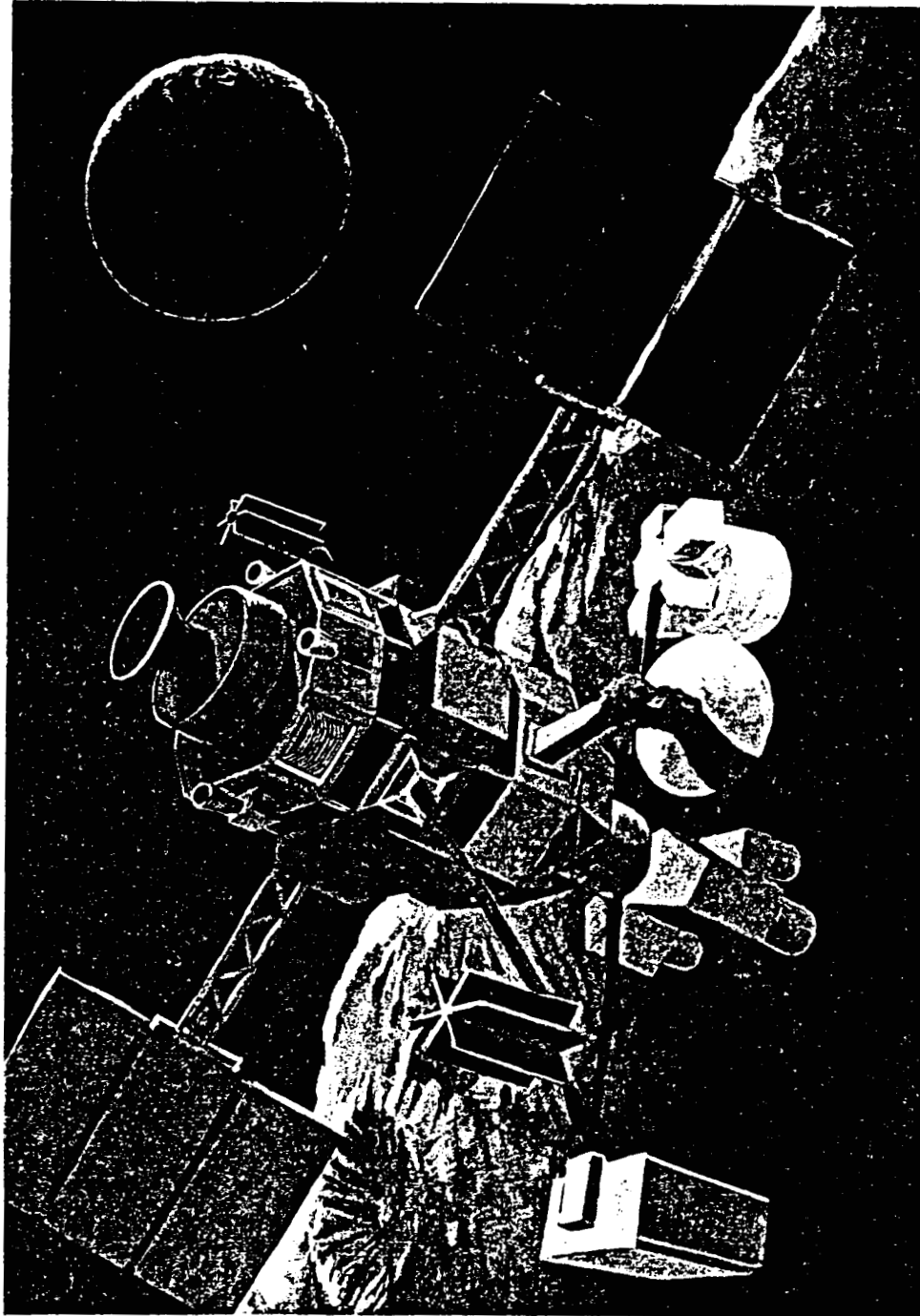


Figure 1.1 Spacecraft configuration. The main body of the platform provides residence for the propulsion system and 24 support subsystem ports. The subsystem ports provide power and communications utilities. The primary remote sensing package is mounted on the lower portion of the platform in the nadir pointing direction.

ORIGINAL PAGE IS
OF POOR QUALITY

Communications is provided by four phased array medium gain antennas mounted on the sides of the spacecraft. These antennae are electronically steered to track relay satellites located at Earth-Moon LaGrange points L1 and L2. The primary remote sensing instrument module is mounted opposite the propulsion module in the nadir pointing direction. This position gives the instruments the required nadir and anti-nadir viewing while providing for unrestricted expansion away from undesired spacecraft thermal and magnetic interference. The spacecraft is expected to continuously pitch to maintain nadir pointing and yaw as required to maintain solar panels normal to incident sunlight.

Orbital Considerations

Mission objectives require orbits stable enough to permit orbital maintenance with a reasonable amount of maneuvering but low enough for good instrument resolution. Due to the Moon's anomalous gravity field, stability of lunar orbits appears to be directly a function of altitude and inclination. Experience from earlier lunar flights and known lunar gravitational harmonics indicates that some orbital inclinations and some low altitude orbits are unstable.

Orbital Strategies

To optimize the relationship between surface coverage and mission requirements, a variety of orbits is required. These orbits may vary in altitude, eccentricity, and inclination. Orbital parameters dictate the type of surface coverage obtained and by varying orbital inclination, eccentricity, and periapsis, various remote sensing mission requirements can be satisfied.

Delta Vee Requirements

An analysis of lunar orbits revealed some surprisingly small velocity requirements for orbital maneuvering. Figure 2 displays velocity requirements for plane changes of various lunar orbits and figure 3 plots delta vee requirements for coplanar orbit changes. With such reasonable maneuvering requirements, many orbital changes are possible with only refueling platform.

Remote Sensing Concepts

Many variations of remote sensing instruments can be flown on the LOP as a result of its modularity. Instruments mentioned represent only a small subset of the possibilities.

Reflectance Spectroscopy

Sunlight reflected from the lunar surface contains absorption lines that are characteristics of minerals present. Mineralogical mapping by this method, combined with data from

other instruments, leads to an improved understanding of the Moon's surface properties and lunar crust history.

Gamma Ray Spectroscopy

Measuring the Moon's natural gamma ray emissions is recognized as a powerful means for measuring the surface elemental abundances. Gamma ray spectrometers were flown on Ranger 3, 4, and 5 missions and on Apollo 15, 16, and 17 command modules.

Ultraviolet Spectrometry

The ultraviolet spectrometer detects the characteristic fluorescence of minerals exposed to ultraviolet energy. In Earth applications, minerals that luminesce have been detected at large distances. Additionally, some rock types show more image contrast when exposed to ultraviolet energy than visible light.

Raman Spectroscopy

Incident light can interact with the molecules by either absorption or scattering. If a photon interacts elastically with the molecule, Rayleigh scattering occurs. If a photon interacts inelastically with the molecule, Raman scattering occurs. The distinguishing characteristic of the Raman effect is the shift in frequency that occurs between the exciting energy and the scattered energy. This frequency difference, called the Raman shift, is directly characteristic of the molecule and is generally independent of the laser excitation frequency.

By measuring the Moon's Raman spectra and correlating this with complimentary reflectance spectra, accurate information on mineral and chemical presence and concentration can be obtained. This has become a powerful laboratory technique and has great potential in lunar remote sensing applications.

Radio Signal Subsurface Mapping

In order to fully understand the subsurface characteristics and engineering qualities of the Moon, an orbital based instrument capable of examining the subsurface is needed. The absence of moisture on the lunar surface indicates that radio frequency electromagnetic energy penetration will be substantially greater than that on Earth. The use of radio frequencies pulsed at the lunar surface can explore the lunar subsurface at depths of at least tens of meters.

Propulsion

Since the primary operating expense of the LOP is likely to be propellant cost, this can be substantially reduced through the use of lunar derived fuels which do not require costly transport out of Earth's gravity well.

Since the Moon is primarily composed of oxygen, oxygen is an obvious choice for a bipropellant oxidizer and can be easily

extracted from lunar minerals by many chemical and thermal processes. The critical element of a lunar derived propellant is thus the fuel. Hydrogen is an excellent fuel when used with oxygen but its lunar concentrations are sorely small. Other lunar derived propellant possibilities include, but are not limited to, Silane (SiH_4/O_2), AlCa/O_2 , Al/O_2 , AlCaMg/O_2 , Ca/O_2 , and lunar soil/ O_2 .

Aluminum based propellants show the most promise of Lunar derived metallic fuels. Aluminum/oxygen has been theorized to perform better than previously mentioned calcium based derivatives and is easily extracted from lunar materials. Powdered aluminum, when used in combination with an Earth based binder and lunar derived oxygen, can provide upwards of a 300 second specific impulse.

A comparison of lunar derived propellants revealed the following:

	<u>Al/LOX</u>	<u>LH₂/LOX</u>	<u>LSiH₄/LOX</u>
Oxid. Mass	1	0.70	0.77
Oxid. Vol.	1	0.70	0.78
Fuel Mass	1	0.78	1.12
Fuel Vol.	1	29.84	4.47
Prod. Time	1	10.86	9.57

Liquid H_2/O_2 gives the best performance of the propellants but production of hydrogen from lunar soils is time intensive. Silane performs well but is also time intensive. Aluminum and oxygen thus show the most promise for lunar derived fuels.

1.0 Background

The Apollo program's scientific output has greatly increased our understanding of the Moon's geophysical and geochemical nature. Vast amounts of data were obtained through surface sampling and orbital based remote sensing measurements. Although a large amount of data was collected, overall surface coverage remains woefully incomplete. The low latitude orbits of the Apollo Command Modules, combined with the relatively small amount of time spent there, provided limited remote sensing of the surface and offered only a tantalizing glimpse of the Moon.

One of the primary rationales for establishing a manned lunar presence is the possibility of exploiting the Moon's resources. The Moon is abundant in oxygen and various metals all of which can find ample application in cis-lunar space. Additionally, undiscovered resources and large deposits of known exploitables may exist on the Moon. Water ice has been theorized to exist in permanently shadowed polar craters (Watson et. al., 1961), and early lunar volcanic activity may have provided a mechanism for forming large ore and mineral deposits near the lunar surface. Given the known resource potential of only a few explored lunar sites, the possibility of large deposits of these resources and other undiscovered resources elsewhere on the Moon seems highly likely. A continued search and exploration for lunar resources on a global scale in conjunction with a manned lunar base will aid in exploiting these resources.

A remote sensing orbital mission, such as the planned Lunar Geoscience Orbiter (LGO), is a necessary precursor to the development of a manned lunar base. The need for a mission of this nature, however, does not end with the establishment of the base. Long term observation of the Moon, a continued search for lunar resources with new techniques, and continued lunar science studies are paramount to understanding the Moon and fully benefitting from its total resource potential.

Accompanying humankind's return to the Moon will be a renewed interest in lunar science studies. A manned lunar base provides an invaluable opportunity to study the Moon via surface sampling and monitoring. However, lunar science at a base site cannot properly address the full spectrum of science questions and objectives. Several of the most fundamental geophysical and geochemical issues, such as the composition, structure, and thermal state of the interior can only be adequately addressed by long term observation and electromagnetic sounding of the lunar surface (Hood et. al., 1985). A long term remote sensing mission in conjunction with a lunar base can expand on LGO's geochemical and geophysical data base and serve as the "eyes and ears" of a manned base by searching for lunar transient events and by

monitoring man's impact on the fragile lunar environment.

1.1 Lunar Prospecting

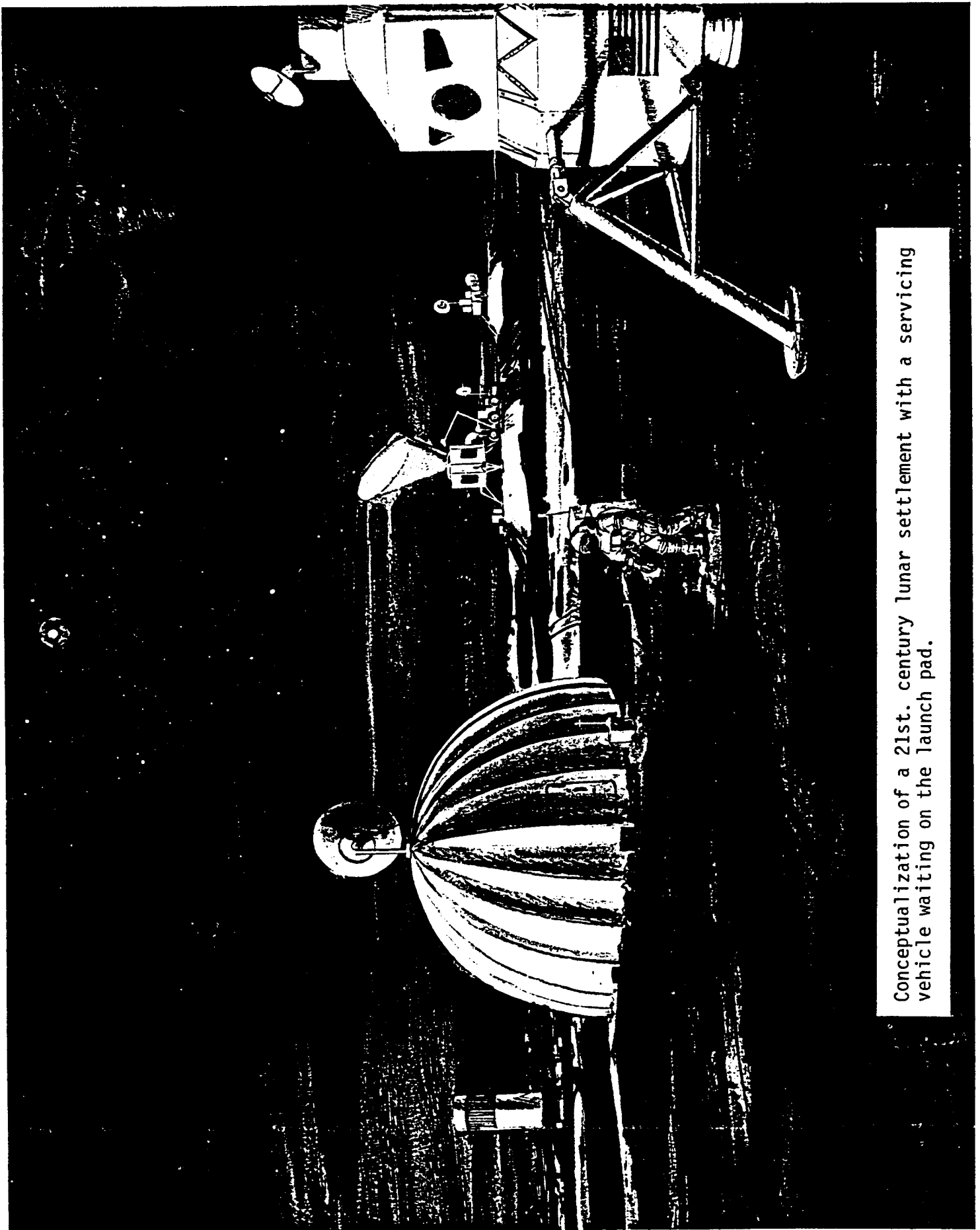
The process of resource exploration on the Moon differs from that on Earth. Prospecting for Earth resources on a large scale typically involves aerial surveys from an aircraft and the use of satellite imaging such as that offered by Landsat. The lack of a lunar atmosphere, however, prevents aerial surveying by any means other than an orbiting satellite. Consequently, global scale prospecting of the Moon is limited, in a practical sense, to orbiting satellites with remote sensing instruments.

The Moon's low mass and lack of an atmosphere make it a very attractive body for remote sensing orbiters. The Moon's mass is small, about 1/80 that of Earth, hence, most orbits about the Moon are generally low in energy relative to equivalent orbits about the Earth. This property substantially reduces propellant requirements for lunar launched and orbiting satellites. The range of possible orbital altitudes about the Moon is also attractive. Since the Moon does not possess an atmosphere, orbital altitudes and lifetimes are limited only by topography and lunar gravitational perturbations. For remote sensing instruments, the lack of an atmosphere is also welcome as scattering and absorption by an atmosphere is not a limitation. This situation is entirely different from that of Earth where orbital altitudes are generally greater than 85 kilometers, energy penalties associated with launch are severe, and the atmosphere limits the resolution and frequency bands of remote sensors.

1.2 Lunar Geoscience Orbiter

As part of NASA's Planetary Observer spacecraft series, the Lunar Geoscience Observer (LGO) is planned to follow the Mars Observer in the 1990's (Wallace et. al. 1986). The LGO is a logical follow up to the lunar scientific investigations of the 1960's and the 1970's. The fundamental objectives of LGO are to map on a global, regional, and local scale the geochemical composition of the Moon, to address geophysical questions, and to survey the Moon for useful resources and candidate lunar base sites. To map the surface chemical composition, LGO's remote sensing instrument package includes a visual and infrared mapping spectrometer (VIMS), an X-ray and gamma ray spectrometer (XGRS), a visual imaging system, a radar altimeter, and a thermal and infrared mapping spectrometer (TIMS). Other LGO instruments addressing the geophysical objectives include a magnetometer and an electrom reflectometer to map the surface magnetic fields and a

ORIGINAL PAGE IS
OF POOR QUALITY



Conceptualization of a 21st. century lunar settlement with a servicing vehicle waiting on the launch pad.

OF POOR QUALITY

microwave radiometer (MRAD) to map the surface heat flow.

The LGO is a polar orbiter with a baseline mission of two years. This will allow global coverage of the lunar surface approximately fifty-two times. Over its mission duration, LGO will map the Moon's surface chemistry and address geophysical questions on a global scale. LGO is essentially serving to fill in the gaps left by previous investigations.

The limited lifetime of the LGO and its inherently limited ability to respond to changes in science and exploration needs are its main deficiencies. The LGO's two year projected lifetime is adequate for its mission objectives but it fails to provide substantial long term observation of the Moon. LGO is also, by its very nature, inflexible to changes in science needs. New methods for locating resources, unforeseen science questions, long term observation, orbits tailored to specific needs, and new instrument technologies cannot be adequately accommodated by LGO.

1.3 The Lunar Orbital Prospector

The Lunar Orbital Prospector (LOP) is a lunar based orbiting platform whose primary mission is to prospect the Moon in support of early lunar colonization and exploitation efforts. Using the LGO mission as a baseline, the LOP mission is designed to direct the next generation of lunar exploration in conjunction with a manned base.

The LOP concept is divided into two distinct parts; an orbiting platform carrying the remote sensing instruments and a servicing vehicle that is lunar launched and landed. The orbiting platform contains its own propulsion system for orbital maneuvering and remains in lunar orbit indefinitely. The platform mounts modular remote sensing instrument packages, communications modules, and power systems. The orbiting platform is the major focus of this year's design efforts.

The primary purpose of the orbiting platform is to map the chemical and mineralogical composition of the Moon, address the next generation of lunar science questions, monitor man's effect on the lunar environment, and to continue LGO's resource exploration. Remote sensing instruments mounted on the platform probe the lunar surface and subsurface with electromagnetic energy. The data returned from the instruments will give an indication of the mineral and chemical species present and an indication of the subsurface geological structure of the Moon. Through careful processing and examination of this data, lunar resource distribution on a global scale can be determined.

ORIGINAL PAGE IS
OF POOR QUALITY

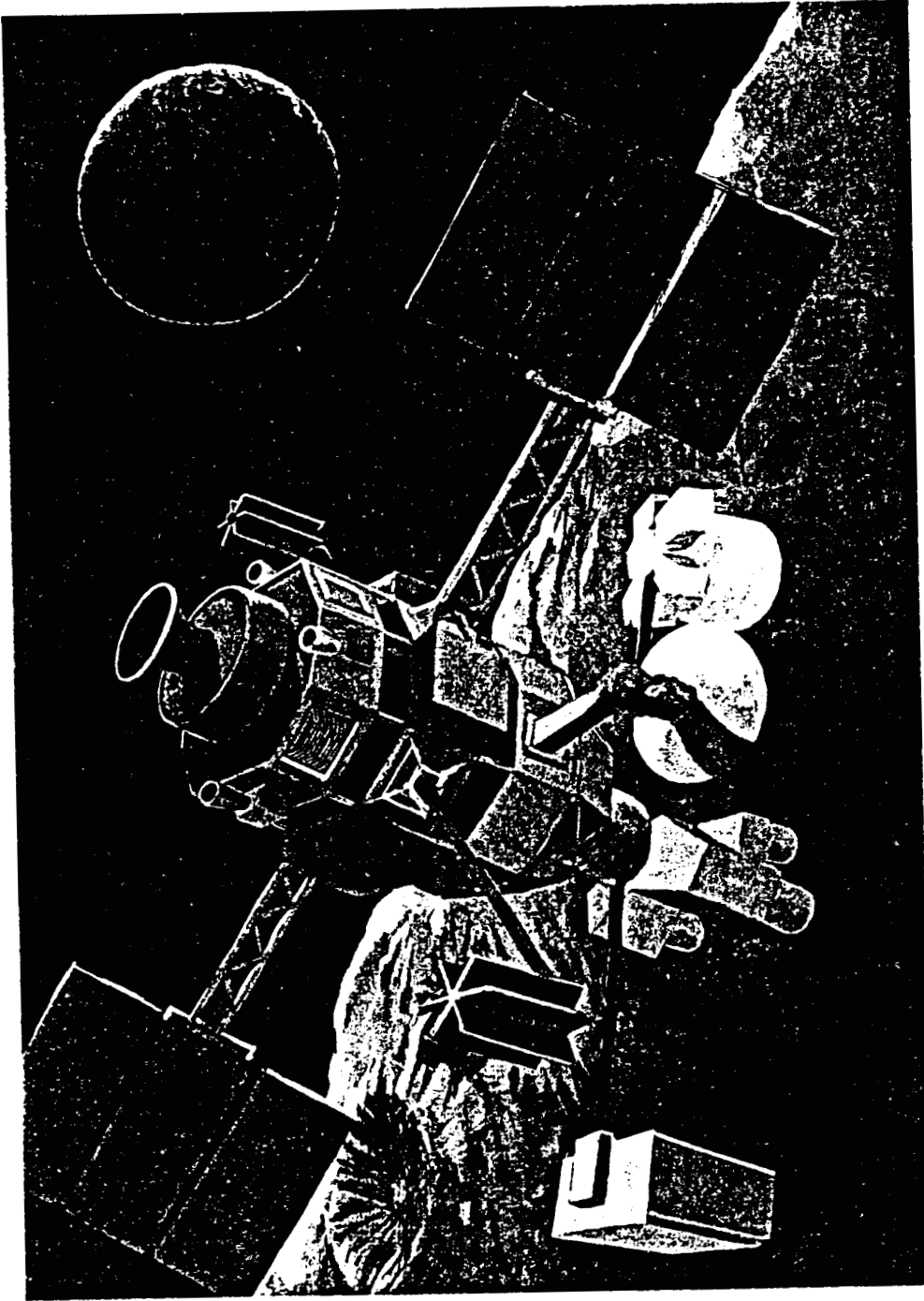


Figure 1. Spacecraft configuration. The main body of the spacecraft houses the propulsion system and provides 24 ports for support subsystems. The primary remote sensing instrument module is mounted on the lower end of the platform in the nadir pointing direction. Each of the ports provides power and communications utilities and the primary port provides up to ten communications channels.

The ability to replace, repair, and upgrade remote sensing instruments is a critical attribute. The concept of modularity permits the orbiting platform to be upgraded and modified as needed. The spacecraft can be repaired, refueled, and its instrument packages upgraded to perform nearly any required remote sensing task. Highly specialized lunar remote sensing missions can be performed and/or small lunar experiments flown without tailoring and deploying an entire spacecraft for each application. The value of this concept has been proven in Earth applications by shuttle based experiments and the second generation Mariner spacecraft.

1.4 GTV

The servicing vehicle, called the Generic Transfer Vehicle (GTV), launches from a base site, rendezvous with the platform for servicing, and returns to the base site. The GTV essentially serves as a "lunar truck" to fly up replacement instrument modules, refueled propulsion modules, etc. and provides servicing of the platform in the event of failure.

This vehicle is similar in concept to a manned base support vehicle currently being investigated by Eagle Engineering and Johnson Space Center (Stecklein et. al., 1988). Servicing could also be accomplished by an Earth orbit based vehicle such as the proposed Utah State University/McDonnell Douglas Manned Assembly Service and Repair vehicle which is space station based. In any event, the design of the orbiting platform is such that the basic requirements of the servicing vehicle are lunar orbit capability, docking ability, and the ability to change instruments. The latter ability is likely to involve some form of man tending.

1.5 Mission Description

The LOP platform mission is divided into three primary phases: transport from Earth to low lunar orbit (LLO), operation in lunar orbit, and platform servicing in lunar orbit. These modes of operation are shown in Figures 1.1, 1.2, and 1.3. Transport of the platform from Earth can be accomplished by a vehicle with a 1000 Kg translunar payload capability. This is within the capabilities of the Titan 34D with an upper stage or a Space Shuttle/upper stage combination. An upper stage, such as the IUS with a reduced propellant mass, provides the initial 3 km/s translunar insertion burn, and the platform's on-board propulsion system provides mid-course corrections and the 300 m/s lunar orbit insertion burn.

After delivery to low lunar orbit, normal orbital operation commences. The initial orbit is baselined to be a 150 Km near polar orbit. Here the platform can alter its orbit to obtain the desired surface viewing, and the orbit can be changed periodically as needed. The initial remote sensing package is baselined to be an updated version of LGO instruments. The initial mission can thus serve as a means for calibrating instruments, gaining experience with the spacecraft, and obtaining an overall remote sensing picture of the Moon.

Since the platform can mount various remote sensing instruments, many types of orbital missions can be contemplated. After completion of the first remote sensing mission, more ambitious and/or complicated prospecting and exploration missions can be performed. When such missions are desired, the servicing vehicle provides a means for changing instrument systems and spacecraft subsystems. The GTV is shown docked to the platform in Figure 1.4 during this mission segment. The propulsion module can also be replaced at this time by a refueled version renewing the platform's orbit change ability. Since other remote sensing mission objectives will require differing orbits, the coincidence of instrument changeouts and platform refueling is necessary. The concept of servicing the platform in lunar orbit gives a great deal of flexibility to mission planning, allows the spacecraft to meet new exploration and science needs, and is vital to the utility and usability of the LOP.

1.6 System Description

The general configuration of the LOP is driven by three major requirements: overall system modularity and expandability, on-board propulsion, and a preferential nadir pointing instrument platform. Figure 1.5 shows the system configuration.

The overall goal of the configuration is to allow the system to grow and adapt to new and different science and exploration needs. The base structure of the spacecraft serves to house the propulsion module and mount the required power, control and communications subsystems. The sides of the spacecraft provide 24 instrument drawers for mounting required subsystems and sensor payloads. The instruments and all other subsystems communicate through an optical spacecraft data bus. The instrument drawers provide the opportunity for replacing, adding, and upgrading any computable instrument system. The primary remote sensing instrument module is mounted opposite the propulsion module in the nadir pointing direction. This position gives the instruments the required nadir and anti-nadir viewing while providing for unrestricted expansion away from undesired spacecraft thermal and magnetic interference.

● EARTH TRANSPORT

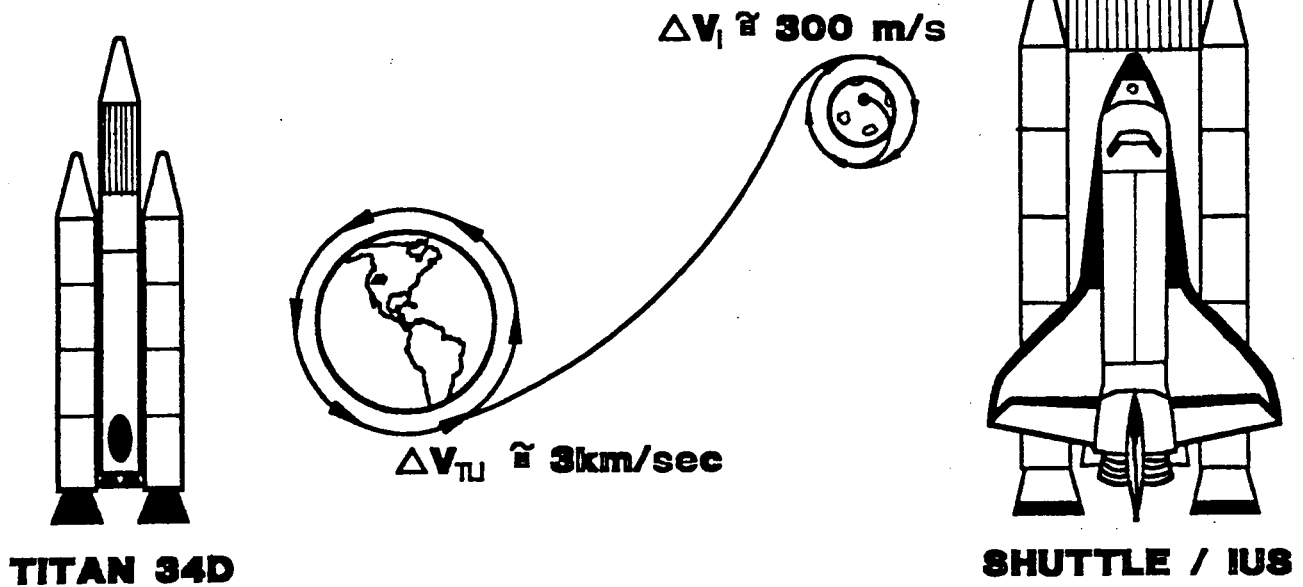


Figure 1.1 Mission phase of platform transport from Earth to lunar orbit. Primary transportation can be provided by Titan 34D/IUS or STS/IUS.

● ORBIT OPERATION

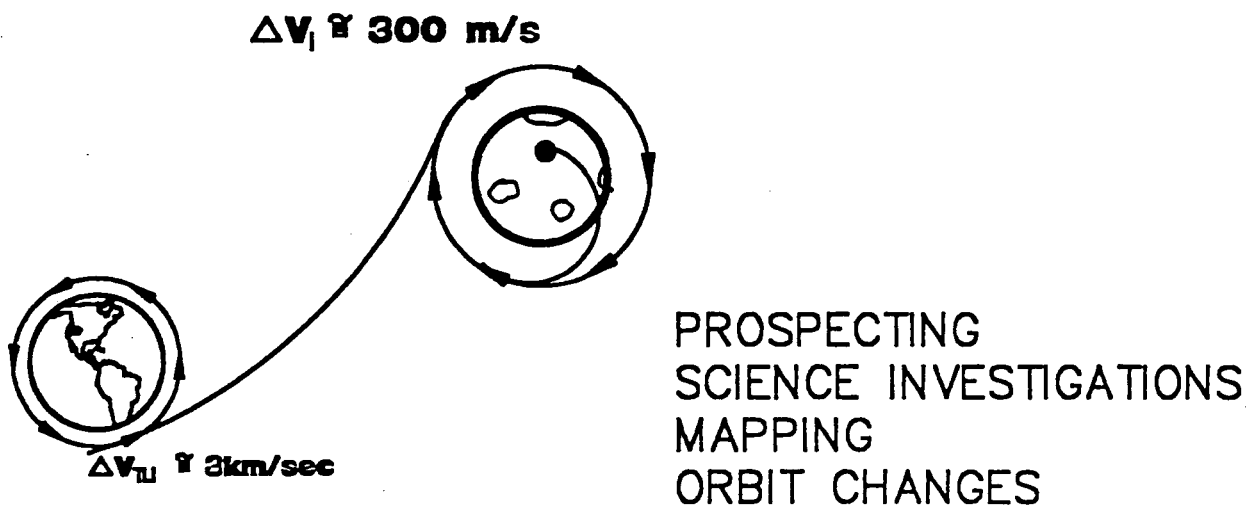


Figure 1.2 Sustained orbit operation of the platform in lunar orbit. The primary objectives of this phase are prospecting, science investigations, and mapping.

● ORBIT SERVICING

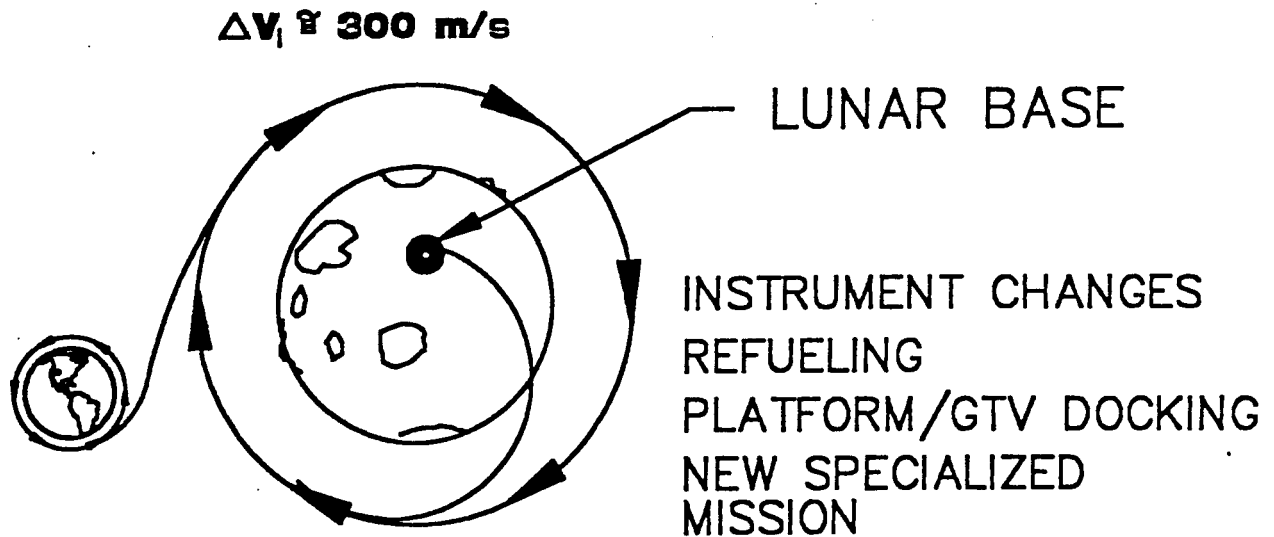


Figure 1.3 Platform servicing in lunar orbit via lunar base launched servicing vehicle (GTV). The concept of servicing in lunar orbit enables platform refueling and instrument changes.

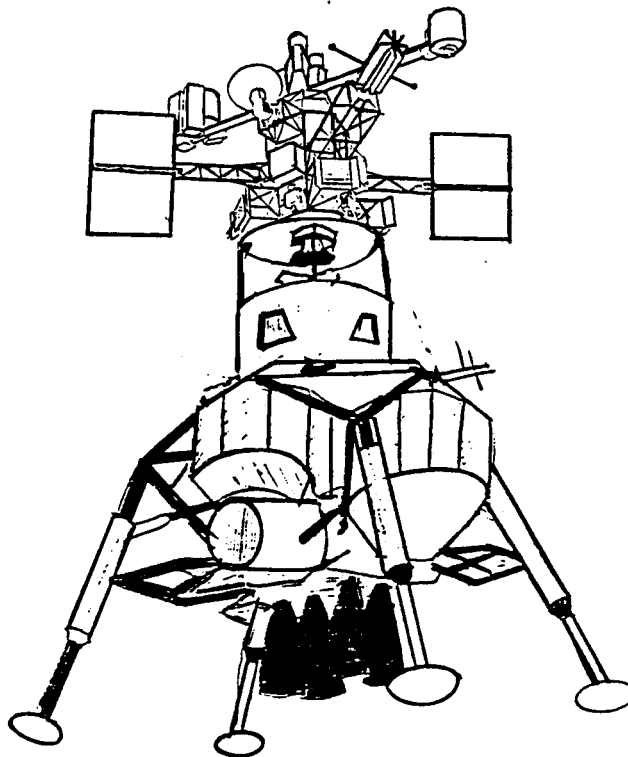


Figure 1.4 Platform and GTV docking in lunar orbit

The spacecraft is expected to continuously pitch to maintain nadir pointing and yaw as required to maintain solar panels normal to incident sunlight. The attitude control system consists of four bias momentum wheels, hydrazine control thrusters, and pitch and roll attitude sensors. Present estimates indicate average pitch pointing accuracy to be approximately ± 2 mrad, and in the event of attitude control failure, the satellite is gravity gradient stabilized.

Communications is provided by four phased array medium gain antennas mounted on the sides of the spacecraft. These antennae are electronically steered to track relay satellites located at LaGrange points L1 and L2. The relay satellites and their locations allow constant data transmission to either the lunar base or Earth.

References

- Barnum, L., personal communication, 1988.
- Barrington, A. R. (1986), Radio frequency reflectivity experiments for AES lunar orbital flights, *Advances in the Astronautical Sciences*, volume 20, pp. 418-433.
- Bond, V, D. Mulichy, Computation of seleocentric orbits using total energy, Lunar bases conference paper 88-172.
- Burke, J. D. (1986), Merits of a lunar polar base location, *Lunar Bases and Space Activities of the 21st Century*, W. W. Mendell ed., pp. 77-84.
- Burke, J. D. (1976), Lunar polar orbiter: a global survey of the Moon, *Acta Astronautica*, volume 4, pp. 907-920.
- Chesley, B., D. Korsmeyer, D. Monroe, Mixed vehicle transportation fleet for missions to lunar polar orbit, Lunar bases conference paper 88-132.
- Cristensen, C., personal communication, 1988.
- Freeman, S. K., *Applications of Laser Raman Spectroscopy*, Wiley and sons, New York, 1974.
- Friesen, L. J. (1986), Search for volatiles and geologic activity from a lunar base, *Lunar Bases and Space Activities of the 21st Century*, W. W. Mendell ed., pp. 239-245.
- Streetman, J. W. (1978), Investigation of the feasibility of chemical rockets using lunar derived fuels, *Proceedings of 14th Joint Propulsion Conference*.
- Hempill, W. R., W. A. Fischer, J. E. Dornbach, Ultraviolet investigations for lunar missions, *Advances in the Astronautical Sciences*, volume 20.
- Hood, L. L., C. P. Sonnet, C. T. Russell (1986), The next generation geophysical investigation of the Moon, *Lunar Bases and Space Activities of the 21st Century*, W. W. Mendell ed., pp. 253-270.
- Lin, R. P., R. E. McGuiire, H. C. Howe, and K. A. Anderson (1975), Mapping of lunar surface remanent magnetic fields by electron scattering, *Proceedings of the 6th Lunar Science Conference*, *Geochim, Cosmochim.*
- McCurdy, G., personal communication, 1988.
- Meline, R., personal communication, 1988.

Rosenberg, S. D. (1986), A lunar based propulsion system, **Lunar Bases and Space Activities of the 21st Century**, W. W. Mendell ed., pp. 169-175.

Simon, M. C. (1986), Aparametric analysis of lunar oxygen production, **Lunar Bases and Space Activities of the 21st Century**, W. W. Mendell ed., pp. 531-543.

Simpson, R. F. (1987), Explorer platform, **AIAA 26th Aerospace Sciences Meeting Proceedings**.

LGO Science Workshop (1986), **Contributions of a Lunar Geoscience Observer**, Dept. of geological sciences and the Anthro-
Graphics lab, Southern Methodist University.

Voyer, P., personal communication, 1988.

Planetary observer planning FY1986, Mission studies report, Wallace, R. A., editor, JPL document D-3649, 1986.

Watson, K., B. C. Murray, and H. Brown (1961), **The behavior of volatiles on the lunar surface**, J. Geopys. Res., 66(9), 3033-3045.

Wilhelms, D. E. (1986), Unmanned spaceflights needed as scientific preparation for a manned lunar base, **Lunar Bases and Space Activity in the 21st Century**, W. W. Mendell ed., pp. 245-255.

2.0 Remote Sensing the Moon

All matter reflects, absorbs, or emits electromagnetic radiation. By reading, or sensing, this radiation, various qualities and quantities of the source can be deduced. This is the concept of remote sensing. Figure 2.2 shows the electromagnetic spectrum and the various bands employed in remote sensing. Different wavelength bands detect different phenomena and thus different characteristics of the source. Figure 2.1 illustrates the source depth of signal received by the remote sensors as a variable of wavelength. It is interesting to note that for wavelengths above three microns, the source depth is approximately 1 wavelength. Thus, any ground data needed to interpret remote spectral emittance measurements must be derived at greater depths for the longer wavelength sensors than for the shorter ones.

Remote sensing can be said to be "passive" or "active". A passive remote sensing system records the energy naturally radiated or reflected from an object. An active system supplies its own source of energy which is directed at the object in order to measure the returned energy. Some examples of active sensing are radar and laser excited emission.

2.1 Reflectance Spectroscopy

Can minerals be identified from orbit by remote sensing instruments? The answer is certainly yes. Minerals emit characteristic wavelengths in the electromagnetic spectrum and this spectrum can be used to identify them. This is due to the fact that most minerals are more or less transparent and the light impinging on them. This light passes into their crystals where it is scattered and reflected from internal surfaces. Some of the light is absorbed selectively by the electronic structures of the ions. This is especially true for Fe and Ti. The fraction of the original light that is re-emitted at the surface of the mineral has a spectrum that expresses the character of the mineral that reflected it (Wood, 1979). Several papers have been published by Hunt et al. (1970, 1971, 1974, and 1977), which list these laboratory spectral signatures for particular minerals and rocks in the visible and near infrared. This range spans from 0.325 μm to 2.5 μm . Ultraviolet, visible, and near infrared signatures are broad bands resulting from absorptions due to electronic processes while the mid and far infrared signatures are sharp bands resulting from absorptions due to vibrational processes.

Laboratory spectral signatures have been used to identify remotely sensed minerals and rocks. Reflectance spectra of several lunar regions is shown in Figure 2.3, and Figure 2.4 illustrates the absorption spectra of an Apollo 15 olivine sample. This is a new field because only in the last few years have instruments existed with sufficient spectral resolution to

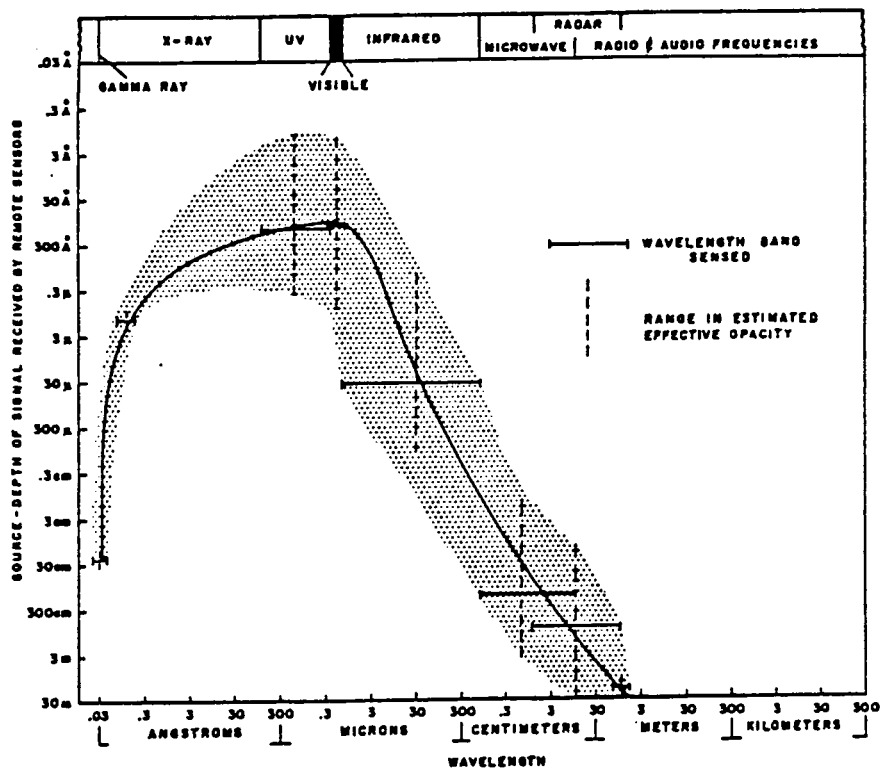
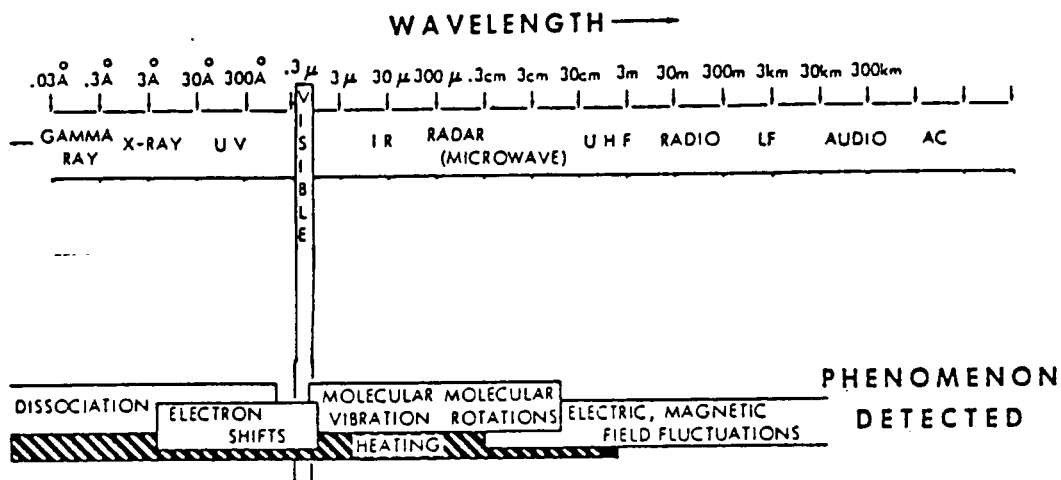


Figure 2.1 Sensor wavelength versus depth of signal penetration. Short wavelength sensors obtain information from the regolith and radar and radio frequencies can reveal subsurface characteristics.



ORIGINAL PAGE IS
OF POOR QUALITY

Figure 2.2 Wavelength versus phenomenon detected at the molecular level.

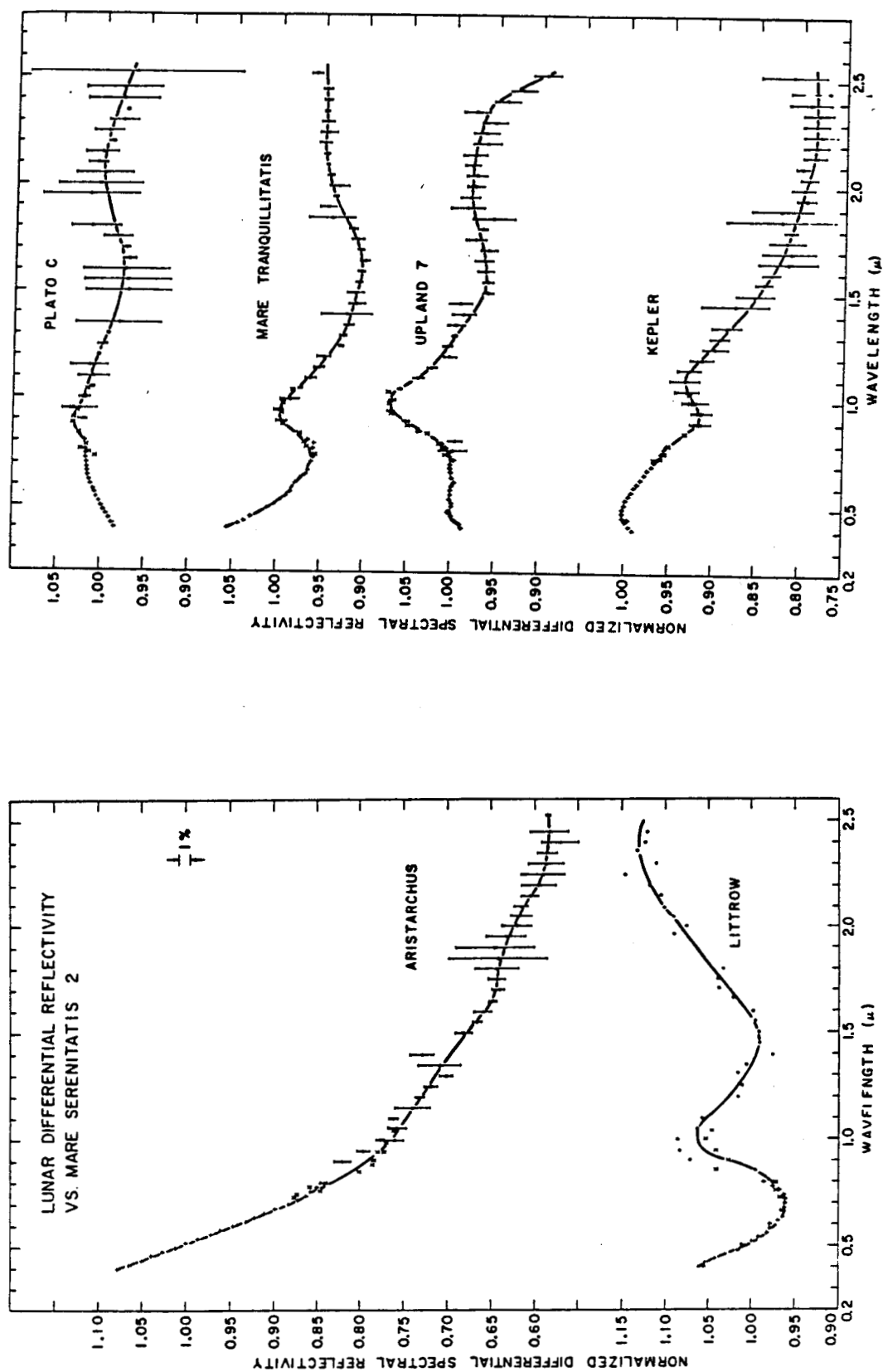


Figure 2.3 Spectral reflectivity curves for various lunar regions.

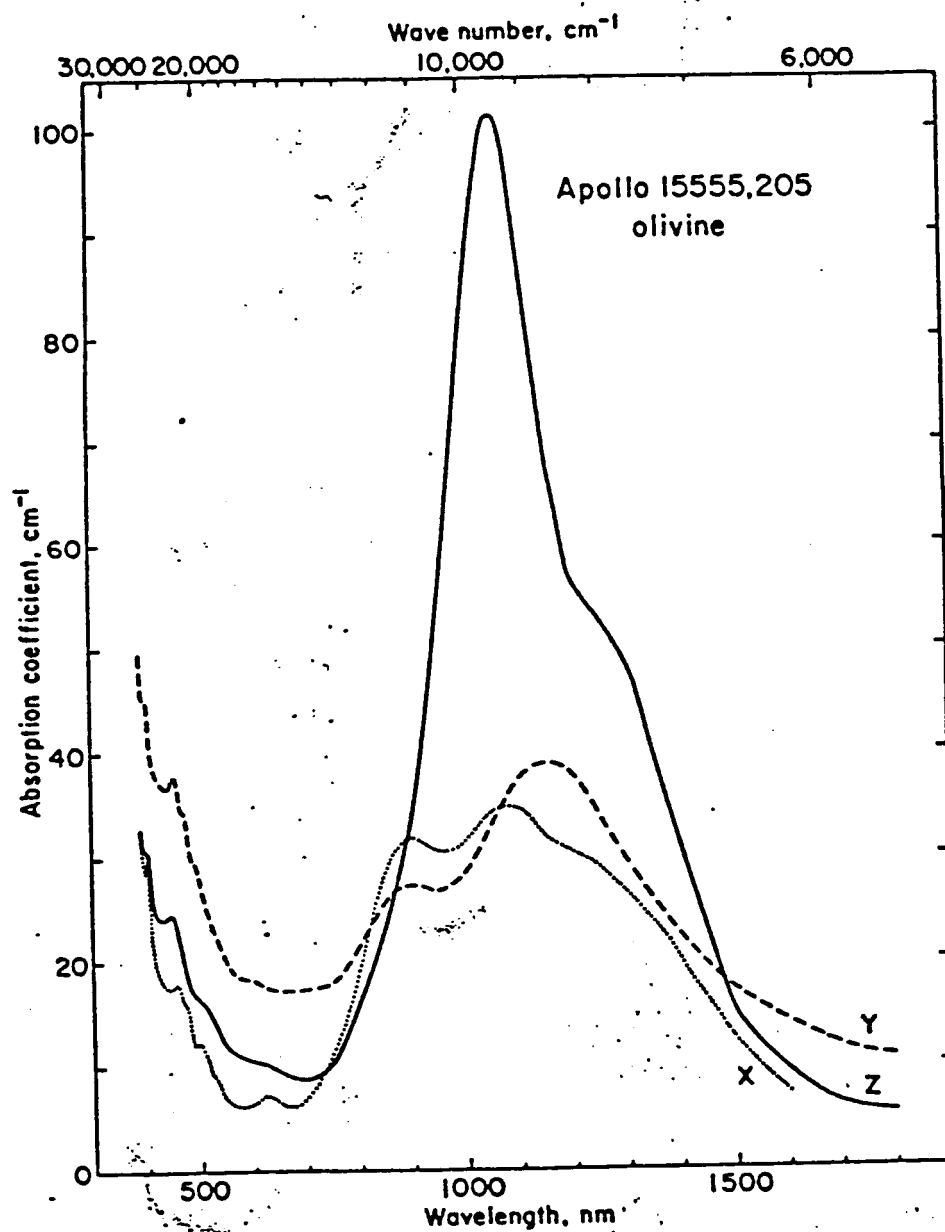


Figure 2.4 Spectral absorption curves for Apollo 15 samples.

identify minerals. It is now possible to distinguish between most silicate and non-silicate rocks and to further discriminate among different silicate rocks and minerals. The mid infrared region between 8 and 12 microns is used to identify the silicate minerals. For example, olivine and quartz can be identified because the fundamental Si-O vibrations of their crystal lattices are different. Olivine exhibits a broad minimum emittance centered at approximately 10 μm , while quartz has an emittance minimum of 8.5 μm (Goetz et al., 1983).

Data from the field is not as simple as lab data, which is usually generated from a "pure" mineral powder. Pure is in quotes because Hunt et al., in the 1970s, discusses the laboratory impurity problems. One type of impurity is the man-made contaminants produced when grinding the mineral into a powder. Grinder steel particles became mixed in with the mineral sample powder, but this is easier to correct than natural impurities. Many mineral samples are contaminated with other minerals in their natural state. Compounding field data problems is the fact that the Moon's regolith contains glass and this glass is almost devoid of the peaks and valleys that characterize laboratory mineral powder spectra, (Wood, 1979).

Instead of using all the spectral lines which identify a rock or mineral in laboratory tests, which can be complicated by impurities, rock and mineral signatures can be derived from only a few lines. McCord and Johnson (1970) compared signatures from Apollo 11 soil samples with their satellite images and found that "mineralogical interpretation can be made of the overall shape of the spectral reflectivity curves". This criteria was used to identify pyroxenes in the lunar soil. Olivine was also detected in the lunar soil by using a few lines (Moore et al., 1980). The 0.95 μm wavelength is a measure of the iron and calcium content of pyroxene and the symmetry of this band can be used to detect the presence of olivine. Furthermore, the 1.0 μm absorption band may indicate basaltic material and titanium can be detected between 0.402 and 0.564 μm .

2.2 Gamma Ray and X-Ray Spectroscopy

The lunar surface is continually bombarded by substantial fluxes of soft x-rays and high energy cosmic particles. Figure 2.5 shows the solar spectrum under quiet conditions which is enough to produce measurable amounts of characteristic x-rays from all of the abundant elements with atomic numbers of 14 (Si) or smaller. With an increase in solar x-ray output, such as a solar flare, the spectrum becomes more energetic such that one might expect to see characteristic x-rays from even higher atomic numbers. Under quiet sun conditions, the solar x-ray flux is most suitable for exciting the light elements, in particular the rock forming elements such as Si, Al, and Mg.

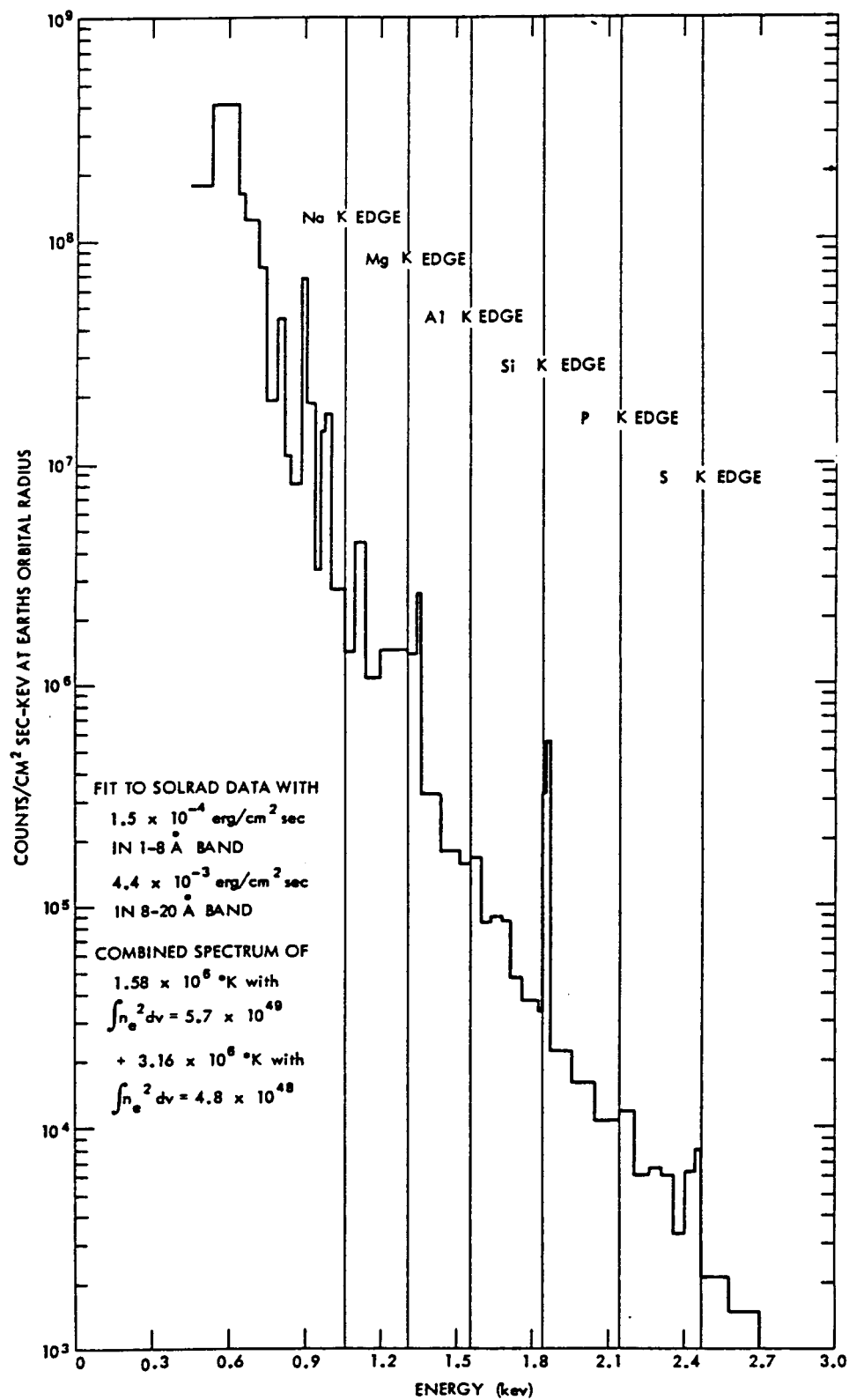


Figure 2.5 Typical solar energy spectrum under 'quiet' conditions.

Lunar surface elements emit characteristic gamma rays as a result of natural radioactive decay and interaction with high energy cosmic particles. The importance of gamma ray measurements to understanding the Moon and mapping its elemental concentrations has been appreciated since the beginning of lunar exploration. Chemical information about surface elements is shown in the gamma ray spectra by discrete lines that have energies characteristic of the individual elements. Typically, cosmic ray particles are protons with energies of the order 10^9 eV. They react with the lunar surface to produce excited nuclei, which in turn emit radiation.

2.3 Subsurface Sensing

On the Earth, plants and hydrothermal alterations can be used to find ore deposits, but this is not useful for the Moon. By using various wavelengths for remote sensing, information at different depths below the lunar surface can be obtained. Radio frequency wavelengths can penetrate deep beneath the surface to reveal subterranean formations. These formations may give clues to the location of ore deposits.

2.4 Conclusion

The answer to the question "Can we use remote sensing to prospect the Moon" is best expressed by Saunders and Mutch, 1980:

"Convincing correlations between certain compositional parameters obtained from Apollo samples and details of both laboratory and remotely acquired spectra have been developed into remote mapping tools that will allow wide-scale mapping of the lunar surface. . . One active group led by Thomas McCord has obtained a large number of spectra for representative lunar regions. Comparison of these curves shows that the important characteristics can be obtained with only three or four selected points on the spectrum. This characteristic allows the important parameters to be contained in a few images of large regions rather than require detailed spectral curves which for equivalent spatial resolution would require an enormous amount of data...The data are in the form of images that have resolution approaching 1 km."

3.0 Environment

The global environment of the Moon and the characteristics of the lunar regolith are important to prospecting and studying the Moon's geology, as well as in the design of a platform. The major environmental parameters discussed are radiation, particles from space, lunar atmosphere and surface pressures, surface

temperatures, magnetism, Moon's center of mass, and moonquakes. Major prospecting parameters include regolith thickness and composition, surface "weathering", and possible sources for mineral concentrations.

3.1 Environmental Parameters

The Apollo program provided vast amounts of data pertaining to the age, composition, and history of the Moon. With the Apollo 11 return of the first lunar samples, old questions were answered and new ones were raised. Gradually, our view of the Moon as homogeneous primordial world changed.

The Moon is a unique world of its own, with a unique environment that has recorded the history of solar activity for billions of years. Through the years of observation and surface exploration, a picture of the Moon has arisen with some expected and some unexpected results. The Moon is an evolved planet that has undergone cataclysmic events such as intense meteorite bombardment and widespread volcanic flows. It is now believed that the Moon once possessed an intrinsic magnetic field that caused residual magnetic fields in lunar rocks. Even though the Moon is now considered geologically inactive, large maria flows are evidence of the planet's once active past. By studying the history of the Moon, one can learn much about planetary formation which helps us understand our own planet Earth better.

The basic physical and orbital properties of the Moon are given in Table 3.1. It is interesting to note the inclination of the Moon to the plane of the ecliptic, nearly 90 degrees. This causes the sunlight to be nearly horizontal at the poles.

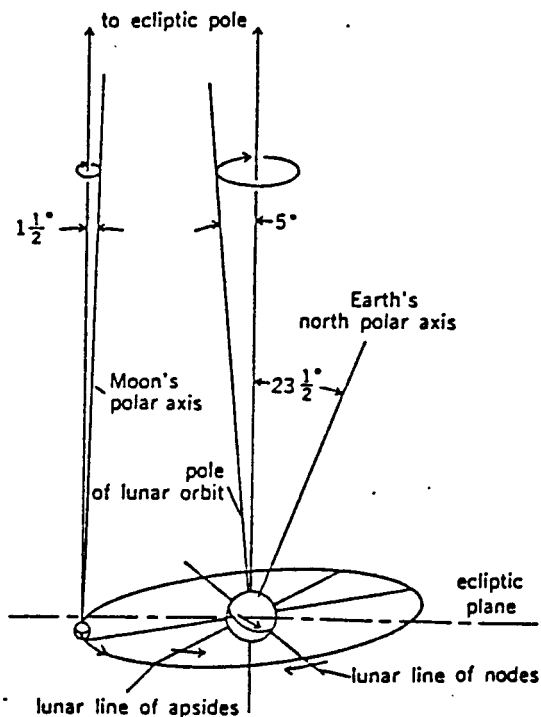
3.1.1 History

The Moon is an evolving planet with a unique geological history. The Moon formed, estimated from return samples, about 4-1/2 billion years ago, around the time the solar system formed. Since then, the Moon has been changed by meteorite bombardment, widespread melting, internal heating, and widespread lava flows. For the past 3 billion years, the Moon has been geologically quiet.

3.1.2 Diversity

The Moon is a diverse world of many minerals, rock types, and surface features. The light colored areas are aluminum and silicon rich "highlands", and the dark areas are volcanic flows known as "maria". The maria are generally flat and are predominately found on the Earth side of the Moon.

3.1.3 Lifeless



MASS- $7.32 \times 10^{22} \text{ Kg}$

MEAN RADIUS- $1.74 \times 10^6 \text{ m}$

MEAN DENSITY- 3340 Kg/m^3

SURFACE GRAVITY (MEAN) -1.67 m/s^2

ESCAPE VELOCITY- 2.38 km/s

PERIOD OF ROTATION - 27.3 DAYS

MEAN DISTANCE TO EARTH - 384,400 KM (center to center)

EARTH/MOON CENTER OF MASS - 4671 KM from the center of Earth

ORBIT ECCENTRICITY - 0.054900489 (MEAN)

Table 3.1 Fundamental properties of the Moon.

Table 1. Apollo Sample Analyses

Compound	Mare, wt %	Highland, wt %
<i>Analyses of Typical Lunar Olivine</i>		
SiO ₂	37.36	37.66
TiO ₂	0.11	0.09
Cr ₂ O ₃	0.20	0.15
Al ₂ O ₃	<0.01	0.02
FeO	27.00	26.24
MnO	0.22	0.32
MgO	35.80	35.76
CaO	0.27	0.16
	<0.01	<0.01
Total	100.97	100.40

Analyses of Typical Lunar Ilmenite

SiO ₂	0.01	0.21
TiO ₂	53.58	54.16
Cr ₂ O ₃	1.08	0.44
Al ₂ O ₃	0.07	<0.01
FeO	44.88	37.38
MnO	0.40	0.46
MgO	2.04	6.56
ZrO	0.08	0.01
V ₂ O ₅	0.01	<0.01
Na ₂ O	<0.01	0.13
Total	102.16	99.37

Analyses of Typical Lunar Pyroxenes

SiO ₂	47.84	53.53
TiO ₂	3.46	0.90
Cr ₂ O ₃	0.80	0.50
Al ₂ O ₃	4.90	0.99
FeO	8.97	15.42
MnO	0.25	0.19
MgO	14.88	26.36
CaO	18.56	2.43
Na ₂ O	0.07	0.06
Total	99.73	100.39

Table 3.2 Chemical composition of several Apollo samples. Chemical distributions is believed to be representative of most of the Moon.

There is no evidence of life existing on the Moon, past or present. This is believed to be due to a fundamental lacking of life's essential elements carbon and nitrogen.

3.1.4 Dryness

The Moon has no known sources of water, unlike most terrestrial rocks. Despite this, the existence of frozen water in permanently shadowed polar craters has been theorized but not confirmed.

3.1.5 Lunar Chemistry

The chemistry of the Moon is of great interest for manufacturing spacecraft materials and, most importantly, propellants. Any usable material that can be manufactured from the Moon saves the cost of transporting it out of the Earth's deep gravity well. Table 3.2 shows the analysis of Apollo samples. Notable among the chemical constituents is oxygen. This is a tremendous advantage to any lunar based spacecraft as the oxygen can be refined for use as propellants.

3.1.6 Gravity

Perturbations in the lunar gravity field exist on a scale of a few hundred kilometers. Large positive anomalies are associated with the circular maria. The gravity potential field, in terms of spherical harmonics, is given in Lunar Scientific Model, JPL document 900-278 and is also shown in Table 3.3.

3.1.7 Radiation and Particles from Space

The solar wind's average speed near the Moon is around 500 km/sec. (Guest and Greeley, 1977). Solar flare particles have been found etched into the Surveyor III TV camera lens. These particles were etched in the lens during its 2 1/2 year exposure on the Moon. There is also an abundance of smaller particles from space impacting the Moon, with one particle as large as a pinhead found in several cubic kilometers of space. However, experience has shown that these particles do not pose a threat to spacecraft or to astronauts on the Moon (French, 1977). An area the size of a dinner plate may be hit by a particle 1 μ m or larger in diameter once a day (Guest and Greeley, 1977).

Cosmic particles impact the moon at several kilometers a second and cosmic rays are strong enough to produce reactions a few meters deep in the lunar soil (French, 1977). Also, gamma rays interact with the uppermost tens of centimeters of soil while x-rays interact with the uppermost tens of micrometers

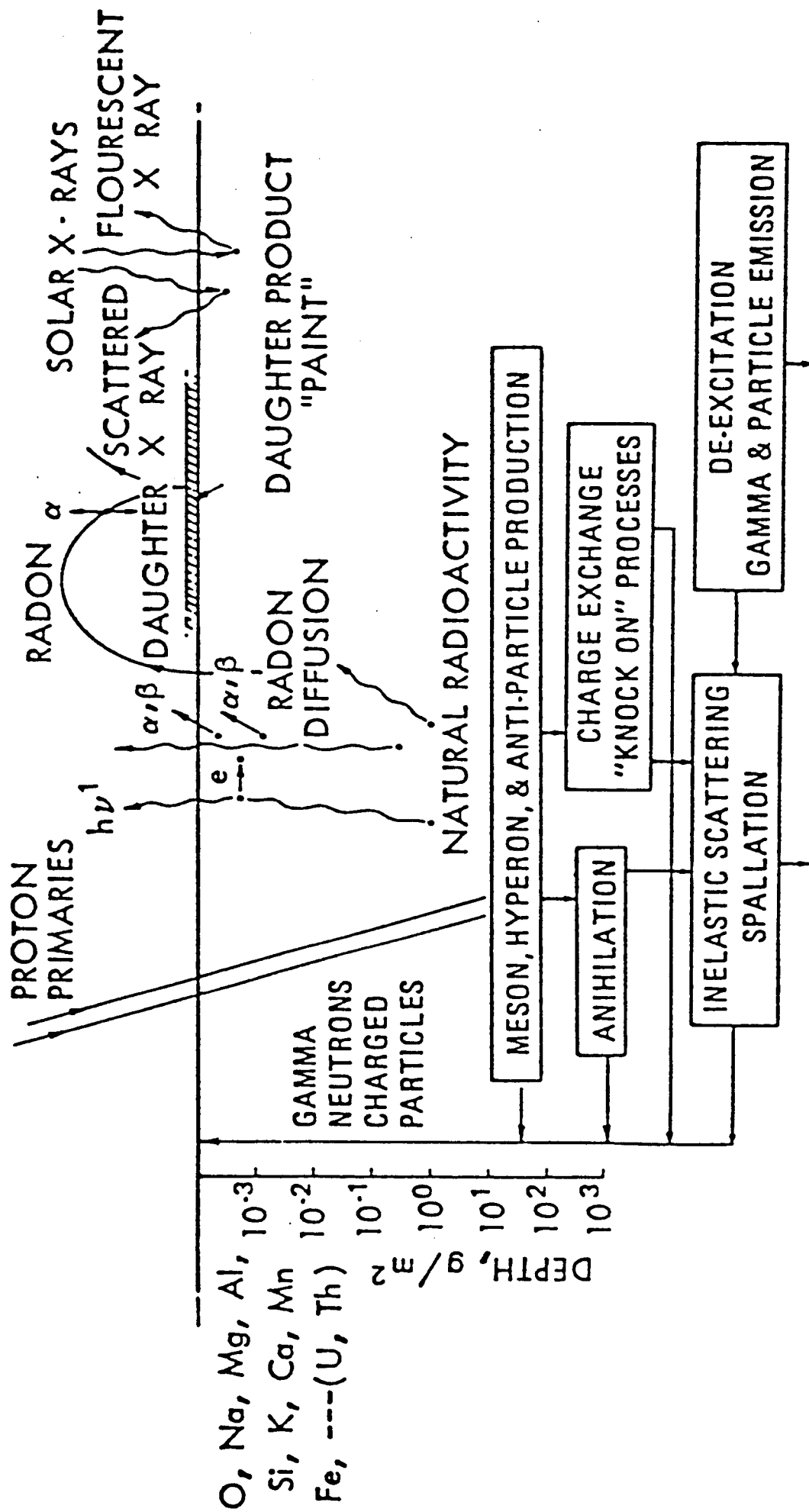


Figure 3.1 Radiation environment at the lunar surface.

$$\Phi(r, \beta, \lambda) = \frac{-GM_{\zeta}}{r} \left\{ \sum_{l=0}^{\infty} \sum_{m=0}^l \left(\frac{a}{r}\right)^l P_{lm}(\sin \beta) (C_{lm} \cos m\lambda + S_{lm} \sin m\lambda) \right\}$$

$$P_{lm}(\mu) = (1 - \mu^2)^{m/2} \frac{d^m}{d\mu^m} P_{l0}(\mu)$$

$$P_{l0}(\mu) = \frac{1}{2^l l!} \frac{d^l}{d\mu^l} (\mu^2 - 1)^l$$

Here r , β , and λ are the selenocentric coordinates above the surface of the Moon. GM_{ζ} is the lunar gravitational mass, a is the mean radius of the Moon, and P_{lm} , C_{lm} , and S_{lm} , are the spherical surface harmonics and coefficients of order l and index m . The determination of the free parameters C_{lm} and S_{lm} by the method of least squares is described in Sec. 1.3.3.

l	m	l = 3, m = 2 Akim (1966)		l = 8, m = 4 GM $_{\zeta}$ = 4902.78 km ³ sec ⁻²			
		C x 10 ⁴	S x 10 ⁴	Lorell and Sjogren (1968)		Lorell (1969) "Mod. 3"	
				C x 10 ⁴	S x 10 ⁴	C x 10 ⁴	S x 10 ⁴
0	0						
2	0	-2.06 ± 0.22	—	-2.026	—	-1.9564	—
3	0	-0.363 ± 0.099	—	-0.2223	—	-0.1299	—
4	0	0.333 ± 0.270	—	0.0941	—	0.1230	—
5	0			-0.1614	—	-0.0365	—
6	0			-0.1089	—	-0.0978	—
7	0			0.1734	—	0.2603	—
8	0			-0.2011	—	-0.0905	—
9	0						
10	0						
11	0						
12	0						
13	0						
2	1	-0.157 ± 0.059	-0.036 ± 0.036	-0.0878	0.0150	-0.1279	0.1290
3	1	0.548 ± 0.026	0.178 ± 0.032	0.3636	0.0740	0.3493	0.0948
4	1			-0.1237	0.0564	-0.1607	0.1099
5	1						
6	1						
7	1						
8	1						
9	1						
10	1						
11	1						
12	1						
13	1						
2	2	0.140 ± 0.012	-0.014 ± 0.015	0.2191	0.1310	0.1587	0.1014
3	2	0.118 ± 0.047	0.001 ± 0.050	-0.0257	-0.0200	0.0076	0.0283
4	2			0.0361	0.0051	0.0265	0.0012
5	2						
6	2						
7	2						
8	2						
9	2						
10	2						
11	2						
12	2						
13	2						
3	3			-0.0265	-0.0496	0.0284	-0.0447
4	3			0.0164	-0.0277	0.0027	0.0148
5	3						
6	3						
7	3						
8	3						
9	3						
10	3						
11	3						
12	3						
13	3						
4	4			0.0091	0.0079	0.0039	0.0001

Table 3.3 Gravity model of the Moon based on spherical harmonics. Various order terms are based on lunar orbiter and Apollo command module observations.

(Wilhelms, 1987). Table 3.4 (adapted from French, 1977) is a summary of these effects. It lists the source, energy and composition of the particles impacting the Moon, along with the effects produced and how deeply they penetrate into the lunar soil.

3.1.8 Lunar Atmosphere and Surface Pressures

Although the Moon's surface environment may be considered to be a vacuum, the solar wind and lunar surface outgassing do produce a slight concentration of gases. The solar wind inputs less than 50 gm/sec into the lunar atmosphere. The solar wind flows directly onto the lunar surface because the Moon lacks a substantial atmosphere or magnetic field. Short, in 1975, suggested that lunar gases are adsorbed on lunar soil particles at night and later released during the daytime heating. He based this suggestion on the fact that the nighttime concentration of ionized lunar gases is about 2×10^5 E ions/cc, which are mostly composed of helium, with some hydrogen, neon, and argon but the nighttime surface pressure is less than 10^{-12} E torr, which increases to 10^{-10} E torr in the day.

About 10^{-4} of the mass of the lunar soil consists of trapped gases. For the gases remaining in the lunar atmosphere, photoionization over weeks and months along with the solar wind are the main loss mechanisms. The predominant nightside gas is neon (LACE gas mass spectrometer measurement of 1×10^5 /cubic cm) and the predominant dayside species are carbon dioxide (solar wind intensity and a model calculations of 6×10^5 /cubic cm). Argon 40, a potassium decay product from the lunar interior, increases the lunar atmosphere by 0.06 gm/s (Vondrak, 1988).

The Moon, like the Earth, has an ionosphere. However, collisions within the ionosphere are unimportant because it is directly coupled to the solar wind. Interactions with the lunar surface control the ionospheric chemistry. Ions formed on the dayside lower hemisphere are driven into the lunar surface while ions formed in the upper hemisphere escape into the solar wind. The surface potential on the Moon's dayside is 30 volts with respect to the solar wind. The electron density on the surface of the Moon is 10^4 /cm³ and extends to an altitude of about 100 meters. The surface potential becomes negative on the nightside, and, at times, the Moon's surface contacts interplanetary plasma and the Earth's magnetospheric plasma tail (Vondrak, 1988).

3.1.9 Lunar Surface Temperature

Surface temperatures at lunar noon reach a maximum of 348 degrees Kelvin, while temperatures drop by almost 255 degrees Kelvin to 93 degrees Kelvin by the end of the lunar night (Short, 1975). The sun is never higher than 1-1/2 degrees at the poles and it is therefore estimated that 2% of the Moon's surface is in

permanent shadow (Guest and Greeley, 1977).

3.1.10 Moon Magnetism

The Moon appears to have a very weak magnetic field, about 2 gammas, but remnant magnetism in the lunar rocks is much stronger, causing some anomalies in the readings (Short, 1975). Measurements of the permanent lunar magnetic field range from 3-313 gammas and are highly regional. The Moon's magnetic field is stronger in the lunar highland regions than in mare regions and stronger on the lunar far side than on the near side. The Earth's field ranges from 30,000 to 60,000 gammas.

Remnant magnetism on the Earth is found in rocks containing iron oxides. On the Moon, metallic iron is the dominant magnetic mineral because "weathering" does not change the elemental iron into iron oxide. Most of this iron is in the form of fine particles produced during meteorite impacts. Apollo 15 recorded maximum field intensities where impact generated breccias are abundant and minimum intensities in regions of undisturbed mare basalts (Guest and Greeley, 1977).

3.1.11 Center of Mass

The center of figure of the Moon is displaced by about 2.5 km from its center of mass, making the far side at higher elevations than the nearside (Guest and Greeley, 1977). This center of mass offset is considerable and produces a limitation on low altitude orbits.

3.1.12 Moonquakes

Apollo seismometers have detected moonquakes with a rating of 2 on the Richter scale. These quakes come from depths ranging from 805 km to 965 km below the surface. By contrast, the Earth's quakes emanate from shallow depths of 97 km (Jastrow, 1977).

3.2 Prospecting Parameters

The Moon is covered by regolith everywhere except where there are steep walls. Since the signals detected from geochemical remote sensing instruments will emanate almost entirely from the regolith, it is important to understand its characteristics (LGO Science Workshop, 1986).

3.2.1 Regolith Thickness

The entire Moon's surface appears to be covered by various

thicknesses of regolith. The cover of regolith ranges in thickness from 1-3 meters in the shallowest areas up to a few kilometers in the highlands. Generally, the regolith is between 5 to 20 meters thick. A thicker layer of regolith covers the older highlands and the younger mare areas. Regolith was produced by millions of years of meteorite impacts that pulverized surface rocks. Therefore, bare bedrock would be found only where there are steep walls, such as on the sides of craters and the walls of rills. Remote sensing the regolith cover does make sense because lab analysis and calculations indicate about 90% of this lunar soil is from the immediate area and only 10% is from craters formed tens to hundreds of kilometers away, or even from the other side of the Moon (French, 1977).

3.2.2 Regolith Composition

Lunar soils contain rock fragments of the underlying bedrock, rock fragments from craters, soil breccias, glassy fragments, and fragments of the impacting meteorites, (less than 1%), (Wood, 1979). Most regolith particles range between 2-60 microns in size, with an average size of 10 microns. This is similar to terrestrial clays. Soil density ranges between 1.3-1.8 g/cc, with an average density of 1.5 g/cc. This soil exhibits a very low (100 m/sec) compression-wave velocity, which is well below the typical Earth soil or Earth alluvium. Porosity can exceed 50% (Short, 1975). Furthermore, Mendell (1985) reports the iron rich mare soils melt at lower temperatures (1473 degrees K) than the highland soils (1673 degrees K).

3.2.3 Lunar Rocks

All of the rock samples returned from the Moon are differentiated rocks from igneous fractionation (Wood, 1979). The two main rock types are the older highland rocks and the younger mare basalts. The highland rocks are feldspar rich (high alumina) while the mare regions are rich in pyroxene and olivine (high magnesium) (Short, 1975). Highland rocks contain as much as 17% Al while mare basalts contain 8% Ti and 15% Fe. Most lunar soils and rocks contain 20% silica, mainly in pyroxene and feldspar (LGO, 1986).

The highland rocks are mostly composed of one type of Plagioclase mineral, Anorthosite. These anorthositic rocks are uncommon on the Earth, except in Greenland where the 3500 million year old rocks form thick bands up to 1 km thick (Guest and Greeley, 1977). The mare basalts are much darker than the highland rocks because they contain an abundance of the mineral ilmenite (Jastrow, 1977). Remote sensing data indicates that there are at least twenty different types of mare basalts (Mendell, 1985).

3.2.4 Surface "Weathering"

Radiation, impacts from micrometeorites, and impacts from the solar wind can make changes in the top of the regolith. An example of this is the creation of glass. The amount of glass present in the regolith can be used as an index of its maturity. Young soils contain less than 10% glass and older soils range between 35-87%. These lunar glasses may be the result of shock melting and vaporization with the loss of volatile elements. This can cause a rise in Fe and Ti compounds which absorb and scatter the light, so there is a general lowering of the albedo. However, the topmost "skin" layer of the regolith is lightened gradually in albedo due to the loss of these glassy coatings by abrasive "scrubbing" from dust impacts and/or radiation bleaching (Short, 1975). Over time, solar wind atoms may also create glass in the regolith by producing many tiny particle tracks in the outer surface of the grains which transforms them into a glass (French, p. 193, 1977).

Compounding surface changes are calculations showing the top one-half millimeter of soil to be thoroughly mixed. This layer is turned over 100 times every million years. However, the top one centimeter of soil is stirred only once every ten million years and billions of years are required to stir the soil to depths of several meters (French, 1977). Most surficial regolith materials do represent underlying materials, however, because the sharp boundaries between mare and highland areas have remained since the maria formed (Wilhelms, 1987).

3.2.5 Possible Sources for Mineral Concentration

Large scale concentrations of metals, water ice, and radio active minerals may be present on the Moon. Iron and titanium are found in dark regoliths, with the darkest mature regoliths containing the most Ti (Wilhelms, 1987). The maria areas show a reduction in radar power, which may be directly related to electric losses due to increased iron and titanium (Arvidson et al., 1983). Since samples of lunar soil collected from permanently cold and shadowy places under large boulders seem to be enriched in low boiling point elements like lead, mercury, bromine, antimony, it is possible these elements were distilled out of the rest of the lunar soil by the hot sun and moved into the shadowed regions where they condensed. Areas near the lunar poles, which have been in permanent shadow, may contain sizable deposits of metals and water ice (French, p.209-210, 1977). Several of the LOP's Passive Instrument Modules, such as the gamma ray spectrometer, x-ray spectrometer, ultraviolet spectrometer, and the active Raman Module can be used to detect metals and the presence of water ice in the permanently shadowed craters might be detected by using the gamma ray spectrometer to detect Hydrogen (Burke, 1977).

The lavas in the lowlands of the western frontside of the

Moon may be distinctly more radioactive than those on the eastern side (Short, 1975). Valuable minerals may be concentrated near the vents through which the lava flowed or in areas of transient events. Since the Moon does not contain liquid water, analogies with mineral concentrations on the Earth may not be valid. New theories about the concentration of minerals on the Moon will develop from the data gathered by the LOP.

REFERENCE

- Barringer, A. R., 1965, "Radio Frequency Reflectivity Experiments Proposed for AES Lunar Orbital Flights", Francis Narin, edit., *Post Apollo Space Exploration*, Vol 20, Part 1, Advances in the Astronautical Sciences: American Astronautical Society Publication Chicago, Ill, pp. 417-434.
- Berlin, Graydon L., Mohammed A. Tarabzouni, Abdullah H. Al-Naser, Kamel M. Sheikho, and Richard W. Larson, July 1986, "SIR-B Subsurface Imaging of a Sand-Buried Landscape: Al Labbah Plateau, Saudi Arabia", *IEEE Transactions on Geoscience and Remote Sensing*, Vol. Ge-24, No. 4, pp. 595-601.
- Blom, Ronald G., Robert E. Crippen, and Charles Elachi, 1984, "Detection of Subsurface Features in SEASAT Radar Images of Meads Valley, Mojave Desert, California": *Geology*, Vol. 12, pp. 346-349.
- Farr, Tom G., Charles Elachi, Philip Hartl, K. Chowdhury, 1986, "Microwave Penetration and Attenuation in Desert Soil: A Field Experiment with the Shuttle Imaging Radar", *IEEE Transactions on Geoscience and Remote Sensing*, Vol. GE-24, No. 4, pp. 590-594.
- McCoy, Roger, 1988, Private communications.
- Mantel, Ellen J. and Elizabeth R. Miller, editors, July 1977, *Catalog of Lunar Mission Data: National Space Science Data Center/World Data Center for Rockets and Satellites 77-02* pp. 93-102.
- Moore, Richard K., 1976, "Active Microwave Systems" in Joseph Lintz Jr., and David S. Simonett, editors, *Remote Sensing of Environment*, Massachusetts, Addison Wesley Publishing Co., ch. 7, p. 234-290.
- NASA, 1986, "Status and Future of Lunar GeoScience": NASA SP-484.
- Peeples, Wayne J., William R. Sill, Thomas W. May, Stanley H. Ward, Roger J. Phillips, Rolando L. Jordan, Elsa A. Abbott, and Terry J. Killpack, 1978, "Orbital Radar Evidence for Lunar Subsurface Layering in Maria Serenitatis and Crisium": *Journal of Geophysical Research*, Vol. 83, No. B7, pp. 3459-3468.
- Phillips, R. J., G. F. Adams, W. E. Brown Jr., R. E. Eggleton, P. Jackson, R. Jordan, W. J. Peeples, I. J. Porcello, J. Ryu, G. Schaber, W. R. Sill, T. W. Thompson, S. H. Ward, and J. S. Zelenka, 1973, "The Apollo 17 Lunar Sounder": *Proceedings of the Fourth Lunar Science Conference*, (Supplement 4, *Geochimica et Cosmochimica Acta*), Vol. 3 pp. 2821-2831.
- Porcello, Leonard J., Rolando L. Jordan, Jerry S. Zelenka, Gary F. Adams, Roger J. Philips, Walter E. Brown Jr., Stanley H.

Ward, and Philip H. Jackson, 1974, "The Apollo Lunar Sounder Radar System": Proceedings of the IEEE, Vol. 62, No. 6, pp. 769-783.

Sabins, Jr., Floyd F., 1987, *Remote Sensing Principles and Interpretation*, second edition, ch 5 & 6 : W. H. Freeman and Company, New York, pp. 181 and 194.

Schaber, Gerald G., John F. McCauley, Carol S. Breed, and Gary R. Olhoeft, 1986, "Shuttle Imaging Radar: Physical Controls on Signal Penetration and Subsurface Scattering in the Eastern Sahara": IEEE Transactions on Geoscience and Remote Sensing, Vol. GE-24, No. 4, pp. 603-623.

Sharpton, Virgil L., and James W. Head III, 1982, "Stratigraphy and Structural Evolution of Southern Mare Serenitatis: A Reinterpretation Based on Apollo Lunar Sounder Experiment Data": Journal of Geophysical Research, Vol. 87, No. B13, pp. 10,983-10998.

Thompson, T. W., 1979, "A Review of Earth-Based Mapping of the Moon": in *The Moon and the Planets*, Vol. 20, D. Reidel Publishing Co., Boston, pp. 179-198.

Ulaby, Fawwaz T., Richard K. Moore, and Adrian K. Fung, 1982, "Radar Remote Sensing and Surface Scattering and Emission Theory", in *Microwave Remote Sensing Active and Passive*, Vol. II: Massachusetts, Addison-Wesley Publishing Company, 1064 P.

4.0 Instruments Groups

The fundamental purpose for the Lunar Orbital Prospector (LOP) is to provide an orbiting platform above the surface of the Moon which will be capable of performing nearly any scientific remote sensing task which researchers on Earth or on the Moon may be inclined to perform. This is a big order, but by trying to anticipate the needs of the scientific community, we think that it is not an impossible task.

To indicate the versatility and some possibilities for the LOP, four mission packages have been postulated to accomplish basic research on the Moon. It must be stressed that these are not the only possible uses of the LOP and its capabilities. If in the future someone has the need of some vital information on the Moon and an instrument is available to obtain that data, the LOP can be available as a platform for that instrument or instrument package.

4.1 LOP Mission Packages

The following is a list of possible scientific packages, their purpose, and the instruments which may be used to accomplish this purpose:

1. Metals and Radioactive Element package.
2. Thermal, Silicates and Water package.
3. Topographic Mapping package.
4. Raman Spectroscopy package.

Each package, except the raman spectrometry package, meets the following specifications:

1. Total system mass less than 200 kg.
2. Total system power requirements less than 500 watts.

The raman spectrometry package, because of its use of a high power laser, will carry part of it's own power supply and will be slightly larger than 200 kg. This will be covered in the section on raman spectrometry.

4.2 Instrument Descriptions and Functions

Because each mission package is made up of several individual sensing instruments, this section will provide a brief description of each instrument, its purpose, and the type of information which can be gained from its use. The Radar surface and subsurface mapping instruments and the Raman Spectroscopy system will each be covered in separate sections.

METALS AND RADIOACTIVE ELEMENTS

- ELECTRON REFLECTOMETER
- MAGNETOMETER
- U V SPECTROMETER
- GAMMA RAY
SPECTROMETER (GRS)
- VISIBLE & INFRARED MAPPING
SPECTROMETER (VIMS)
- X-RAY SPECROMETER
- RADAR ALTIMETER

THERMAL, SILICATES AND WATER

- MICROWAVE RADIOMETER
- GAMMA RAY
SPECTROMETER (GRS)
- HIGH RESOLUTION SOLID
STATE IMAGER (HRSSI)
- VISIBLE & INFRARED MAPPING
SPECTROMETER (VIMS)
- RADAR ALTIMETER

Table 4.1 Passive instrument systems

TOPOGRAPHIC MAPPING

- LASER ALTIMETER
- GEODESIC IMAGER
- RADAR SURFACE AND
SUBSURFACE MAPPER
- RADAR ALTIMETER

RAMAN SPECTROSCOPY

- RAMAN SPECTROMETER
- RADAR ALTIMETER

Table 4.2 Active instrument packages

4.2.1 Radar Altimeter

One instrument which will be present in all of these packages is the Radar Altimeter. Because of its universal use in all of the packages it will be mounted directly to the body of the platform. It consists of a radar instrument which measures the distance of the LOP above the surface of the Moon. The Radar Altimeter will provide a link between the data taken on each mission, and it will provide a standard for researchers to correlate between the individual missions and packages.

The Radar Altimeter has a mass including the antenna of 17kg and a power consumption of 28 watts. The antenna is a nadir pointing parabolic dish of 1 m diameter. The electronics fit in a box which is 120 X 60 X 10 cm [1]. The antenna will be mounted on a boom out to one side of the LOP.

4.2.2 Gamma Ray Spectrometer (GRS)

Gamma rays are emitted by a nucleus which decays from a certain state to a lower energy level, or they may come from annihilation of a proton or an inelastic collision between a beta particle and an atom [4]. This instrument will detect gamma rays emitted as a product of natural radio active decay from Thorium, Uranium and Potassium. It will also be able to detect emissions as a result of high energy cosmic rays interacting with Iron, Titanium, Hydrogen, and Oxygen [5]. The information obtained by the GRS must be collected over a particular spot several times to get useful information. This necessitates a long mission. The mission length proposed for the Lunar Geoscience Observer (LGO) is one year. Although shorter missions may be adequate, it is proposed that a mission period of 1 year be used as a baseline for this instrument.

The GRS was flown on the Apollo 15 and 16 Command Service Modules. It will also be included on the LGO. The Apollo gamma ray spectrometer is shown in Figure 4.1 and the results of radioactive element surface mapping is shown in Figure 4.2. At an orbital altitude of 100 km, resolution is expected to be about 30 km [1]. At an altitude of 30 km, resolution should be about 22.9 km. See appendix 4 for details of the method used to estimate resolution.

The GRS is sensitive to radioisotopes from RTGs, thoriated alloys, and potassium paints. It is also sensitive to magnetic fields greater than 1 gauss. The instrument must be boomed to greater than one space craft diameter from the craft and shielded from the RTGs. The precision of measurements are strongly dependent upon the duration of the measurements and the observing geometry.

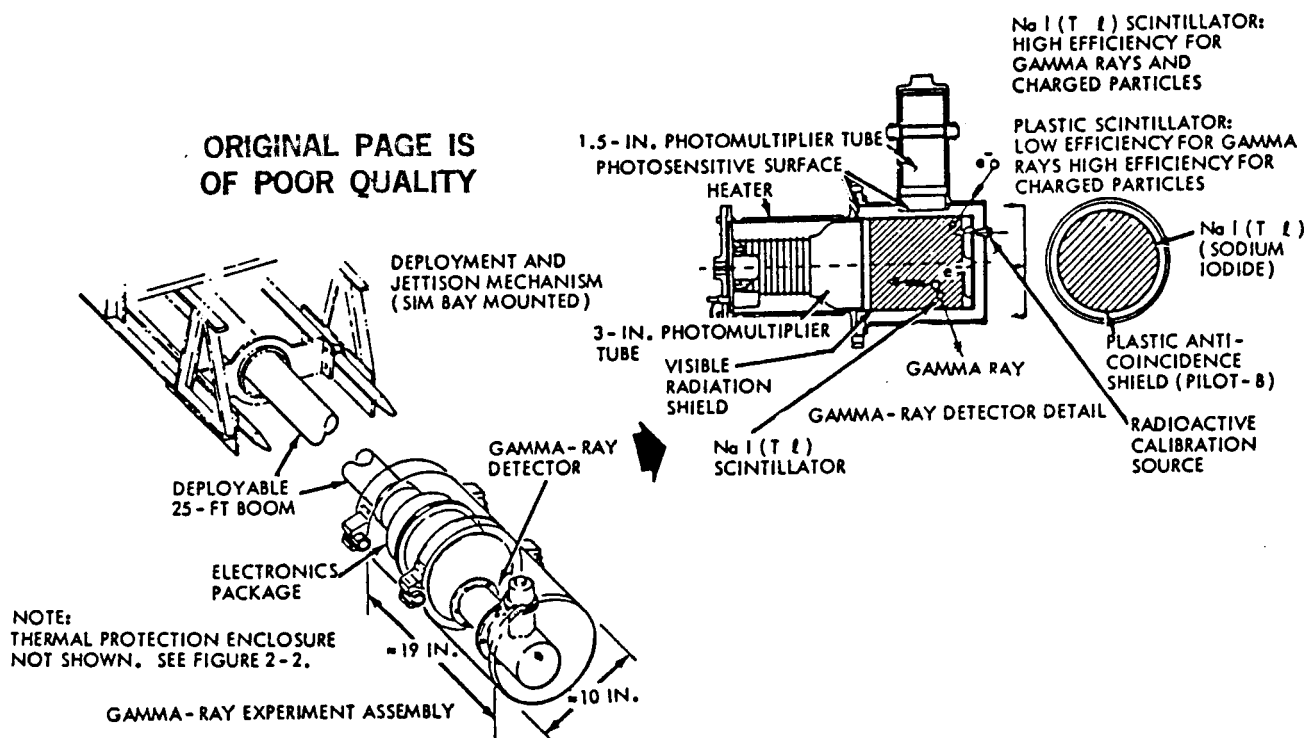


Figure 4.1 Apollo gamma ray spectrometer

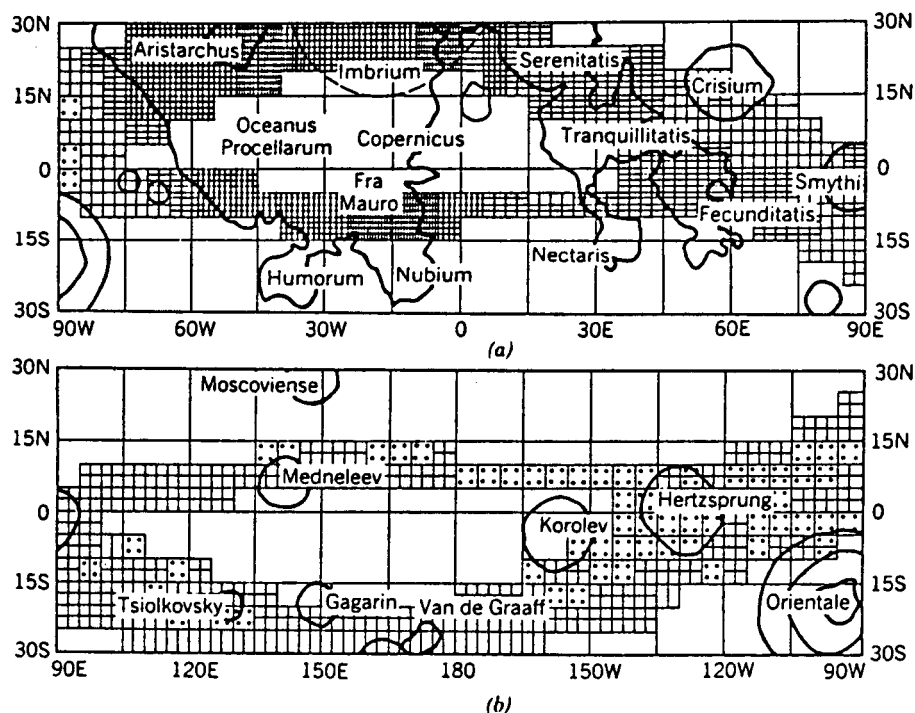


Figure 4.2 Apollo orbital gamma ray spectrometer results

4.2.3 Thermal Infrared Mapping Spectrometer (TIMS)

The use of a spectrometer sensitive to the $6\mu\text{m}$ to $20\mu\text{m}$ range of reflections and emissions from the surface will allow the detection of silicon based minerals. TIMS is designed to look at this spectral region and will provide a more complete picture of the composition of the surface of the Moon [1].

TIMS will consume approximately 12 W of power and has a mass of 16 kg. The field of view for this instrument as proposed in the LGO mission is 30° . For a 100 km circular orbit and a 30° field of view it will take 8.5 days to completely map the surface assuming that it didn't pass over the same region twice. To compensate for this possibility, a 30 day mission period should provide full coverage of the surface.

4.2.4 Visible and Infrared Mapping Spectrometer (VIMS)

The VIMS will be used to continue identification of specific mineral species. This will allow the identification of some minerals by comparison to spectra of known Moon minerals. The data obtained will also allow the mapping of the surface of the Moon with respect to these minerals for later reference.

The detector is a CCD type with 128×128 elements. The optics have a focal length of approximately 1 m and a focal ratio of f3.0. This is based on some improvement over the system used on Galileo and proposed for the LGO mission [4]. The field of view of the TIMS on the LGO is 30° which would allow full coverage of the surface in less than 20 days, assuming no overlap and looking at the light side of the Moon only. The instrument for the LOP will have a smaller field of view as a result of higher resolution, therefore a mission length of 60 to 90 days should provide the needed data. This accounts for the decreased field of view and also for the fact that it would be nearly impossible to have an orbit which exactly covered the whole surface of the Moon without any wasted overlap on the images.

The power requirement of the VIMS is 20 watts and the mass is 30 kg. The mass of the mirror was estimated using a baseline of 166 kg per square meter of surface area on the primary mirror [5]. This is a more powerful instrument than that proposed for LGO and Galileo, but it is within the projected instrument information contained in the CRC Handbook of Space Technology [4]. It will use a cassegrain optical system which is the most economical in terms of space and mass. Because of the cassegrain optical system, the overall size of the VIMS will be smaller than that of the system used on the LGO. The housing and detector of the VIMS must be kept at very low temperatures, and the optics of the instrument must be kept free of gas and particulate contaminants. The VIMS operates on the sunlit side of the Moon only.

4.2.5 Visible High Resolution Solid State Imager (VHRSSI)

The purpose of this instrument is to allow investigators to look at specific areas at very high resolution. VHRSSI consists of an optic system with a focal length of 880mm and a focal ratio of f5.6. The three CCD focal planes each consist of 1024 X 1024 pixels at 15 μ m center to center spacing. The light entering the system is split by a prism through three filters and onto each CCD. This allows each area photographed to be observed either in color (red, green and blue filters) or at three other spectral regions. This configuration will give a 1° field of view. Because of the very small field of view, it is impractical to assume that total coverage of the lunar surface is possible.

VHRSSI will be used to obtain high resolution images of specific areas of the surface of the Moon. This instrument will enable scientists to obtain resolutions per picture element (pixel) ranging from 45 cm at 25 km above the surface to 6.8 m at 400 km above the surface of the Moon. It may be possible to obtain even higher resolution by exposing all three focal planes to the same field in the same spectral range. In this case each individual pixel on each focal plane will probably be exposed to a slightly different area than the corresponding pixel on the other focal planes. By combining the images received from all three CCDs the resolution may be increased by nearly a factor of three.

By using a cassegrain optical system, the total size and mass of the system can be minimized. The total mass of the system is 15 kg, and it will use 20 watts. Because of the weight savings in this system, the total mass is the same as the refraction system proposed for the LGO mission but with a much higher resolution [5].

Two other options were considered for the optics of the VHRSSI. A "minimum" configuration which would be the same as that proposed for the LGO. This system has a focal length of 250 mm and a field of view of 4°. The resolution at 25 km is 1.5 m and is 24.0 m at 400 km. This is a refraction system which is inherently heavier. Because of this difference, the overall mass is the same as the system proposed in the preceding paragraph for the LOP mission.

A "maximum" configuration was considered which was aimed at a total mass of under 100 kg. This system would use a 3.9 m focal length with cassegrain optics. The total mass would be 95 kg. The resolution would be 10 cm at 25 km above the surface and 1.9 m at 400k m above the surface. The major drawback, other than mass, is that the field of view is only 13.6 minutes of arc. This small field of view would severely limit the useful information in a frame.

4.2.6 Magnetometer and Electron Reflectometer

The magnetometer, along with the electron reflectometer, will be used to locate iron and other magnetic minerals through the measurement of local magnetic fields. They are also used to determine the size of the metallic core of the Moon and to determine the most probable origins of local remnant magnetism.

The magnetometer maps surface magnetic fields at low altitudes, and the electron reflectometer provides complimentary measurements by mapping magnetic field distributions. For best results, the two instruments should be flown together. The field patterns are mapped by measuring the movement of solar and interplanetary charged particles, which are easily scattered in moving to a region of increased magnetic field strength as they approach the Moon. If no surface magnetization is present, the particles are absorbed into the lunar surface. If magnetization is present, a fraction of the particles are reflected back with an intensity that increases with the strength of the total surface field.

A magnetometer was flown on Voyager, Pioneers, ISPM, Galileo, and it is included on the LGO. Surface magnetometers on Apollo 12 discovered high local surface magnetic fields on the Moon and an Electron Reflectometer was flown on Apollo 15 and 16 subsatellites. This instrument is also included in the instrument list for the LOP.

Resolution of a few kilometers is possible at low altitudes, but the Magnetometer is basically ineffective at altitudes above 60 km. The Electron Reflectometer results are independent of altitude, however.

The Magnetometer is sensitive to spacecraft-generated magnetic fields, and must be boomed out to greater than 3 space craft diameters. It works only when solar wind disturbances are minimal. The electron reflectometer is sensitive to the same space craft magnetic fields as the magnetometer, and is also sensitive to electrostatic charging. The electron reflectometer results are not sensitive to solar wind disturbances.

4.2.7 X-Ray Spectrometer

The x-ray spectrometer will be used to measure amounts of elements on the Moon's surface which emit x-rays due to excitation by solar radiation. These elements include magnesium, aluminum, and calcium. During periods of high solar activity, it can also detect iron, potassium and titanium. The spectrometer measures and accumulates data over many orbits.

The x-ray spectrometer was flown with the Apollo 15 Scientific Instrument Module and on the Apollo 16 Command Service Module. An x-ray spectrometer is also planned as part

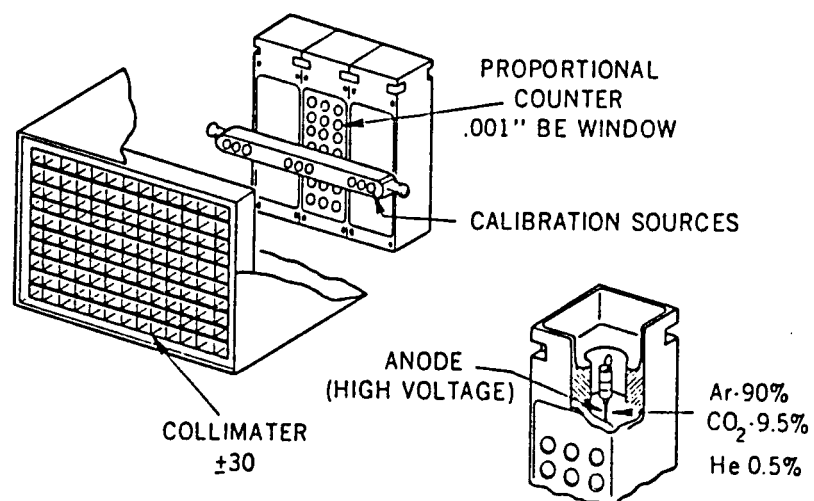


Figure 4.3 Apollo x-ray spectrometer

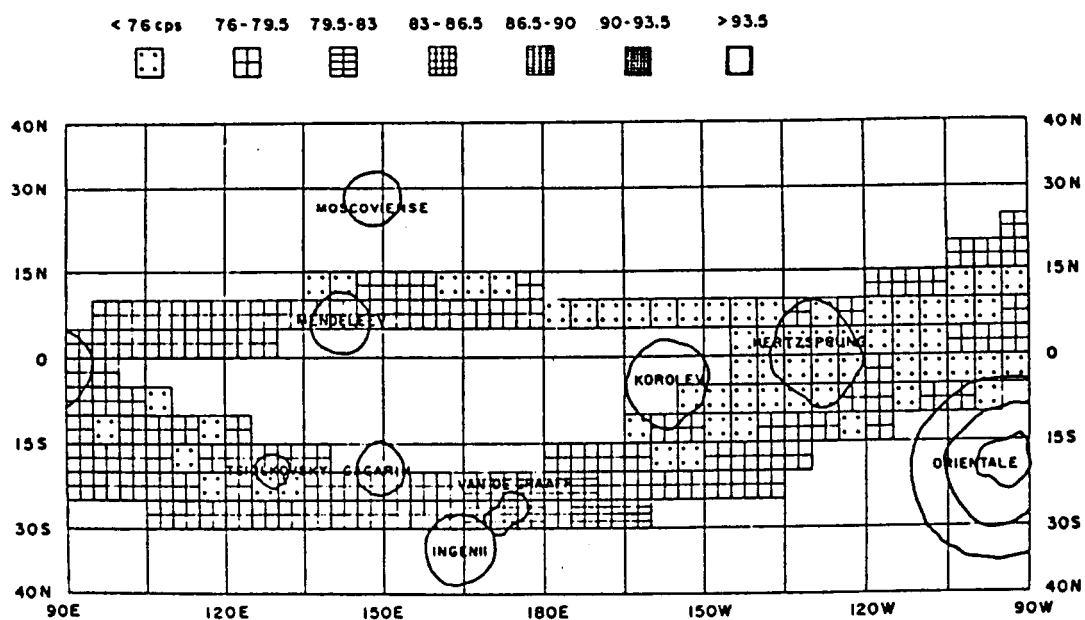


Figure 4.4 Apollo x-ray spectrometer orbital results

of the LGO instrument package. The Apollo x-ray spectrometer is shown in Figure 4.3, and the results of AL/Si and Mg/Si profiles obtained by this instrument is shown in Figure 4.4. Complimenting the spectrometer is a solar monitor to record readings in solar x-ray outputs. At an orbital altitude of 100 km, the resolution is expected to be about 30 km, and at an altitude of 30 km the resolution will be about 8.9 km. Resolution is also dependant upon solar output since the spectrometer uses proportional counters.

The solar detector, which is sensitive to solar radiation reflected by other space craft components, must point in an anti-nadir direction. To avoid problems with reflected radiation it will be boomed out away from the space craft far enough that no reflected radiation will be within the 20° field of view of the solar detector. The x-ray spectrometer operates on the daylight side of the Moon only.

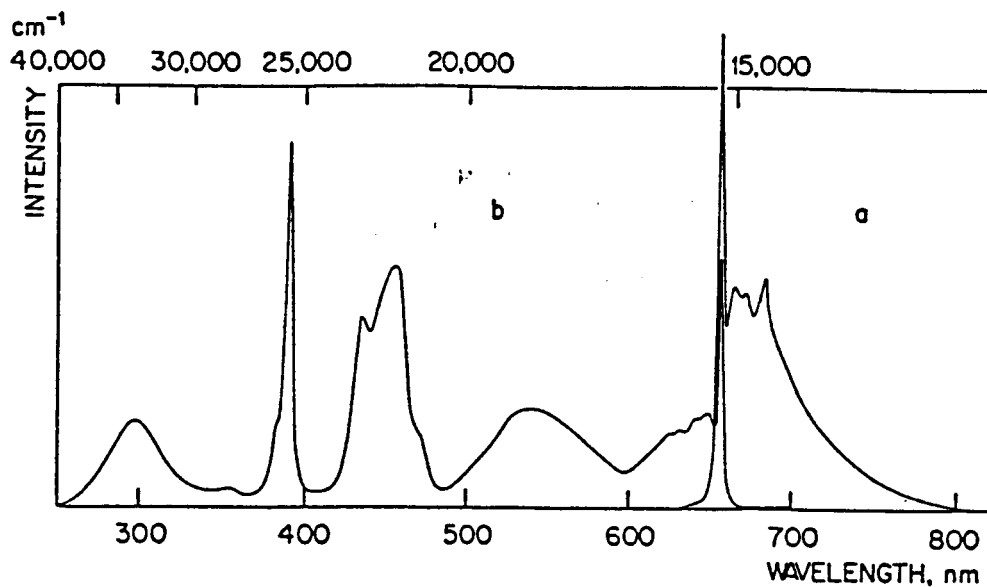
4.2.8 Ultraviolet Spectrometer

The ultraviolet spectrometer can be used to compliment imagery from visible, infrared, and radar spectrometers in identifying minerals, particularly those that luminesce in the UV wavelength range (metallic substances). It can also be used to compliment visible imagery to map surface features (some lunar features are seen with more contrast in the UV range). The ultraviolet spectrometer operates in a manner similar to that of the VIMS. Ultraviolet solar energy reflected from the Moon's surface is focused onto a photomultiplier which has an output proportional to the intensity of the UV reflectance. It will be used on the sunlit side of the Moon.

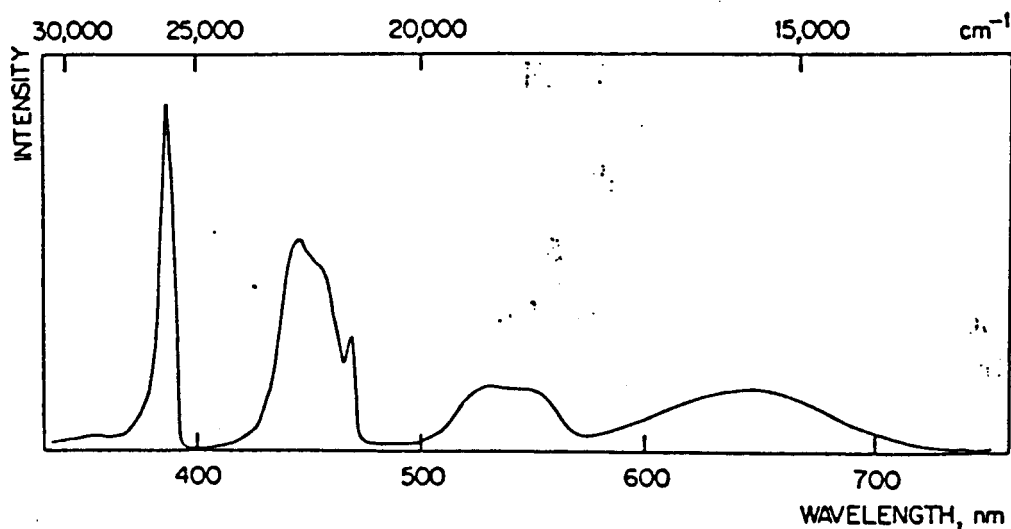
An ultraviolet spectrometer was flown on Apollo 17 which provided some observations of the lunar surface and lunar atmosphere, along with some additional Earth, and galactic observations. Luminescence spectras of different lunar minerals in the UV and visible range are shown in Figure 4.5. Ultraviolet spectrometers have also been used to study the lunar atmosphere. Thus, UV spectrometers may be an especially valuable tool to monitor environmental changes to the lunar atmosphere due to the human presence after a lunar base has been established.

4.2.9 Geodesic Imager

The geodesic imager is a medium resolution imaging system which takes images both in the nadir direction and at an angle 50° forward of nadir. When these images are later combined and correlated, it will give a three dimensional representation of the surface of the Moon. This system will only be used on the daylight side of the Moon.



Luminescence excitation and emission spectra of $\text{LiAl}_5\text{O}_8: \text{Fe}^{3+}$, measured at 77°K. (From Pott and McNicol, 1972.)



Luminescence excitation spectrum of $\beta\text{-NaAlO}_2: \text{Fe}^{3+}$, measured at 77°K. (From Pott and McNicol, 1971a.)

Figure 4.5 Ultraviolet luminescence of several Apollo lunar samples

The LGO will have a geodesic imager as part of its instrument package, and this basic instrument is baselined to be on the LOP. But, because of the limited data rates available on the LGO, it will only image 1200 frames in the one year mission of the spacecraft [1]. The LGO instrument uses a 1024 X 1024 pixel CCD; but, because of the limited data rates, only one half of the CCD is being used to image the surface. The other half is used as storage for the preceding image. The increased data capabilities of the LOP will allow the use of the full CCD focal plane, doubling the amount of data in each image. A geodesic imager on the LOP will greatly improve the visible mapping of the Moon.

4.2.10 Microwave Radiometer

The microwave radiometer is an instrument which detects noise-like radiation from a body [9]. It will be used to measure heat flow from the surface of the Moon which will allow scientists to map the global heat flow providing data for the effect of solar heating at different latitudes. The instrument may also provide data concerning the thermal inertia of the Moon's surface. Thermal inertia is a measure of the responsiveness of a material to changes in the thermal environment [2]. The microwave radiometer will consume about 10 watts and has a mass of 10 kg. This is based on the proposed model for the LGO mission. The total mass includes the mass of a parabolic dish type antenna with a diameter of 1m [1]. The field of view of the microwave radiometer is about 30°, so the total mission time to map the surface of the Moon is less than that of TIMS.

4.2.11 Laser Altimeter

The laser altimeter is similar to the radar altimeter in function. The major difference is that it uses much shorter laser wavelengths to map the surface. The shorter wavelengths also allow much more accurate determination of altitude. Currently an Earth-based system has been developed using a laser as part of an altimetry and ranging system. This system in the altimetric mode will give vertical precision to within decimeters and will give a 70-100 m horizontal resolution, as well as provide nearly contiguous coverage when operating at 40 pulses per second [10]. Laser altimeters were used on the Apollo missions.

REFERENCES

- [1] Contributions of a Lunar Geoscience Observer (LGO) Mission, Department of Geological Sciences, Southern Methodist University, Dallas, Texas.
- [2] Carr, Micheal H., The Geology of the Terrestrial Planets, NASA Scientific and Technical Information Branch, 1984. p.212.
- [3] Duivenstijn, A. J., and Venverloo, L. A. J., Practical Gamma Spectrometry, Charles C. Thomas - Publisher, 1963. p.11-12.
- [4] CRC Handbook of Space Technology: Status and Projections, p.140-141.
- [5] NASA Space System Technology Model, Vol. III, January 1984. p.93.
- [6] Lunar Remote Sensing and Measurements, Geological Survey Professional Paper 1046-B, U.S. Government Printing Office, 1980.
- [7] Post Apollo Space Exploration, Advances in the Astronautical Sciences, Volume 20, Part One, American Astronautical Society Publication, 1965.
- [8] Catalog of Lunar Mission Data, National Space Science Data Center/World Data Center A for Rockets and Sattelites, July 1980.
- [9] Oliver, Frank J., Academic American Encyclopedia, Grolier Inc., Danbury, Conneticut, 1987.
- [10] Cohen, S.C.; Degnan III, J.J.; Bufton, J.L.; Garvin, J.B.; and Abshire, J.B.; The Geoscience Laser Altimetry/Ranging System, IEEE Transactions Geoscience and Remote Sensing, Vol. GE-25, September, 1987.

5.0 Passive Packages

Two passive remote sensing instrument packages are utilized; the Metals and Radioactive Element package and the Thermal, Silicates and Water package. The passive packages utilize concepts of reflectance, gamma, and x-ray spectroscopy as well as magnetic field mapping techniques. A discussion of each package follows.

5.1 Metals and Radioactive Element Package

The Metals and Radioactive Element Package will be used to determine the position of certain metallic minerals. It will also be able to map the positions of radioactive elements in the lunar surface. This data is important because metals and other elements found on the Moon can be used to support the manufacture of lunar derived propellants, and used for other important purposes by an established lunar colony. This package will include the following instruments:

1. Magnetometer
2. Electron Reflectometer
3. Gamma Ray Spectrometer
4. X-Ray Spectrometer
5. Visible and Infrared Mapping Spectrometer (VIMS)
6. Ultraviolet Spectrometer
7. Radar Altimeter

The total mass of this package is estimated to be less than 100 kg and the total power requirements is less than 100 watts, which is well within the design constraints. The total mission time is estimated to be 1 year, and is baselined for a 50 Km polar orbit.

5.2 Thermal, Silicates and Water Package

The Thermal, Silicates and Water package will allow researchers to map the positions of higher and lower concentrations of silicates which may be useful in future manufacture of fuels from the lunar soil. It will also provide data on the heating and cooling characteristics of the lunar surface. This package is also capable of detecting small quantities of Hydrogen which is locked up in the soil and which will be extremely useful if found. This package contains the following instruments:

1. Thermal Infrared Mapping Spectrometer (TIMS)
2. Microwave Radiometer
3. Gamma Ray Spectrometer
4. Visual and Infrared Mapping Spectrometer (VIMS)
5. Visible High-Resolution Solid State Imager (VHRSSI)
6. Radar Altimeter

The total mass of this package is less than 100 kg and the power required is approximately 100 watts. The mission length of this package is estimated to be approximately one year. Most of the mission time for this package is in gathering information from the GRS. Since this instrument is also being used on the Metals and Radioactive Element package, it will be possible to cut the mission time to less than six months if the other package is also flown and the data is available.

6.0 Active Sensing Packages

Two active remote sensing instrument packages are utilized; Topographic Mapping and the Raman Spectroscopy package. Both packages utilize spacecraft generated electromagnetic energy to stimulate surface reflections and emissions respectively. A brief discussion of each package follows, and more indepth discussions are given in sections 7 and 8.

6.1 Topographic Mapping Package

The Topographic Mapping package will provide more thorough information on the topography of the lunar surface. It will also have the ability to "see" beneath the lunar regolith, which could give more clues to the evolution of the Moon and other bodies in the solar system. This package is an "active" package in that it will be sending out signals and recording the lunar reactions to those signals. It includes the following instruments:

1. Geodesic Imager
2. Radar Surface and Subsurface mapper
3. Laser Altimeter
4. Radar Altimeter

The specifics of this package will be covered in the section on Radar Surface and Subsurface Mapping.

6.2 Raman Spectroscopy

The other active package is the Raman Spectroscopy package. This mission will attempt to use Raman Spectroscopy to analyze the composition of the lunar soil. This technique has proven very useful in the laboratory but has never been tried in a remote sensing application. The package contains the following instruments:

1. Tunable Laser
2. Raman Detector and Optics
3. Extra Power Supply

The total mass of the raman package is approximately 225 kg. This is larger than the original mass budget but within the design limits of the system. The extra mass is a combination of large batteries for the power and an optical system which includes a large collection mirror to gather the maximum number of photons returning from the surface after it is hit by the laser. This instrument package will be explained in further detail in the separate section on raman spectroscopy.

7.0 Application of Raman Spectroscopy in Lunar Remote Sensing

The purpose of the Raman spectroscopy sensing package is to identify and detect abundances of mineral species on the surface of the Moon. This information will be used, along with complementary data obtained by Infrared spectroscopy and other techniques, to form a global map of the geologic composition of the lunar surface. This data is important because metals and other elements found on the Moon could be used to support manufacture of lunar derived propellants and used for other important purposes by an established lunar colony. In order to develop an application of Raman spectroscopy for lunar remote sensing, various resources were studied to find out how it has been used previously. Physical principles of Raman spectroscopy and differences and similarities to infrared spectroscopy were also studied. An application and mission scenario were planned which should fulfill the goals outlined above. The specifications that the system was required to meet are:

- Total mass of system less than 200 Kg
- Total power requirements of system less than 1500 watts.

As a baseline for calculating expected resolutions, signal intensities, etc., a circular polar orbit at an altitude of 25 Km was assumed. The period for this orbit is about 2 hours with an orbital velocity of 1.67 Km/s (resulting in 1.64 Km/s of the lunar surface to be covered by a static nadir pointing system).

The final estimate of the total mass of the package is approximately 235 Kg, which slightly exceeds the mass budget, while the total power requirement is estimated to be 1500 watts, which is within the power budget constraints.

7.1 Current Applications

Raman spectroscopy is a method of studying substances by observing energy changes in the molecules which make up that substance. It is being used extensively in laboratory and short distance atmospheric sensing applications, but we are not aware of it being used previously in a far-remote sensing application. It is currently being used by chemists and other scientists to identify complex and compound organic substances by comparing the Raman spectrum of an unknown to the spectra of known compounds. It is also used to study molecular structures, to observe chemical reactions taking place, and in the quantitative analysis of compounds.^{1,2}

Raman spectroscopy has also been used in limited atmospheric studies and pollution control monitoring.⁷ Atmospheric H₂O has been detected to 2 km altitudes and at distances of a few hundred meters trace elements such as nitric oxide, sulfur dioxide, nitrogen, benzene, or ammonia can be detected in the tens of a ppm range. Figure 7.1 illustrates the remote raman system.⁹

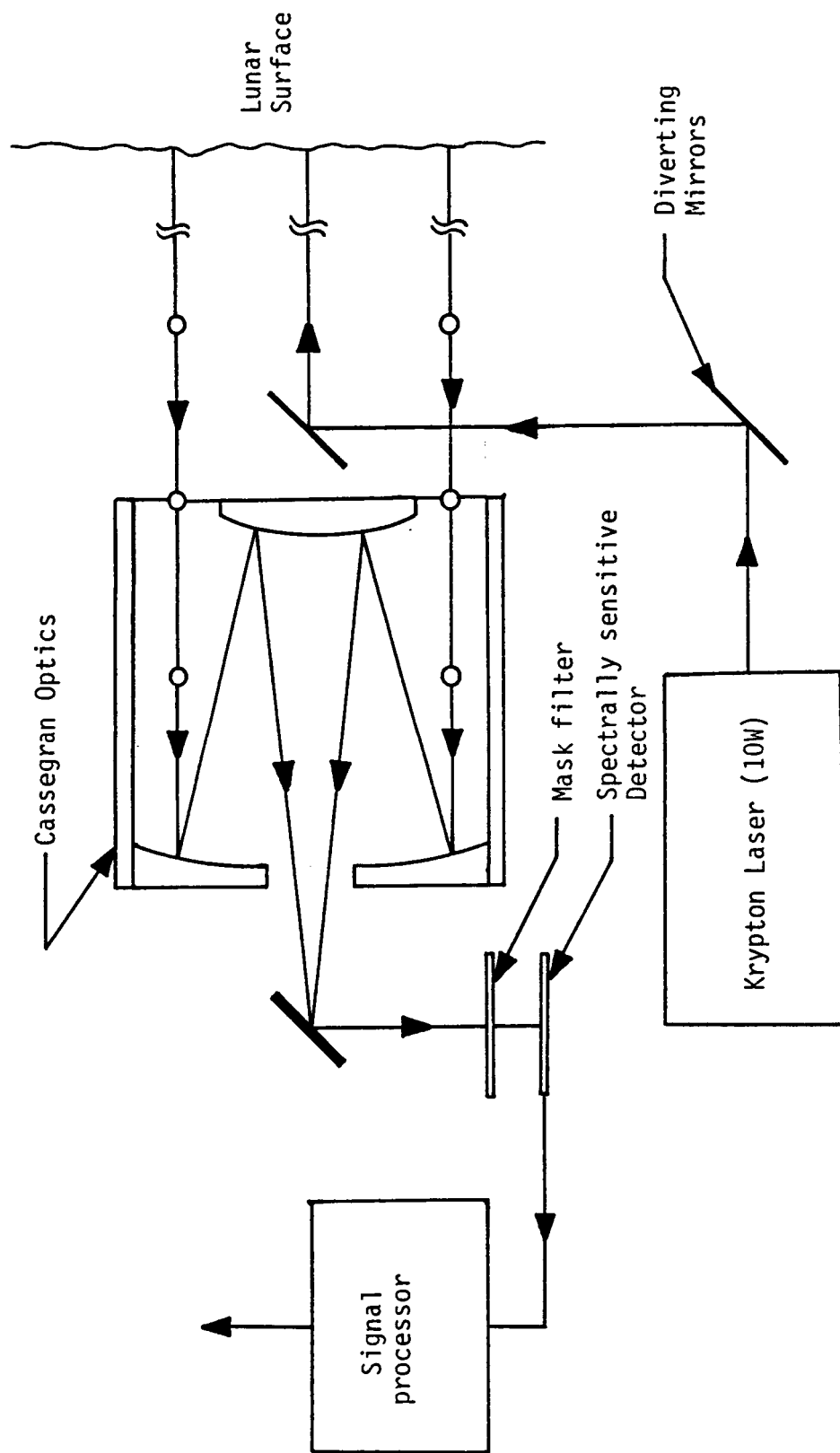


Figure 7.1 Schematic of a remote raman sensing system.

One reason that Raman spectroscopy hasn't been used for remote sensing at large distances is that it is a very weak phenomena. It requires a large power input, gives a poor return, and the presence of any appreciable amount of light, other than the laser light used to excite the sample, makes the Raman effect extremely difficult to observe. Another problem is that the light scattered back by the Raman effect is readily dispersed by the earth's atmosphere. For these reasons, Raman spectroscopy has been mainly a laboratory or localized procedure.

7.2 Principles of Raman Spectroscopy

Raman scattering occurs as a result of an inelastic collision of a quantum of light and a molecule of a substance. As a result of this collision, a dipole moment is temporarily induced in the molecule. The dipole moment oscillates with the frequency of oscillation dependent on the polarizability of the molecule. The polarizability of most of the molecules in the sample does not change due to the collision, and the molecules return to the same energy level that they were in before the collision took place (see Figure 7.1). As a result of the dipole moment oscillations, the energy from the collision takes the form of light scattered back from the molecule in all directions. This light is at the same frequency as the incident light, and is known as Rayleigh scattering. Figure 7.2 illustrates both Raman and Rayleigh scattering.

Some of the molecules, however, return to a different energy level than the one they were in before the collision (Figure 7.3). This net change in energy is due to a change in the polarizability of the molecule. Because of the polarizability change, the temporarily induced dipole moment can vibrate not only at the frequency of the incident light, but at frequencies above and below the incident frequency. These oscillations can be rotational, vibrational, or both. Since the rotational and vibrational energy levels of a molecule are quantized, the light scattered is shifted by the amount of energy between the different rotational/vibrational energy levels of the molecule. The light scattered back as a result of the dipole moment oscillations can then be of frequencies which are above or below the frequency of the incident light. This is known as Raman scattering. A typical laboratory Raman spectrum is shown in Figure 7.4. The spectral lines due to light at a frequency lower than the incident light frequency are called Stokes lines, and the lines due to light at a higher frequency are called Anti-Stokes lines.

The Stokes lines and the Anti-Stokes lines are shifted the same amount on either side of the frequency of the incident light. Ideally, this would result in the Stokes lines and Anti-Stokes lines being mirror-images of each other, but in practice, the Stokes lines are usually much stronger than the Anti-Stokes lines. For this reason, usually only the Stokes

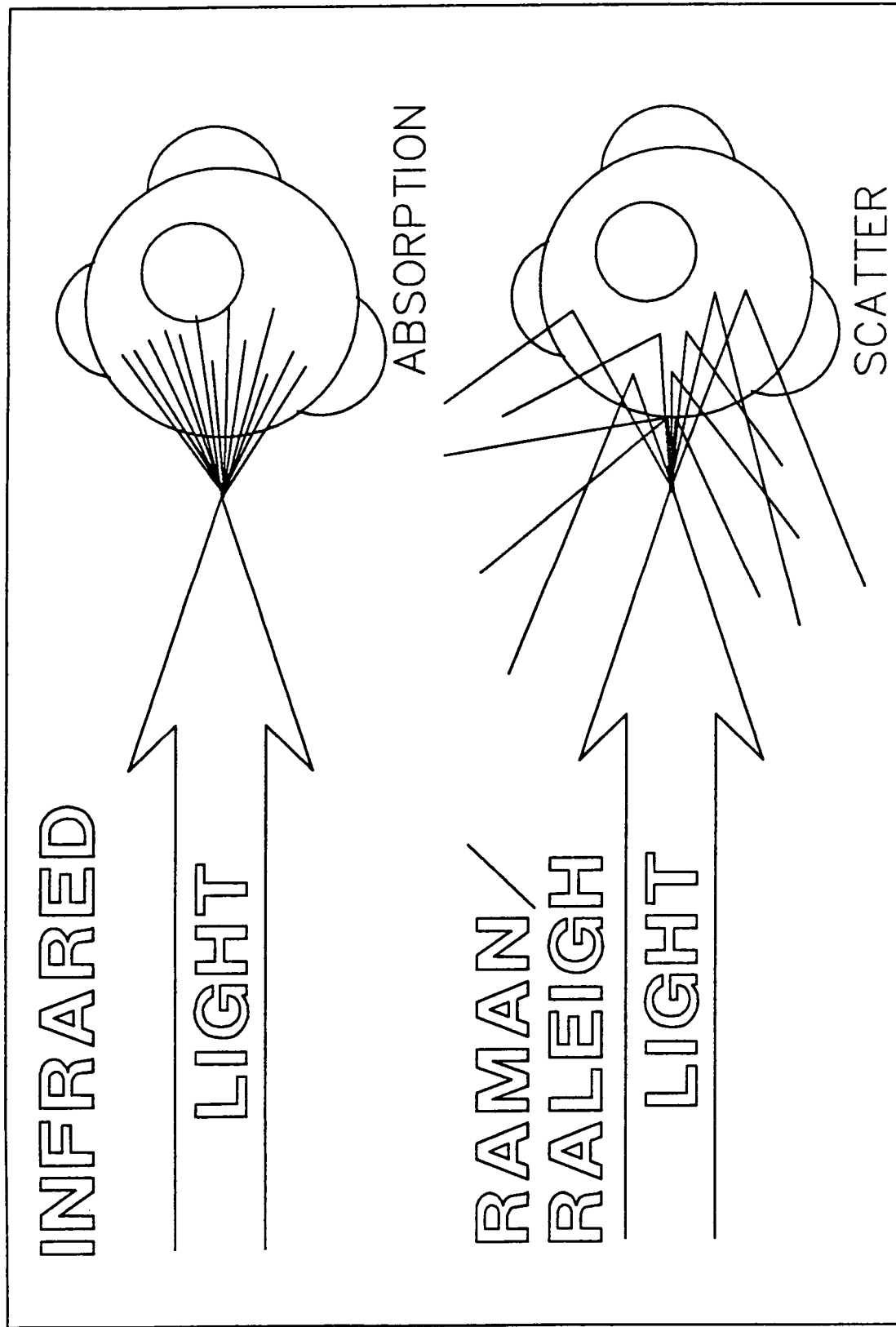


Figure 7.2 Graphic representation of Raman and Raleigh scattering and infrared sensing and the primary difference in the methods. Raman is an emission phenomena while infrared sensing is an absorbtion phenomena.

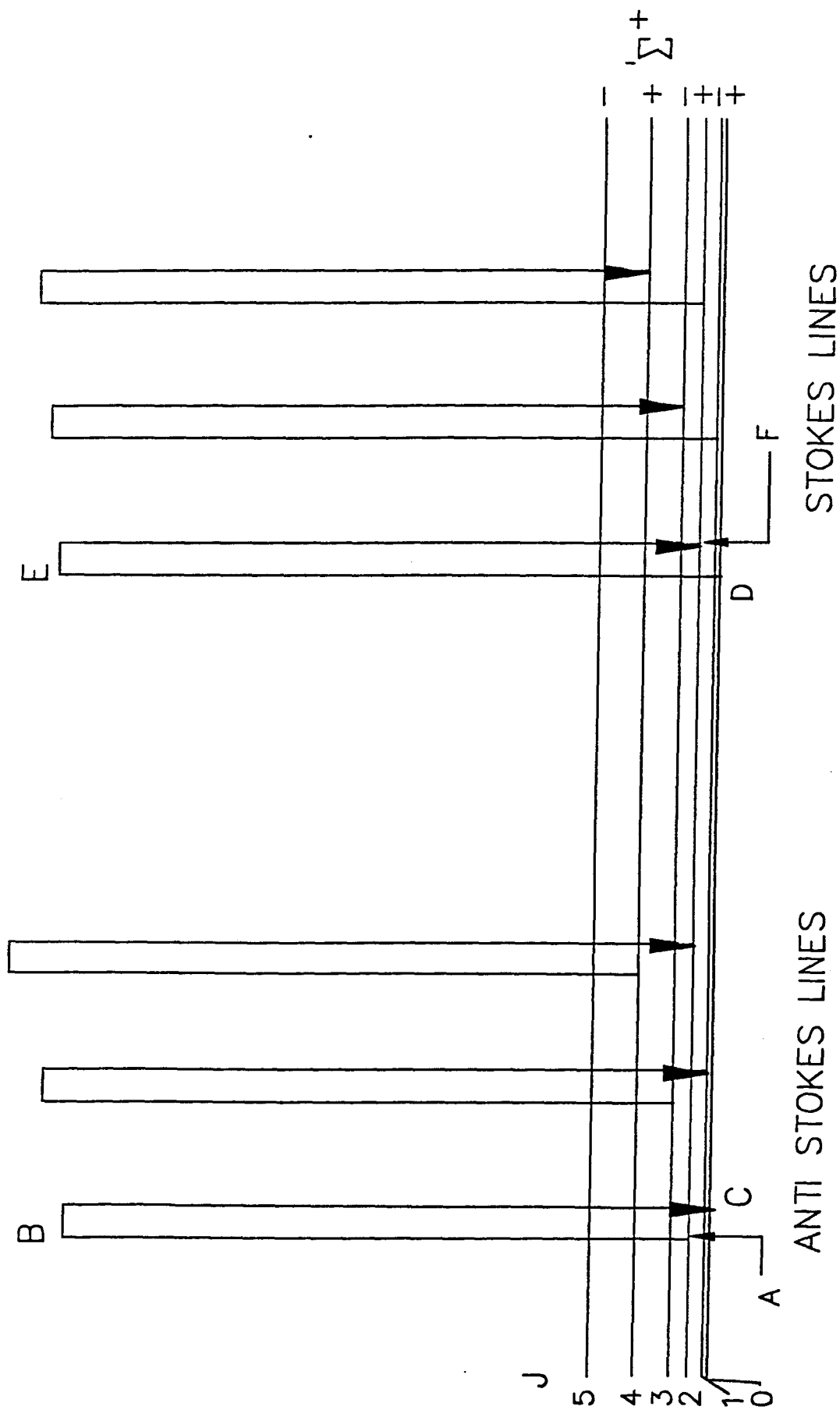
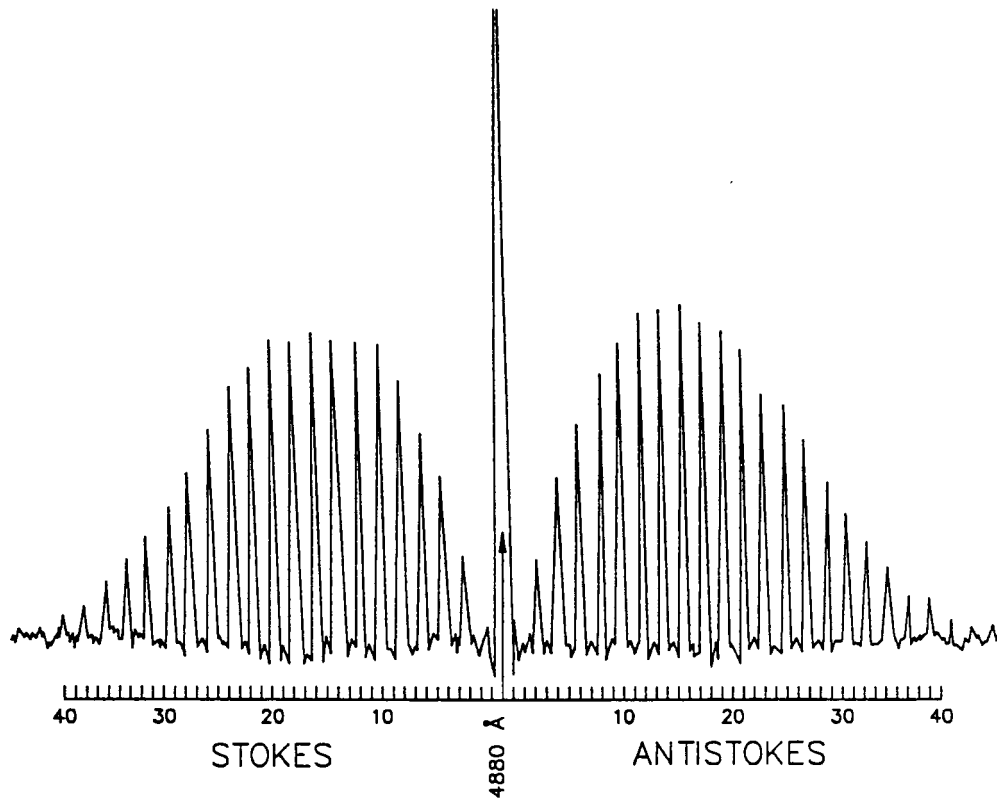
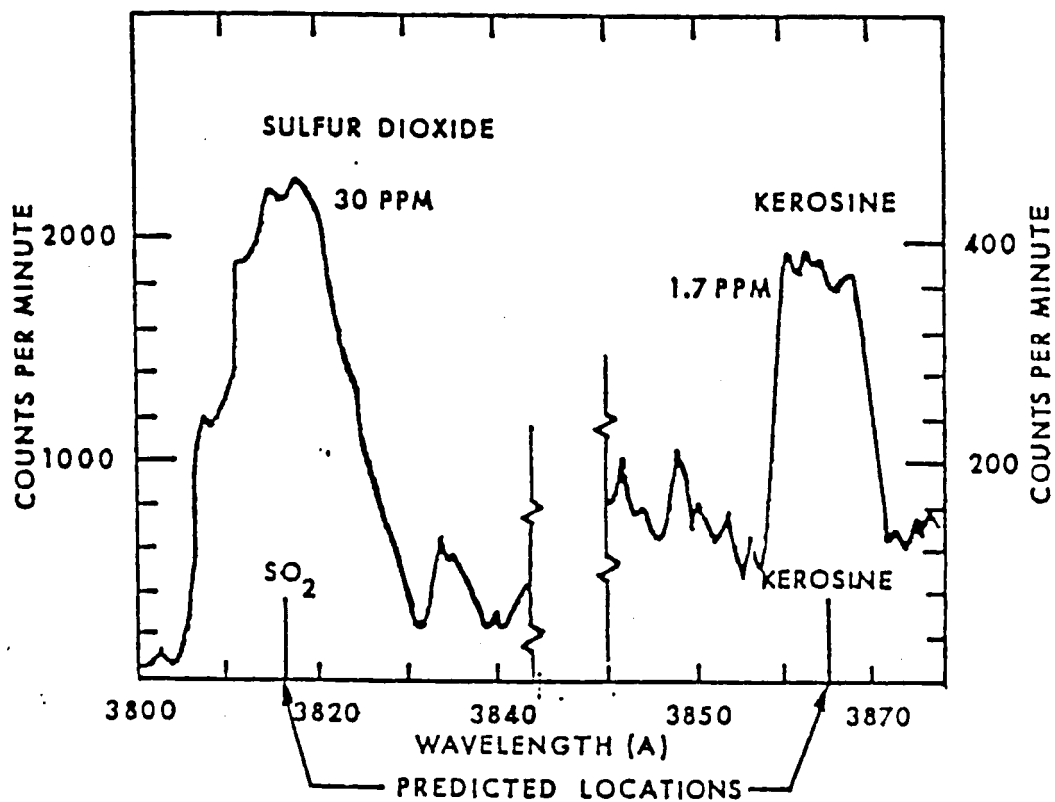


Figure 7.3 Electron and molecular energy level changes occurring during raman scattering result in energy changes in the quantum states and thus stokes and anti-stokes lines.



Laboratory spectrum of CO₂.



Remote sensed raman spectra of atmospheric pollutants.

Figure 7.4 Raman spectrums of both laboratory and remotely sensed samples.

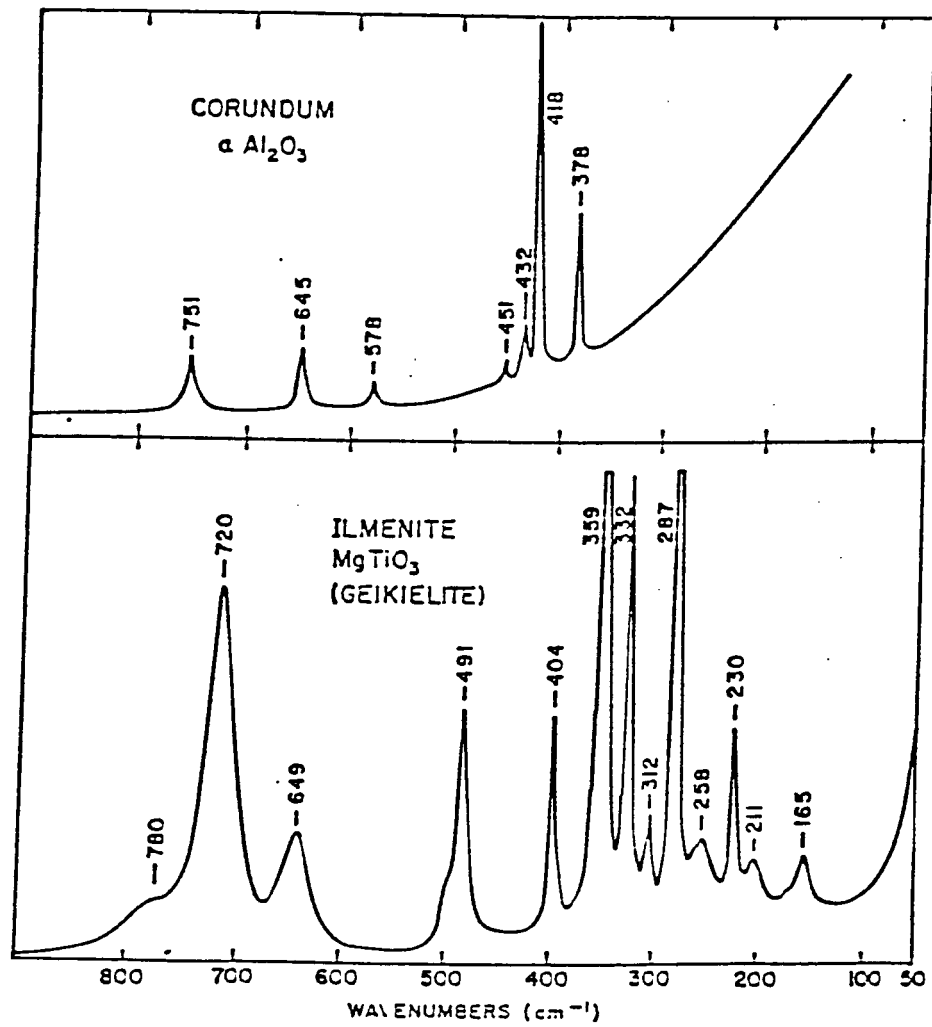


Figure 7.5 Raman spectra of Apollo lunar samples.

lines are studied. The spectral lines are always displaced the same amount from the incident frequency, as long as the incident light is not of a frequency which is absorbed by the compound, in which case very little light scattering occurs.

Raman scattering is a very weak phenomenon. Since only a fraction of the molecules in a substance undergo a net energy change, the intensity of the Raman scattered light is only about 10^{-6} of the incident light intensity. Because of this, a monochromatic light source, such as a laser, is necessary to avoid swamping out the Raman lines.

The spacing of the spectral lines is a characteristic of the particular substance causing the Raman scattering differences between quantized energy levels and studying the Raman spectrum of a substance, it can be identified. The Raman spectrum of a given sample will be a composite of all the spectra of the individual substances in it. Therefore, by studying the Raman spectrum of the Moon's surface, we should be able to identify and map it's mineral composition.

An advantage that Raman spectroscopy has over infrared spectroscopy is that the intensity of the Raman spectrum is proportional to the amount of the substance present in the sample being examined. This yields the possibility of finding quantitatively how much of a mineral is present in the area examined.

7.3 Lunar Orbiting Platform Application of Raman Spectroscopy

As mentioned above, the Raman effect is easily swamped out by any appreciable light at frequencies other than the exciting frequency of the laser. The Raman spectroscopy study of the lunar surface will be done on dark side of Moon while the space craft is in the Moon's shadow or with the Raman spectrometer shielded from the sun. Since there is no atmosphere on the Moon to disperse the Raman scattered light, we should be able to observe the Raman effect. (See Appendix 7)

Remote sensing using the Raman effect has been successfully used to examine atmospheric pollutants. Figure 7.4 shows the type of results that can be returned. It can be seen that very small quantities of atmospheric pollutants can be detected. The spectral differences between gaseous and solid materials can be seen if Figure 7.4 is compared with Figure 7.5, which shows the Raman spectrum for two materials typical of the Moon. Notice how the motion of the gas causes the wide band broadening around the predicted locations Also note that the horizontal axis for each graph is different, wavelength for the gas and wavenumber for the powders.

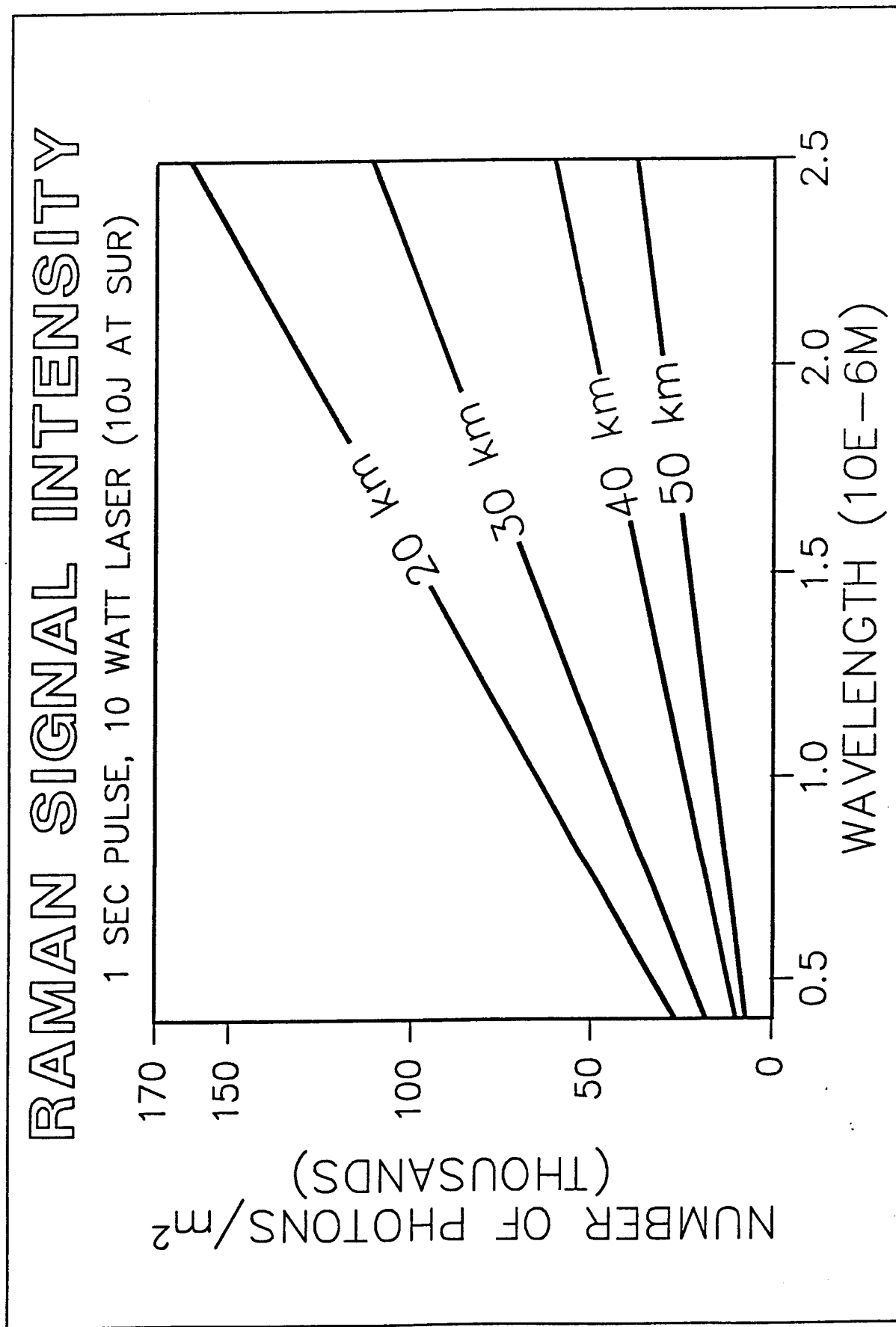


Figure 7.6 Intensity of Raman effect recieved at the spacecraft based on a 10 watt laser.

7.4 Laser Sources

A laser light source will be used to excite the lunar surface. It is essential that the laser to be used have at least a medium power output, in the range of one watt to one hundred watts, and a very narrow, stable range of output frequencies.

A high output power would be desired for two reasons. First, as mentioned previously, only about 10^{-6} of the incident power is Raman scattered. Secondly, since light which is Raman scattered is considered diffuse and radiates out in all directions, the intensity of the light received at the point of observation will vary as the inverse square of the distance from the surface of the Moon. Figure 7.6 shows an example of the intensity that would be observed by the spacecraft at different altitudes with different power lasers when considering these circumstances. See Appendix 7 for more considerations. Because of this, the more power used to stimulate the Raman effect, the better will be the results obtained.

A narrow, stable range of output frequencies is needed from the laser to be able to effectively observe the Raman spectrum. Ideally, the output should be of only one frequency. This exciting frequency must be such that it is not absorbed by the sample. It is not likely that there is one frequency which every possible mineral on the surface will not absorb. It is therefore proposed that the Raman spectroscopy experiment be repeated several times, with different exciting light frequencies. This could be accomplished with multiple small lasers which have different output frequencies, or with a single tunable laser that has good tuning characteristics. The tunable lasers presently available have the problem of a very narrow range of tuning capability, on the order of tens of nanometers, but advances in laser technology will likely extend this tuning range.

Lasers which are currently in use for Raman spectroscopy in the laboratory are rated in the 20 milliwatt to 500 milliwatt range. NASA is currently developing a laser in the ten to one-hundred watt output power range, which is in the range required for this application. Many types of laser sources are available. The particular type which would be best suited to this application is an area which requires further study, but current estimates indicate that a Krypton laser may be suitable.

Advantages found in interferometers or fourier analysis systems could even be used to allow use of multiple excitation frequencies. The use of a pulsed or continuous beam laser would depend on specific mission objectives. A pulsed laser would allow the best spectrum possible to be gathered while a continuous laser would give a more thorough coverage of the surface.

Contrary to a passive observing system, the footprint of the

system would depend on the width of the beam on the surface and the time of the laser pulse or the sample rate of the spectrometer. Current designs show a fixed nonsteerable laser and spectrometer.

A very sensitive detector must be used to observe the Raman effect. A cassegrain type optic system (157mm objective diameter minimum) will be used, coupled to an imaging array spectrometer, similar to sensor technology being developed for the HIRIS spacecraft.⁶ The optics will have a narrow field of view (1 to 2 degrees : .5 to 1 km footprint), and be aimed at the same spot which the laser is aimed at in order to maximize energy return. Detailed analysis of this system is given in Appendix 7.

7.5 Differences and Similarities to Infrared Spectroscopy

Some of the results which are expected from the Raman spectroscopy package are similar to results expected from infrared sensing. In particular, mineral species can be identified by both methods. Some differences in the results exist, however, which make the two methods complimentary.

7.5.1 Surface Resolution Different

The degree of surface resolution expected from each method is different. A surface "footprint" of about one meter wide and variable length depending on laser pulse rate is expected from the Raman system at an orbital height of 25 kilometers. The footprint is shown in Figure 7.8. Adjustable optics in the laser could facilitate changing the laser beam width. The laser source will be used for operation only on the dark side of the Moon, with different laser frequencies chosen so that no mineral species are missed because of absorption. This will make it impractical or impossible to completely cover the lunar surface with this method. This method would be highly suited for high resolution site specific coverage.

With the infrared spectrometer, a surface "footprint" of about 150 meters in diameter is expected at an orbital height of 30 kilometers. The infrared spectrometer will operate continuously on the sunlit side of the Moon, and complete surface coverage is expected to be possible in about 250 days. (See Appendix 7 for a detailed description of the method used to estimate surface resolution and mission time).

7.5.2 Bandwidths

The bandwidth of the individual bands in the Raman spectrum is narrower than bandwidth of the individual bands in a typical infrared spectrum. With a Raman spectrum the bandwidth is proportional to the square root of the temperature of the sample.

Because of this, it is possible to get a better resolution of individual mineral species. Also overtones and combination bands (second order spectra) are rarely seen in Raman spectra under normal conditions. This aids in making the spectra clearer and more simplistic to analyze.¹⁰

With the Raman spectroscopy package, since the light source, surface area detected, and detector will all be moving, the bandwidth of the spectrum received should not be affected appreciably by distortion from the Doppler effect. The infrared spectrometer, on the other hand, will have a stationary light source, (the sun), a stationary surface area detected, and the detector will be on the moving space craft. This could make the spectrum received subject to distortion due to the Doppler effect.

7.5.3 Spectra Different

The spectra produced by infrared and Raman spectroscopy is different. Since the spectrum of the surface of the Moon will be a composite spectrum of all the minerals which are found on it, it may be difficult to pick out the spectra of some individual minerals. With two independent spectra to study, identification of some minerals should be easier. Infrared spectral bands are generally numerous and broad while Raman spectral bands are generally fewer and narrower. It can not be overemphasized that Raman and Infrared spectroscopy are complimentary techniques. Benzene is shown in Figure 7.8 as an example.

The Raman spectrum can also be polarized by crystals. Using optical filters on the sensor, crystals formed or ejected during meteoric impact, and the orientation of these crystals, could be detected.¹⁰

7.5.4 Intensity of spectral lines different

Unlike infrared spectrum lines, the intensity of the Raman spectrum lines is directly proportional to the volumetric concentration of the mineral present in the sample. This is because the Raman spectrum is an emission spectrum, while the infrared spectrum is an absorption spectrum. For an absorption spectrum, the presence of any amount of a material is sufficient to absorb all the light frequencies characteristic of that material. Conversely, for an emission spectrum, the amount of energy a substance can emit is proportional to the amount which is present. Raman spectroscopy will therefore enable a better estimate of what amounts of minerals are found on the lunar surface.

7.6 Mission Scenario

The mission scenario has been planned so as to take advantage of the differences and similarities in the lunar surface study. The best way to do this is to first send up the infrared spectrometer to obtain a complete characterization of the lunar surface. From this preliminary map, specific areas of geologic interest on the surface can be identified for more detailed study. The Raman sensing package can then be used to obtain confirmation of the infrared results, with better surface resolution, and to obtain a better estimate of the amounts of minerals present. These complementary results will make possible a better, more accurate map of the lunar surface than would be possible with either method alone. The Raman spectroscopy package is baselined to operate from an elliptical orbit with a low periapsis of around 25 Km (for more information, see orbits section).

REFERENCES

1. **Spectroscopy Vol. 2**; ed. by B.P. Straughan and S. Walker, Chapman and Hall, 1976.
2. **Introduction to Infrared and Raman Spectroscopy**; (second edition) Colthrup, Daly, and Wiberly, Academic Press, 1975.
3. **Optical and Laser Remote Sensing**; ed. by D.K. Killinger, A. Moorgdian, (Springer series in Optical Sciences, #39), Springer-Verlag 1983.
4. **Tunable Solid State Lasers for Remote Sensing**; ed. by Byer, Gustafsen, and Trebino, (Springer series in Optical Sciences, #51) Springer-Verlag 1984.
5. **Scientific and Engineering Applications of Commercial Laser Devices**; Proceedings of the International Society for Optical Engineering, vol. 610, ed. by R. Feinberg, L. Holmes, M. Levitt, 1986.
6. **Earth Observing System Reports**, vol. IIC, HIRIS; NASA Publications, 1987.
7. **Laser Monitoring of the Atmosphere**; ed. by E.D. Hinckley, (Topics in Applied Physics, Series by Springer-Verlag) #14, 1978.
8. **Handbook of Space Technology: Status and Projections**; R. Michael Hord, CRC Press, 1984.
9. **Applications of Laser Raman Spectroscopy**; Stanley K. Freeman, Wiley-Interscience, 1974.
10. **Infrared and Raman Spectroscopy of Lunar and Terrestrial Mineral**; Clarence Karr, Jr., Academic Press, 1975.
11. **Introduction to the Theory of Molecular Vibrations and Vibrational Spectroscopy**; L. A. Woodward, Oxford University Press, 1972.
12. **Laser and Coherence Spectroscopy**; ed by Jeffery I. Steinfeld, Plenum Press, 1978.

8.0 Radar Surface and Subsurface Mapping

Most of the instrument modules on the LOP (Lunar Orbital Prospector) are used to identify minerals or elements. The LOP Radar module, on the other hand, is used to identify structures. Short wavelength radar produces excellent topographic maps of the Moon's surface. Long wavelength radar produces both surface maps and penetrates the regolith to produce subsurface maps.

On the Earth, subsurface maps are used to locate valuable mineral deposits which natural processes can concentrate in structures or certain rock layers. These structures may or may not be exposed at the Earth's surface. One method of finding these hidden structures and tracing rock layers is to drill rock cores at various locations. The rock core samples are then correlated with their locations to generate a subsurface map.

On the Moon however, subsurface maps can be generated by using a long wavelength radar system mounted on a platform orbiting the Moon. Buried structures have been located and the lateral extents of rock layers have been traced as they disappeared from the surface under the cover of other rock layers (Peeples et al., 1978). Mapping deep below the Moon's regolith is possible because, unlike the Earth, no liquid water or clay minerals are present around the lunar soil grains to attenuate the radar signal's power (Barringer, 1965).

Table 8.1 summarizes the subsurface depths detected on the Moon and the Earth. A 60 meter radar wavelength was used to detect a Moon layer 1.6 km deep. On the Earth, radar wavelengths of 23 cm were used to detect depths of only a few meters below desert areas and the Earth's ice caps can be penetrated more deeply than the desert areas.

In the future, the LOP radar subsurface mapper will map features such as the buried surfaces and Mascons (areas of gravity anomalies which are believed to be caused by portions of the Moon's mantle caught in its crust), buried craters, and buried lava flows. The lateral extent of beds partially exposed on the Moon's surface can also be traced. The mapper can also be used to detect if there is any depth to the Reiner Gamma Formation, an unusual albedo marking in Western Oceanus Procellarum which correlates to a strong magnetic anomaly. Some believe it was a comet which impacted the Moon (NASA, 1986).

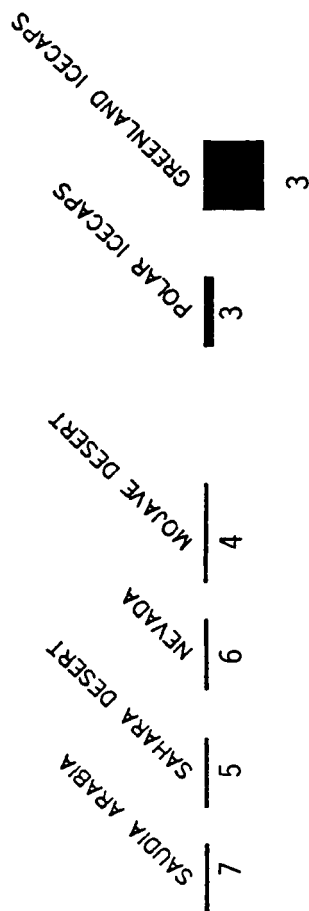
8.1 Mission Objectives

8.1.1 Surface Mapper

The data needed to map the Moon's surface is generated simultaneously with the subsurface map information. The primary objective of the surface mapper system is to complete the topographic map coverage of the entire Moon's surface which was

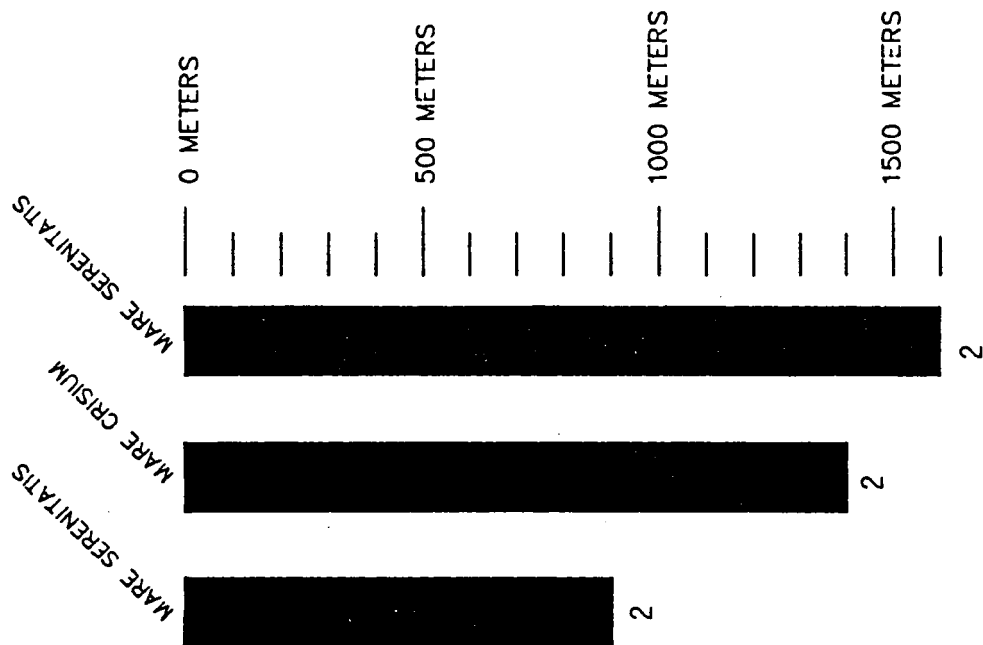
EARTH

(23 CENTIMETERS) (75 CENTIMETERS)



MOON

(60 METERS) — WAVELENGTH



DETECTION OF SUBSURFACE LAYERS ON THE MOON AND EARTH

1. Mantel and Miller, 1977
2. Peebles et al., 1978
3. Barringer, 1965
4. Blom et al., 1984
5. Schaber et al., 1986
6. Farr et al., 1986
7. Berlin et al., 1986

begun in the 1960's and 1970's. At this time, Earth based radio telescopes at the Arecibo and Haystack Observatories made high resolution lunar radar maps of the entire Earth-side lunar hemisphere with resolutions of 1 km to 10 km. The radar wavelengths available for these Earth-based observations ranged from 3.8 cm to 7.5 m. This wavelength window was imposed on these observations because 3.8 cm radar is absorbed by the water in the Earth's atmosphere and 7.5 m radar is limited by the Earth's ionosphere (Thompson, 1979). Since the Moon has no real atmosphere (refer to the Environment section of this report) there are no restrictions on the radar wavelengths the LOP radar mapper system can use.

8.1.2 Subsurface Mapper

The subsurface mapper's primary objective is to continue mapping the Moon's subsurface for the features previously mentioned. Subsurface maps have been made of only two areas on the Moon and these were made during the last manned flight to the Moon. In 1972, Apollo 17 subsurface mapped in Mare Serenitatis and in Mare Crisium using a radar wavelength of 60 meters (Peeples et al., 1978). Figure 8.1 is a photomosaic of the southern portion of the surface of the Moon's Mare Serenitatis and its radar subsurface cross section taken from point A to A'. The surface radar returns in this area exhibit constructive and destructive interference. Perhaps this interference phenomena is also responsible for the two subsurface layers appearing as discontinuous dots instead of as continuous lines (Sharpton and Head III, 1982). Radar soundings of other lunar regions are shown in Figures 8.2 and 8.3.

8.2 General System Operation

Radio frequencies between 3 MHz and 300 MHz, which correspond to wavelengths between 100m to 1 m respectively, are transmitted from the LOP to the Moon where they are reflected, refracted or absorbed by the Moon's surface and subsurface as shown in Figure 8.4.

A major problem with subsurface mapping is that whatever radar wavelength is used, the stronger surface returns may mask the weaker subsurface returns. Several methods have been used to distinguish subsurface features from surface features. One method is to compare maps produced by different wavelengths. If a feature on a subsurface map does not appear on a surface map of the same area made by a wavelength too short to penetrate the surface, the feature is not a surface feature and is probably a subsurface feature. Another method, used by Peeples et al. (1978), is to correlate images obtained during multiple orbits. Figure 8.5 illustrates how a subsurface layer extending over at least two orbits can be separated from surface reflections. The radar return from this subsurface will have the same time delay

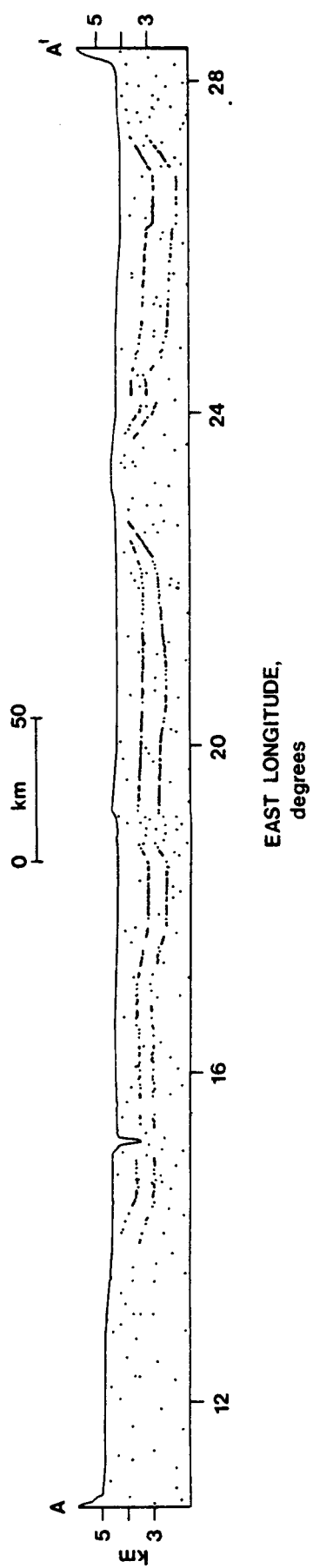
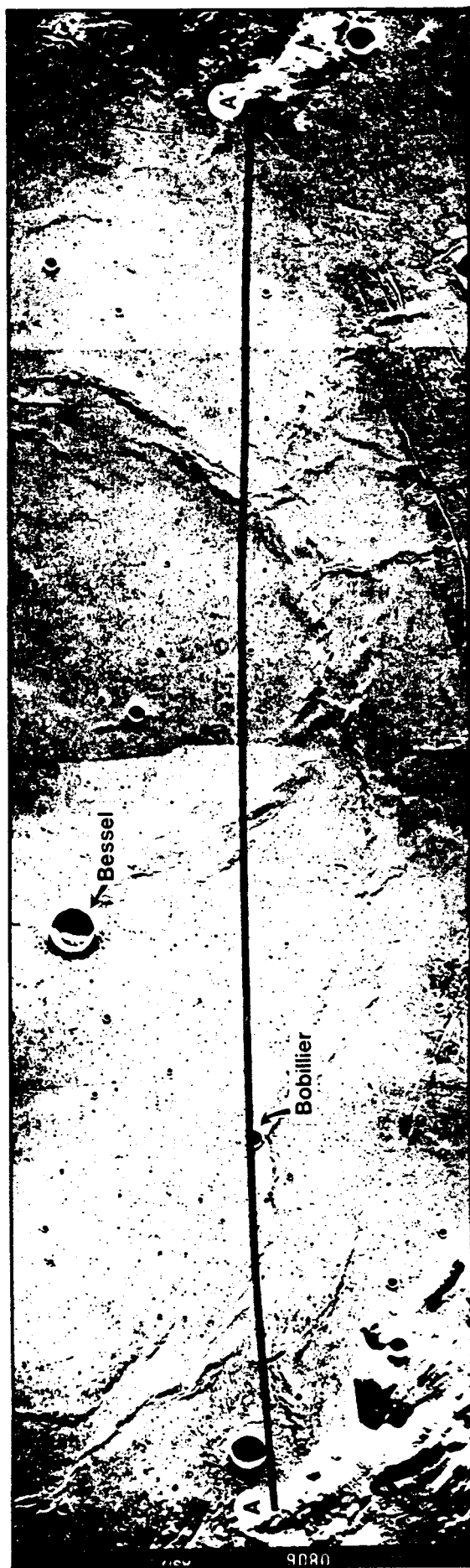


Figure 8.1 Apollo 17 photomosaic and radar cross section from points A to A' of the portion of Mare Serenitatis (Sharpton and Head III, 1982)

ORIGINAL PAGE IS
OF POOR QUALITY



APOLLO 17 LUNAR SOUNDER (ALSE) RADAR IMAGERY

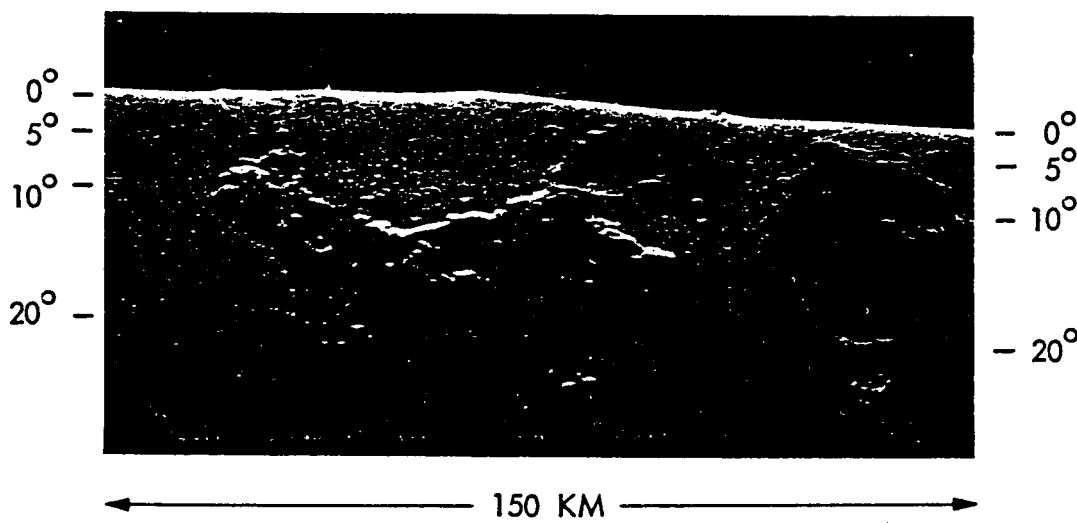
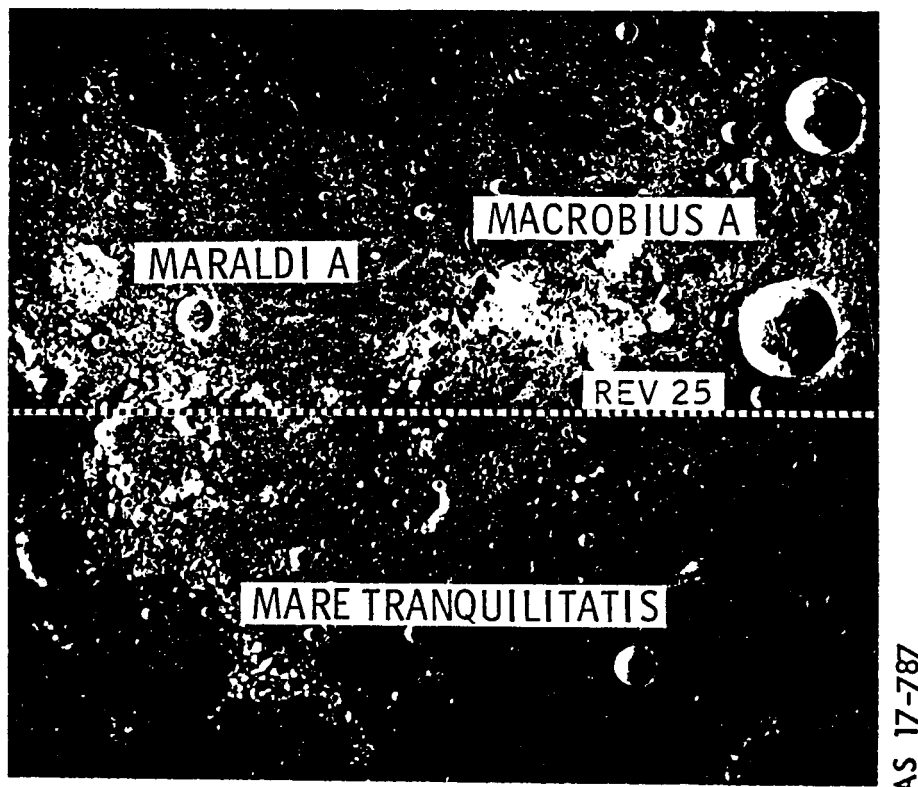


Figure 8.2 Radar sounding of Mare Tranquilitas lunar region. Subsurface reflections can be seen in the bottom photo where these bright portions are buried subsurface layers.

ORIGINAL PAGE IS
OF POOR QUALITY



APOLLO 17 LUNAR SOUNDER (ALSE) RADAR IMAGERY

LUNAR HIGHLANDS

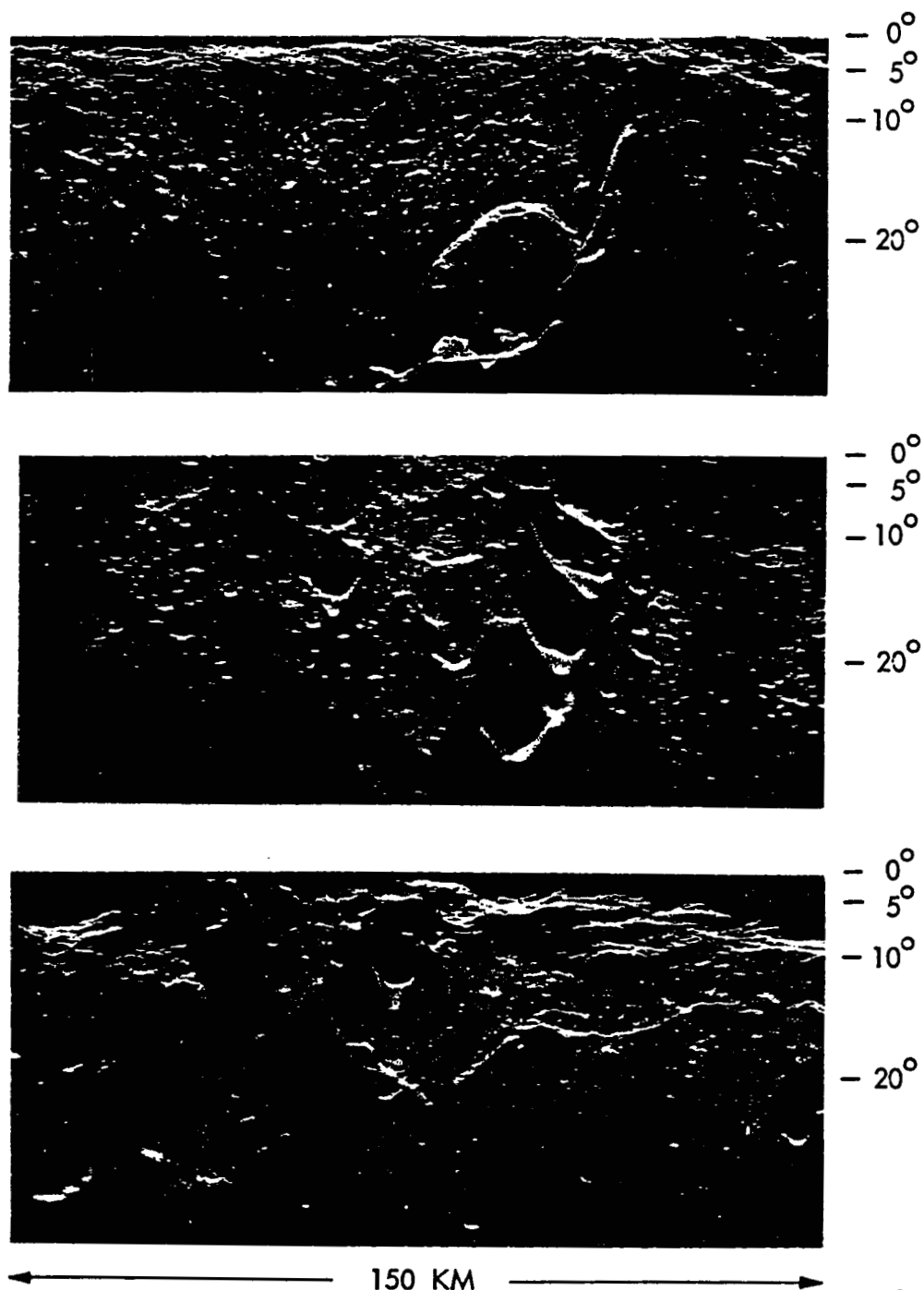


Figure 8.3 Radar sounding images of cross sections of Lunar Highlands. Cross sections show bright reflections which indicate subsurface layers.

RADAR REFLECTION, REFLECTION, AND ABSORPTION

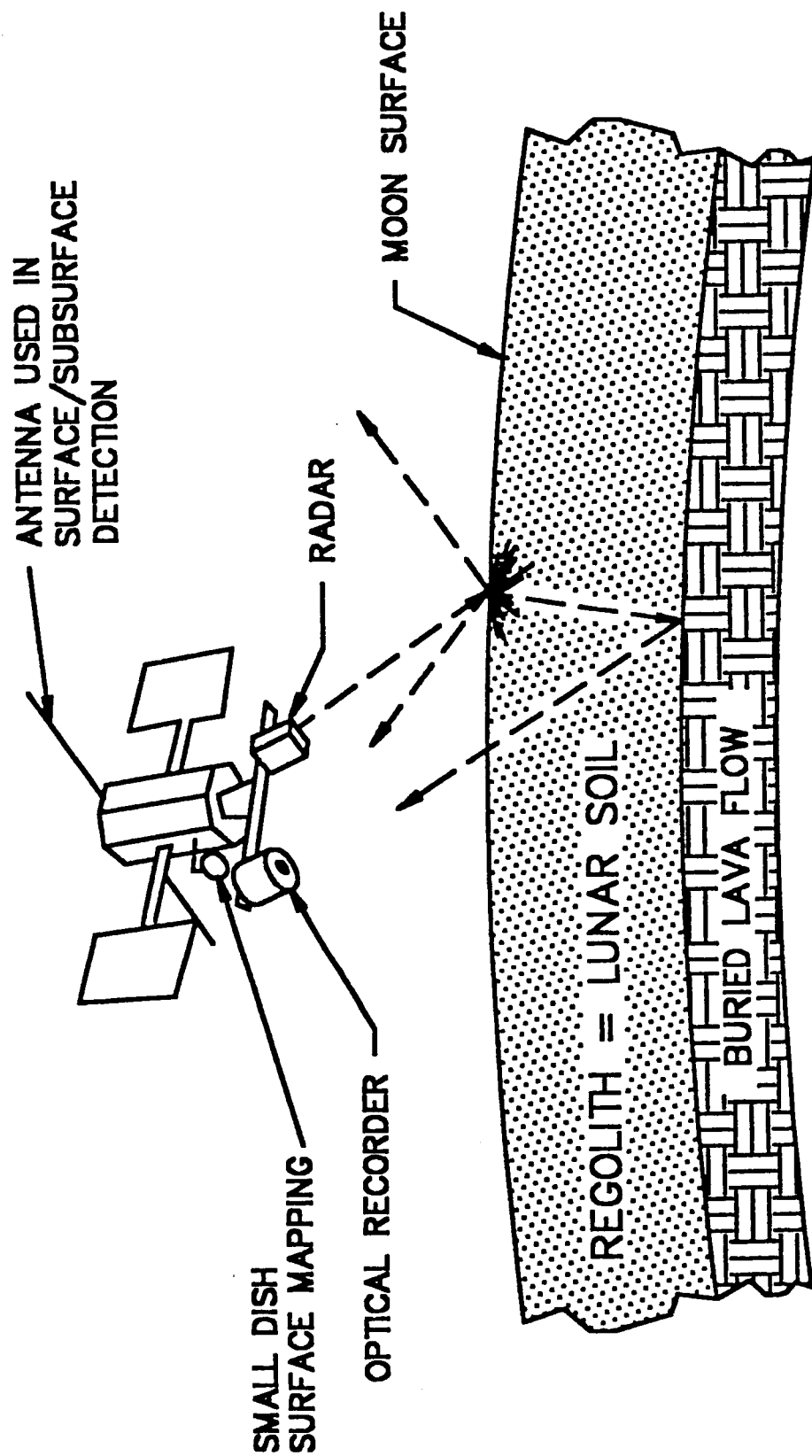


Figure 8.4 Diagram of radar subsurface mapping operation. The radar signal is absorbed and reflected at the surface while some of the signal penetrates the surface to reflect from subsurface layers. The small dish antenna is used with short wavelengths to obtain surface maps and to subtract the surface reflection from the subsurface signal.

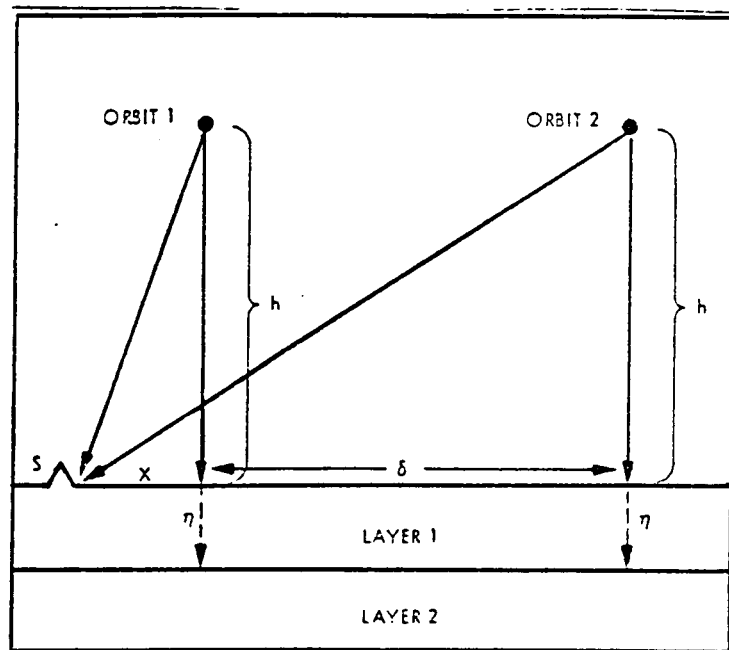


Figure 8.5 The geometry of the multiple orbit correlation technique. The spacecraft is denoted for two orbits (Orbits perpendicular to the plane of the figure) at height H and orbital separation δ . A sub-surface reflecting layer is at depth η , and a surface reflector S is at an offtrack distance X from the nadir point of orbit 1 (Peeples et. al. , 1978).

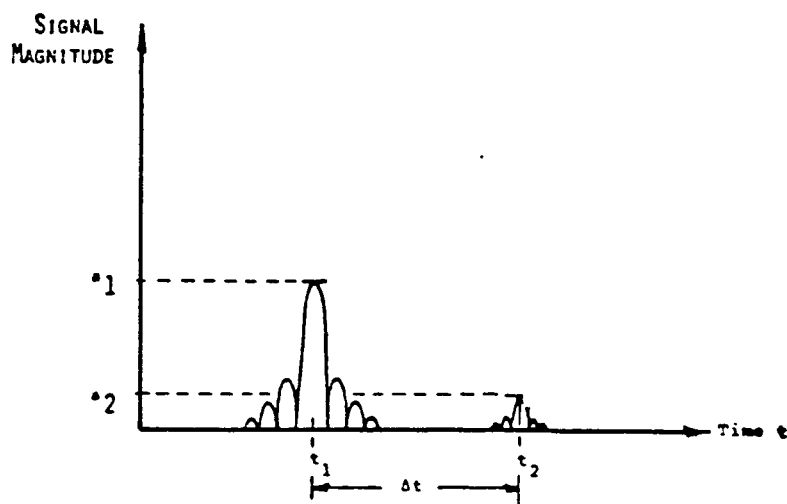


Figure 8.6 Amplitude response of surface (T_1) and subsurface (T_2) features. Long time delays (δt) between the signals produces good signal resolution. Figure adapted from Porcello et. al. 1974.

in orbit 1 and orbit 2. However, the individual surface feature reflector S will not be recorded at the same relative time delay on orbit 1 and orbit 2 because of the translation of the orbit.

The strength of the subsurface return is controlled by several factors. Table 8.2, an adaptation of the basic radar formula, computes the total power reflected from a smooth subsurface. The surface roughness and material dielectric constant information are contained in the reflection coefficient terms. Several of the other terms can be controlled by the LOP radar design to increase the subsurface signal intensity. Of course, a strong transmitter and high gain antenna increase the return signal intensity.

There is a tradeoff between the length of radar wavelength transmitted and the depth of Moon penetrated. The longer the wavelength, the more power is returned. However, longer wavelengths penetrate further and the depth of penetration is inversely proportional to the return intensity. Since the altitude of the system above the Moon's surface is also inversely proportional to the return intensity, the LOP's orbital geometry can enhance the subsurface signal returns. In 1972, the Apollo 17 Lunar Sounder orbited 110 km above the Moon and transmitted a 60 meter wavelength. The LOP will be orbiting at a lower altitude of 50 km and the radar returns will be stronger, and perhaps even deeper subsurface layers will be detected when the 60 meter wavelength is transmitted.

Another primary variable is the length of the time delay between the surface and subsurface returns. The smaller the time delay, the more intense the subsurface return. However, the closer together the signals, the more apt they are to interfere with each other. In Figure 8.6, the surface return (1) is much larger in intensity than the subsurface return (2), but the side lobes of the surface return are near the amplitude of the subsurface return. If the time separating the reception of these returns is too short, then the smaller subsurface return may be covered by the surface return sidelobes. Several methods of controlling the time delay are discussed under Fixed Parameters and Experimental Parameters.

The major problem with subsurface mapping is that the stronger surface returns may mask the weaker subsurface returns. To further address this problem, the LOP Radar Subsurface Mapper System has been baselined as an experimental system. Several parameters affecting the intensity of the subsurface returns will be varied, one at a time, until the brightest subsurface return for each parameter is received. Refer to Experimental Parameter section.

8.3 The Instrument

8.3.1 Introduction

The LOP Radar Mapper uses some of the features from the past Radar Mappers. From the Apollo 17 Lunar Sounder, the LOP borrows ideas on the hardware, such as coherent synthetic aperture radar, high gain dipole antenna, and optical recording. A small dish antenna is added for 1 cm wavelength surface mapping, discussed in the Instrument Hardware Components section. In the Fixed Parameter section, the LOP borrows ideas from the Lunar Sounder on the use of a large dynamic range and precise side lobe control. Although both mappers have circular orbits, the LOP will be in a lower orbit, 50 km instead of 110 km. The Lunar Sounder subsurface data was used only for sounding, which is the detection and location of subsurface discontinuities. The LOP subsurface data is also used for lunar subsurface profiles and subsurface images. The Lunar Sounder used 3 wavelengths and the LOP Mapper will enlarge this choice by scanning over 7.

Sabins (1987) discusses the characteristics of the Seasat satellite, Shuttle Imaging Radar-A (SIR-A) and SIR-B. All of these radar systems produced surface maps along with subsurface maps in dry areas on the Earth. Their technique of a variable depression angle was borrowed and slightly enlarged for the LOP. SIR-B used a depression angle ranging from 30 to 75 degrees and the LOP depression angle ranges from 30 to 80 degrees.

Several techniques were borrowed from airborne radar systems. In the Fixed Parameter section, the LOP uses two look directions. This concept has been proposed for the future SIR-C in the form of a squint mode discussed later. The technique of variable polarization is borrowed from airborne radar and has been proposed to be used in the future SIR-C. The LOP adds circular polarization to the proposed types of polarization.

The LOP adds different forms of FM modulation in the Experimental Parameters. This idea was not used in the Lunar Sounder, Seasat, SIR-A, SIR-B or proposed for the SIR-C. The LOP will determine if the intensity of subsurface returns is influenced by signal modulation.

8.3.2 Instrument Hardware Components

Figure 8.7 illustrates the major hardware components. They include:

1. Coherent Synthetic Aperture Radar (CSAR) (transmitter and receiver)
2. Small Dish Antenna (Surface Mapping only)
3. High gain Matched Wide Bandwidth Dipole Antenna (surface and subsurface mapping)
4. Optical Recording and Holograms--The Communications

- system will provide a digital recording system.
5. Space radiators for thermal control

This system is estimated to have a mass of 50 kg and uses 200 watts. The small dish antenna will produce excellent surface topographic maps from 1 cm radar. Since this wavelength is too short to appreciably penetrate the surface, it can also be used to extract subsurface information from the total return information. Since the total return of the longer wavelengths contains both the surface and subsurface returns, the surface only return obtained from the small dish will be subtracted from the total, leaving only the hidden subsurface return information (McCoy, 1988).

The Optical Recording system employs holographic techniques to record and later view the output of the optical processor. Holograph images are useful for two reasons. First, they can store more of the processed data produced by the Coherent Synthetic Aperture Radar than photographic films. They can preserve the CSAR phase information which allows the user to adjust the image focus and view or filter the spectrum as the image is viewed (Porcello, 1974).

8.3.3 Fixed Parameters

These parameters are held constant while the experimental parameters are varied. However, at a future date, some of these fixed parameters may also be changed. The fixed parameters are:

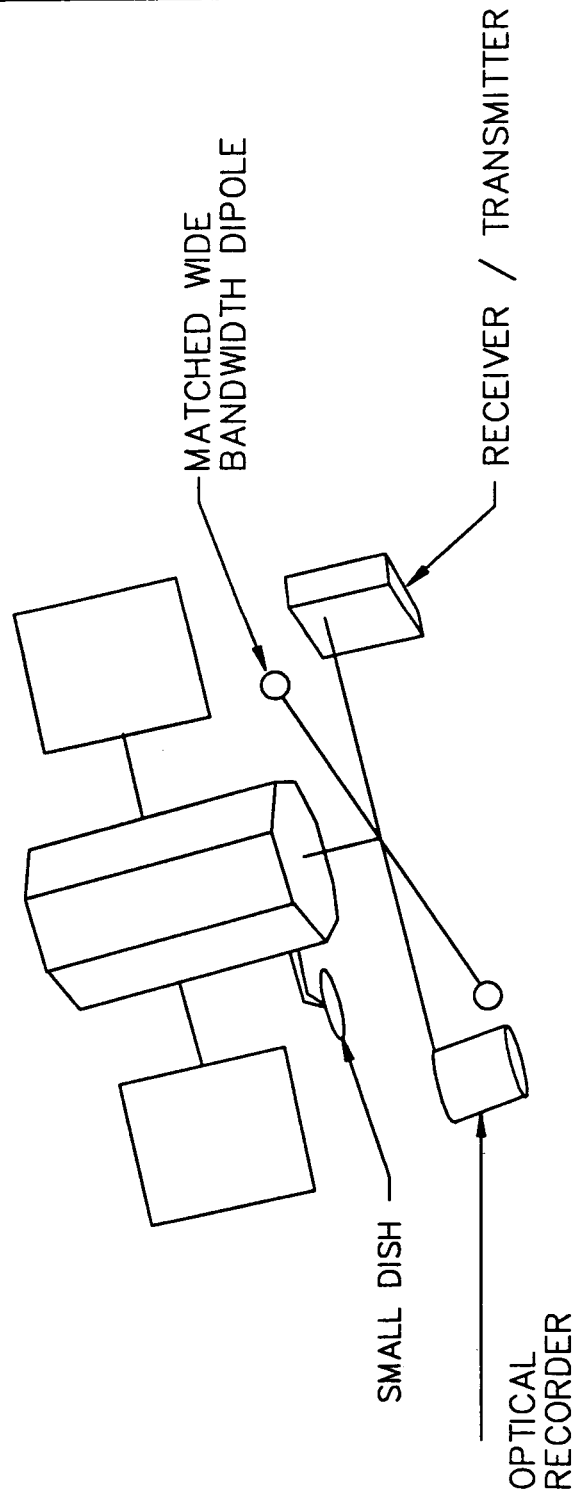
1. Altitude 50 km
2. Circular Near Polar Orbit
3. Large Dynamic Range (dB)
4. Precise Side Lobe Control
5. Two Look Directions
6. Processing Data (Profile, Image and Sounding)

In order for the computer to generate a synthetic aperture from the Coherent Synthetic Aperture Radar system, large amounts of processed data are used. Therefore, a large dynamic range in the processed data is required as was used by the Lunar Sounder, around 40-50 dB (Porcello, 1974).

Precise side lobe control is important so that the weaker subsurface signal is not lost in the main signal side lobes. Refer to Figure 8.6. Side lobe control is accomplished by combining the shape of the radiated waveform in the transmitter with the spectral weighting in the signal processor (Phillips et al., 1973).

Several concepts used in surface radar mapping are applied to mapping the subsurface. The technique of looking at an area from two perpendicular directions will help to detect faults and other linear features in the subsurface. However this squint

S.A.R. INSTRUMENT



MASS = 50Kg POWER = 200 WATTS

Figure 8.7 Radar subsurface mapping instrument system.

mode, where the platform alternately switches the beam behind and in front of the usual sideways look direction, creates computational problems. The computer must account for the movement of the signal from a particular target across various range cells. These problems are discussed by Moore, 1976, and Ulaby et al, 1982.

Other surface radar mapping techniques applied to the subsurface mapping involve the processing of the data. The Lunar Sounder Radar used sounding for subsurface data and imaging and profiling for surface data (Phillips, 1973). Computer processing should be able to make images and profiles of the surface of at least the first subsurface layer encountered below the regolith.

8.3.4 Experimental Parameters

To reduce the amount of data the computer must process simultaneously, each of the following 4 tests will be conducted one at a time. After one test has been adjusted to produce the maximum subsurface return, the next test will begin. The tests are:

1. Multi-Wavelength (1 meter to 100 meters)
2. Variable Modulation (FM, OOK, FSK, PSK)
3. Variable Polarization (HH, VV, HV, VH, Circular)
4. Variable Depression Angle (30-80 degrees)

The first experiment is to produce a map of the Moon to indicate which radar wavelengths are best suited for locating lunar subsurfaces at each region of interest. This test is necessary because the actual subsurface layer depths vary along with the ability of different wavelengths to penetrate to different depths. Each wavelength has its own subsurface detection window. The upper window boundary for each wavelength is defined as where the computer recognition of subsurface detail is not permitted because of bandwidth limitations (Sharpton, 1982). The lower window boundary for each wavelength is defined as where the signal has attenuated to skin depth (Schaber et al., 1986). As the LOP Radar system orbits the Moon, the radar wavelengths will be varied in seven sequential steps from 1 m to 100 m (1m, 10m, 20m, 40m, 60m, 80m, 100m). When subsurface reflections are detected, the wavelength used and location of the subsurface on the Moon is recorded. If later computer data enhancement uncovers other subsurface layers between the recorded step wavelengths, the appropriate wavelength can be interpolated. Once these wavelengths are known, testing can begin for the modulation type which produces the brightest subsurface return.

FM modulation rather than AM modulation is used so that the signal is always at its highest intensity. Three other forms of FM communication modulations will be tested.

In addition to the variations of HV polarization planned to

$$P_r = P_t \left(\frac{G \lambda}{8\pi(H+x)} \right)^2 (1 - |R_{01}|^2)^2 |R_{12}|^2 (0.10)^{-2.74} \Upsilon f \tan \delta$$

P_r = power from subsurface

P_t = Peak effective transmitter power

G = Antenna gain

λ = Radar wavelength

H = Altitude

x = Depth of the subsurface interface

R_{01} = reflection coefficient at the lunar surface / freespace boundary

R_{12} = reflection coefficient at the subsurface layer interface

Υ = time delay between the arrival of both returns

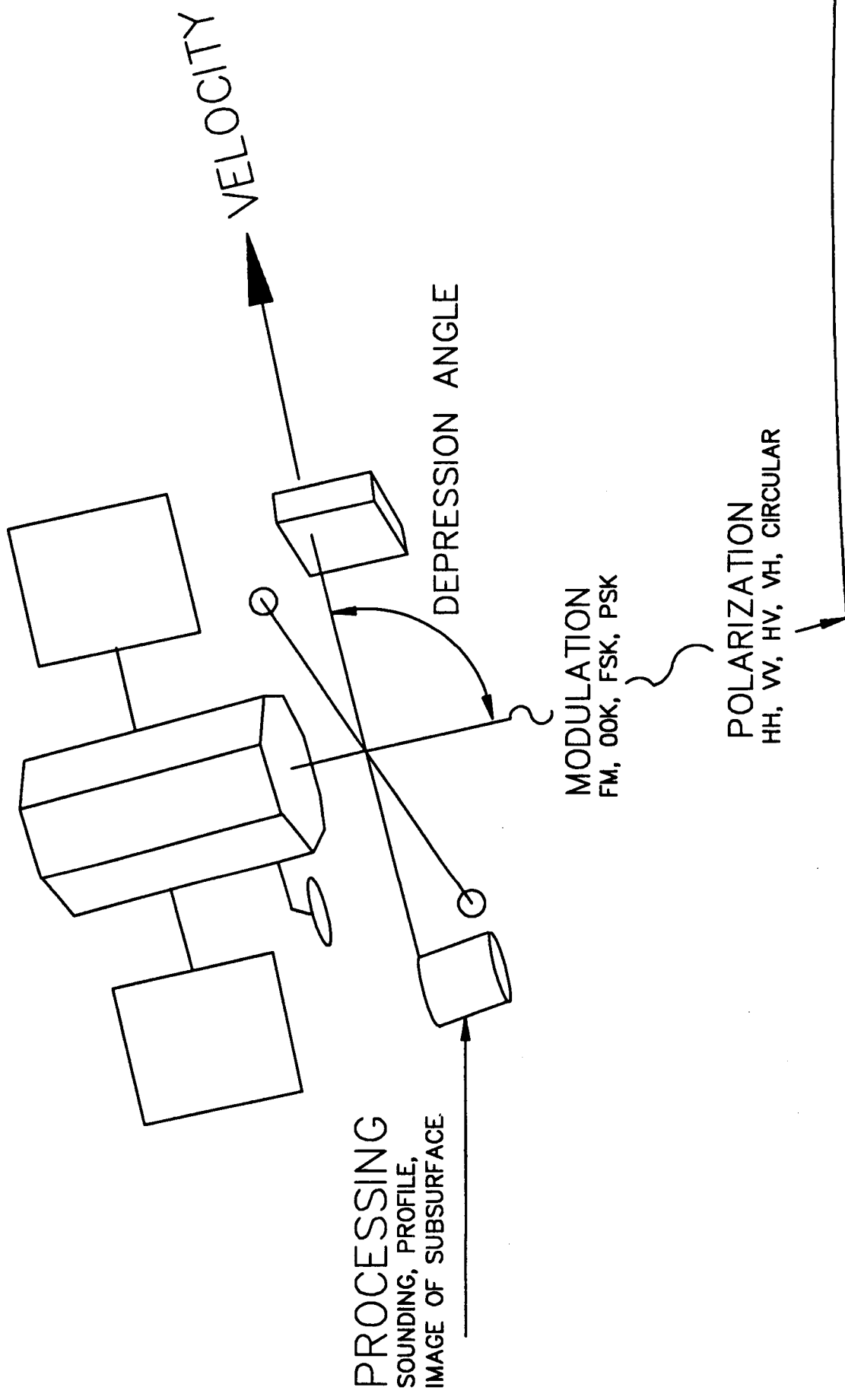
$\tan \delta$ = lunar material loss tangent

f = radiated frequency

Porcello et. al. 1974

Table 8.2 Radar power return formula.

VARIABLE PARAMETERS



be used on SIR-C, the LOP adds circular polarization. Computers should be able to handle the increase in information produced by circular polarization.

The depression angle can be manipulated to change the time between the arrival of the surface return and the subsurface return. The equation in Table 8.2 shows that if the delay time is short, then the subsurface signal intensity is stronger. There is a tradeoff with the size of the depression angle, for while large values of the angle of depression increase the intensity of the subsurface signal, smaller depression angles may be necessary to keep this subsurface signal visible in the surface signal sidebands, as seen in Figure 8.6.

8.4 Conclusion

The LOP Radar Mapper System is an experimental instrument. It is designed to adjust several parameters one at a time until the best radar subsurface return is received. In future experiments, several parameters may be varied simultaneously to further fine tune their adjustment to produce the brightest subsurface return.

The geologic history of the Moon will be better understood when subsurface maps define the relationships between the isolated rock units on the Moon's surface. Perhaps some lunar subsurface structures will be found to be associated with concentrations of valuable minerals. This is a new area of scientific exploration since the water processes of weathering and hydrothermal alteration, responsible for so many of the valuable mineral concentrations on the Earth, are absent on the Moon.

REFERENCE

Barringer, A. R., 1965, "Radio Frequency Reflectivity Experiments Proposed for AES Lunar Orbital Flights", Francis Narin, edit., *Post Apollo Space Exploration*, Vol 20, Part 1, *Advances in the Astronautical Sciences*: American Astronautical Society Publication Chicago, Ill, pp. 417-434.

Berlin, Graydon L., Mohammed A. Tarabzouni, Abdullah H. Al-Naser, Kamel M. Sheikho, and Richard W. Larson, July 1986, "SIR-B Subsurface Imaging of a Sand-Buried Landscape: Al Labbah Plateau, Saudi Arabia", *IEEE Transactions on Geoscience and Remote Sensing*, Vol. Ge-24, No. 4, pp. 595-601.

Blom, Ronald G., Robert E. Crippen, and Charles Elachi, 1984, "Detection of Subsurface Features in SEASAT Radar Images of Meads Valley, Mojave Desert, California": *Geology*, Vol. 12, pp. 346-349.

Farr, Tom G., Charles Elachi, Philip Hartl, K. Chowdhury, 1986, "Microwave Penetration and Attenuation in Desert Soil: A Field Experiment with the Shuttle Imaging Radar", *IEEE Transactions on Geoscience and Remote Sensing*, Vol. GE-24, No. 4, pp. 590-594.

McCoy, Roger, 1988, Private communications.

Mantel, Ellen J. and Elizabeth R. Miller, editors, July 1977, *Catalog of Lunar Mission Data: National Space Science Data Center/World Data Center for Rockets and Satellites 77-02* pp. 93-102.

Moore, Richard K., 1976, "Active Microwave Systems" in Joseph Lintz Jr., and David S. Simonett, editors, *Remote Sensing of Environment*, Massachusetts, Addison Wesley Publishing Co., ch. 7, p. 234-290.

NASA, 1986, "Status and Future of Lunar GeoScience": NASA SP-484.

Peeples, Wayne J., William R. Sill, Thomas W. May, Stanley H. Ward, Roger J. Phillips, Rolando L. Jordan, Elsa A. Abbott, and Terry J. Killpack, 1978, "Orbital Radar Evidence for Lunar Subsurface Layering in Maria Serenitatis and Crisium": *Journal of Geophysical Research*, Vol. 83, No. B7, pp. 3459-3468.

Phillips, R. J., G. F. Adams, W. E. Brown Jr., R. E. Eggleton, P. Jackson, R. Jordan, W. J. Peeples, I. J. Porcello, J. Ryu, G. Schaber, W. R. Sill, T. W. Thompson, S. H. Ward, and J. S. Zelenka, 1973, "The Apollo 17 Lunar Sounder": *Proceedings of the Fourth Lunar Science Conference*, (Supplement 4, *Geochimica et Cosmochimica Acta*), Vol. 3 pp. 2821-2831.

Porcello, Leonard J., Rolando L. Jordan, Jerry S. Zelenka, Gary F. Adams, Roger J. Philips, Walter E. Brown Jr., Stanley H.

Ward, and Philip H. Jackson, 1974, "The Apollo Lunar Sounder Radar System": Proceedings of the IEEE, Vol. 62, No. 6, pp. 769-783.

Sabins, Jr., Floyd F., 1987, Remote Sensing Principles and Interpretation, second edition, ch 5 & 6 : W. H. Freeman and Company, New York, pp. 181 and 194.

Schaber, Gerald G., John F. McCauley, Carol S. Breed, and Gary R. Olhoeft, 1986, "Shuttle Imaging Radar: Physical Controls on Signal Penetration and Subsurface Scattering in the Eastern Sahara": IEEE Transactions on Geoscience and Remote Sensing, Vol. GE-24, No. 4, pp. 603-623.

Sharpton, Virgil L., and James W. Head III, 1982, "Stratigraphy and Structural Evolution of Southern Mare Serenitatis: A Reinterpretation Based on Apollo Lunar Sounder Experiment Data": Journal of Geophysical Research, Vol. 87, No. B13, pp. 10,983-10998.

Thompson, T. W., 1979, "A Review of Earth-Based Mapping of the Moon": in The Moon and the Planets, Vol. 20, D. Reidel Publishing Co., Boston, pp. 179-198.

Ulaby, Fawwaz T., Richard K. Moore, and Adrian K. Fung, 1982, "Radar Remote Sensing and Surface Scattering and Emission Theory", in Microwave Remote Sensing Active and Passive, Vol. II: Massachusetts, Addison-Wesley Publishing Company, 1064 P.

9.0 Orbital Analysis

Two baseline altitudes for the LOP are needed for the different mission scenarios. The RAMAN Spectroscopy system, an active laser sensing package, and other high resolution instrument packages require low orbits. For these instrument packages, a near polar elliptical orbit of 25 Km at its nearest approach to the Moon and 2000 Km at its most distant point is utilized. This allows for high resolution remote sensing at the 25 Km periapsis. For the other missions, a near polar circular orbit of 50 Km will be utilized.

9.1 Constraints

Instrument resolution dictates the need for low lunar orbits, but many problems arise from these orbits. The Moon's topography and gravity field, coupled with the platforms fuel consumption and the need for complete surface coverage, are the primary constraints addressed in this orbital analysis.

9.1.1 Topography and Center of Mass

The topography of the Moon varies greatly. The near side of the Moon is relatively flat while the far side is very choppy due to a large quantity of meteorite impacts. Additionally, the center of figure of the Moon is shifted 2.5 Km from its center of mass making the lunar farside at higher elevations. The feature of the center of mass of the Moon offset from the physical center, results in a circular orbit about the center of mass appearing elliptical with respect to the lunar surface. The highest point on the Moon, measured from the Moon's 1731 Km reference radius (Moon's sea level), is a peak on the lunar farside. The peak is located near the Sierpienski Crater and has an altitude of 16 Km.

Due to the unique lunar environment, no significant atmosphere, the minimum orbit altitude is 20 Km with a safety factor due to the topography limitation and the offset center of mass. The actual minimum orbit used for computations is set at 25 Km.

9.2 Gravity Field

A significant feature of the lunar surface is the presence of large gravity anomalies. These gravity anomalies are the result of large concentrations of dense mass and uplifts in the mantle (see Figure 9.1). These dense mass concentrations and mantle uplifts are scattered across the lunar surface with no apparent pattern.

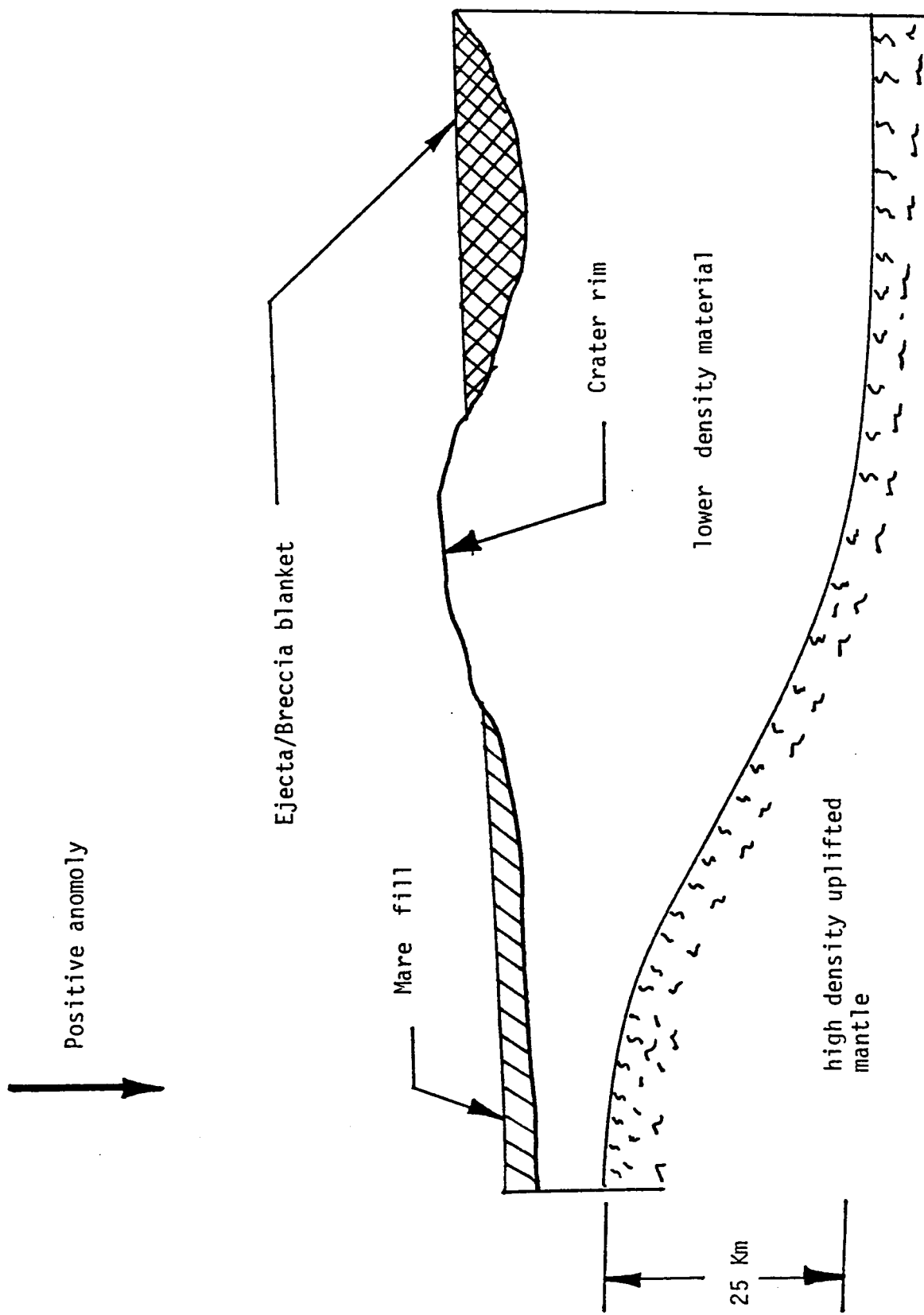


Figure 9.1 Grimaldi crater positive gravity anomaly. Uplifted mantle of higher density creates the higher gravitational attraction.

The randomly placed gravity anomalies distort the orbit of a lunar satellite. The University of Texas at Austin performed a study based on data collected from the Apollo 8, 12, 15, and 16 Missions and the Lunar Orbiter Missions 1-5. For the U. of Texas study a circular polar orbit of 111 Km altitude was analyzed over a period of one year. The orbit was substantially distorted after a period of nine months (see Figure 9.2).

The apoapsis, the most distant point in the orbit from the Moon's surface, began at 111 Km and increased to 220 Km. The periapsis, the nearest point in the orbit from the Moon's surface, began at 111 Km and deteriorated to 7 Km. The satellite crashed into the lunar surface after approximately nine months. One could safely classify this behavior as unstable.

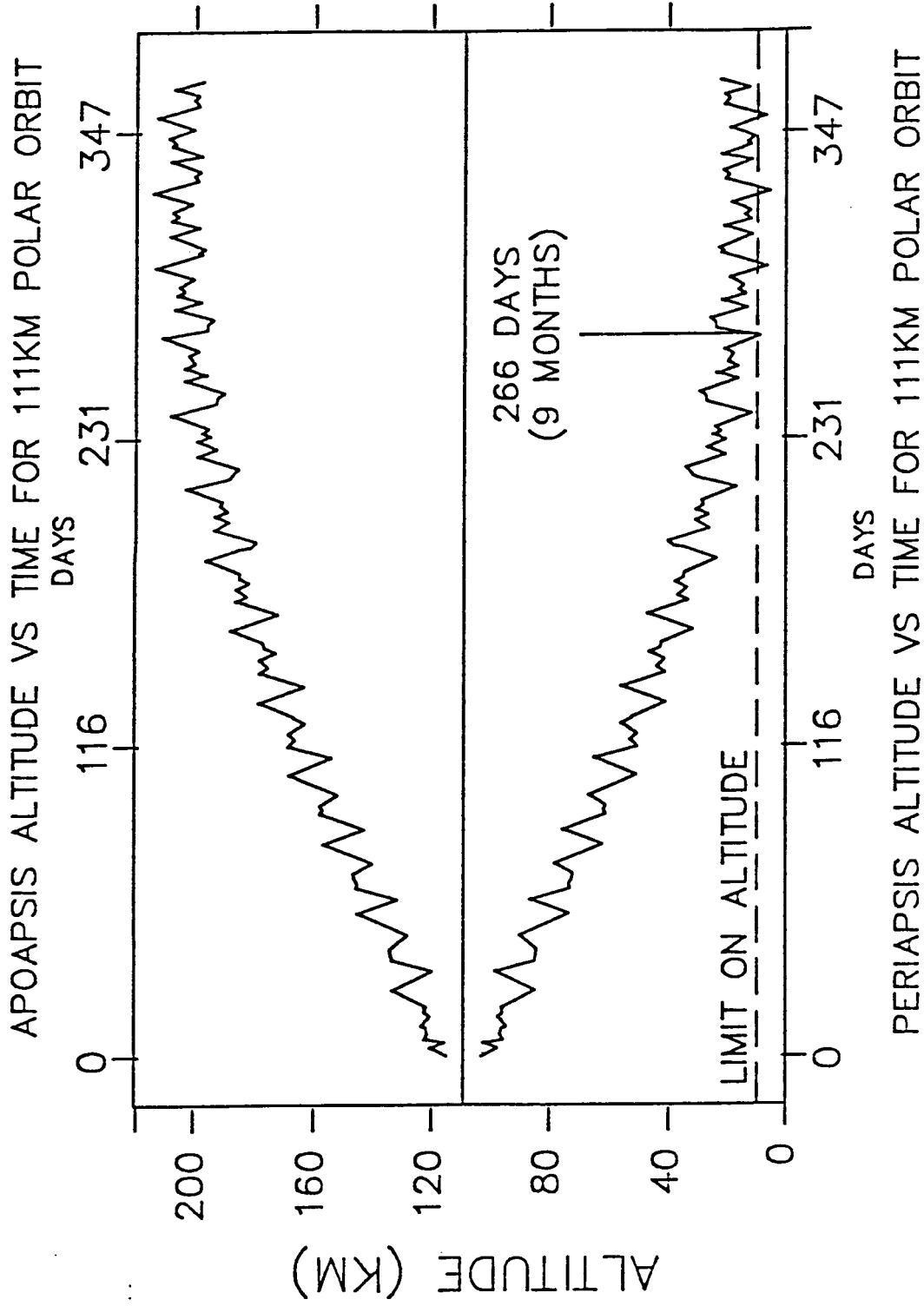
The gravity anomalies create a major problem for orbit stability. A method around this instability problem is to place the LOP in a elliptical or highly eccentric orbit (eccentricity: $e=1-\text{width/length}$, circle=0, line=1). Here the velocity of the satellite at the periapsis is great while the velocity at the apoapsis is much slower. This places the satellite near the apoapsis for most of the orbital period and this does not allow the gravity anomalies to have a great effect upon the orbit. In a circular orbit, the orbital velocity is constant and thus allows the gravity anomalies a greater time per period to distort the orbit.

The orbits of the LOP will be elliptical to avoid excessive orbital distortion. The attitude control system will correct any minor distortions in the orbit due to the gravity anomalies. Additionally, the elliptical orbit allows for greater "hang time" over a point at the apoapsis and also allows for low altitude coverage at the periapsis.

9.3 Orbital Strategies

The platform's ability to change orbital parameters is important to achieving the desired mission versatility. To optimize the relationship between surface coverage and mission requirements, a variety of orbits is required. These orbits may vary in altitude, eccentricity, and inclination. Each instrument package will require an orbit tailored to its specific need and the platform must be capable of a wide variety of orbits. Several classes of orbital coverage are considered: optimal global surface coverage at moderate to low resolution, regional coverage at moderate to high resolution, and very high resolution site specific coverage. Orbital parameters dictate the type of surface coverage obtained, and by varying orbital inclination, eccentricity, and periapsis, various remote sensing mission objectives can be realized.

Orbit inclination strongly influences the quality of regional surface coverage. Figure 9.9 illustrates the effect of



UNIVERSITY OF TEXAS AT AUSTIN

Figure 9.2 Effect of lunar gravitational perturbations on a 111 Km polar orbit. Note the rapid increase in eccentricity resulting in perapsis lowering and apoapsis raising. The stability criteria, crashing into the Moon, is effected after 9months of unassisted orbiting.

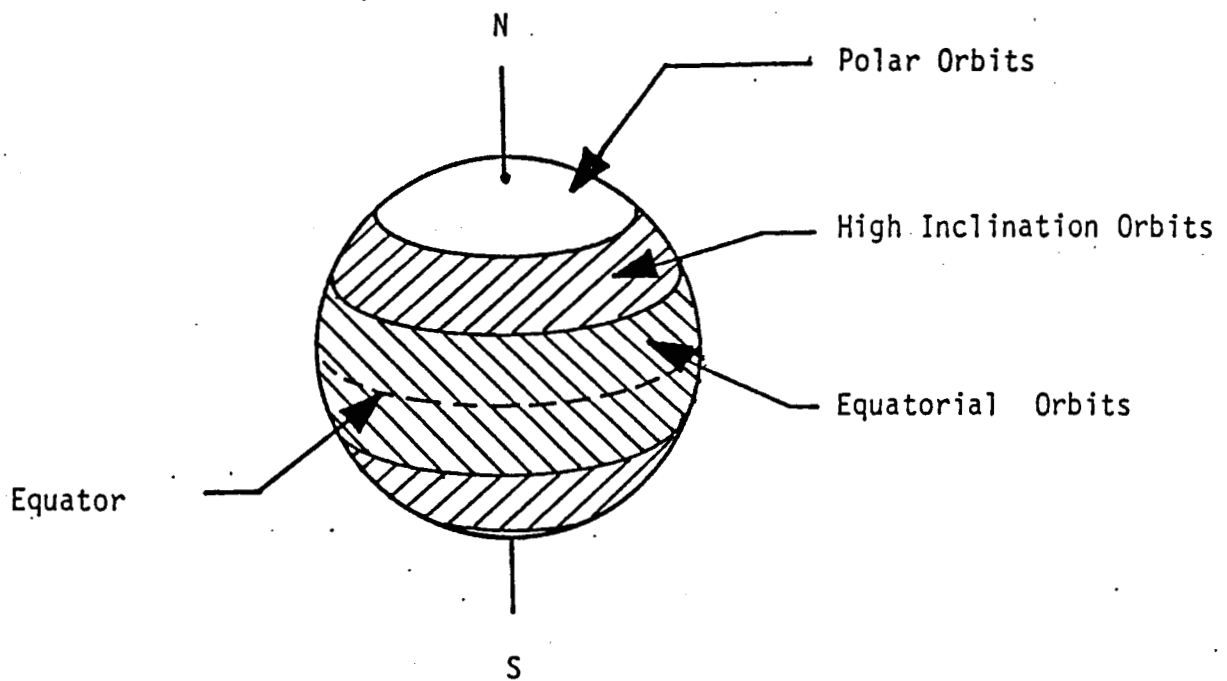


Figure 9.9 Orbit inclination vs. regional coverage. Optimal surface coverage is obtained at the latitude corresponding to the orbit inclination angle.

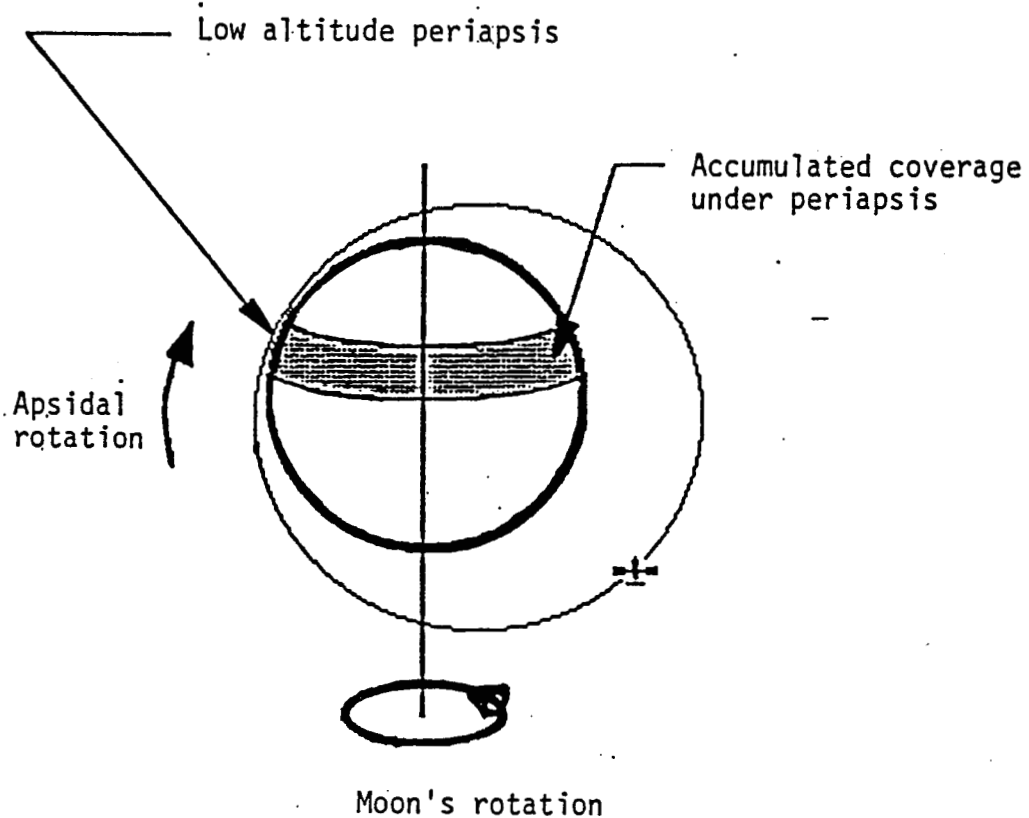


Figure 9.10 A method for obtaining global high resolution coverage of the Moon by rotating a low altitude periapsis at appropriate intervals.

various orbit inclinations on local coverage. In general, viewing is most complete at the lunar latitudes corresponding to the orbit inclination angle. Viewing of the entire lunar surface is offered only by polar orbits but this advantage is offset by sparse coverage at low latitude regions where successive orbit tracks are far apart. Reducing orbit inclination from 90 degrees improves the coverage at low latitudes and equatorial regions but this completely eliminates polar coverage. Low inclination orbits are consequently best suited to high resolution, site specific coverage at low latitude regions and polar orbits are best suited to lower resolution, global coverage and high resolution coverage of the polar regions.

Orbital altitude exerts a strong influence on instrument resolution. High altitudes decrease optical resolution and increase instrument dwell time while low altitude orbits increase resolution and decrease dwell time. Higher orbital velocities, which are directly coupled to low altitudes, decrease the amount of time available for instruments to sense the surface. For reasonably small altitude differences, dwell time is not a significant factor here as lunar orbits exhibit small changes in orbital velocity with changes in orbital altitude. Orbit altitude selection is therefore a primary function of instrument optical resolution, viewing needs, and orbital stability considerations.

9.3.1 Orbital considerations

Mission objectives require orbits stable enough to permit orbital maintenance with a reasonable amount of maneuvering but low enough for good instrument resolution. Due to the Moon's anomalous gravity field, the stability of lunar orbits appears to be directly a function of altitude and inclination. Experience from earlier lunar flights and known lunar gravitational harmonics indicates that polar orbital inclinations and low altitude orbits are unstable. Exactly polar orbits exhibit a rapid rise in eccentricity leading to periapsis lowering and therefore crashing into the lunar surface. Large lunar gravitational anomalies are known to exist but the overall gravity field and its effect on low altitude orbit stability is poorly known. Numerical simulations of lunar orbits, based on low order spherical harmonics, suggest a pattern of rising eccentricity on polar orbits (Chesley et. al., 1988) and on oscillating eccentricity on equatorial orbits (Bond and Mulcihy, 1988). Present estimates of a 100 Km polar orbit lifetime, before periapsis crash, are 9 months.

The net effect of orbital instabilities is to increase propellant use for orbital sustenance. General avoidance of very low altitudes and certain inclinations can partially negate stability problems. Estimates of lunar gravity harmonics indicates stable near polar orbits may be available. These are the so-called "frozen" orbits (Burke, 1976). This family of slightly eccentric orbits have the periapsis fixed near the

Moon's south pole and may remain stable for up to two years (Uphoff, 1976).

9.3.2 High Resolution Strategies

Several surface coverage strategies are made possible by simply varying the orbital altitude (eg. large regions at low resolution, small regions at high resolution, and global coverage at moderate to high resolution). Global coverage at moderate resolution can be achieved through the use of a 100 Km polar orbit such as that planned with the LGO mission. Higher altitudes reduce the resolution obtained but increase the instruments' field of view thus allowing the equatorial regions to be more adequately viewed. Complete surface coverage from a polar orbit can be obtained in 27 days.

A highly elliptical orbit with a low periapsis over the region of interest gives a high resolution sensing opportunity without the stability problems caused by strong lunar gravity anomalies that are associated with low circular orbits. Since a small fraction of the orbit is spent at low altitudes, the net effect is to provide a low altitude sensing opportunity while maintaining a higher average orbital altitude. The drawback to this method is the small region of coverage that accumulates under the periapsis. The highly eccentric orbit is also capable of giving low resolution, large regional coverage on the apoapsis side with a smaller delta vee requirement than is associated with an equivalent transfer to a high circular orbit. The elliptical orbit offers a variety of surface coverage opportunities, and by properly choosing periapsis latitude and orbit eccentricity, a significant variation in surface coverage can be obtained in one orbit.

A possibility exists for high resolution global coverage by using a highly eccentric orbit and periodically shifting the latitude of periapsis. Figure 9.10 illustrates this concept. Since the orbit precession is small, the orbit can be considered to be fixed in space while the Moon rotates under it. By rotating the orbit line of apsides at appropriate intervals, enough to allow high resolution coverage under the periapsis to accumulate, the entire lunar surface can be viewed from a low altitude without severe orbital stability problems.

9.3.3 Specific Missions

The Radar Subsurface instrument package requires a low altitude circular orbit to sufficiently probe the lunar surface. A proposed orbit for this package is a 50 Km near polar circular orbit. From the existing data, this orbit appears to be stable for a period long enough to allow sufficient data to be collected.

The RAMAN Spectroscopy package requires a low, highly eccentric orbit which will be used to probe the dark side of the Moon. For good instrument resolution, a highly eccentric and very low periapsis orbit is required. Elliptical orbits of varied inclinations, and eccentricity of 0.36, and a periapsis fixed at 25 Km satisfies the needs of the RAMAN package. These orbits may be stable enough to permit short data gathering operations, but it will probably be necessary to enter these orbits a number of times to acquire the required data or to provide large amounts of orbit sustenance propulsion to maintain orbit ephemeris.

With the LOP being modular, many other instrument packages will be flown to perform a variety of missions. The LOP having its own propulsion system, can also accommodate these missions by simply changing orbit parameters to fill individual requirements.

9.4 Fuel Consumption

The propellant used is an aluminum/binder mixture with liquid oxygen as the oxidizer. To minimize the usage of the propellant, a limit was placed on the largest velocity change experienced by the platform. A limit of 1500 m/s for the delta vee for any set of orbital maneuvers was set. This delta vee requires 417 Kg of propellant. The specific impulse of the propellant is taken to be 275/s and the mass of the platform is 560 Kg. The platform fully loaded thus has a mass of 977 Kg.

If future missions require more mass intensive instrument packages, the delta vee budget will decrease with fixed propulsion mass. If one desires the same delta vee capacity with more platform mass or with the same mass, the propulsion system can be replaced by one with more propellant capacity. This feature is a result of the LOP's modularity and a lot of extra space to house extra fuel.

9.4.1 Coplanar Orbital Maneuvers

As this platform is an observation vehicle, the time required to execute different orbital maneuvers is not a factor in choosing the transfer orbit energy. Due to this lack of a time limit and the desire to utilize the propellant most effectively, a Hohmann transfer is used for coplanar orbit transfers.

A Hohmann transfer (see Figure 9.3) is a transfer between two circular coplanar orbits. This is achieved by using an elliptical orbit tangent to the initial and final orbits (Fundamentals of Astrodynamics, 1971).

Using a Hohmann transfer to change from a circular 25 Km orbit to a 2000 Km circular orbit requires a delta vee of 524 m/s

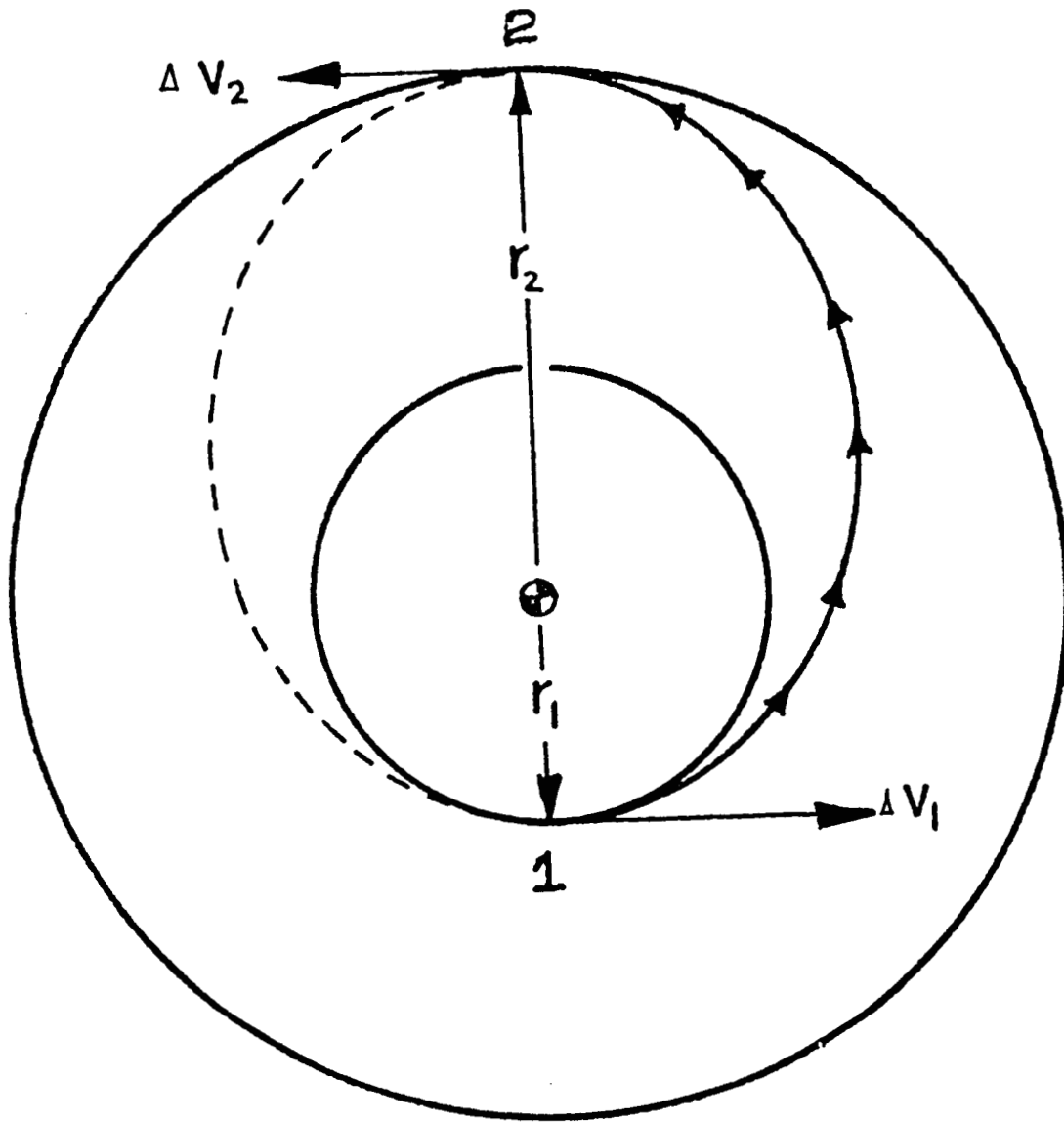


Figure 9.3 Diagram of a Hohmann transfer between two coplanar circular orbits. The Hohmann transfer is the most fuel efficient method for orbit transfer. The procedure consists of two delta-vees to transfer into an elliptical orbit and then circularize the final orbit.

HOHMANN TRANSFER

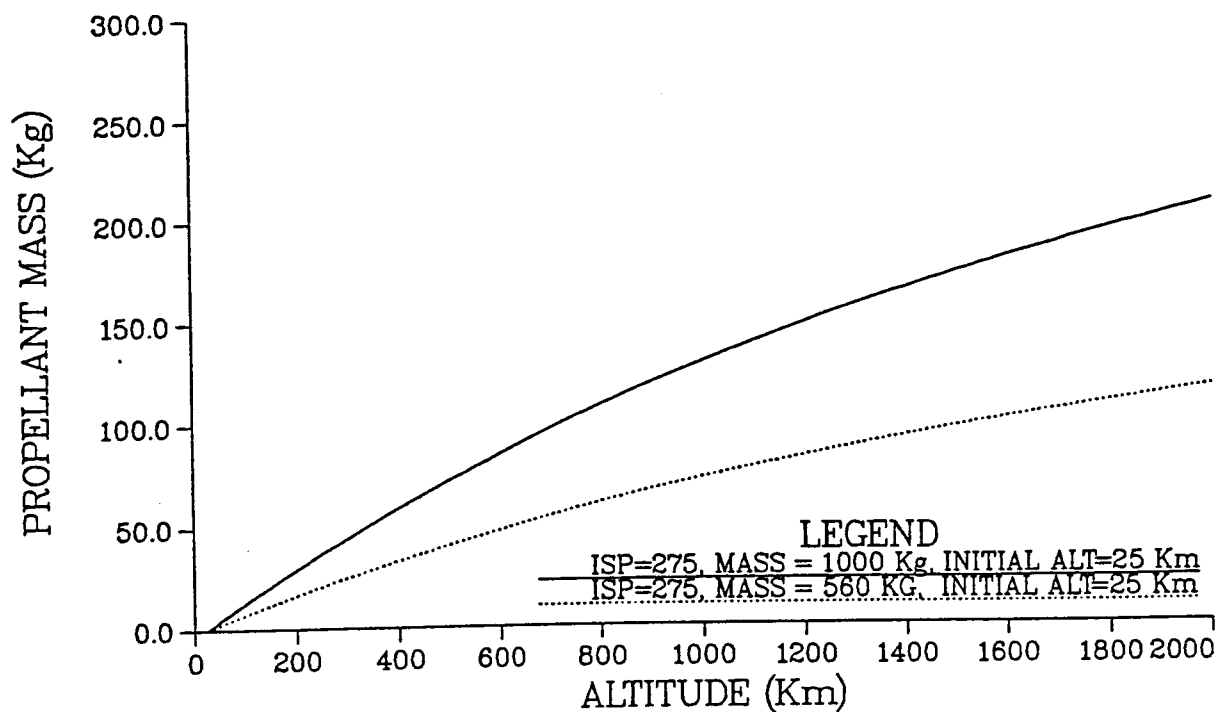
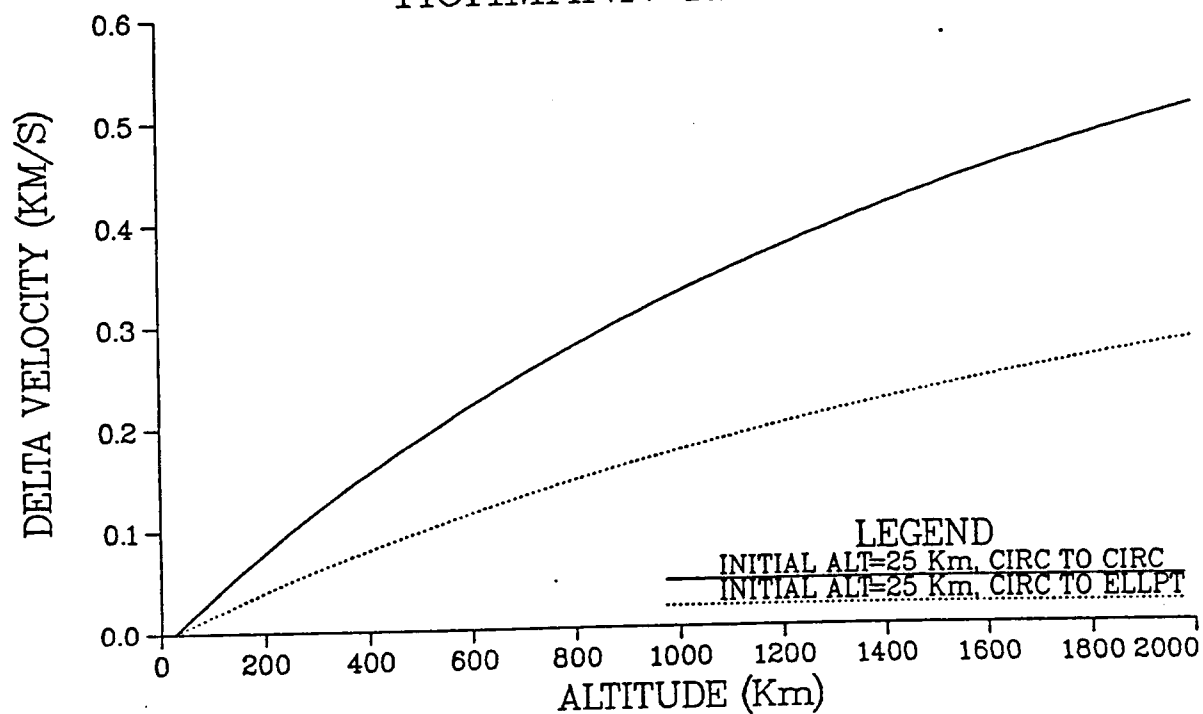


Figure 9.4 Delta Vee and propellant requirements for coplanar circular and elliptical orbit transfer.

which translates to 120 Kg of propellant. If the final orbit is to be elliptical with an apoapsis of 2000 Km, the delta vee is 318 m/s and the propellant mass is 70 Kg (see Figure 9.4).

9.4.2 Plane Changes

Orbital plane changes, the rotation of the orbit plane, are needed for complete Moon coverage and to reach different orbits as required by the mission to be performed. Orbital plane changes are executed at the point of minimum velocity in the orbit to minimize propellant usage. For elliptical orbits, the minimum velocity occurs at the apoapsis. For circular orbits, the velocity is constant, and, therefore, the maneuver can be executed at any time.

For an elliptical orbit with the periapsis at 25 Km and the apoapsis at 1300 Km (eccentricity = 0.27), the orbit can be rotated 90 degrees (see Figure 9.5). The more eccentric an orbit, the greater the angle through which the orbit can be rotated and still remain within the given delta vee budget.

In a circular orbit, the maximum plane change is limited by the propellant mass constraint (see Figure 9.5). For a 25 Km circular orbit, the maximum angle that the orbit can be rotated is 55 degrees. As the altitude increases, the maximum angle of rotation also increases.

9.5 Conclusions

To avoid perturbations due to gravity anomalies, elliptical orbits will be utilized. All coplanar orbit changes will be made using a Hohmann Transfer and all plane changes will be made at the apoapsis when possible. Two standard baseline orbits will be used to accommodate the different instrument packages and to cover the entire lunar surface. Both will be near polar elliptical orbits with their periapsis at 25 and 50 Km respectively, and their apoapses varying from 25 Km to 2000 Km. The elliptical orbit allows for greater "hang time" over a point at the apoapsis and also allows low altitude coverage at the periapsis.

PLANE CHANGE: OCCURS AT APOAPSIS

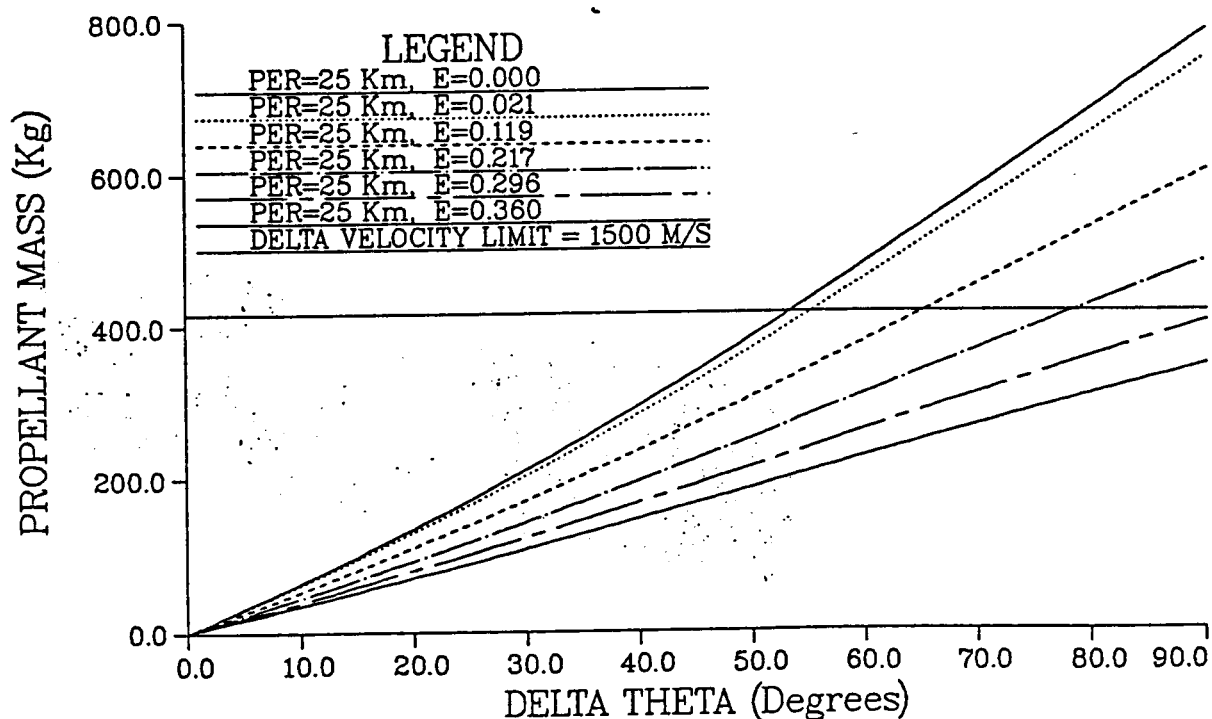
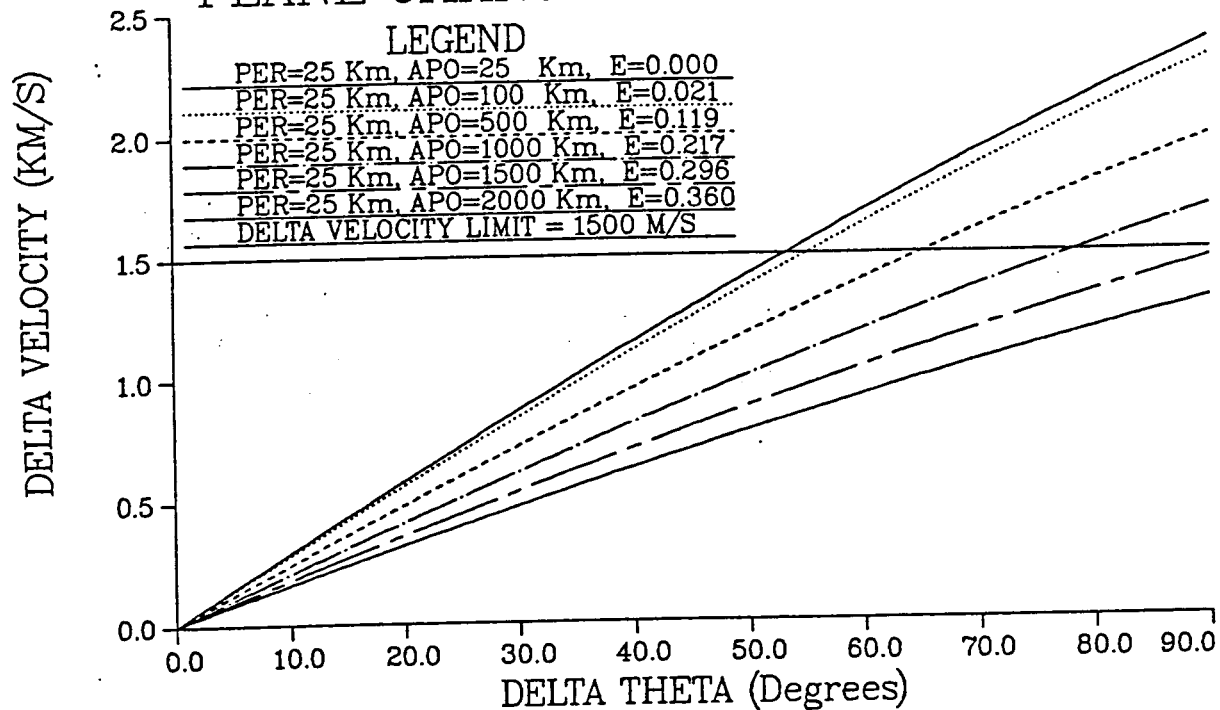
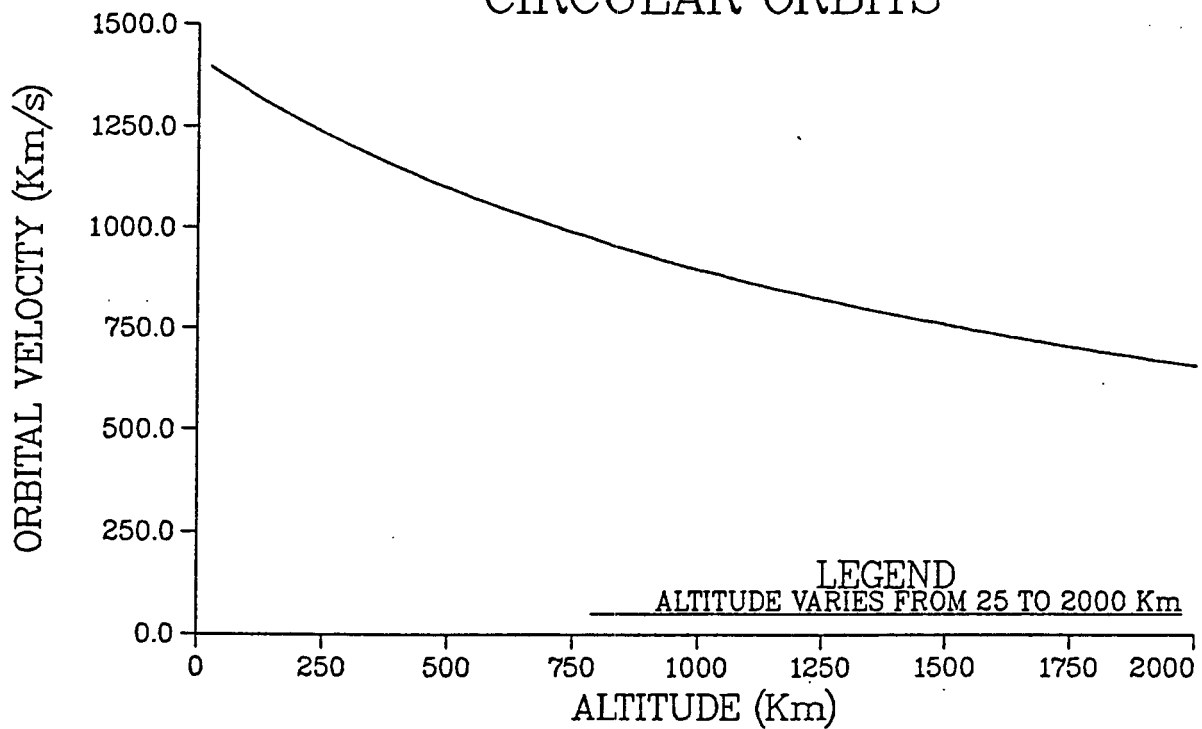


Figure 9.5 Delta vee and propellant requirements for orbit inclination changes.

CIRCULAR ORBITS



ELLIPTICAL ORBIT

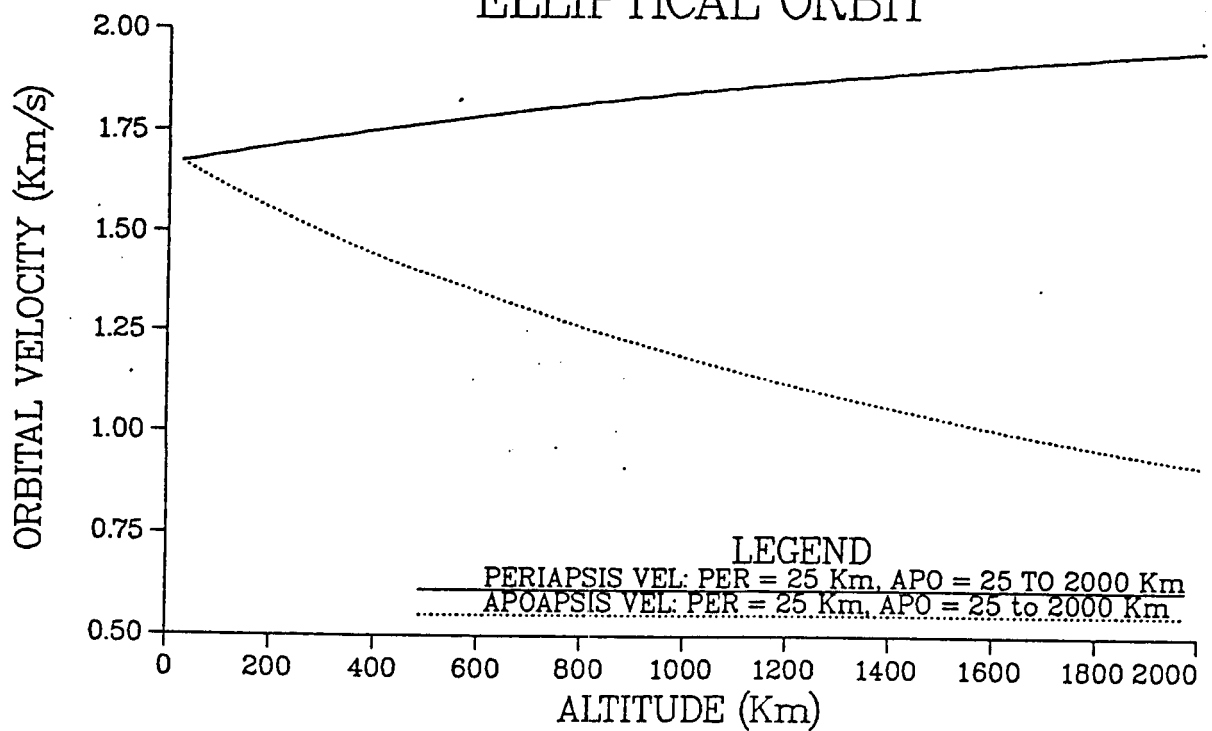
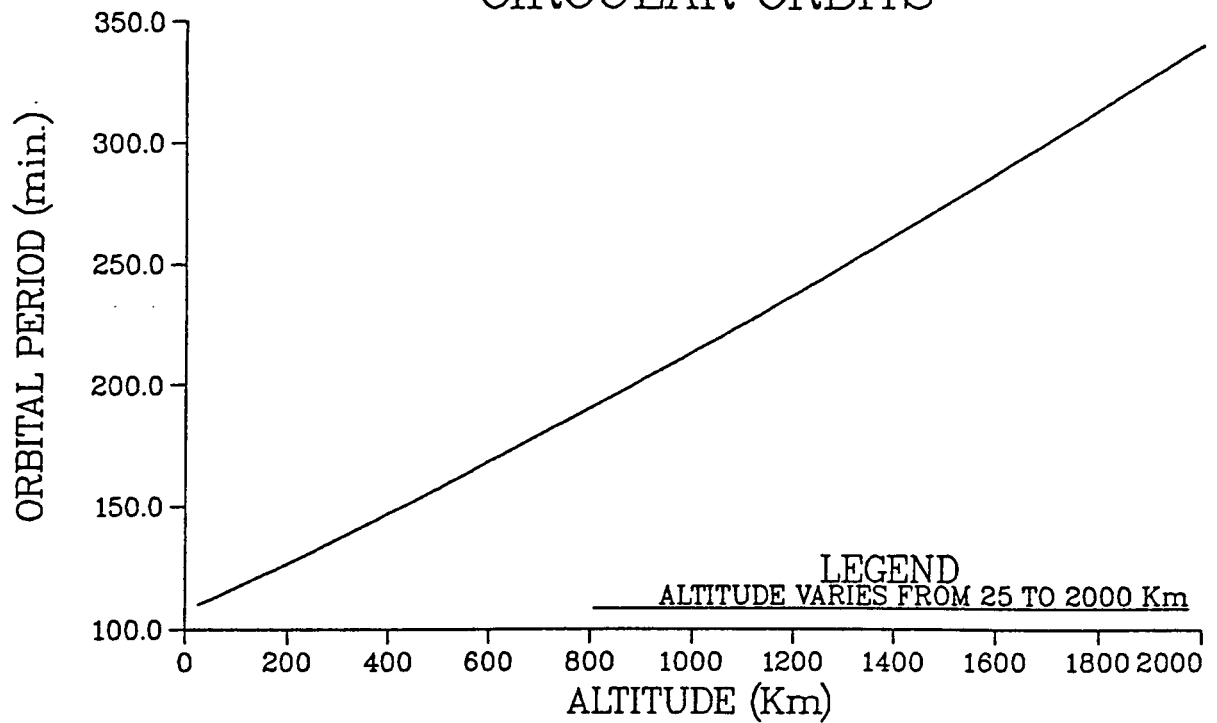


Figure 9.6 Orbital velocities for elliptical and circular orbits.

CIRCULAR ORBITS



ELLIPTICAL ORBITS

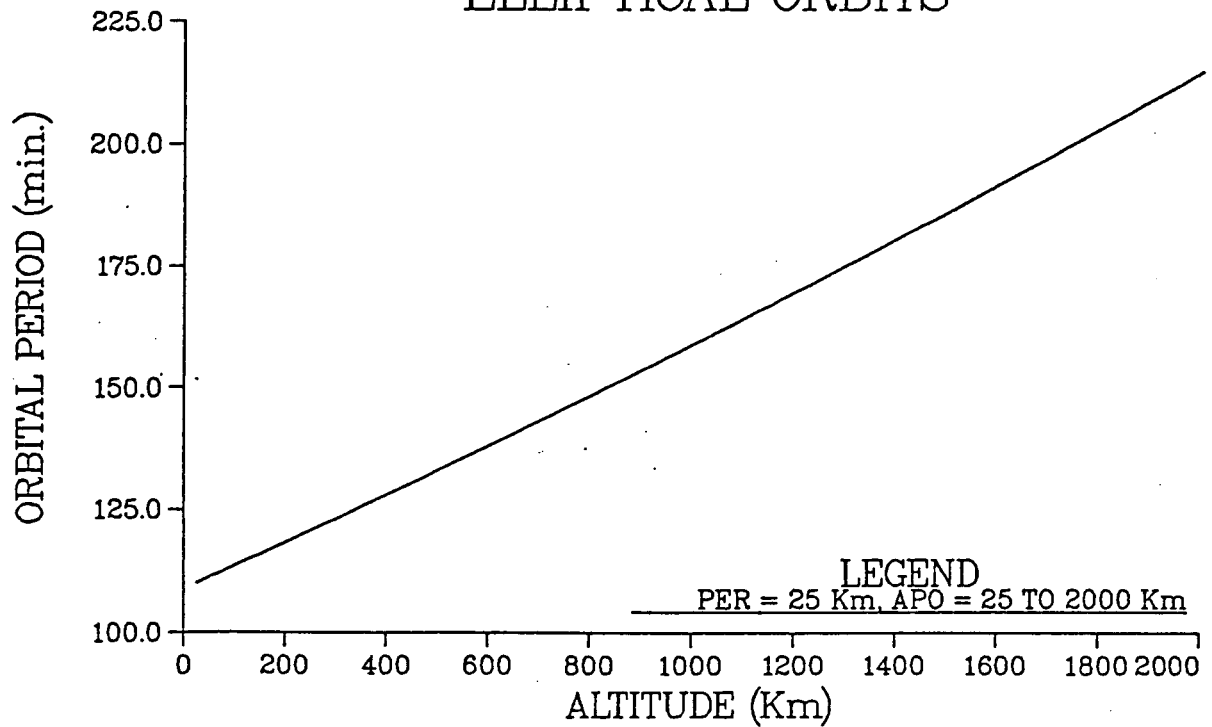
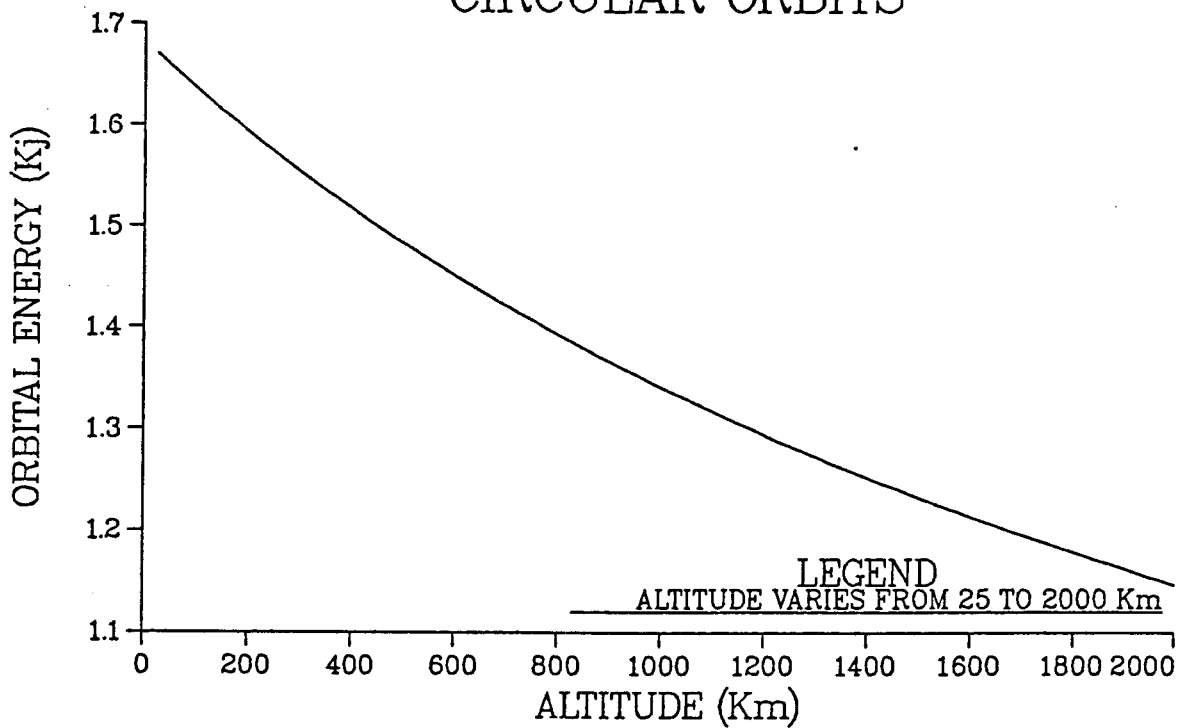


Figure 9.7 Orbital periods for elliptical and circular orbits.

CIRCULAR ORBITS



ELLIPTICAL ORBITS

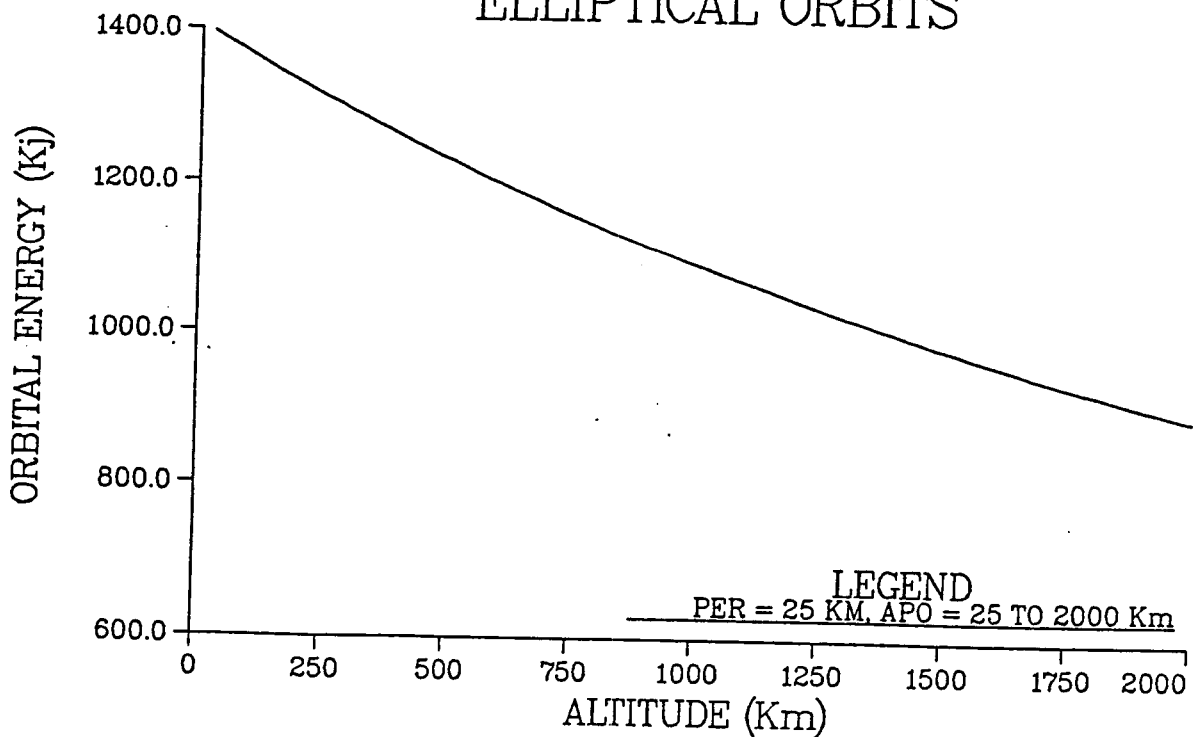


Figure 9.8 Orbital energies for elliptical and circular orbits.

REFERENCES

Bate, R. R., D. D. Mueller, and J. E. White, **Fundamentals of Astrodynamics**, New York, Dover Publications, 1971.

Chelsey, B., D. Korsmeyer, D. Monroe, **Mixed-Vehicle Transportation Fleet to Lunar Polar Orbit**, University of Texas at Austin, April, 1988.

Lunar Viking Feasability Study: Final Report, Volume 1, Martin Marietta, 1971.

Monte Riphaes LM76, Lunar Map, Mecator Projection, NASA.

Status and Future of Lunar Geoscience, NASA, 1986.

10.0 Propulsion System

The Apollo missions went to the Moon, landed, and returned lunar samples of rocks and regolith. They amassed great knowledge of our closest celestial neighbor. Along with this knowledge and information they brought back new questions and these questions require another look at the Moon on a global scale.

The Moon has a great deal of scientific value since it has recorded over 4 billion years of exogenic events in the solar system in its surface. Also, because it is made of mostly silicates it is an excellent candidate for developing models for other similar silicate bodies in the solar system such as asteroids, moons, etc. Perhaps the most valuable feature of the Moon to mankind at this time is that it is a potential source of raw materials that can be utilized in the future to support long term programs of space exploration. The production of goods such as fuel, glass, alloys, composites, etc., from lunar derived materials represents a considerable reduction in the cost of accomplishing any given extraterrestrial mission.

The time scale for the launch of LOP is in the early 21st century. At this time a lunar base will have been established with lunar processing plants. The LOP places a requirement upon itself to use a lunar-derived propellant system. This is a unique criteria that involved many investigations into mineral and elemental concentrations. Possibilities of deriving propellant sources from these minerals are a major concern.

Lunar propellant quantities are derived from mineral concentrations of the lunar rocks and regolith returned by the Apollo missions. An analysis of the production rates possible, feasibility, and cost of production of lunar derived propellants was undertaken. A propellant scenario was developed and two propellant systems will be incorporated into this scenario. The platform will use a LO_2/Al propellant system and the GTV will use a LH_2/LO_2 propellant system. The platform will use a hybrid turbopump propulsion system. Some of these parameters are given for this propellant system.

10.1 Mineral and Element Concentrations

Lunar minerals that show the most promise for propellant production are:¹

Olivine	$[(\text{Mg}, \text{Fe})_2 \text{SiO}_4]$
Pyroxene	$[(\text{Ca}, \text{Mg}, \text{Fe}) \text{SiO}_3]$
Ilmenite	$[\text{FeTiO}_3]$

Olivine and Pyroxene occur in concentrations approaching 60%². Ilmenite occurs at concentrations of up to 20%¹. These minerals are good sources for lunar oxygen production. High percentages of oxygen in these rocks may be removed by many processes.

Elemental concentrations from the Apollo missions are shown below:

<u>Element</u>	<u>Moon (PPM/Wt) ³</u>	
	<u>Mare</u>	<u>Highlands</u>
O	417000	446000
Si	212000	210000
Al	69700	133000
Fe	132000	48700
Ca	78000	106800
Na	2900	3100
K	1100	800
Mg	57600	45500
Ti	31000	3100
H	54	56
P	660	500
Mn	1700	675
C	100	100
Cl	26	17
Cr	2600	850

The elements in bold are possible propellant sources. The only lunar derived propellant oxidizer possible is oxygen, and it makes up almost half of the lunar material. Liquid oxygen is used very heavily as a propellant oxidizer in Earth applications.

Other elements may be used as propellant fuels. Many of them can be used as the sole propellant fuel or in chemical combination with other elements to form various fuels.

10.2 Lunar Production Processes

There are many lunar production processes under study at the present time. Oxygen and hydrogen production are among the most studied processes. There are, however, many problems to be looked at before a lunar processing plant can be commenced. Many of the production processes under study have reconfigured terrestrial processes to lunar processes.

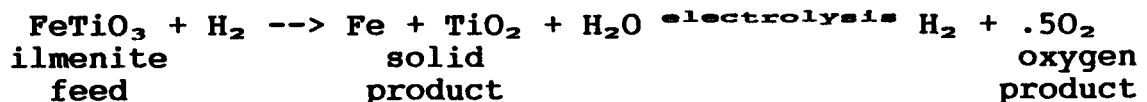
Many questions must be answered before an efficient lunar production process can be brought into operation. Some of these questions are:

1. Production rates
2. Processing plant mass
3. Power consumption
4. Lunar material extraction rates
5. Processing plant performance factors (temperature, pressure, carbon deposit rates, etc.)
6. Terrestrial supply quantities
7. Technological feasibility

These questions are just a few of the many that need to be answered. The questions shouldn't be overlooked if a lunar base is to be built to provide an economic return on a processing plant built at the Moon base.

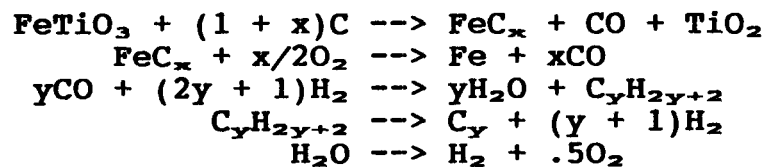
10.3 Lunar Oxygen Production

There are many viable processes for producing lunar oxygen and one of the most promising of these processes is ilmenite reduction. The basic reaction is:⁴



Note that a hydrogen source is required, and the hydrogen source will have to be renewed, possibly as a terrestrially supplied source. This will increase the production cost and rates of the oxygen reduction.

Another possible process is the carbothermal process. Its reactions are:⁶

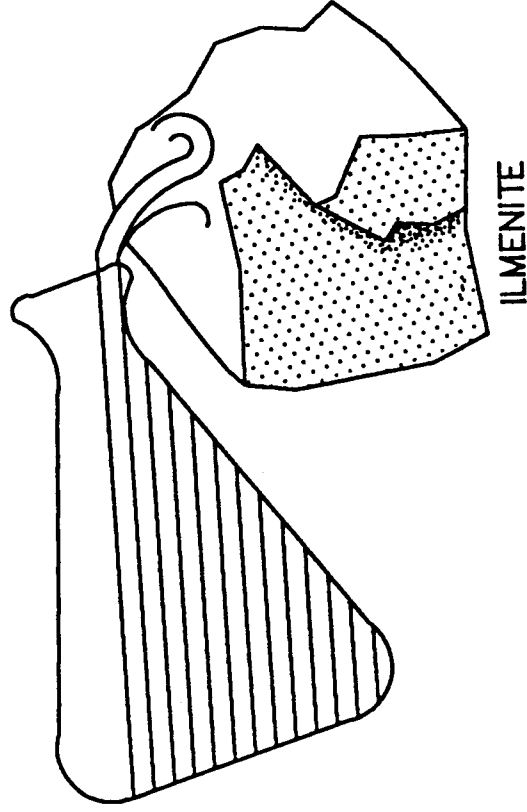


This process requires a carbon source along with a hydrogen source. The terrestrial supply problem associated with the hydrogen source applies to the carbon source also. Another potential problem with the carbothermal process is in dealing with possible carbon deposits during oxygen production in the processing plant.

With 10% of the lunar material consisting of ilmenite, a yield of 1% of lunar oxygen can be produced with a 100% efficient processing plant.¹ The yield can increase greatly if beneficiation (only transporting to the processing plant the material needed in the reactions) is employed.

A method of transporting the required carbon and hydrogen sources is in the form of methane or ammonia from the Earth.⁷ Methane and ammonia are easier to transport than hydrogen and can provide savings in terms of storage tank volume, cooling hardware, and transportation cost. The methane and ammonia can be chemically reacted once on the Moon to produce the needed carbon and hydrogen sources for mineral processing.

OXYGEN PRODUCTION



ILMENITE REDUCTION – REQUIRES HYDROGEN
CARBOTHERMAL PROCESS –
REQUIRES HYDROGEN AND CARBON

10.4 Lunar Hydrogen Production

Elemental hydrogen concentrations are very low (50 ppm). A 100% efficient hydrogen recovery method would only yield 0.005% of hydrogen.

A possible hydrogen production process involves the use of solar energy directed into a furnace to liberate the hydrogen gas. This process has a relatively good efficiency with 20 micrometer diameter soil grains, but this would mean a beneficiation process to the soil before processing.

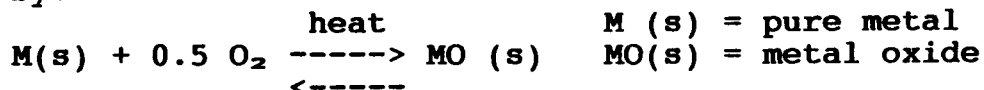
Another option with unlimited yield is to transport the hydrogen from Earth. It can be transported as hydrogen, methane or ammonia. Methane and ammonia require chemical reduction, and transported hydrogen increases the cost of availability of the hydrogen and oxygen.

10.5 Vacuum Reduction of Minerals

Vacuum Reduction is the decomposition of metal oxides into pure metals and gaseous oxygen.¹⁹ This reaction occurs when the metal oxide is heated in an ultra-vacuum environment where the oxygen partial pressures are low. The major metal oxides found in lunar soils are SiO₂ (40-48%), MgO (6-11%), TiO₂ (0.5-9%), Al₂O₃ (10-20%), and CaO (9-15%).¹⁹

This technique is not an efficient method for metal extraction on the Earth because of the difficulty in producing such a high vacuum. On the other hand, this technique is suited for extracting metals in moons and asteroids since these bodies already possess ultra-high vacuums because they lack an atmosphere.

Vacuum reduction is probably the most efficient method of obtaining pure metals because no additional chemical reducing agents such as H₂, CH₄ or the supporting equipment are required in the process. The metal oxide to metal decomposition is described by:

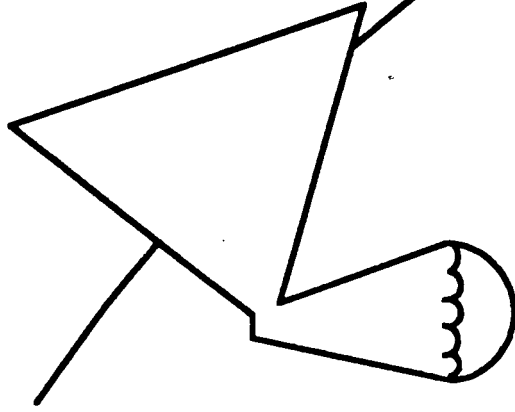
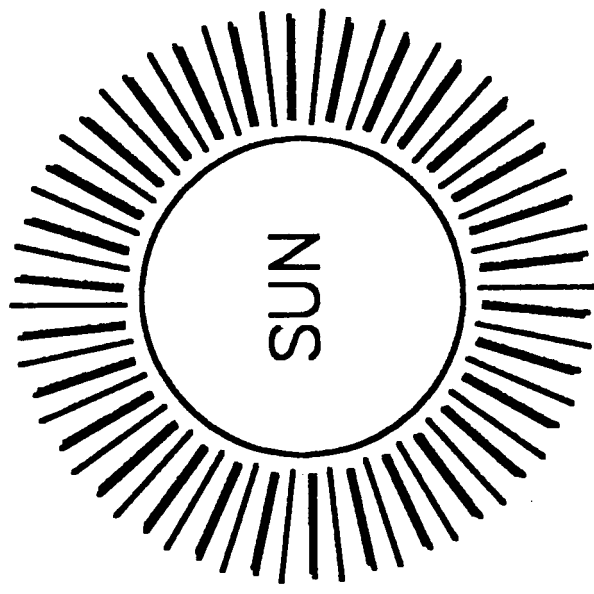


Studies show that at oxygen partial pressure of 10⁻¹⁹ atm, metallic Fe, Ti, Si, Mg, and Al are all stable phases at temperatures around 2000 C.

10.6 Lunar Derived Fuels from Human Wastes

Humans produce a great deal of metabolic wastes at very high rates (see Table 10.1 and 10.2). These materials require immediate attention because of the potential ill effects caused

HYDROGEN PRODUCTION



COLLECTOR/HEATER

= 0.005% YIELD

LIBERATE HYDROGEN FROM SOLAR ENERGY

1

by poor sanitation. Based on estimates of average metabolism, these wastes can amount to a vast supply of raw materials for fuel production and also represent important sources of reclaimable materials in a closed environment life support system (CELSS)²¹, even when the population of the base is small. There are several processes by which chemicals necessary for fuel production can be reclaimed from such wastes produced on a Moon base.²⁰

A physico-chemical waste processing plant consisting of a waste combustor module and a water hydrolysis module was studied. The amounts of gases produced from wastes produced by a 25 man crew in 360 days using a waste combustor are shown in Table 10.4. The values were calculated from the combustor reactions tabulated in Table 10.3. The total amounts of gases were recovered (see Table 10.5) with an overall efficiency of recovery of 56.5%, if we assume that only food, water, and oxygen for the crew is resupplied. This scheme is maximized to produce O₂ and H₂ since these are to be used to support the GTV and platform propellant requirements. It is assumed that 60% of transpiration water is recovered and hydrolyzed to produce enough O₂ to be used in the waste combustor.

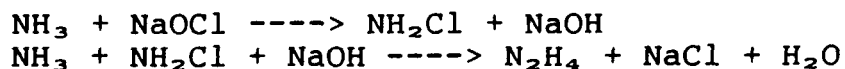
Other considerations, such as what percentage of reclaimed water needs to be allotted for life support, may affect this scheme. Nevertheless, the results show (Table 10.5) that this process is sufficient to support the O₂ and H₂ refueling needs of the LOP mission during the initial stages of a Moon base. To provide more O₂, in the event of a need for multiple refueling events, then adding a Bosch reactor to the system would release more O₂ from part of the CO₂ supply at the expense of some H₂ (see Table 10.4 and Table 10.5).

Another method of releasing H₂ from human wastes is through the anaerobic digestion by methane producing bacteria in a biogas bioreactor, but this method could not be used to support the fuel needs since it has a low rate of CH₄ production (see Table 10.7).

The waste combustor process is able to produce substantial N₂ (4125 Kg/yr). This represents a possible route to the synthesis of Hydrazine from lunar derived H₂ and N₂ although it needs to be evaluated further since it requires resupply of sodium hypochlorite (NaOCl) and sodium hydroxide (NaOH). Hydrazine (N₂H₄) may be produced from the following scheme:^{17, 18}

step 1) Lunar Derived Ammonia Production
- 500 C 250 atm, fine Fe catalyst
$$\text{N}_2 + 3 \text{H}_2 \rightleftharpoons 2 \text{NH}_3$$

step 2) Lunar Derived Hydrazine Production



10.7 Fuels Derived from Agricultural Wastes

In the event that the LOP mission was to take place at a time when a large Moon base capable of supporting lunar agriculture, it would be possible to produce suitable fuels from agricultural wastes. The scheme would involve the production of CH_4 (Table 10.7) from such wastes in a bioreactor, which can then be used to reduce ilmenite or pyroxene (Table 10.9).

It was assumed that as the size of the lunar colony reaches a population numbering greater than 500⁵, then it would be feasible to produce food using lunar agriculture. Table 10.8 shows that this size of base with agriculture capabilities is necessary in order to produce enough lunar derived H_2 and O_2 to support the LOP mission.

10.8 Other Production Elements

Production of the other elements have been considered but not as in great detail as oxygen and hydrogen production. There are several production processes that yield various elements. Production rates are not specified for these processes.

A carbochlorination process will produce silica, silicates, and aluminium. Electrolysis of molten silicates provides oxygen, silica, aluminium, and other elements. To obtain various elements a basic acid leach process is advised. A specific hydrogen fluoride acid leach process produces silica and metal oxides.

10.9 Production Constraints

A constant 20 m^3/day digging rate with a 33% error to account for equipment maintenance and work slow downs due to crew rotations⁵ was assumed. With a lunar soil density of 1300 to 1800 kg/m^3 , a digging rate considering the mass per day would range from 8580 to 11880 kg/day . These constraints are applicable to the beginning days of a lunar base in the year 2010. There is room for improvement in these figures but these were used to keep a conservative estimate of production rates of the elements considered as a propellant source.

10.10 Production Rates

The production rates were determined from known production processes explained in section 10.1. There are many unknown factors affecting the production rates. A 50% efficiency was assumed for many of the rates.

Lunar oxygen:	85.8 - 118.8 kg/day	(100% efficient)
Lunar hydrogen:	0.215 - 0.297 kg/day	(50% efficient)

Lunar aluminium: 3.00 - 4.14 kg/day (50% efficient)
Lunar MgO: 0.875 - 1.21 kg/day (50% efficient)

Lunar oxygen and hydrogen production rates are obtained from the production constraints and from the production process used. No precise production rates for lunar aluminium and MgO are available. These rates were taken from the expected lunar oxygen production rates multiplied by the concentration of the aluminium and MgO. These are reasonable values taking into account that lunar material is collected at the same rates and manner of extraction. MgO is given here because it is a factor in the production time of a propellant fuel called Silane (SiH_4).

10.11 Processing Plant Sizing

The production rates will mean nothing if there isn't a method of producing what is desired. This section sizes a 10000 kg oxygen per year processing plant. These values were determined with the use of reference 6:

6.82×10^{11} J	- energy required
21 600 W	- power required/year
326 kg	- required processing plant mass
120 kg	- mining and beneficiation equipment required
540 kg	- power plant required
$\$9.86 \times 10^6$	- transportaion cost (\$10000/kg)

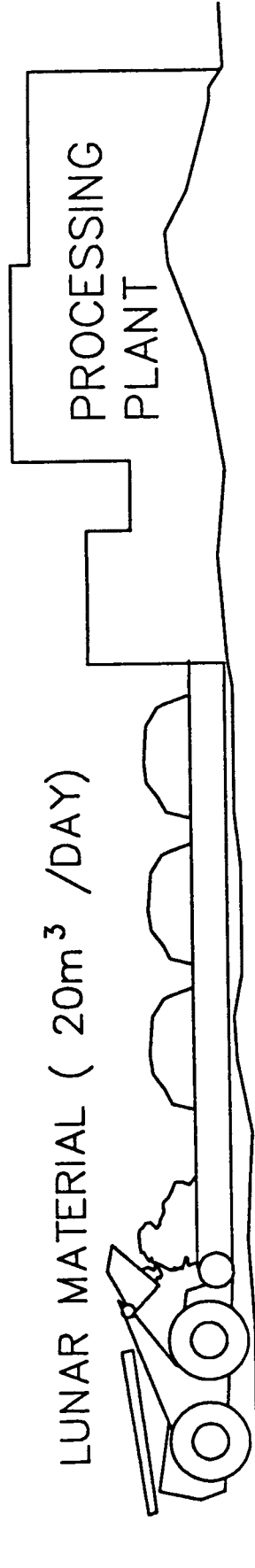
The ten million dollar transportaion cost (transportaion from Earth to the lunar base) would pay for itself in a very short time if one considers the cost of transporting all the required fuel from Earth.

The power and mass requirements of the plant isn't excessively large. From this simple analysis, a 10000 kg of oxygen per year is a viable production rate. This also shows that a processing plant for the LOP, or some other lunar fueled spacecraft, is a worthwhile investment not only for the propellant required for LOP but also to produce lunar building materials and water for the Lunarians working at the base.

A processing plant doesn't require any beneficiation equipment but it helps a great deal in the yeilds of the required materials.

The processing plant sizes for production of the other necessary products can be assumed to be much smaller than the oxygen production plants due to beneficiation performed from the lunar oxygen production.

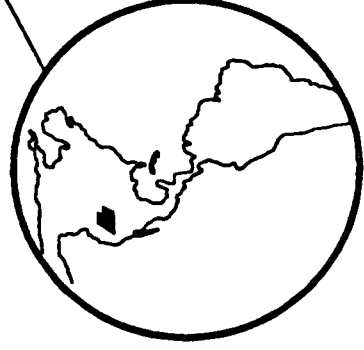
PROCESSING AND COSTS



ELEMENT	Kg/day	COST
OXYGEN	85.8	\$62.00
HYDROGEN	0.215	\$10.00
ALUMINUM	3.00	\$200.00
SILANE	0.350	\$45600.00



\$10,000 /kg



10.12 Lunar-Derived Propellant Possibilities

From all this initial information, many propellant sources can be defined. They are but not confined to:

LSiH₄/LOX
AlCa/LOX

LH₂/LOX
AlCaMg/LOX
Lunar Soil/LOX

Al/LOX
Ca/LOX

Liquid oxygen (LOX) is the obvious choice for the propellant oxidizer. The primary question is what propellant fuel would be most effective and practical for the LOP.

Three of the seven possibilities here were considered in an evaluation. Liquid silane (LSiH₄)/liquid oxygen, liquid hydrogen/liquid oxygen, and aluminium/liquid oxygen were considered. The rest of the seven are derivatives of the Al/LOX propellant system.

Liquid silane has not been used before but has been theorized to perform well. It has good characteristics. This would incorporate a liquid bipropellant system which is a well used system with spacecrafts. To produce liquid silane, magnesium oxide (MgO) must be lunar produced. MgO is one of the first reactants used in the production of silane which is the controlling factor in the silane production time.

LH₂/LOX has been used for a long time. It has proven its reliability and its worthiness time after time. This propellant source is also a liquid bipropellant.

Al/LOX will contain a solid fuel source and a liquid oxidizer. Two possible rocket schemes are possible.⁹ One is using a pump-pressure fed concept where this system provides the LOX from a pressurized tank and a passivated powder fuel supplied by a spiral screw feed. The other method is the hybrid, turbopump concept. This concept requires the additional transportation of a binder for the fuel source. The hybrid system is more reliable, safer, and a proven method of rocket propulsion than the pump-pressure fed concept.

10.13 Propellant System Quantities

An analysis between the three chosen propellant possibilities was performed. The platform propellant would be in storage with the platform until used, and an assumed storage time was taken to be one year. Boiloff rates of the liquid propellants was included in the analysis. The propellant masses do not change for various acceleration loads, only the time of propellant burn changes. Production times were taken from the production rates and the masses required for the propellants. All propellants were assumed to be totally lunar-derived. The relative quantities are shown in Figure 10.1.

RELATIVE PROPELLANT QUANTITIES

	AL/LOX	LH /LOX	LSIH /LOX
OXIDIZER MASS	1	0.70	0.77
OXIDIZER VOLUME	1	0.70	0.77
FUEL MASS	1	0.78	1.12
FUEL VOLUME	1	31.33	4.69
PRODUCTION TIME	1	10.82	9.53

Figure 10.1 Relative propellant quantities

LOX was not the overriding time factor for these propellant systems. The fuels were the production time controllers. All the systems have reasonable production times except for LSiH_4/LOX system. The yield of LSiH_4 is very low. The cost (which will be given in the next section) is very high. From this analysis LSiH_4/LOX propellant system was not considered further in the study.

A delta V of 1500 m/s was assumed early in the study to provide for platform orbital changes. The two GTV delta V's are divided into two 2000 m/s delta's. One delta V is for the detachment from the platform after refueling to a lunar landing. The mass used for this maneuver was the GTV mass plus the mass of the required propellant to land. The other delta V was for launching of the GTV from the lunar base to platform rendezvous. Its mass consisted of the GTV, platform fuel needs, and the GTV fuel needs from the lunar base to platform rendezvous.

10.14 Production Costs

Production costs consisted solely of Earth to Moon transportation. The cost of this transportation is taken to be \$10000/kg. This is about the cost of gold. The production costs are taken from the production rates and process scenarios.

To produce lunar silane, hydrochloric acid is required which must be totally terrestrially supplied. Magnesium oxide used to produce silane can be lunar derived. For just the cost of transporting the required amounts of hydrochloric acid a cost of \$45600/kg of silane is required.

To produce lunar oxygen requires hydrogen to perform the necessary reactions. All systems require the lunar oxygen so this must be taken into account no matter what the situation is. The \$62/kg cost of lunar oxygen is essentially the transportation cost of hydrogen from Earth with an expected 5% conversion loss of hydrogen per pass in the oxygen production process.

Aluminium production cost is a pure guess. \$100/kg of aluminium was assumed. It can be anything!

Liquid hydrogen production is also a hypothesized guess. \$10/kg of hydrogen is a reasonable assumption because the solar energy is free (comes from the sun) and doesn't require any chemical reduction processes.

10.15 Propellant System Decision

A final propellant decision was decided upon for many reasons. Relative propellant quantities are shown in Figure 10.1. The use of Al/LOX as the propellant source for the platform was decided upon for its storability, low production

time, low volume and possible low system mass requirements, low cost, transfer capabilities from the GTV to the platform, and its reliability. The transfer capabilities is that its low volume requirements makes it easy to transfer as one complete system in itself.

LH₂/LOX will be used as the GTV propellant system. Its reasons are for its low mass requirements, proven reliability, high performance capabilities, promising hydrogen production rates from human remains, and it is most likely to be transported anyhow so why not transport enough hydrogen for the GTV anyway. This is a very reasonable decision based on many lunar base design configurations. Water will be needed for human survival which can double as a hydrogen source for the propulsion system.

10.16 Effect of Rate of Fuel Production on LOP Mission

The LOP mission requires periodic refueling and refurbishing due to its modular nature because it is able to alter its orbits depending on the specific remote sensing task to be accomplished. The time between each refurbishing event will be determined by the rate of production of GTV propellant mass and the propellant mass for platform maneuvering.

The platform weighs 560 Kg dry mass and is capable of a Delta vee = 1500 m/s, which translates into 390 Kg O₂ and 143 Kg Al. The GTV dry mass is 460 Kg and must perform two Delta vee = 2000 m/s per refurbishing event, thus requiring 624 Kg O₂ and 105 Kg H₂. Therefore, assuming that the platform was delivered to the Moon from a LEO orbiting space station, then at least 1014 Kg of O₂, 105 Kg of H₂ and 143 Kg of Al must be produced in the lunar base before the first refueling and instrument maintenance GTV - platform rendezvous can be performed.

The refueling frequency of the platform will depend on rates of fuel production, so that methods with high production yields are desirable. The availability of lunar derived fuels will determine in part when the LOP could be deployed, assuming of course that no fuel is resupplied from LEO. If the LOP platform can function for 6 months without refueling or maintenance during its initial deployment, then it could be deployed together with the first lunar base crew (see Table 4, 5). The GTV could be deployed after a landing pad was constructed. On the other hand, if the LOP required maintenance every 3 months then it could not be deployed until one year after the lunar base was fully established.

10.17 Establishing a Lunar Materials Processing Plant and Base

The availability of materials on the Moon will depend on the size of the Moon base present and also on the specific activities that are carried out at the base. The sequential colonization

scheme developed by the University of Texas⁷ was used as a baseline scenario to determine how many inhabitants could be present and what tasks they would perform. The base is established in four phases, all through which the base grows in size and becomes increasingly self-sufficient.

The LOCO base construction scenario begins with the landing of a crew of 6-8. During this first phase, the crew sets up a power plant and communication antennae, constructs a permanent landing pad, and begin to excavate a larger, radiation shielded base. About 6 months later, the crew is now 8-12 and the landing pad and buried shelter are complete. Also a pilot processing plant is now extracting LOX and metals from the regolith. As manned power is needed to expand fuel production, the crew size increases to 50-100 so as to build a larger base. During this phase, lunar agriculture is reasearched, raw materials export begins, and permanent lunar processing facilities are built. A list of what equipment may be present at the base at this time is tabulated in Table 10. At a much later time, the base contains 500+ inhabitants that work in full production of LOX, matals, and other lunar derived finished products. It is expected that at this stage full scale lunar agriculture is underway.

10.18 Propulsion System Analysis

The thruster configuration is shown in Figure 10.2. The nozzle analysis considered the nozzle to be operating at its operating condition (third critical point). A chamber pressure of 400 psi (2.76×10^6 Pa) and an exit pressure of .0404 atm (4094 Pa) was used in the analysis. A constant flow rate and acceleration rate was assumed for the total propellant burn. An acceleration rate of 0.5g was taken to control the force exerted on the boomed objects of the platform. The areas of the throat and exit depend upon the flow rate of the propellant which is controlled by the acceleration rate. A chamber temperature of 4500 K and an exit temperature of 3000 K were assumed⁹.

With an acceleration rate of .5g a throat area of 6.16 cm², an exit area of 358.9 cm², and a thruster length of 33.61 cm would be required for a conical 15 degree nozzle⁹. The thruster configuration is shown in Figure 10.2.

The specific impulse of this Al/LOX system is approx. 275 s. The thrust chamber will contain the solid aluminum fuel, carbon refractory material for insulation purposes, rubber to dissipate the acoustical vibrations which can affect the propellant flow rates, and on the outside will be stainless steel. The thrust chamber and nozzle will be further cooled by a regenerative cooling system. This system incorporates the use of the cryogenically stored liquid oxygen to circulate around the thrust chamber and nozzle to cool it during firing.

PROPOSAL NOISE SYSTEM

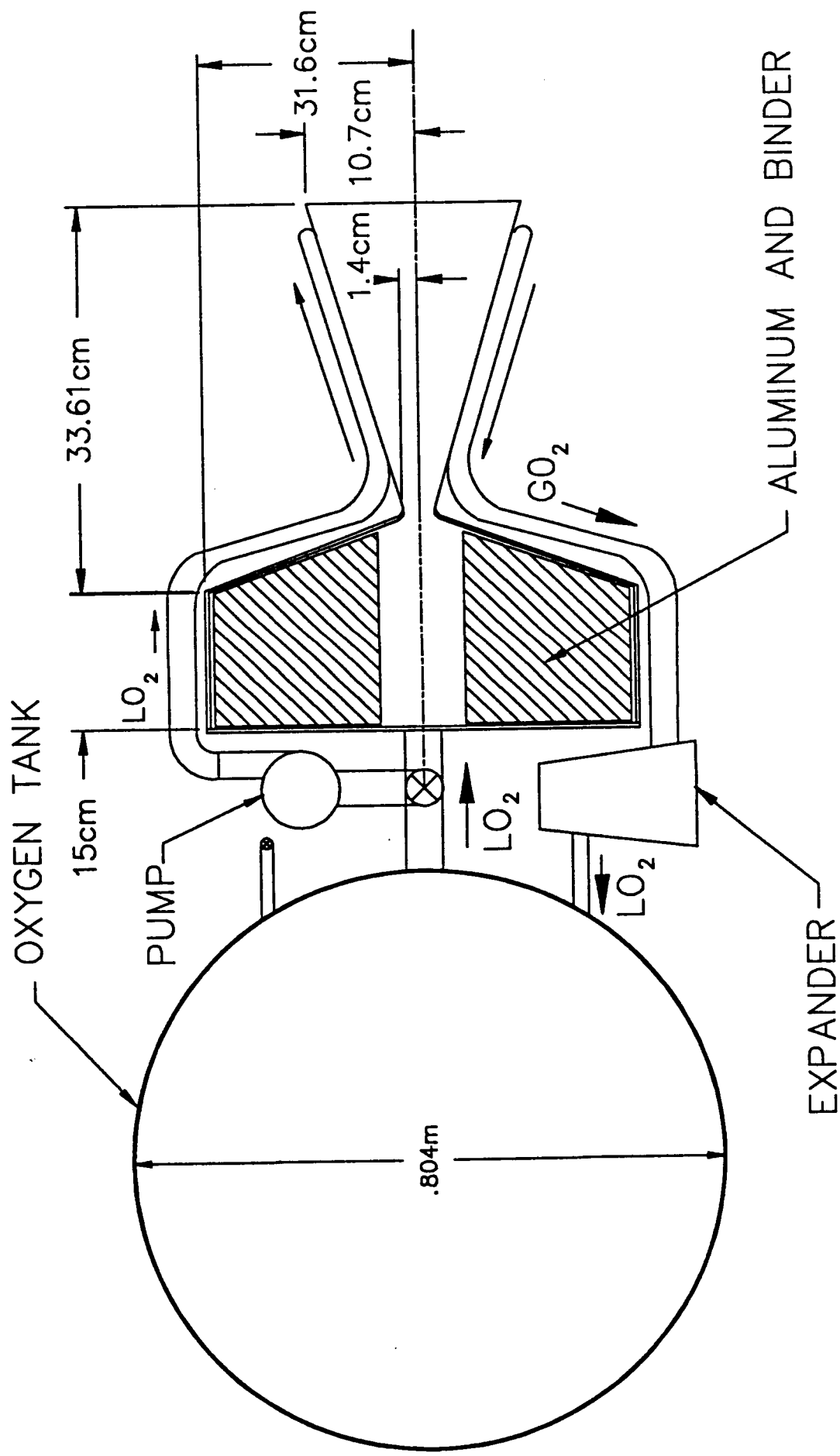


Figure 10.2 Thruster configuration. Thermal control of this design is given in thermal considerations section.

10.19 Thrust Chamber

The thrust chamber will contain the solid aluminum fuel as mentioned earlier. To burn this fuel a temperature of 4500 K and a pressure of 2.76 MPa is required. With this an area ratio of burn area to throat area of 168 is required, and a burn area equal to 1035 cm² is required. A thrust chamber length of 15 cm was taken and a 6 cm radius of the inside propellant fuel was also used from the fact that a liquid oxygen injector with a 6 cm radius injector would be used. The outside radius therefore is 31.6 cm to incorporate the aluminum fuel volume of 0.0454 m³. The thrust chamber length was decided on as 15 cm for thermal considerations. An accurate design may result in a more practical assessment of the thrust chamber length.

Using a short tube with conical entrance injector orifice type⁹ with a 3.18 mm diameter orifice and a discharge coefficient of 0.78, 93 holes will be possible on an injector diameter of 12 cm which fits nicely inside the thrust chamber. An approximate injector spray length is on the order of 1 to 2 cm depending on injector design and thrust chamber conditions. A total pressure loss through the 93 orifices is on the range of 1.4 MPa. This would set the liquid oxygen tank pressure at about 4.16 MPa. This liquid oxygen tank pressure can be accomplished with a turbopump sytem which will be demonstrated in the next section.

Injector design is a very empirical design process. This injector design is just an approximation to show the capability of using an effective injector. Much work can be conducted with respect to this effect.

A total propellant burn time of 285 s is obtainable from this propulsion scenario at the 0.5g acceleration rate.

10.20 Liquid Oxygen System

The liquid oxygen volume required with a 5% boiloff rate is .2712 m³ which gives the inside diameter of a spherical tank to be .804 m.

Four MPa pressure inside the liquid oxygen tank was assumed. Trying to produce this pressure with some inert gases such as Neon, Argon, and Helium would require an approximate spherical tank volume of 0.5 m. This is much too large to be acceptable for the platform. An inert pressure tank pressure of 24 MPa was assumed in the calculations which is an acceptable value for this kind of tank application. The masses of the inert gases varied for the different types of gases used. The tank mass was relatively constant because the diameter of the tank and internal pressure of the tank were assumed constant.

A pressure bladder will be used inside the liquid oxygen tank to force the liquid oxygen out with a constant flow rate and to prevent contamination of the return oxygen with the oxygen being used.

The pressure fed concept was too large to make it work so a turbopump system was incorporated. The oxygen flow rate out of the tank will be 1.35 kg/s of which 1.25 kg/s is required to the thrust chamber which leaves 0.10 kg/s to be routed to the turbopump system. The flow rate in the turbopump system was kept low to keep the heat readmitted to the liquid oxygen tank low. This was on the order of 8.7 kW. The work done by the turbine is 4.7 kW with a 30% efficient turbine¹² which is much greater than the required 0.15 kW to operate the 80% efficient pump. The heat extracted from the regenerative cooling of the thrust chamber and nozzle is 24.1 kW.

All the oxygen returned to the liquid oxygen tank from the turbine will not be useful because it will be outside of the pressure bladder. It will have an accumulated mass of 23.5 kg of oxygen and a volume of 0.118 m³.

The turbopump system is reliable and has been used on many missions. It will be used also on this mission in a hybrid, regenerative cooling system. Much design work can accompany this scenario. These preliminary investigations yield a feasible possibility of the use of this system.

10.21 Starting Problems

It is not known if Aluminum/Liquid Oxygen is hypergolic or not. The assumption in this paper is that it is because the melting point of its metal oxides is less than the melting point of the metal itself. This means that it will be in a vapor phase combustion process. Much time and effort was taken to determine accurately if this system is hypergolic, and the conclusion is that it is.

The equilibrium constants for a reaction were determined with the use of Ref. 8 mole fractions. They showed promise in that the forward reaction of the combination of the aluminum and oxygen is definitely the manner the reaction would like to attain. Much future work in this aspect can also be undertaken. If the reaction is not hypergolic then we are confident that an igniter may be used in order to start the propulsion system.

10.22 Future Considerations

The expected insertion of LOP is in the year 2010 or after a lunar base has been developed. In this time range many new insights into production rates and lunar-derived propellant systems may come about. This is always the case with a future project. Things can change for the better in this time frame.

A computer program can be written for outputs such as given in this paper for various inputted information. Detail analysis of boiloff rates and cryogenic storage can be analyzed. Projection costs and thruster parameters can also be included in future considerations.

Preliminary details reveal a lunar-derived propulsion system capability. Much additional design work can improve upon the feasibility of such a system.

10.23 Conclusions

A lunar-derived propellant system is possible. Various fuels may be used each with thier own benefits. Propellant production from lunar materials is a worthwhile undertaking. Small processing plants are capable of producing the required LOP propellant amounts with ease.

Concentrations of elements are present on the lunar surface in amounts needed for propellant production. Transportation of material is needed but this is offset by the need of this material for the lunar base workers.

The need of lunar-derived propellants is evident. For future exploration beyond our planet, propellant production is a necessary factor. Propellant systems can be designed and made to work by the use of our nearest celestial neighbor. It is the means to expand our existence beyond the boundaries of earth.

REFERENCES

1. Rosenberg, Sanders D. (1985) "A Lunar-Based Propulsion System", **Lunar Bases and Space Activities of the 21st Century** (W. W. Mendell, ed.), pg. 169
2. LGO Science Workshop Members (1986) **Contributions of a Lunar Geoscience Observer (LGO) Mission to Fundamental Questions in Lunar Science**, Dept. of Geol. Sciences and the Anthro-Graphics Lab of Southern Methodist University
3. General Dynamics Convair Division (1979), **Lunar Resources Utilization for Space Construction Final Report Volume II**, NASA Lyndon B. Johnson Space Center, pg. 4-32
4. Gibson, Michael A. and Knudsen, Christian W. (1985), "Lunar Oxygen Production from Ilmenite", **Lunar Bases and Space Activities of the 21st Century** (W. W. Mendell, ed.), pg. 543
5. Lunar Operations Company (1987), **A Final Design Review for a Bootstrap Lunar Base**, The University of Texas at Austin
6. Cutler, Andrew Hall and Krag, Peter (1985) "A Carbothermal Scheme for Lunar Oxygen Production", **Lunar Bases and Space Activities of the 21st Century** (W. W. Mendell, ed.), pg. 559
7. Friedlander, Herbert N. (1985), "An Analysis of Alternate Hydrogen Sources for Lunar Manufacture", **Lunar Bases and Space Activities of the 21st Century** (W. W. Mendell, ed.), pg. 611
8. Streetman, J. W. (1978) "Preliminary Investigation of the Feasibility of Chemical Rockets Using Lunar-Derived Propellants", AIAA/SAE 14th Joint Propulsion Conference
9. Sutton, George P. (1986), **Rocket Propulsion Elements**. John Wiley & Sons, New York
10. Criswell, David R. (1978), **Extraterrestrial Materials Processing and Construction**, Lyndon B. Johnson Space Center
11. Siegel, Bernard (1964), **Energetics of Propellant Chemistry**, John Wiley & Sons, Inc., New York
12. Donovan, R. M., et. al. (1984), "Space Station Propulsion Analysis Study", prepared for the Twentieth Joint Propulsion Conference, Cincinnati, Ohio, June 11-13, 1984, NASA-TM-83715
13. Cornelisse, J. W., et. al. (1979), **Rocket Propulsion and Spaceflight Dynamics**, Fearon-Pitman Publishers, Inc., London

14. Oates, Gordon C. (1984), **Aerothermodynamics of Gas Turbine and Rocket Propulsion**, American Institute of Aeronautics and Astronautics, Inc., New York, New York
15. Loh, W. H. T. (1968), **Jet, Rocket, Nuclear, Ion, and Electric Propulsion: Theory and Design**, Springer-Verlag New York Inc.
16. Shepherd, Dennis G. (1972), **Aerospace Propulsion**, American Elsevier Publishing Company, Inc., New York, N. Y.
17. Cotton and Wilkinson (1980), **Advance Chemistry: A Comprehensive Text**, p. 695, John Wiley & Sons, Inc., New York.
18. Nebergall, Smith, and Holtzclaw (1972), **General Chemistry** Fourth Edition, pp. 522-3, D.C. Health & Co.
19. Sparks, D. R. (July 1985), **The Vacuum Reduction of Extraterrestrial Silicates**, General Motors Corp.
20. Hotzapple, M.T., F.E. Little, M.E. Makela, C.O. Patterson (Feb 22 1988), **Analysis of an Algae-Based CELSS. Part I. Model Development**, CELSS Research Conference, Texas A & M University.
21. Sauer, R. L., **Metabolic Support for a Lunar Base**, pp. 647-651.

11.0 Communications System

11.1 Introduction

The platform communication system must handle two basic functions of the craft. First, the system must provide control and maintenance communications for the platform. Second, the system must handle the data communication between platform and lunar base. These both must be solved with the platform's goal of modularity and redundancy to meet the mission objectives.

11.1.1 Control and Maintenance

Functioning of the craft can be monitored and corrected if necessary at all times if the craft has a constant communication link with the base. Some examples of this may be data from the altimeter relaying information concerning height above Moon, or internal navigation equipment confirming the present location. Other critical information concerning status of power supply, internal temperature, fuel supply, and other systems are included in this communications goal.

11.1.2 Data Transmission

The platform's major mission is to sample the lunar surface electromagnetically searching for lunar materials. Each of these instruments will need a link back to the lunar base for this information to be useful. Two possibilities exist: data can be transferred as soon as it is collected from the instruments, or data can be stored on the platform and transferred at some later time.

One of the instruments on the platform will be a high resolution imaging camera for analyzing various electromagnetic spectra. High resolution imaging requires a high data rate for real-time data analysis. For example, using a 1024 X 1024 pixel grid with 256 color levels per pixel, and have each picture transmitted at 30 frames per second, the data transfer speeds could approach 800 Mega-bits per seconds. The data requirements of this device alone could overload the communications system.

Designing a system to meet these high data rates will ensure future usefulness as well of efficient handling of slower data rates through multiplexing.

11.2 Internal System Schematic

With all the major components mounted in modules on the outside of the platform, an internal network is needed to link these modules together. These modules must accept data from instrument modules, process data, and transfer data to lunar base. The general configuration is shown in Figure 11.1.

COMMUNICATIONS

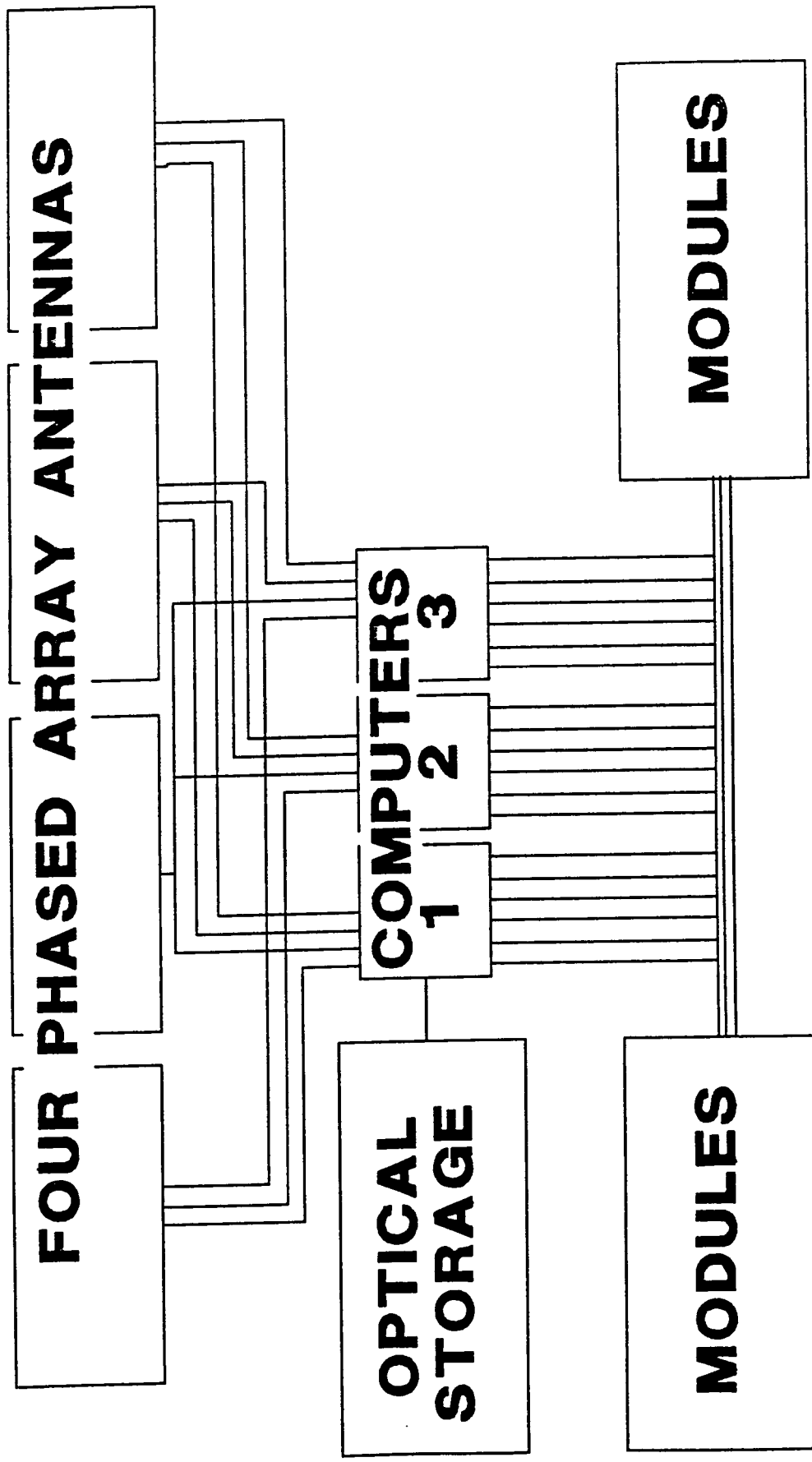


Figure 11.1 System Configuration

11.2.1 Optical Fiber System

Data from each module will be linked to the main communication computers by optical fiber. Optical fiber has the potential for very high data rates with few disadvantages as compared with conventional copper cables.

In order to allow maximum flexibility in replacing the modules, the physical connection between module and optical fiber bus will be linked by an infrared transmitter-receiver pair. Each module will have three transmitter-receiver infrared links and optical fibers. Each optical fiber will connect to one of the three central computers. Data rates approaching 10 Giga bits/sec are possible using optical fiber lines.

The receiver/transmitter pair would consist of a high speed gallium-aluminum-arsenide light emitting diodes as source, and photodiodes as receivers. The transmitter would emit infrared radiation at approximately 1 micron wavelengths.

Work has been done to protect optical fiber lines against bending and shock. Glass fibers break quickly if they are subjected to even a slight manufacturing defect and are not coated immediately after being drawn. A fiber optics cable used by NASA has an aluminum-sheathed pressurized outer jacket housing a polyethylene inner jacket containing 10 fibers. Each fiber is in a buffer tube which is filled with a gel material that acts as a cushion. The fiber itself is coated with a sealant. All of this protection is designed to reduce micro-bending and prevent moisturization.

11.2.2 Communication Computers

The communications package will use three computers for data processing. These computers will provide the following functions: 1) Supervise data transmission to/from modules. 2) Provide Long-term storage for slow data rate modules, short-term storage for medium data rate modules. 3) Provide data compression on slow data rate telemetry for more efficient packing in storage memory. 4) Provide re-routing control in case a key communications system component fails.

11.2.3 Antenna Modules

The antenna modules will be linked directly with the central computers. Each module will contain a phased array and a communications transceiver. Phased array antennas are different from the standard parabolic dish in that they are electronically steered by changing the phasing of the array elements. No mechanical orientation system is needed. The central computers will control the phasing for proper orientation of the signal

beam toward the relay stations. To lower the power consumption of the system, only one of the four phase array/transceiver systems will be enabled at one time.

11.3 External Design

The external system will include the antenna/transmitter units mounted in modules on four of the eight sides of the platform, module for the communications computer, and one for optical on-board memory storage.

11.3.1 Antenna/transceiver units

Although the system is modular, the antenna/transceiver units must always occupy the same four modules for proper operation. The phased array antennae are sensitive to out-gassing from the attitude control motors. Consideration must be taken to keep exhaust from passing over these modules.

11.3.2 Central Computer Module

The central computer module must also occupy a specific module because of the link to this module from all the other modules with optical fiber. Making this location anywhere on the platform would vastly increase the number of optical fibers connections.

Data from modules will be linked to central fiber optic network by using a light link instead of physically splicing the optical fiber with the modules system. By using a infrared light link, replacing modules would be easier for remote vehicles.

11.3.3 Optical Storage Module

The optical memory module would use laser/magnetic technology to provide a read/write storage system. Data could be stored temporarily during system changeovers, or as a permanent location for non-critical data to be stored and later removed by the GTV as a complete module.

11.4 Data Format

With the current state of data communications, many options are available for transmission of data to/from the Moon base. But because of power restrictions and desire for small error rates, some of the newer communications formats out-perform older analog modulation techniques.

11.4.1 Pulse Coded Modulation

Pulse Coded Modulation (PCM) techniques are useful for data communication because of its binary structure. All pulses are the same height and shape; therefore, it is only necessary for the receiving equipment to detect the presence or absence of a pulse for signal detection. Distorted pulses do not degrade the signal as long as the pulses can be recognized.

PCM systems are becoming increasingly more important as a result of certain inherent advantages:

1. In long-distance communications, PCM signals can be completely regenerated at intermediate repeater stations because all the information is contained in the code. Essentially a new, noise-free signal is regenerated each time the signal is repeated. Noise doesn't propagate as the signal is repeated.
2. The modulation and demodulating circuitry is all digital, thus affording high reliability, and is compatible with on-board computer systems.
3. Signals may be stored in a digital format using present digital storage techniques. Data may be stored as data is gathered, and transferred when platform is within direct communication range with the lunar base. Storage allows slow data to be transferred in a fast burst, thus increasing system efficiency.
4. Efficient data compression techniques can be performed on data while in a digital state to reduce transmission rates and increase system efficiency.
5. Appropriate algorithms exist that can reduce the effects of noise and interference on the digital signal. Digital signal enhancement can be used to filter noise out of the original signal.

11.4.2 Data Bit Rates

The bandwidth required for transmission is proportional to the baud rate. The need for high data rates becomes apparent when many modules are connected through one communication system. Data rates of several hundred Mbps will be possible with improved communication system designs. This number may increase to 1 Gbps by 1995.

Slower data could be multiplexed into a dense signal with present day technology. For example, the present PCM telephone systems in the United States multiplex 24 4-KHZ telephone conversations on a single channel. These 24 lines are time-multiplexed to give 192 bits per frame. One extra bit is inserted to give frame synchronization, yielding 193 bits/frame. Each

input channel is sampled at an 8 KHZ rate resulting in a frame interval of $1/8$ KHZ or 125 micro seconds and a clock rate of $(193)(8 \text{ KHZ}) = 1.544 \text{ Mbps}$.

The bandwidth of the signal is a direct function of data rate. Using a Non Return to Zero binary encoding format, the signal bandwidth is approximately $1/2$ of the data rate. For data transfer at 1.544 Mbps, a bandwidth of 777 KHZ would be required.

11.5 Power Budget

Because of the limited power aboard the platform, the complete communications system power will be limited to 100 watts. This power must be divided between the Antenna/transceiver modules, and the communication system computers. The Antenna/transceiver modules will take 50 watts, and the computers, optical storage, and optical bus system will use the rest.

11.5.1 Transmitter/Receiver Power Requirements

Transmitter will require a large amount of power because of the need to transfer data across large distances to the relay sites. The transmitter power requirements can be reduced if paired with an antenna system with a directional pattern. For example, if our system needs at least 50 watts of transmitter power to provide reliable communications, the transmitter would need to supply 50 watts of RF power to a isotropic antenna to fulfill this requirement. If instead of a isotropic antenna we used a parabolic dish with 37 DB gain, the transmitter would only need to supply 10 Milli-watts for a 50 watt effective output signal.

11.5.2 Communication Computers/Storage Power Requirements

Computer power requirements are a direct function of the processing speed of system, and the materials used to construct the system hardware. Power requirements can be reduced further by operating the system in a semi-cryogenic environment. With a total power budget of 45 watts for this subsystem, each one of the three computer systems would require approximately 10 watts of power. Data storage would be limited to 10 watts, and the optical bus 5 watts.

11.6 Size and Mass Budgets

Mass for the communications system will be limited to 50 kgs for the complete system. Size will be limited to the maximum dimensions of a module on the platform which is approximately $0.57 \times 0.57 \times 0.3$ meters cubed.

11.6.1 Transceiver/Antenna Size and Mass Budgets

Most space communications are done with a large parabolic dish, but using a dish would defeat the design constraints for modularity. Phased arrays on the other hand are flat, and would provide the necessary directional gain. Phased arrays are comparatively light in weight and each package with transmitter would be limited to 10 kgs. Thus four packages would require 40 Kgs.

11.6.2 Communications Computers Size and Mass Budgets

The communications system's three central computers will fit in a single module. The total weight for the computers will be 30 kgs.

11.7 Communication System Backup

System Back-up is an integral part to any communication system design, especially on a space vehicle that will not carry a maintenance crew. Possible failures could be in the following systems: 1) Antenna failure, 2) Transmitter/Receiver failure, 3) Communications Computer failure, 4) Optical Data bus failure.

11.7.1 Antenna Failure

In the event of a major failure in one of the four phased arrays, one of the other three systems can replace the defective unit with a command from the central computers. The platform might have to rotate slightly to permit the other array a direct line to relay satellites. During a next GTV mission to the platform, the damaged antenna can be replaced.

Phased arrays are generally tolerant to minor damage. A study done on a phased array radar antenna designed for the B-1 bomber showed that 6% of the array elements needs to be damaged before the system performance falls below specifications.

11.7.2 Transmitter/Receiver Failure

Since each of the four antenna/transceiver modules contain a complete system, failure correction would follow the same procedure as for a damaged antenna system.

11.7.3 Communications Computer Failure

A single computer failure would be detected by the other two computers during routine error checking routines. The defective

EARTH-MOON SYSTEM

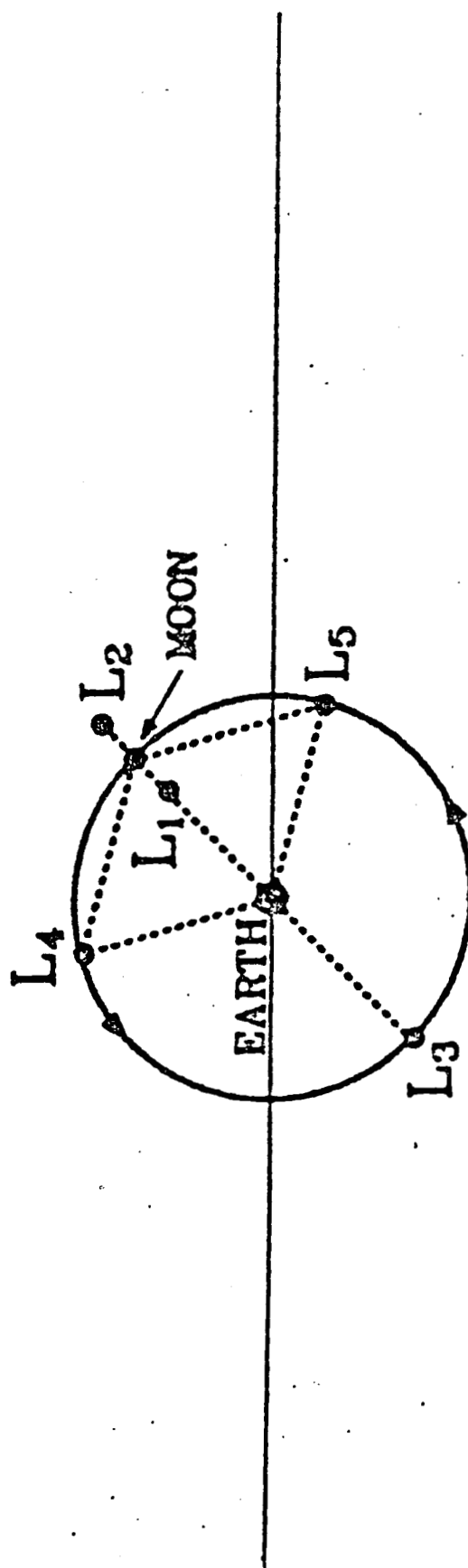
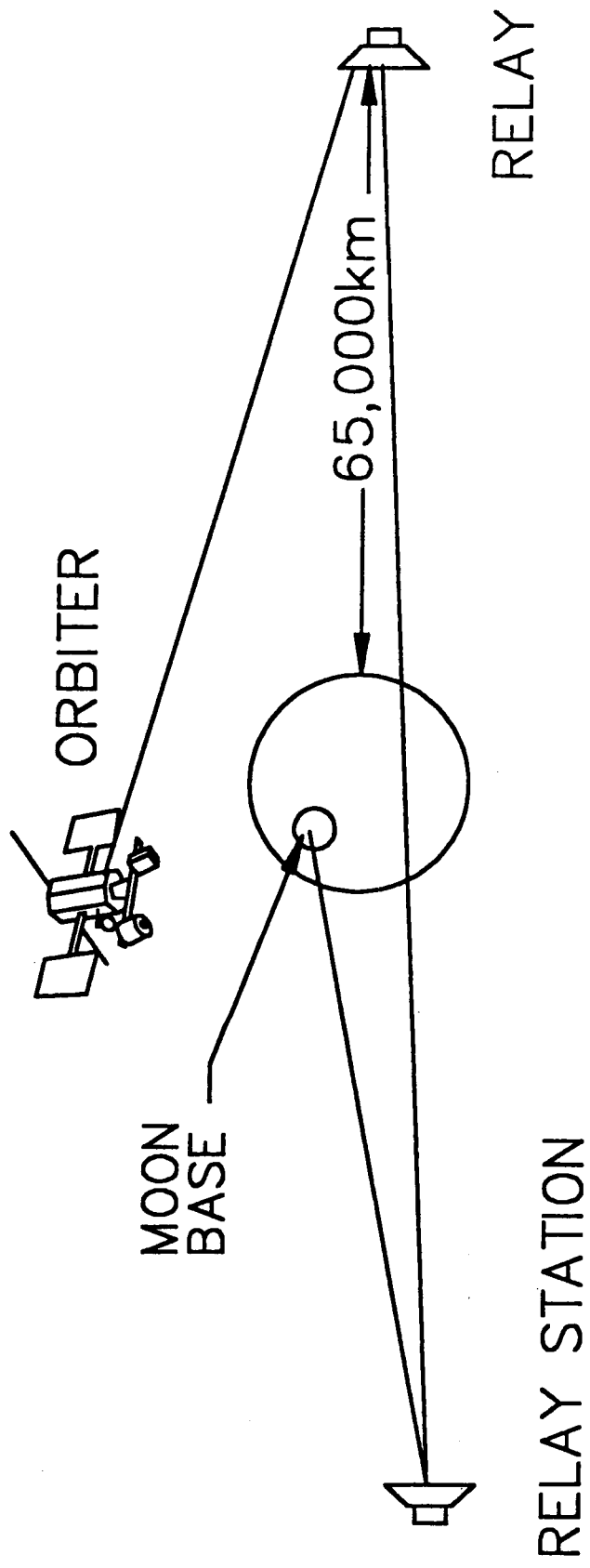


Figure 11.2 Earth-Moon Lagrange Points

RELAY STATIONS



MOON RADIUS = 1730km

Figure 11.3 Relay Satellite Location

computer would be turned off by the other two computers and work load transferred accordingly, and the defective computer would be replaced during a GTV visit.

11.7.4 Optical Data Bus Failure

Should a optical fiber link from a module fail, two other lines would provide backup communication potential since three lines feed each module. This failure could be caused by the Gallium-aluminum-arsenide transmitter or photo detectors on each line. In any case the other two lines would handle the load until the line could be replaced.

11.8 Relay Sites

To fulfil the system goal of continuous communications with platform and base, many options for relay stations were investigated. Two of the most promising are discussed below.

11.8.1 Ground Based Relay Stations

A system of ground based relay stations could be erected on the Moon's surface to provide a constant communication link with platform and base. Because of the vast distances between sites, and the general topography of the Moon, this system would be complex and hard to maintain for a successful communication link. Possibilities exist of using dielectric-slab surface-wave modes for radio communication on the Moon over long distances (1000 km or more), but these have yet to be proven for a reliable communications system.

11.8.2 Satellite Relay Stations

Orbits exist that allow a lunar base to have a lunar synchronous system equivalent to a geosynchronous system on Earth. These orbits are called Lagrange points. The Lagrange points are located approximately 65,000 Km between Earth and Moon, and behind the Moon. Two satellites located in these points would provide complete coverage for platform to base. Figure 12.2 shows the Lagrange points in relation to the Earth-Moon system, and Figure 12.3 shows a possible worst case communication path between platform and base. These satellites should be equipped with a new generation space antenna technology with diameters approaching 300 meters. These have been configured for launch into space using the present Space Shuttle system. Using large parabolic dishes would further reduce platform transmitter power while allowing the same communications system performance.

REFERENCES

Okoshi, Takanori, **Optical Fibers**, Academic Press, New York, New York, 1982

Stutzman, Warren L., **Antenna Theory and Design**, John Wiley & Sons, Inc., 1981.

Krauss, John, **Electromagnetics**, McGraw-Hill Series in Electrical Engineering.

Stremmer, Ferrel G., **Introduction to Communication Systems**, Addison-Wesley Publishing Company.

CRC Handbook of Space Technology: Status and Projections.

Kolcum, Edward H., **Shuttle Transmission Links Will Rely on Fiber Optics**, Aviation Week, v120, March 12, 1984 p 249.

NASA Plans Infrared Devices for Communications in Shuttle, Aviation Week, v118, Feb 21, 1983 p 69.

Klass, Philip J., **B-1 Pioneers Airborne Phased Array**, Aviation Week, v120, April 9, 1984, p 84.

Elson, Benjamin M., **Shuttle-Compatible Antenna Developed**, Aviation Week, v115, May 5, 1981 p 46.

12.0 Power System

The purpose of the power system group in the design of the LOP was to create a modular power system which could meet the varying power requirements of the LOP as well as maintain operational power during power module changes and during power system failures. The mass budget set for the power system was 70 kg. It was found that the power requirements would be normally about 660 W continuously but that during the operation of the Raman package as much as 1900 W would be required while in the shadow with an accompanying requirement of 400 W while in the light. In order to meet these requirements, as well as others, the power system consists of two solar panels, several battery packs, and two 50 W Radioisotope Thermal Generators. The optimal physical size of the various components of the power system and the configuration of this power system will also be discussed.

12.1 Options and Considerations

Three main system design options were considered for powering the LOP: (1) Solar arrays with secondary batteries, (2) Radioisotope Thermal Generators (RTG's), and (3) Solar arrays and secondary batteries in combination with RTG's. Because of the mission duration of the LOP platform, primary (nonrechargeable) batteries were discarded as a consideration for system power. These options represent the main power sources used in spacecraft design today and are expected to be the main sources in the future as well. Conversion efficiencies and mass efficiencies on all these options are predicted to improve by the year 2020, our proposed launch date. In our analysis, we tried to use conservative estimates of all these projections.

There were several considerations which affected our decisions; these were: (1) reliability, (2) life span, (3) efficiency, (4) modularity, and (5) thermal and environmental effects. These considerations were used to determine the type of power system that would be used. They were evaluated and ranked in a decision matrix with the result that a solar array/secondary battery system with accompanying RTG's was determined to be the best power system for the LOP's needs (see Figure 12.1). The reasons for the weightings used in the decision matrix follow.

12.2 Solar Array, Secondary Batteries

Solar arrays/batteries are the most efficient of all the power sources evaluated even when considering the additional mass of the batteries. Solar arrays in conjunction with batteries are however not as reliable as RTG's. The solar arrays are also rather fragile in comparison with RTG's and can be damaged by short circuits, small meteors or any number of occurrences. If the solar arrays were to fail, the LOP would have power only as long as the secondary batteries held a charge. Therefore the

DECISION MATRIX FOR LOP PLATFORM POWER SYSTEM

	Life Span (8)	Efficiency (w/kg) (7)	Thermal/Environmental Effects (3)	Reliability (9)	Modularity (5)	Totals
Solar Array With Batteries	6 / 48	9 / 63	8 / 24	4 / 36	6 / 30	201
RTGs	9 / 72	3 / 21	3 / 9	8 / 72	8 / 40	214
Solar Arrays With Batteries and RTGs	6 / 42	7 / 49	4 / 12	8 / 72	9 / 45	226

Figure 12.1 Decision Matrix

solar array/battery power system was given a high efficiency rating (9) and a low reliability rating (3). Solar arrays have a relatively good life span but gradual degradation of efficiency due to solar erosion limits their output power after about 15 years to between 70% to 85% of the beginning of life value. Thus this power system was given a medium rating for life span (6). The modularity of solar arrays is slightly less than the other power options (transport, connection to orienting motors and precise directional placement being somewhat more difficult), however array placement can partially compensate for this shortcoming so the system was given an average rating (6) for modularity. except for a small amount of heat the environmental effects of this system are almost nil therefore it was given a favorable rating in this area (8).

Two types of secondary batteries were considered for use in conjunction with the solar arrays. These are:

1. Nickel-Cadmium (Ni/Cd) approx 50 W/Kg by the year 2020
2. Nickel-Hydrogen (Ni/H₂) approx 60 W/Kg by the year 2020

Ni/Cd batteries have been used extensively in past scientific missions but are nearing the limits of their technological capabilities. Ni/H₂ batteries, however, are beginning their developmental life and by the year 2020 will probably provide a greater efficiency than Ni/Cds. Therefore Ni/H₂ batteries were chosen for array support.

The life span of a Ni/H₂ battery pack for the LOP can only be estimated. The high cycling demands of the platform will serve to reduce battery life but the low depth of discharge will tend to increase it (see depth of discharge later in this report). By keeping the batteries cool and with deep discharge reconditioning (controlled discharging of the batteries over "long" time periods) battery life should be well over 12 years.

Alkali metal high-energy couples (Na/X and Li/X) are another possible source of battery power which may be feasible by 2020 but they are currently far behind Ni/H₂ batteries in terms of development and were not considered for this application.

12.3 Thermal Power

Radioisotope thermoelectric generators are reliable and can be incorporated into an extremely versatile power module that can be replaced or repaired by a small shuttle type repair vehicle. The reliability of RTG's has been demonstrated by several missions including the deep space Voyager missions. Thus, they were given high ratings in the areas of reliability and modularity, (8) and (9) respectively. RTG's can also provide nearly constant power output over long periods of time very well, depreciating only small amounts. They were therefore given a high rating in the area of lifespan (9). Their shortcomings are

LOP Power Requirements for Different Instrument Modules

In all cases 100 W was assumed for communications, 75 W For miscellaneous needs and 200 W for growth except for the Topographic Mapping mission which assumes only 170 W for growth.

Metals and Radioactive Elements Mission

	Power in light	Power in shadow
Communications	100 W	100 W
Miscellaneous	75	75
Growth	200	200
Electron Reflectometer	5	5
Magnetometer	3	3
Ultraviolet Spectrometer	13	0
Gamma ray Spectrometer	10	10
Visible and Infrared Mapping Spectrometer	10	0
X-ray Spectrometer	10	0
Radar Altimeter	28	28
Total	457	421

Topographic Mapping

	Power in light	Power in shadow
Communications	100 W	100 W
Miscellaneous	75	75
Growth	170	170
Geodesic Imager	15	0
Radar subsurface mapper	200	200
Laser Altimeter	50	50
Radar Altimeter	28	28
Total	638	623

Thermal, Silicates and Water

	power in light	power in dark
Communication	100 W	100 W
Miscellaneous	75	75
Growth	200	200
Thermal Infrared Mapping Spectrometer	12	12
Microwave Radiometer	10	10
Gamma ray Spectrometer	10	10
Visible and Infrared Mapping Spectrometer	20	20
Visible High Resolution Solid State Imager	20	20
Radar Altimeter	28	28
Total	475	475

Active Mineral and Element Detection

	power in light	power in dark
Communication	100 W	100 W
Miscellaneous	75	75
Growth	200	200
Raman Spectrometer	0	1500
Altimeter	28	28
Total	403	1903

Figure 12.2 Power Requirements for Mission

ORIGINAL PAGE IS
OF POOR QUALITY

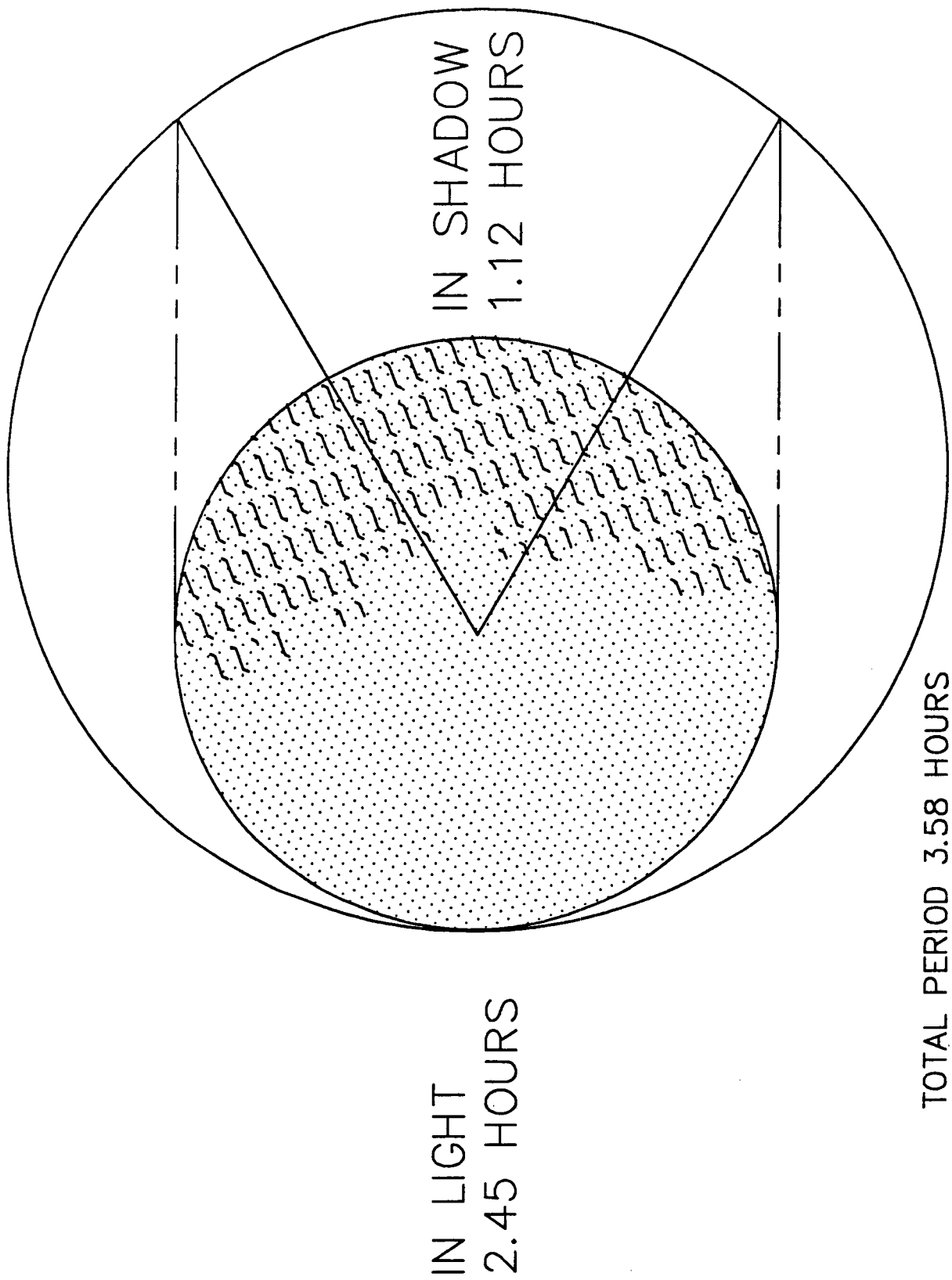


Figure 12.3 Orbit Sunlight Environment

evident, however. Since RTG's produce a high amount of excess heat, they could pose problems for some of the scientific instruments that are to accompany the platform. Sensitive instruments would either have to be shielded from the RTG's or the RTG's would have to be placed some distance from the main body of the spacecraft. Therefore, RTG's received a low rating in the area of thermal/environmental effects (3). RTG's are also extremely inefficient sources of power so their mass is quite high in comparison to the other power alternatives, and they received a low rating in this area also (3). Cost was only of minor importance in our decision but must be kept in mind as the cost of RTG's is and is expected to remain astronomical even if today's efficiencies are significantly improved.

12.4 Solar Array/Batteries/RTG's

In considering the diversity of scientific operations and the expected length of time the platform will be in orbit, the power system that we found most appealing is an integration of all the best assets of the systems mentioned above. Such a system requires a more complex implementation than the one source options but there are many factors in its favor.

The use of solar arrays and batteries allows the utilization of the most efficient of all the systems for the production of power, and thus the solar array/battery/RTG system still receives a fairly high efficiency rating (7). The reliability of an RTG would be particularly advantageous for essential mission systems such as communications and attitude control. In the case of a solar array/battery failure, the integrated system gets a good rating in this area (8). The modularity of this system would be even better than the other two systems since it would be easier to change the power system modules while still maintaining essential power to the LOP. It has been given a rating of (9) in modularity. The life span of the system will only be as long as that of the solar arrays, so it receives a rating of (6) for life span. Furthermore the thermal/environmental effects would only be slightly better than that of the RTG system since there would be less RTG mass in this system. It was given a rating of (4). As can be seen from the decision matrix in Figure 12.1, this system is clearly the best one for the LOP's needs.

12.4.1 Power Needs

The LOP's power needs will vary greatly depending on what instrument modules are being used. Power consumption by the non-'scientific instrument' portions of the LOP remain fairly constant. A power need of about 100 continuous Watts was assumed for communications while 75 continuous Watts was deemed to be sufficient power for both losses in the system and intermittent needs such as attitude control, propulsion, orienting motors, and others. An additional 170 to 200 W continuous power was

SOLAR ARRAYS

ORIGINAL PAGE IS
OF POOR QUALITY

Type: Multiple Band Gap
Conversion Efficiency (Energy Out/ Energy In) - 20%
Specific power: EOL - 220 W/Kg BOL - 286 W/Kg
Total Mass - 4.087 Kg
Degradation over lifetime - 30%
Total Power Produced: EOL - 899.23 W BOL - 1652 W
Maximum Acceleration: .5g
Cell Size - 2cm X 6cm
Cell Voltage - .5 V
Power per Cell (EOL) - .196 W
Current per Cell (EOL) - .392 Amps
Array Voltage - 33V
Total Number of Cells - 4590
Number of cells per Column - 66 (This is necessary in order to
get required voltage.)
Packing Factor 10% additional area
Total Final Array Area - 6.92 m²
Operating temperature: 50 degrees Celcius
Maximum angle off normal to the sun: 6.5 degrees Raman module
33 degrees other modules
Life: approx. 20 Yrs.

BATTERY

Type: Ni/H₂
Energy Density: 60 W-Hr/Kg
Mass: 59.6 Kg, 149 Kg Raman
Capacity: 3576 W-Hr, 8940 W-Hr Raman
Density: 2000 Kg/m³
Volume: .0298 m³, 7.45m³ Raman
Life: approx. 14 Yrs.

RTG

Power: 100 W
Mass: 13.3 Kg
Specific Power: 7.5 W/Kg
Life: Approx. 20 Yrs

TOTAL MASS

77 Kg, 166.5 Kg Raman

Figure 12.4 Values Used in Power System Computations

considered necessary as a 'growth' factor to make it possible for the LOP to carry other instrument modules with greater power requirements than those considered in this study and to create a 'cushion' for other unforeseen changes in power needs. If more than an additional 200 W is needed, the modularity of the power system will make it possible to replace the existing system with one capable of meeting this new demand.

Using these requirements and the power requirements for the individual scientific instruments determined by the instrument group, the power needs of the LOP while carrying the various instrument modules, both in the light and in the shadow of the Moon, was determined (see Figure 12.2). Three of the instrument modules will require about the same power, the maximum amount being required by the topographic mapping module. With this module, the LOP will require 638 W while in the light and 623 W while in the shadow. However, the power requirements of the Raman Spectroscopy package far exceed these power requirements. It requires 403 W while in the light and 1900 W while in the shadow.

12.4.2 Component size

The actual size of the different components of the power system were determined by creating a FORTRAN program (see Appendix 12) to minimize the total mass of the system while still producing power sufficient to meet the LOP's needs both in the light and in the shadow. Because the instrument packages have two very different power needs, the program was run twice, once for the Raman module and once for the other three modules. In each case a 'worst case' orbit was assumed. The worst case orbit being one in which a maximum amount of the orbit was spent in the shadow of the Moon where the solar array can not generate power. This orbit, as determined by the orbit group, has a shadow time of 1.12 hrs and a light time of 2.456 hrs and is shown in Figure 12.3. It was also assumed that the Raman module would only operate for 45 min while in the shadow. The efficiencies and specific powers for the different power producers are conservative estimates for the year 2020 obtained mainly from the CRC Handbook of Space Technology: Status & Projections. These values are listed in Figure 12.4.

The FORTRAN program was created using the examples in Spacecraft Systems Design and Engineering Space Power Subsystem (see references). A hard copy, explanation, and results of this program can also be found in the Appendix.

It was found that the minimum mass for the system occurred when the RTG mass was zero for both the Raman module and the other three modules power requirements (see Figure 12.5), but it was also found that the addition of two 50 W RTG's only increased the mass of both systems by 1.27 Kg. It was therefore decided that the additional mass was worth the reliability that these two 50 W RTG's would entail. If the solar array/battery

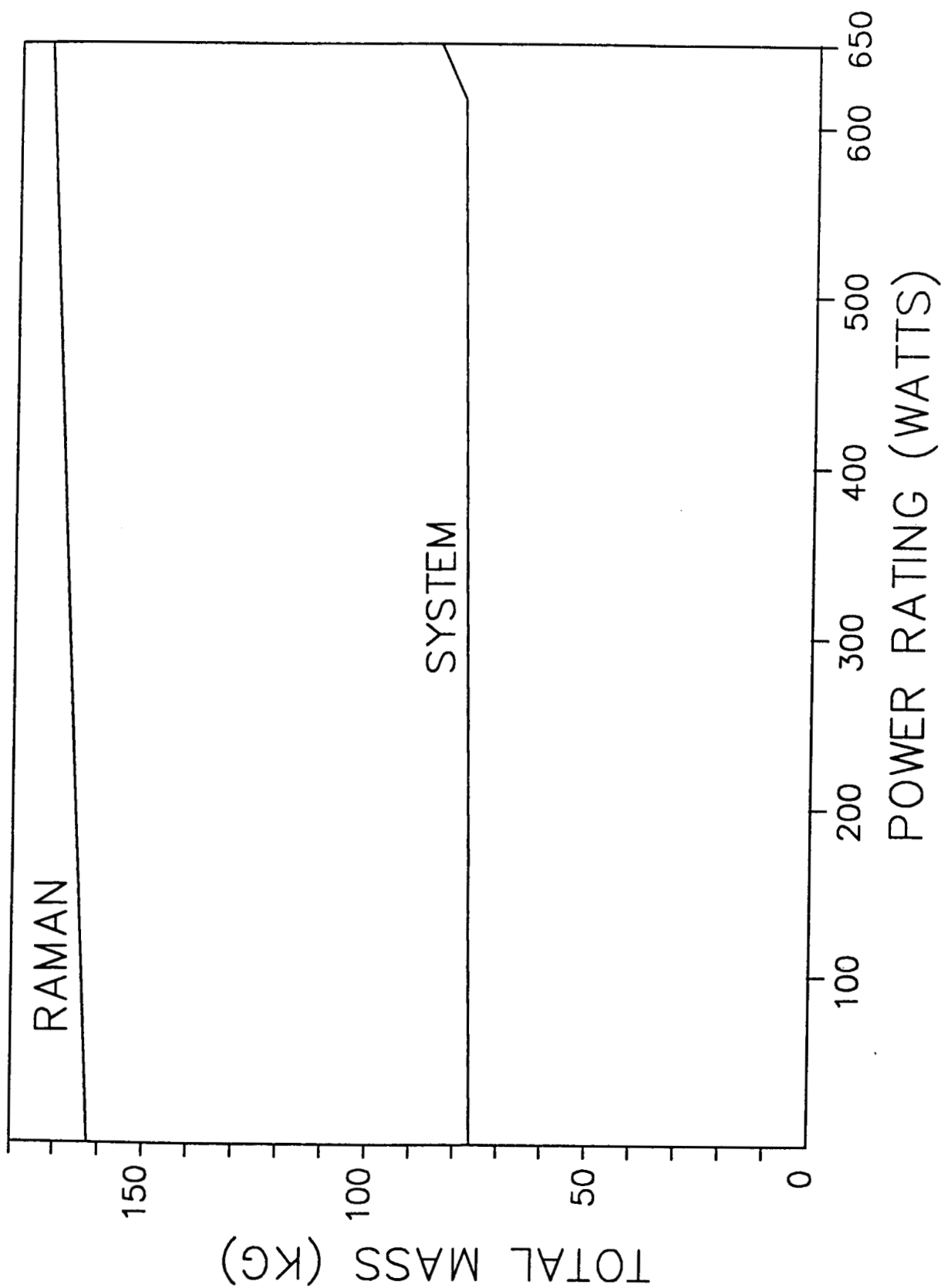


Figure 12.5 RTG Power vs. Total System Mass

system were to fail, the RTG's could still supply 100 W continuous power until repairs could be affected. This 100 W should be sufficient to keep the LOP in orbit until that time.

Comparison of the masses for the components of the two different systems showed that the difference in their masses was composed mainly of 89.43 Kg of batteries and only .56 Kg of solar array. Therefore, it would be best to have a solar array capable of supporting the Raman module on the LOP at all times, then to carry up the additional batteries needed for the Raman module with it. Thus the total mass of the power system will be 77 kg, usually, and 166.5 kg when the Raman module is in use. This is fairly close to the mass budget set by systems engineering for the power system. The masses of the various components of the power system are listed in the Appendix.

It may also be noted that the depth of discharge (DOD) in the results portion of the computer program is constant and very low, only 16%. This is because the DOD in the example used to create the program actually reduces to being the time in shadow divided by 15 and so becomes constant. This calculation is shown in the Appendix. The DOD is extremely small because of short orbital period and the high demands placed on the batteries while the LOP is in the shadow. The maximum recharge rate of the batteries is a function of battery mass. Since the time in the light (where the solar panels can supply energy) is so short and the drain on the batteries has been so large while in the shadow, a recharge rate in the range of 460 W is required. This requires a relatively large battery mass which makes for a very small depth of discharge.

12.5 Solar Array Sizing

In order for the solar arrays to be able to charge the batteries, they must have a higher voltage than the batteries. A voltage of 28 V was assumed for the batteries, so a voltage of 33 V was used to size the solar arrays. Unfortunately, the sizing of the arrays can only be very rough because the voltage and current characteristics of photovoltaic cells are usually determined by empirical testing of an assembled cell. Since the cells that would be used on the LOP have not been built yet, their characteristics have not been determined. Therefore, the values used are ones which are reasonable to expect in the year 2020. The computations were done by again following the solar array sizing examples in reference 1. They were also done in such a way that the array will produce the power necessary at its end of life. The values used and the computations are recreated in the Appendix.

To reduce stress on the solar panels during plain changes, it would be best to make them tall rather than long. Therefore, the solar cells will be divided into four arrays, two on each

LOP Platform Power Diagram

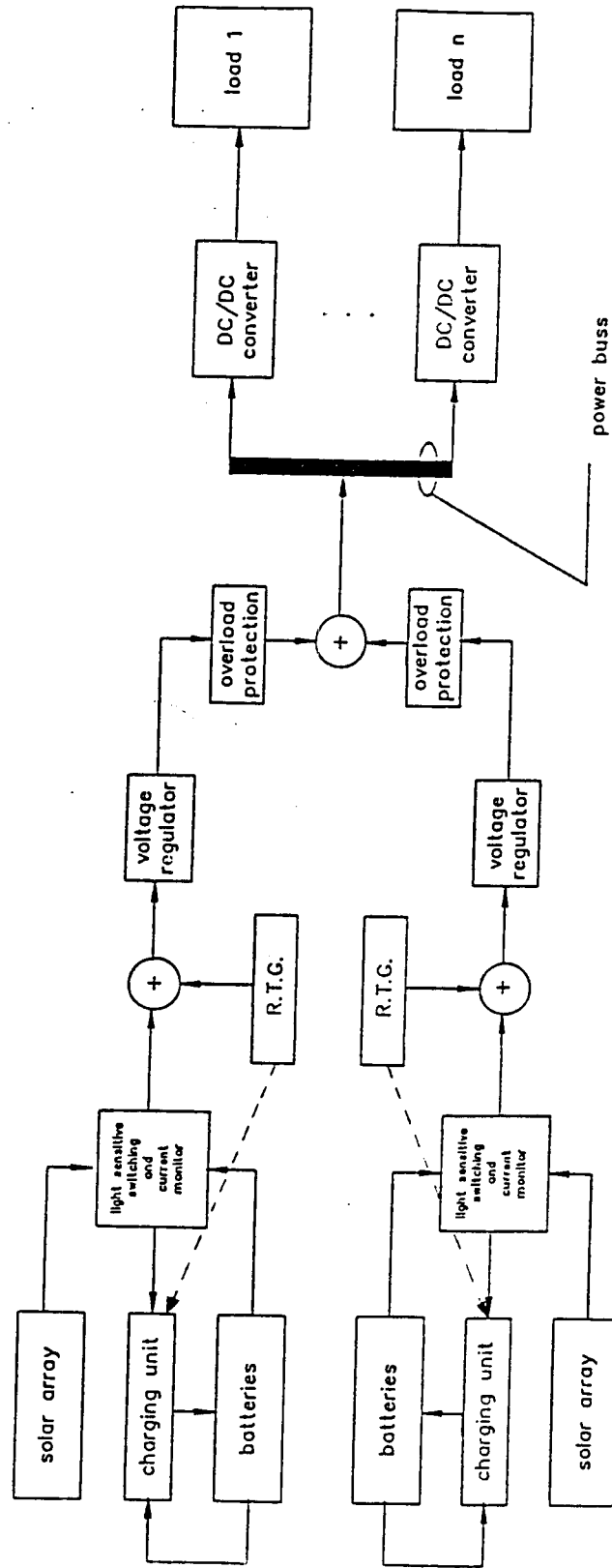


Figure 12.6 Power Diagram

boom, stacked on top of each other. It is interesting to note that although the arrays would only be able to be 6.5 degrees off normal to the sun while the Raman Spectroscopy module is being used, they can be as much as 33 degrees off normal while the other packages are operating and still produce sufficient power.

12.6 Design Parameters

The LOP platform Power Diagram, shown in Figure 12.6, provides a schematic representation of what the main considerations for the power distribution system were. Headlining the considerations list was the possibility of one or more of the power providing components completely malfunctioning. A simple solution came, in addition to using both solar array/batteries and RTG's, in the form of redundancy. A single branch of the power system consists of a solar array with dependent batteries and a single RTG. In case of emergency, a low power distress signal can be sent by the power produced by any one of the three components. However, since the batteries depend upon the solar cells for their charge, the level of redundancy in a single branch can only be something less than two. A second branch mirrors the first branch and provides a substantial increase in redundancy. Should a branch completely fail, it's image is still capable of producing enough power to run the entire communications system, the attitude control system, and some low power instruments.

A priority sensitive power bus is also necessary. In an emergency its first priority must be to provide power to the communication and attitude control systems. By connecting the high priority loads to their corresponding positions on the bus, they will receive their necessary current before the lower priority loads. It is also necessary to isolate each load with a current sensing switch (not shown on the diagram). When the current is too low, the load is cut off from the bus. The power bus is designed to supply a constant 28 V DC which is a NASA satellite voltage standard. A DC/DC converter can be used for loads operating at voltages other than 28 V DC.

Light sensitive switches will determine whether power will be drawn from the solar arrays or the batteries. During times of sunlight, a current monitor determines how much current to send to the battery charger and how much current is required by the rest of the system. When the batteries are charged, it must divert current from the charger to prevent overcharging.

Overload protection devices are used to prevent a short in one branch from crashing the whole system. Fuses or circuit breakers will isolate the individual loads for the same reason. A connection between the RTG's and the battery charger will also make it possible for the RTG's to charge the batteries during a time of emergency.

REFERENCES

1. CRC Handbook of Space Technology: Status and Projections, P. Michael Hord, CRC Press Inc., 1984.
2. Little Dipper Final Report, Utah State University, 1986.
3. NASA Space Systems Technology Model, NASA, 1984.
4. Technology Trends in Space Power Systems, E. W. Frank Jr. and H. Weiner, the Aerospace Corporation, 1984.
5. Scientific Satellites, W. R. Corliss, NASA, 1967.
6. Contributions of a Lunar Geoscience Observer (LGO) Mission to Fundamental Questions in Lunar Science, LGO Science Workshop Memembers, 1986.
7. Mars Lander/Rover Vehicle Development, Final Report, Utah State University, 1987.

13.0 Configuration and Structure

The lunar orbital prospector, LOP, is a satellite used in conjunction with a manned lunar base to examine the Moon. The LOP is to be executed around the year 2010 and uses projected 2010 technology. Originally, the LOP was to land and orbit the Moon as one unit, but further synthesis set the design to a permanently orbiting platform, the LOP, which would be serviced by a generic transfer vehicle, GTV. The LOP is the major design thrust for 1987-1988; the GTV may be designed in 1988-1989.

The LOP is a multi-mission modular spacecraft, MMS. It is similar to the EXPLORER platform [1] which has a central triangular region for modules as well as module attachment to top and bottom. The LOP, however, has eight sides for more modules and the capacity of expanding the base structure. The modules on the LOP range from propulsion to communications to scientific packages.

This report addresses four topics: Configuration, structure, material, and thermal control of the LOP. To have a strong, dependable spacecraft these topics must be addressed.

13.1 Configuration

The general configuration of any space vehicle is determined by the mission requirements. The configuration of the LOP is driven by three primary mission goals: an on board propulsion system, a science package requirement, and modularity. These mission requirements have been met as discussed below.

13.1.1 Propulsion System

Of all the factors contributing to the LOP design, the most significant is the propulsion system with its storage and thrust requirements. The fluctuating mass of the propellant and the large physical size of the propulsion system dictate that this module be at the center of mass of the system.

With this fact in mind, the basic structure of the spacecraft is baselined after the structure of INTELSAT V (International Telecommunications Satellite V). The main structure consists of a load bearing cylinder, housing the propulsion module, and two transverse load bearing plates. This is shown in Figure 13.1.

13.1.2 Altitude Thrust

The large loads of escape from Earth and orbital changes are supported by the central load-bearing cylinder. The cylinder structure has the advantage of carrying large axial loads with

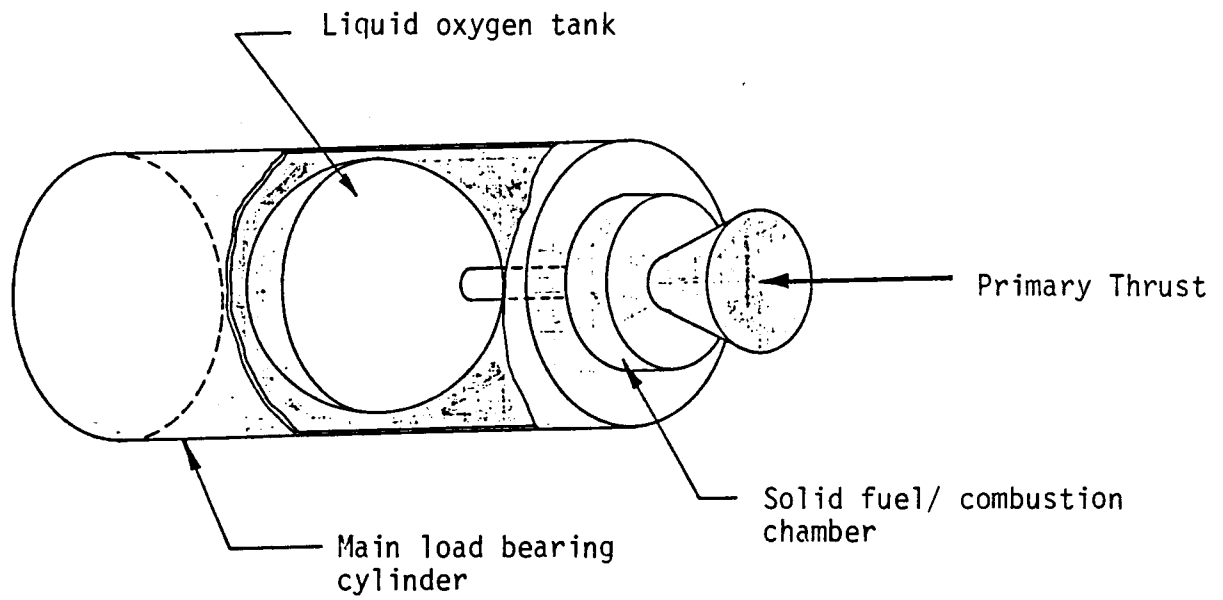


Figure 13.1 Main load bearing cylinder and propulsion system

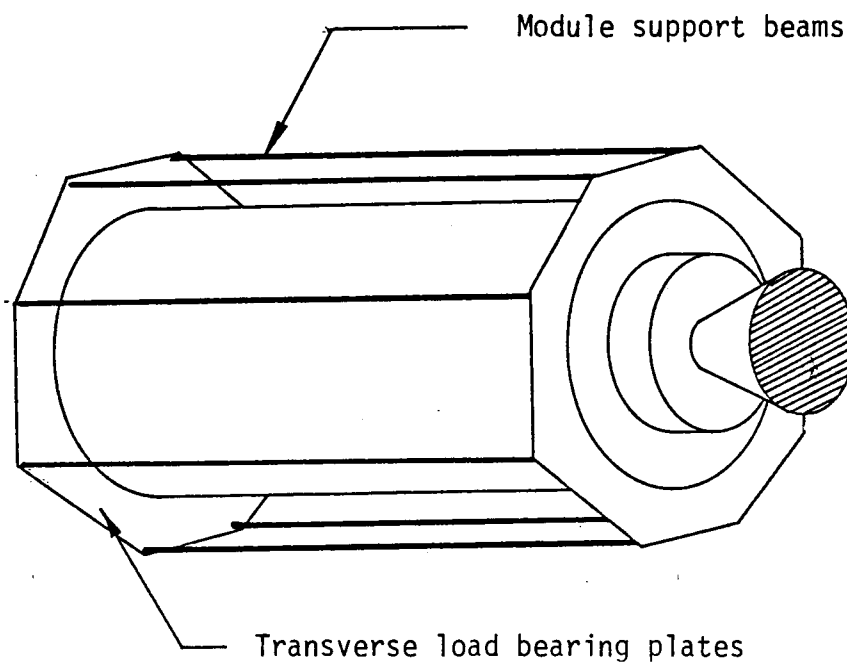


Figure 13.2 Construction diagram showing end plates and module support beams.

very thin walls, much like a soda can that supports a person's weight.

13.1.3 Attitude Thrust

The transverse loads to the LOP from attitude thrusts would damage the main cylinder if they were transmitted directly to the side of the cylinder, just like the soda can crumples when the person standing on it reaches down and taps it on the side. To handle this, octagonal plates are attached to top and bottom of the cylinder. These plates are made of honeycomb aluminum sandwiched between two layers of graphite/epoxy. The plates convey the transverse loads of attitude thrusts to the main cylinder without damaging the cylinder.

13.1.4 Module Support

The modules are supported by a truss structure that runs between the two transverse load bearing plates. This keeps the main cylinder untouched. This load bearing structure is strong and has the advantage of being lightweight. See Figure 13.2 for cylinder and plate conceptualization with the attached struts.

The propulsion module is placed at the center of the load bearing cylinder, ensuring that the fluctuation mass of the propellant is at the center of mass of the satellite. The module is shown with main structure Figure 13.3.

13.1.5 Science Packages

The satellite would be worthless without science packages. These packages contribute to the overall configuration of the LOP. These packages require nadir pointing for lenses, antinadir viewing for instrument cooling, and clearance from spacecraft thermal and magnetic interference of the spacecraft.

The requirements are met by placing the science module at the lower end of the spacecraft as shown in Figure 13.4. This provides an unobstructed view of the Moon and an unlimited distance to escape magnetic and thermal interference of the spacecraft.

13.1.6 Modularity

The concept of modularity requires docking locations be provided for a service vehicle. Although it would be convenient to dock immediately adjacent to the module to be serviced or replaced, the reality of being able to do this without damaging other nearby modules becomes obscure. Therefore, the design team proposes a soft docking location. A docking ring above the

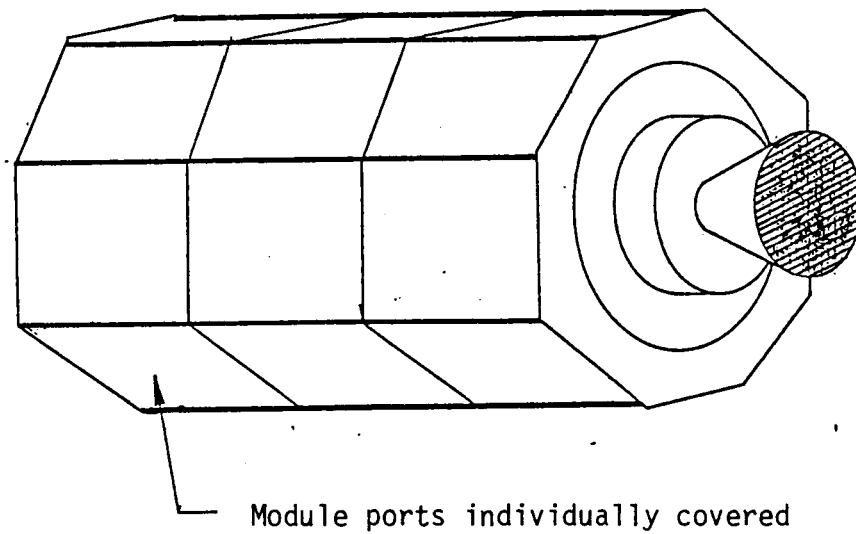


Figure 13.3 Configuration diagram showing module ports. The spacecraft provides 24 support module ports with communication and power utilities to operate attached subsystems.

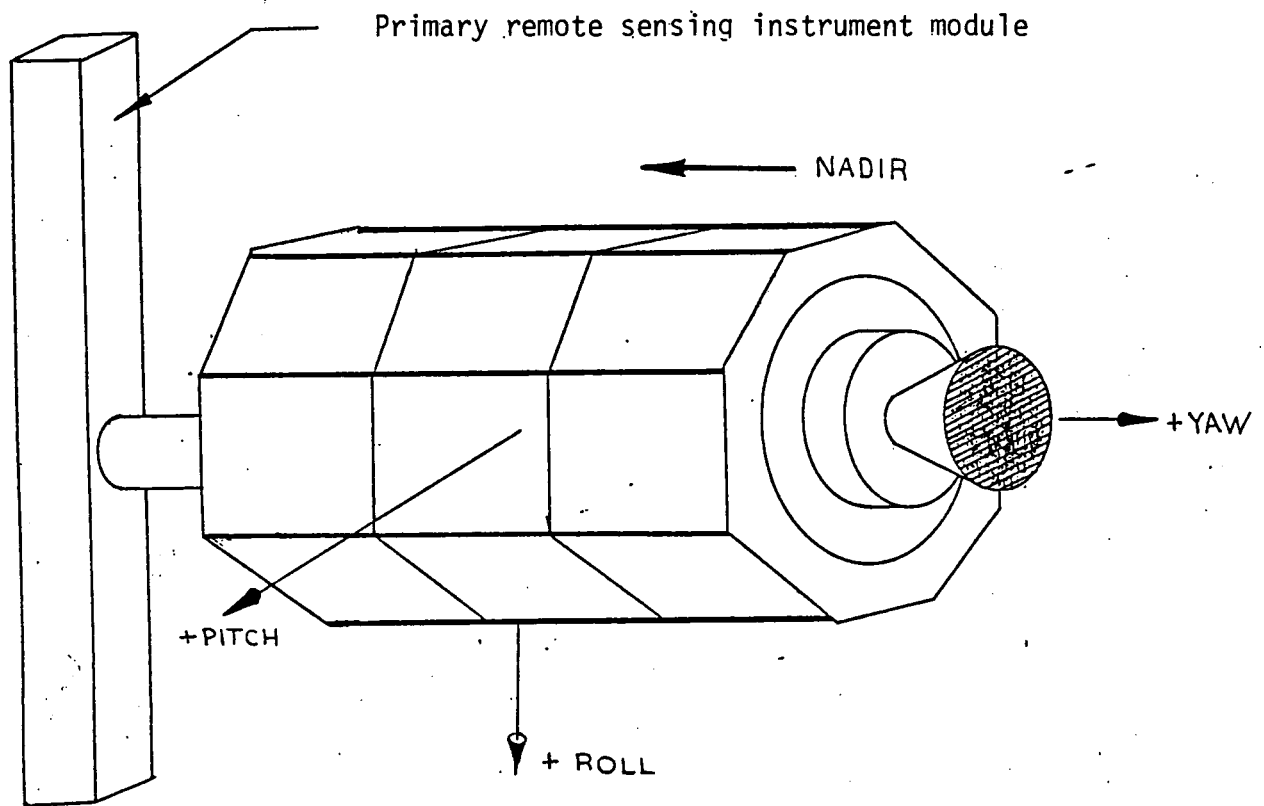


Figure 13.4 Configuration showing primary remote sensing module placement.

propulsion nozzle is supplied for the service vehicle to dock. See Figure 13.5 with the docking ring added.

A preliminary design of the service vehicle is essential to complete the docking aspect of the design. The design team proposes this as the next step in the Lunar Orbital Prospector mission design.

Making a system completely modular calls for standard mounts for the various modules. The locations of these mounts are found on the structure's support trusses. Details of the attach locations are not provided at this time, but it is considered a relatively trivial problem.

13.1.7 Other Modules

Miscellaneous power, communications, and instrument systems are located in several of 24 spacecraft side ports. Four phased array antennas are mounted symmetrically on the spacecraft. This is done to ensure that communication is possible in all directions (reference Communications section of this report). The multi-module power system complete with RTG's, solar panels, and battery modules is added to the system also. The excessive heat radiated by the RTG's requires that they be boomed away from the satellite. The solar panels are placed on rotating hinges in order for them to be near normal to the sun for maximum performance. These panels are also boomed away from the spacecraft to avoid contamination due to attitude control thrusters. The altimeter is mounted on the nadir pointing end of the spacecraft and boomed out a short distance to ensure an unobstructed view of the Moon.

The attitude control system described earlier is shown with the attitude control thrusters mounted on the momentum wheel modules. The complete artistic drawing and the technical drawing are shown in Figures 13.6 and 13.7.

13.2 Sizing the Structure

With the determination of the material to be used for the structure and the booms, graphite epoxy, it is necessary to do a stress analysis on the satellite to determine the mass of the structure without the modules. To do this, the type of trusses to be used for the booms must be determined. M. S. Anderson indicates that a statically determinant truss "has the advantages of being free of thermal stresses for all temperature distributions." This fact is significant for the applications of the LOP. However, a statically determinant structure is not as strong as a truss with additional reinforcing diagonal members attached.

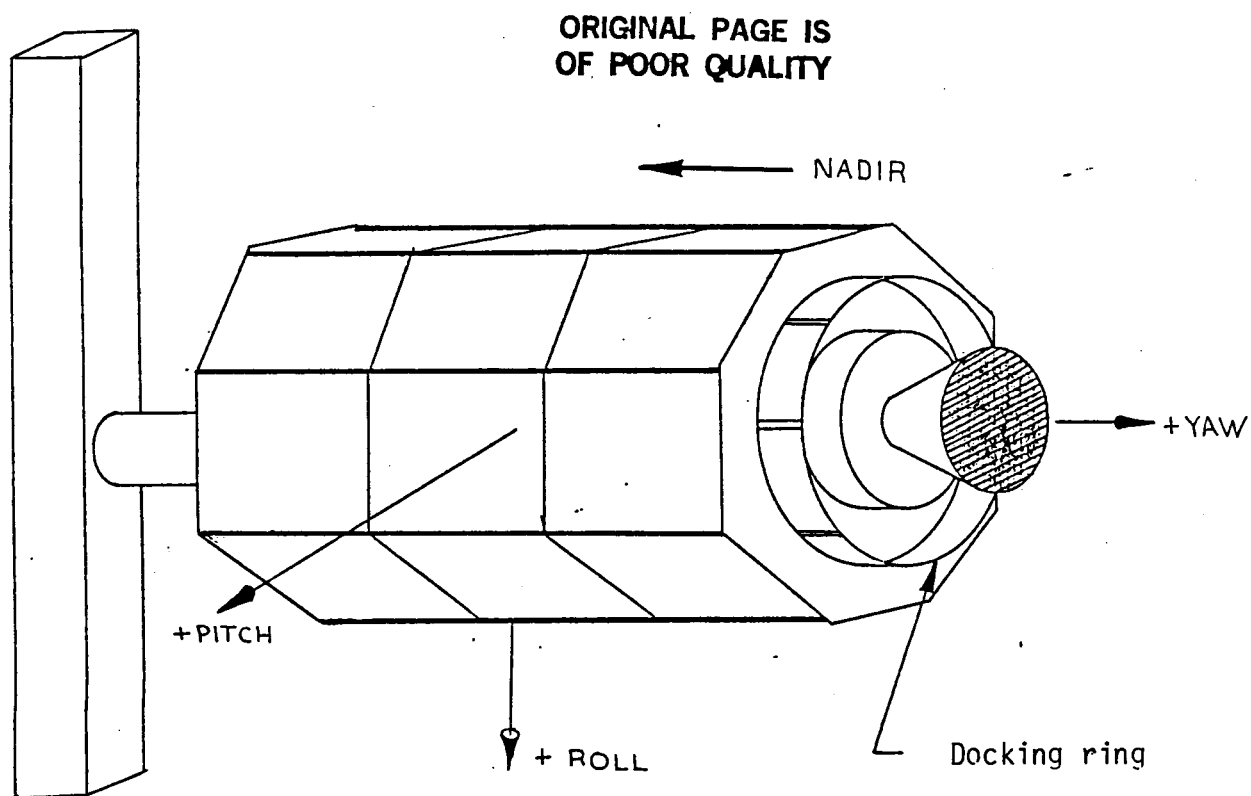


Figure 13.5 Docking ring surrounds propulsion system and provides location for service vehicle docking.

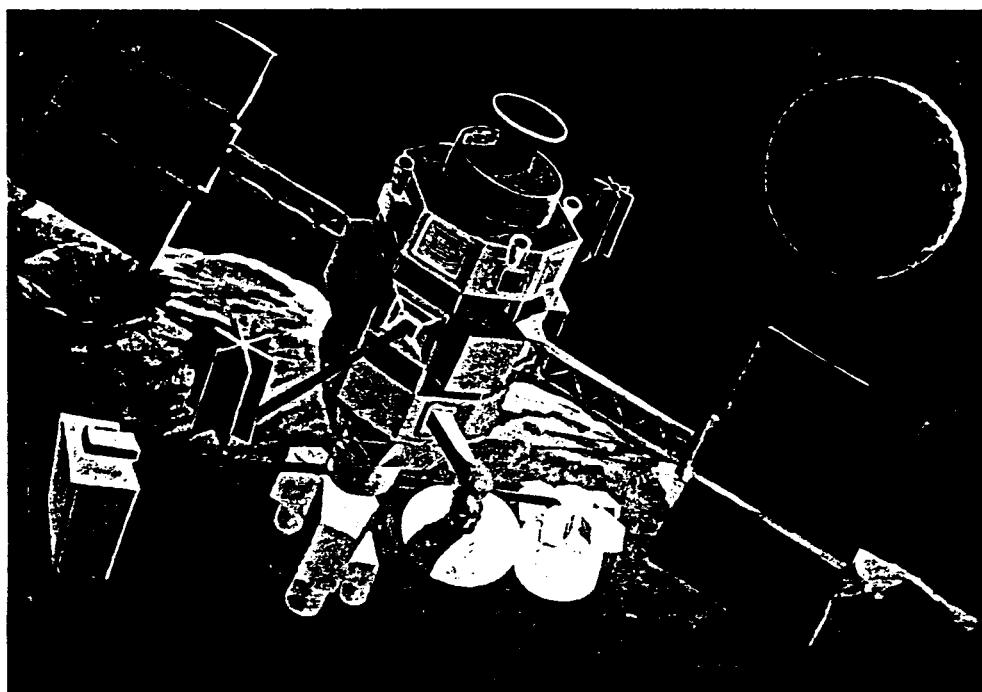
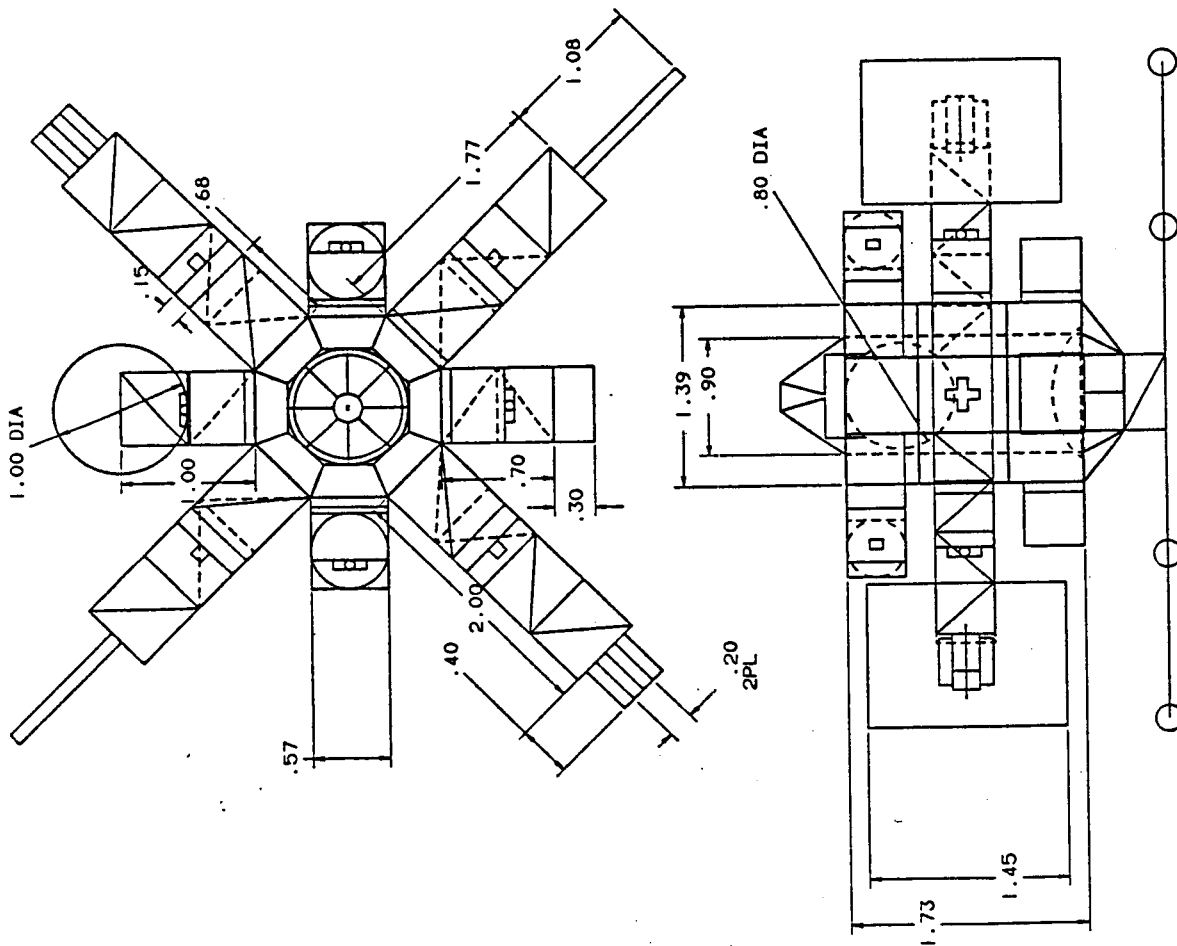


Figure 13.6 Artistic rendering of final configuration.

ORIGINAL PAGE IS
OF POOR QUALITY




 USU/CAD/CAM COLLEGE OF ENGINEERING	
TITLE PLATFORM DESIGN	
DATE 01/10/00 DRAWN BY KYLE ADAMS CHECKED BY ME 595	SHEET 01 OF 01 Dwg Line C DRAWING NUMBER

Figure 13.7 Technical drawing of final configuration. All dimensions are given in meters.

The on board propulsion system's acceleration of 0.5 g's must be handled by the trusses. They must have a high natural frequency and be capable of rapidly damping out any vibrations that may occur through docking or through any other impacting force.

To have both the advantages of a high natural frequency and relieved thermal stresses, M. S. Anderson suggests additional diagonal stiffeners. These stiffeners have dampers which are designed to provide stiffness at the frequencies of concern, but at lower frequencies resistive forces through these additional members would be negligible. These trusses will be used and are shown in Figure 13.8.

Although for the final design it would be pertinent to have a complete dynamic analysis coupled with a finite element analysis, this approach is beyond the scope of a preliminary design. It was determined by the design team that a static structural analysis with some factors of safety added would give sufficient results for a good preliminary estimation. This approach has been verified by Jim Burke (Jet Propulsion Laboratories) to be common for preliminary designs.

The force applied to the trusses is calculated using Newton's law, $F = ma$. Using four member trusses, the analysis is simplified by analyzing one member with one-fourth the force applied. A computer program has been written to solve for the maximum moment on the beam for various outside diameters which is at the point of attachment to the platform (see appendix). Using $\sigma = Mc/I$, as explained in most mechanics of materials texts, the program then calculates the required thickness of the booms. The results have been spot checked and are listed in the appendix. The design team has chosen 10 cm O.D. members for the trusses.

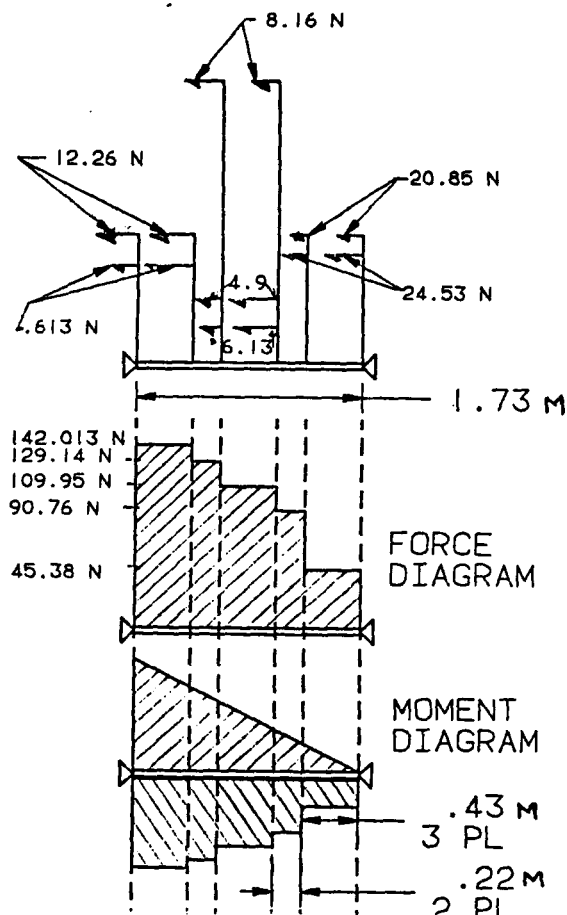
The results of the analysis indicate that the beams can be very thin, and the thickness will be limited by construction constraints. Jim Burke has verified that this is common in satellite design.

The main beams of the platform are analyzed by means of a force-moment diagram (see Figure 13.9). Once again the required thickness is small and these will be lightweight.

The thickness of the main load bearing cylinder has been determined by the method explained earlier. Construction restraints are also the limiting factor in this case.

13.3 Material

A suitable platform for the LOP must satisfy the launch requirements as well as incorporate the proposed docking of the GTV, the orbit changes, the thermal cycling of the LOP in and out



Element being analyzed is the vertical module support bars which bear the primary instrument inertial loading.

MAXIMUM MOMENT = 45.25 N-M


 USU/CAD/CAM COLLEGE OF ENGINEERING			
TITLE FORCE/MOMENT DIAGRAM			
DATE 06/07/88	SCALE NONE	DWG SIZE A	SHEET 01 OF 01
DRAWN BY		DRAWING NUMBER	
JAMES ADAMS		ME 505	

Figure 13.9 Force and moment diagram used to analyze the peak stresses on the instrument module port.

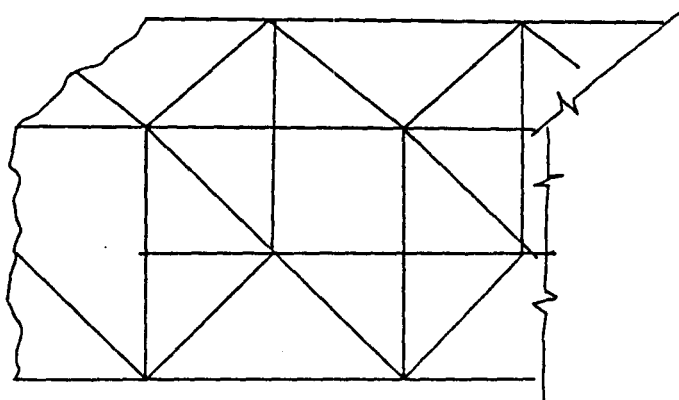


Figure 13.8 Truss structure of zero thermal expansion design. Each node is statically determinate. This basic structure is used to support each of the support modules.

of the Moon's shadow, and total mass of the platform. Two sources are considered for materials: the Moon, and Earth. If material could be made on the Moon the cost of transportation from the Earth might be reduced. The third section of MATERIAL addresses space environments.

13.3.1 Lunar Material

Lunar fiberglass is being studied by Clemson University [3] but they have only addressed how to make it, and not what its mechanical properties are. For analysis purposes this is about as useful as making the LOP out of green cheese from the Moon.

Aluminum from the Moon was also considered, but the yield rate is only enough for the fuel requirements and not the actual structure. Since the bulk of the LOP is to be launched from Earth the best method is to fabricate it on Earth.

13.3.2 Earth Material

The behavior of the spacecraft structure is directly related to the materials used to construct it. In order to determine the best material to build the structure of the platform, several different materials were considered:

- * Titanium
- * Aluminum
- * Composites (graphite/epoxy)

A comparison of the considered materials is summarized in Table 13.1.

The spacecraft materials which determine the platform behavior must satisfy the following conditions to be effective in the LOP mission:

- * Lightweight
- * Low thermal expansion
- * Stiff
- * Vibration resistant
- * Fatigue resistant
- * Creep resistant
- * Impact resistant

Graphite/epoxy composite is the best choice for the platform material. Gr/Ep is rapidly finding increased use in aerospace. The first Gr/Ep structure to be flown in space was the support truss for the Application Technology Satellite. It was chosen principally for its low coefficient of thermal expansion. "NASA is using composites for the antenna reflectors of its Advanced Communications Satellite

SPACECRAFT MATERIALS

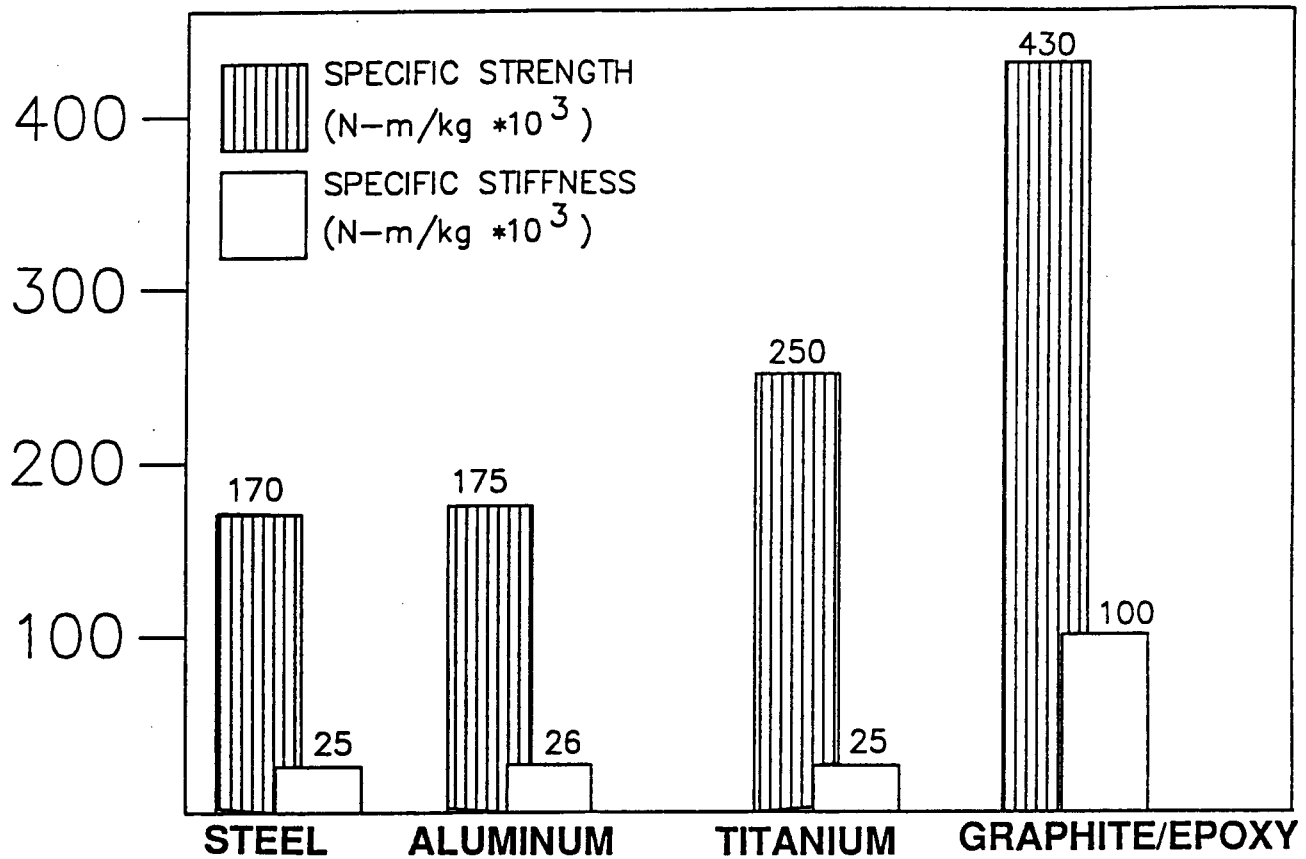


Table 13.1 Summary of different spacecraft materials considered for the LOP.

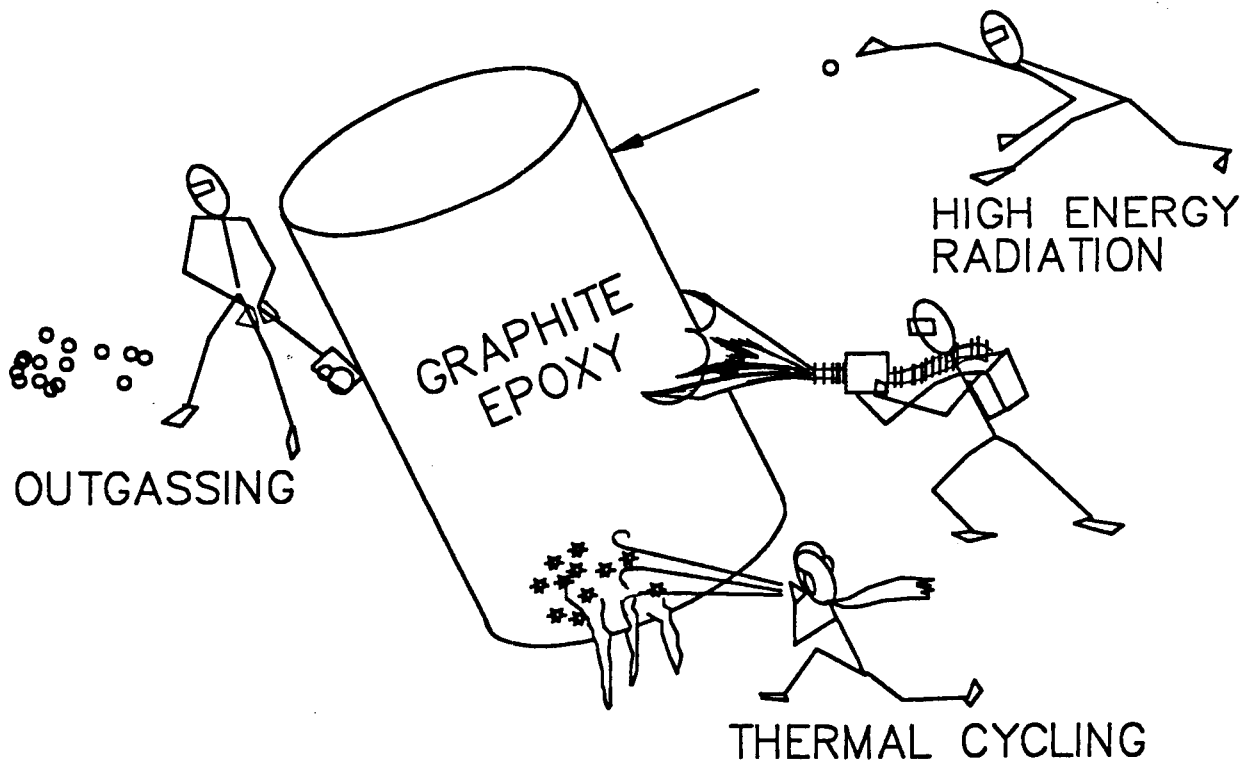


Figure 13.10 Graphical illustration of lunarians attacking a composite structure in the space environment.

(ACTS)," which is scheduled for launch in 1989 [3]. Further discussion of Gr/Ep advantages over titanium and aluminum is detailed below.

13.3.2.1 Lightweight

Graphite/Epoxy is 40% lighter than aluminum. Table 13.1 shows, using specific strength, the relative advantage of graphite/epoxy over other materials. All properties of materials are taken from [2].

The advantage of weight reduction using composites over aluminum and titanium is illustrated in the following example. Assuming a cylinder diameter of 1m-diameter, and 1m-height, and a thrust on the cylinder of 27 kN (the thrust on the OMS engine of the space shuttle) the three main materials were compared for the mass required to prevent buckling of the main cylinder. The details of these calculations are shown in Appendix 13. The results are summarized in Table 1. F.S. is the factor of safety on the applied load (a F.S. of 2 means 2×27 kN).

Table 1. Mass comparisons of materials for the main load bearing cylinder (diam=1m).

<u>Material</u>	<u>Mass(F.S.=1)</u>	<u>Mass(F.S.=2)</u>
Gr/Ep	2.17 kg	2.86 kg
Aluminum	5.44 kg	8.13 kg
Titanium	7.38 kg	9.60 kg

The most lightweight choice would be the composite at less than 3 kg for the main load bearing cylinder. This is the principle advantage of composites over the metals. And a definitive one since transportation costs in space are important considerations.

13.3.2.2 Low Coefficient of Thermal Expansion

Depending on how the composite is layed up, it can be designed for a zero coefficient of thermal expansion, CTE [4].

Titanium has a CTE of $8.8 \times 10^{-6}/K$, steel is $11 \times 10^{-6}/K$, and aluminum is a whopping $23 \times 10^{-6}/K$. The composite is the better choice for the LOP with a CTE of $-.36 \times 10^{-6}/K$ to zero.

A low CTE is desirable since the satellite is cycling in and out of the Moon's shadow, and in space one side of an object can be heated by the sun while the far side is nearly frozen from pointing away from the sun. With this hot and cold environment it would be difficult to maintain pointing

accuracies of scientific instruments and communications equipment if the material expanded a great deal with temperature. Fortunately Gr/Ep performs outstandingly with a low CTE.

13.3.2.3 Stiff

Gr/Ep is stiffer than Titanium, which is stiffer than steel and aluminum [4]. A stiff structure maintains pointing ability which is important for the scientific instruments and the communications equipment. Gr/Ep is also the stiffest of the materials being compared per unit weight. See appendix 2 for graphical comparison of specific stiffness of materials.

13.3.2.4 Vibration Resistant

Composites have excellent structural damping as compared to the metals [4]. Damping is important since the platform will have many different mechanical disturbances from the attitude control system (momentum wheels, and thrusters), pointing of solar panels, altitude control, docking of the GTV, mounting of modules, and other unforeseen disturbances.

13.3.2.5 Fatigue Resistant

Composites have shown an appreciable fatigue resistance to mechanical cycling, however there have been studies that indicate that thermal cycling might be a problem with the reduction in property values for composites.

13.3.2.6 Creep Resistant

Gr/Ep is more creep resistant than the metals. This is of course important since it is not easy to go into space and then find out that a beam has sagged.

13.3.2.7 Impact Resistant

Gr/Ep is poor in impact resistance, but the assumption is that by the year 2010, these developments will have been worked out. Assuming that composites will be more impact resistant in the future, all the other outstanding properties of Gr/Ep overshadow this problem.

13.4 Space Environment

Graphite/Epoxy is a strong and lightweight material, however it is more prone to attack in a space environment

than the isotropic materials aluminum and titanium. Primarily it suffers from outgassing, thermal cycling, and radiation. The space environment is shown graphically in Figure 13.10. Each of these problems will be briefly discussed.

13.4.1 Outgassing

In the vacuum of space, organic compounds outgas, or sublimate. This is not a major problem since it is slow and can be slowed further with various coatings. For example coating the composite with a foil wrap or an integral aluminum cladding. Covering the composite solves another problem of ultraviolet attack of the epoxy [3]. Composites wrapped in a foil will also reflect insolation slowing the heat into the spacecraft.

13.4.2 Thermal Cycling

Thermal cycling results from the spacecraft being heated and cooled as it passes from the sun to the shaded portion of its orbit and back again. D. E. Bowles [5] found that thermal cycling produces microcracks in the matrix which reduces the stiffness and significantly changes the CTE. Others have found similar results [6], and [7].

Utah State University has thermally cycled a Gr/Ep composite tube 10,000 times to determine the damage if any that is done to the microstructure of the tube. This experiment has not been published, but the results show no microcracks on the surface of the tube [8]. If this is true the problems with thermal cycling will not be limiting in space.

13.4.3 Radiation

C. L. Leung [10] says, "...the greatest [adverse] effect from space environments [on composite materials] is a decrease in the mechanical properties due to high-energy radiations." Essentially the mechanism in weakening the composites is the high energy particles slam into the composite and excite molecules and bonds in organic materials such that they are removed from the macromolecular chain.

Leung found that the composite increased in strength to begin with then the strength began to drop off as the radiation level increased. He found that the "mechanical and shear strength generally will be comparable to that of the unexposed system after about 3 years of service (or about 3×10^8 rads)" [10]. However the levels of high energy particles at the Moon are much lower than at those

experienced in the Van Allen radiation belts. The levels of radiation felt at the Moon for one year, assuming three solar flares (a very conservative estimate), is 200 rads/week of solar particles, and at worst 10 rads/year of cosmic radiation [11]. For comparable levels of radiation in Leung's study this says the LOP can last at the Moon for 28×10^3 years.

The CRC Handbook of Space Technology Projections [9] predicts that by the year 1991, resin matrix composites will have a space environment lifetime of 22 years. Assuming this is correct, there should be no concern over the degradation of the properties of composites in space applications.

13.5 Thermal Control

The objective of thermal control is to keep instruments and packages at the proper operating temperatures. The LOP has two areas that need control, the liquid oxygen (LOX) tanks, and the scientific instruments.

13.5.1 LOX Tank

The outside of the LOP was found to be about 334 K for a worst case. The internal pressure of the LOX tank is to be 4 MPa for propulsion purposes. With these parameters, a spherical tank was sized at .80 m nominal diameter with a wall thickness of 4.5 mm and a mass of 25 kg. This is for an aluminum tank designed with a factor of safety of 3. See Appendix 4 and 5 for graphs of tank thickness and mass versus pressure of the tank (note these graphs are for a factor of safety of 1). Appendix 6 is the computer program used to generate these plots. For a saturation pressure of 4 MPa the temperature of the LOX is 147 K.

The amount of boil-off is a concern, but by insulating the spherical tank with multiple layer insulation, MLI, the boil-off can be reduced to manageable proportions. Using 5 cm of Southampton test 8.7 micro Al foil + carbon loaded fiberglass paper (30 layers per cm) with an effective thermal conductivity of 0.1×10^{-4} W/m-K [12]. It takes about 0.58 years for 5% of the LOX (294.3 kg total) to boil-off. This was found from the equation:

$$q = KA \frac{T}{\text{insulation thickness}} = \text{mass flow rate} \cdot H_{fg}$$

and

$$\text{time to boil-off} = \frac{\text{mass of LOX}}{\text{mass flow rate}}$$

This selection of MLI fits around the tank, and inside the cylinder, and gives a good design for the LOX tank with minimal boil-off rates.

13.5.2 Scientific Instruments

Each of the instruments has its own thermal control in the form of some type of radiating plate to space. The radioisotope thermal generators, RTG's, also have their own radiating fins to cool the loads.

If something needs extra heat dissipation there is existing technology that can probably handle the needed cooling loads. For example, there is a passive radiator that promises to dissipate 75 mW maintaining a temperature of 60 K [13]. The radiator for this type of load is approximately 58.4 X 30.5 X 0.127 cm.

It would be desirable to keep the thermal control techniques passive, like heat pipes and radiator plates, but if something like the raman laser needs extra cooling, an active refrigeration cycle will have to be used. It is not known at this point what type of thermal loads will be generated by the raman laser, so no sizing can be done. The raman module is only one of the packages to fly on the LOP, and when it is needed, the necessary engineering can be done. The combustion chamber and nozzle of the propulsion module may also need a special application of cooling.

13.6 Conclusion

The lunar orbiting prospector, LOP must have a stable strong load bearing structure. This is accomplished with a load bearing cylinder to bear the launch and orbit change loads of propulsion. Two plates on either end of the cylinder bear the transverse loads of attitude control.

The best material to make the LOP out of is graphite/epoxy since it is lightweight, has a low coefficient of thermal expansion, is stiff, vibration resistant, fatigue resistant, and creep resistant. The adverse effects of outgassing, thermal cycling, and attack by high energy particles on graphite/epoxy are not extensive or crippling to the LOP and its applications.

An effective liquid oxygen tank has been sized with 5 cm of multiple layer insulation to slow the heat penetration of the tank. The tank is 25 kg, made of aluminum, and is about 5 mm thick. This arrangement loses 5% of the oxygen stored in about 6 months.

Scientific instruments each have their own control techniques. If something else is needed it can be developed for that specific application.

REFERENCES

1. Simpson, R. F., "Explorer Platform", AIAA 26th Aerospace Sciences Meeting, AIAA-88-0066, January 1988, pp. 1-5.
2. Agrawal, B. N., Design of Geosynchronous Spacecraft, Prentice-Hall, Inc., Englewood Cliffs, N. J., 1986, pp. 179-251.
3. Leonard, L., Advanced Composites, Vol.1, 1986, pp. 35-37.
4. Hercules Aerospace, Promotional Literature, Salt Lake City, Utah.
5. Bowles, D. E., Journal of Composite Materials, Vol. 17, 1984, pp.173-184.
6. Babel, H. W., T. P. Schumate, P. F. Thompson, SAMPE Journal, May/June 1987.
7. Tompkins, S. S., S. L. Williams, Journal Spacecraft, Vol. 21, No. 3, May/June 1984, pp. 274-280.
8. Redd, F. J., Personal Communication, Utah State University, 1988.
9. CRC Handbook of Space Technology Projections, pp. 87-96.
10. Leung, C. L., "Space Environmental Effects on Graphite/Epoxy Composites".
11. NASA Technical Memo 78119, pp. 1-2,1-3.
12. Scurlock, R. G., "Croygenic Engineering I", Institute of Cryogenics, pp. 2-6, 2-7.
13. Bard, S., Journal Spacecraft, Vol. 24, No. 3, May/June 1987, pp. 193-197.

14.0 Thermal Considerations

The thermal analysis of an orbiting satellite is very complex. A preliminary analysis was performed with some simplifying assumptions. These assumptions were made so that some rough calculations could be made and the problem areas could be identified. The assumptions will be stated throughout.

It is well recognized that a more in-depth thermal analysis, usually including a test of a thermal mockup to verify the model, is needed before the design is complete.

14.1 Sources of Heat

There are four major sources of heat that affect the lunar satellite. They are: solar radiation, reflected sunlight from the lunar surface, thermal radiation from the lunar surface, and internally generated heat loads (see Figure 14.1). Solar radiation and the heat radiation from the lunar surface have the greatest influence on the satellites's temperature.

14.1.1 Solar Radiation

Solar radiation has a profound effect on the temperature of the satellite. The solar flux is taken as 1400 W/m^2 which is an approximate average value over one years time. Since the satellite is a great distance from the sun, it is assumed that the solar flux impinges on the satellite with parallel rays. The solar intensity is then taken as a product of the solar flux and the projected surface area normal to the sun's rays.

14.1.2 Reflected Solar Radiation

The reflected solar radiation is a fraction of the total incident solar radiation on the Moon which is reflected back into space. This reflected radiation is also know as the albedo flux.

The amount of reflected solar radiation depends on the satellite's position, altitude, and the orientation of the sun. The albedo for the Moon is taken as 0.85. For the calculations performed, it was assumed that no reflected solar radiation came from the unlit portions of the Moon.

HEAT LOADS

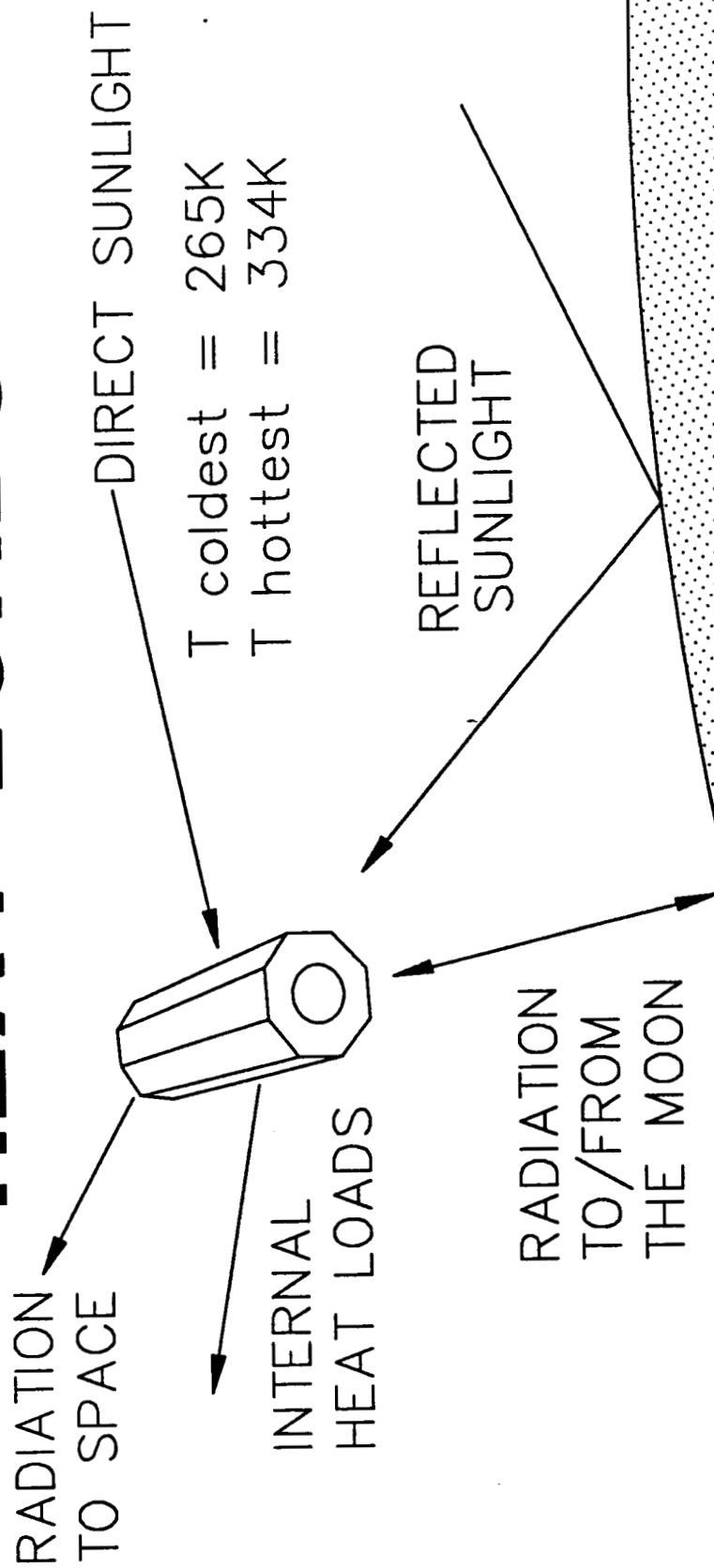


Figure 14.1 Heat Balance on Orbiter

14.1.3 Thermal Radiation from the Moon

The Moon absorbs a portion of the incident solar radiation which it re-emits as thermal radiation in accordance to the Stefan-Boltzman law. It is assumed that the emitted radiation is constant over the entire lunar surface. The lunar surface emits diffusely and obeys Lambert's cosine law (White, 1984).

The amount of thermal radiation absorbed by the satellite is a function of the temperature difference between the satellite and the Moon, the area, emissivity, and altitude of the satellite. The thermal radiation absorbed has a large value and therefore is a predominant factor in the temperature of the satellite.

14.1.4 Internally Generated Heat Loads

These heat loads are generated by the different instruments on board the satellite. These loads are generally small in comparison with the other heat inputs.

Most of the primary remote sensing instruments contain their own thermal control systems. The exception to this is the RAMAN Spectroscopy package. The laser will have to be cooled, and this will need to be done by an active cooler.

The communication, data storage, and processing equipment may need to be cooled or warmed depending on their individual needs. When the specific pieces of equipment are chosen their thermal control can be specified.

The RTG's will radiate approximately 900 W of thermal energy. The RTG's are placed on booms away from the main body and radiation shields will be placed around them. This will prevent thermal radiation from reaching the main body of the spacecraft. A coupling, having a very low thermal conductivity, will be placed in the booms to prevent excessive thermal conduction through the material. If needed some of this excess heat may be used to heat some of the equipment or instruments.

For all calculations the internally generated heat load was taken as 1100 W. This is a worst case approximation. The RTG's are taken to be partially shielded, and the internal heat loads are high.

14.2 Radiation Out

While there are many thermal inputs to the satellite, radiation is the only method of heat transfer out of the satellite. An effective method of thermal control is the prevention of the absorption of solar irradiation. By

coating the outer skin of the satellite with a material of high emissivity and low absorptivity, preventive control is achieved. Absorptivity is the ratio of the absorbed radiation to the total incident radiation. The lower the surface absorptivity, the less radiation absorbed. Emissivity is a ratio of the radiation emitted to the maximum possible radiation emitted.

Several methods may be used to radiate the excess heat out into space. These may be passive radiators or active systems. Passive radiators are preferred when possible but may become too large to be feasible. Active systems are generally complex and expensive. These systems are also prone to failure.

The satellite will incorporate both passive and active systems. The liquid oxygen tank will require cooling while most of the instruments will be passively cooled.

14.3 Equilibrium Skin Temperature

The equilibrium skin temperature was calculated using an energy balance of the incoming and the outgoing heat. By modeling the spacecraft as an octagon and varying the surface coatings, the following temperatures were found (see Table 14.1). For the worst cases the satellite was assumed to be in an orbit totally in the dark and totally in the sun. The actual temperature of the satellite will be between these values depending on the orbit it is in. The temperatures of the Moon in the sunlight and in the dark were 350 K and 90 K respectively. The internal heat load was taken to be 1100 W.

<u>SURFACE</u>	<u>Tmin (k)</u>	<u>Tmax (k)</u>
White Paint	257.7	330.0
Anodized Al.	265.3	334.0
Graphite Epoxy	308.3	358.4
Gold	305.9	356.9

Table 14.1 Satellite Surface Temperatures

14.4 Recommendations for Surface Coating

From the calculations that were performed, the best coating for the surface is a special white paint or anodized aluminum. To help with the even distribution of the heat over the entire surface of the satellite and to avoid thermal stresses in the composite frame, the aluminum coating was chosen.

The aluminum coating will also help protect the satellite from harmful particles and rays. If after a period of time the aluminum coating begins to lose its effectiveness, a coat of the special white paint can be applied. This new coat will help in the thermal control while the aluminum will also help to distribute the heat evenly.

14.5 Special Problems

A unique problem arises when the satellite's engine is fired. The combustion chamber becomes very hot almost instantaneously. The inside temperature is 4500 K while the outer skin temperature is approximately 700 K. To protect the liquid oxygen tank from this surge of heat, the combustion chamber is located outside the main body of the satellite. Radiation shields will be placed between the combustion chamber and the main body. A couple with a low thermal conductivity will be placed in the liquid oxygen line to prevent thermal conduction (see Figure 14.2).

To cool the nozzle, part of the liquid oxygen will pass over the nozzle and then enter the liquid oxygen tank on the outside of the bladder to help keep the oxygen pressurized.

14.6 Conclusion

The satellite will be coated with anodized aluminum to help prevent the absorption of radiation and the emittance of radiation. The aluminum will also help distribute the heat in an even fashion around the satellite.

Passive and active cooling systems will be used on the satellite to achieve the desired temperatures. Passive radiators will be used when feasible.

A more in-depth thermal analysis, including a test of a thermal mockup to verify the model is needed to complete the design.

THERMAL CONTROL

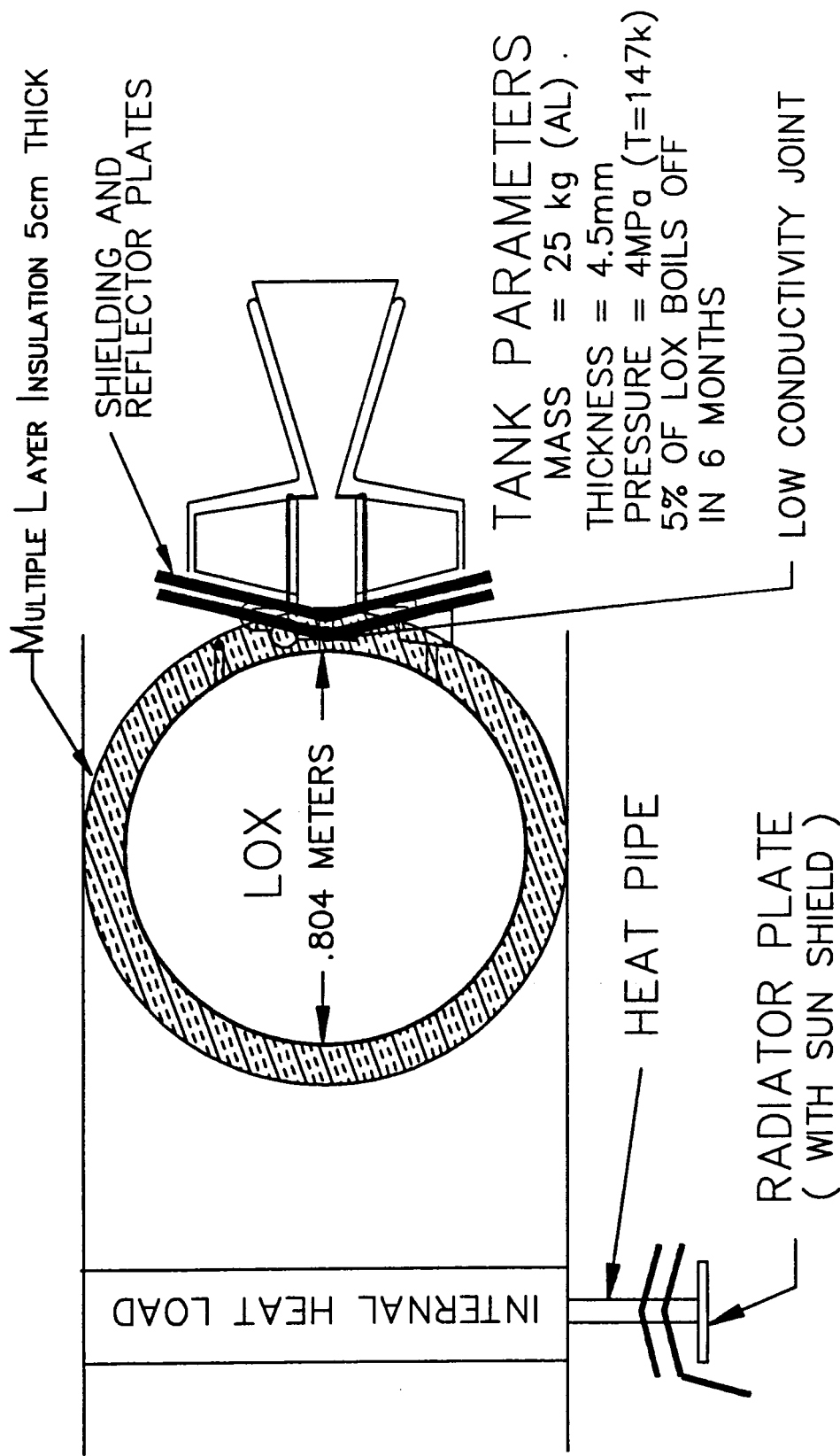


Figure 14.2 Thruster Thermal Control

REFERENCES

Agrawal, B.N., Design of Geosynchronous Spacecraft, INTELESAT, Washington D.C., Prentice-Hall, Inc., Englewood Cliffs, NJ, 1986.

Spacecraft Design and Engineering: Thermal Control,

Space Systems Technology Model: Volume 3, Analysis of Technology Needs and Future Considerations, NASA, January 1984.

White, F.M., Heat Transfer, Addison-Wesley, Reading, Mass., 1984.

DESIGN OF A BIAS MOMENTUM WHEEL

15.0 Introduction

It has been recognized for some time in the history of gravity gradient stabilization that a small momentum wheel nominally oriented along the pitch axis enhances roll/yaw coupling and thereby provides greater liberty in arranging the inertia distribution, as is so all important for gravity gradient designs¹.

Although a small pitch momentum wheel can sometimes be used to augment gravity gradient stabilization, the term "bias momentum" really refers to a larger momentum wheel, used on a satellite that does not rely on the gravity gradient for stabilization. The basic idea in its simplest form is shown in Fig. 1. The satellite is intended to be stabilized to the orbiting axes. The orbiting axes are defined as the roll (x) in the velocity direction, the pitch (y) normal to the orbital plane, and the yaw (z) in the local vertical direction. An active attitude sensor measures any deviation from pitch/roll and attitude errors are fed to appropriate control systems which in turn cause corrective pitch and roll torques to be applied.

The momentum wheel used on the orbiting platform is a double-gimbaled momentum wheel attitude control system. The system provides three-axis stability, and offers control about all three vehicle axes through wheel speed control and two-degree of freedom gyrotorquing.

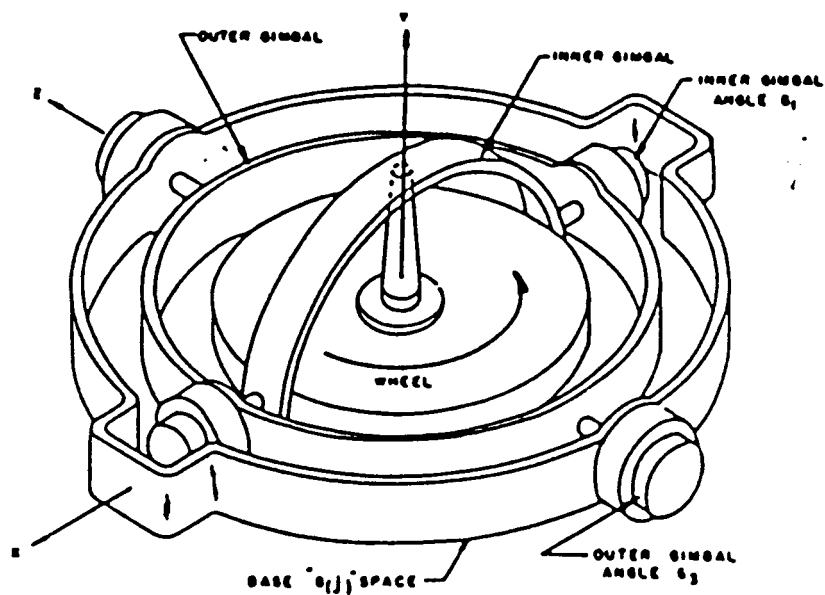
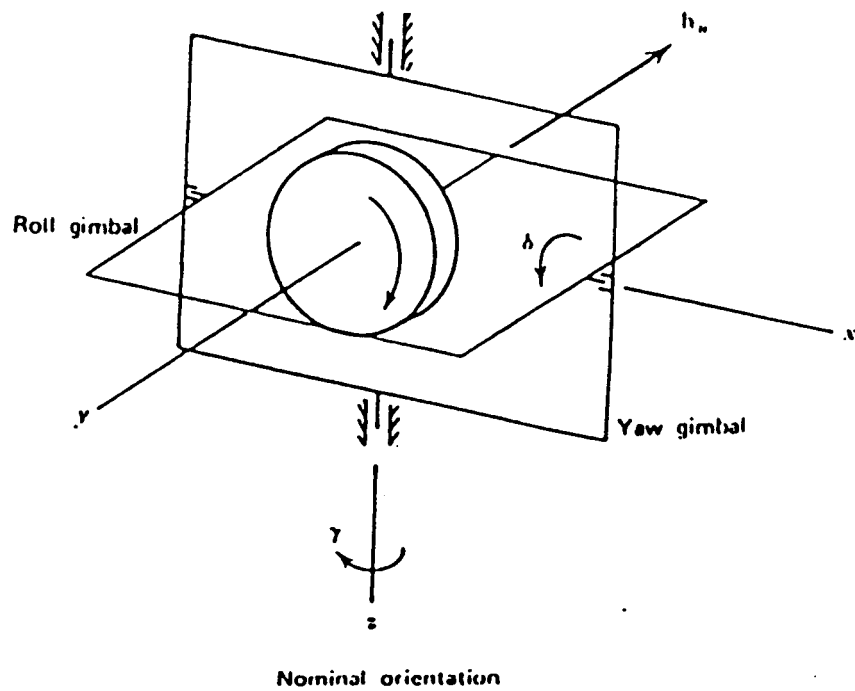
The advantages of the momentum wheel are: (1) capability of high accuracy pointing control; (2) short term stability against disturbance torques; (3) roll/yaw coupling that permits yaw angle stabilization without a yaw sensor; (4) the system can be used to provide scanning motion across the celestial sphere for a horizon sensor; (5) compensation for cyclic torques without fuel consumption. Thus, the momentum bias system can provide three-axis control with less instrumentation than a three-axis reaction wheel system.

15.1 Theoretical Analysis and Equations of Motion

The satellite configuration is illustrated in Fig. 2. and the reference frame (x, y, z) is rotating with respect to an inertial frame at the rate, ω_o . The satellite pitch:roll:yaw moments of inertia are 1253:1017:652 $kg \cdot m^2$.

For simplicity of the analysis, the body axes coincide with the principal axes and the analysis is based on the following assumptions. (1) the satellite is a rigid

ORIGINAL PAGE IS
OF POOR QUALITY



Double Gimbaled CMG

Figure 1. Orientation of the gimbal².

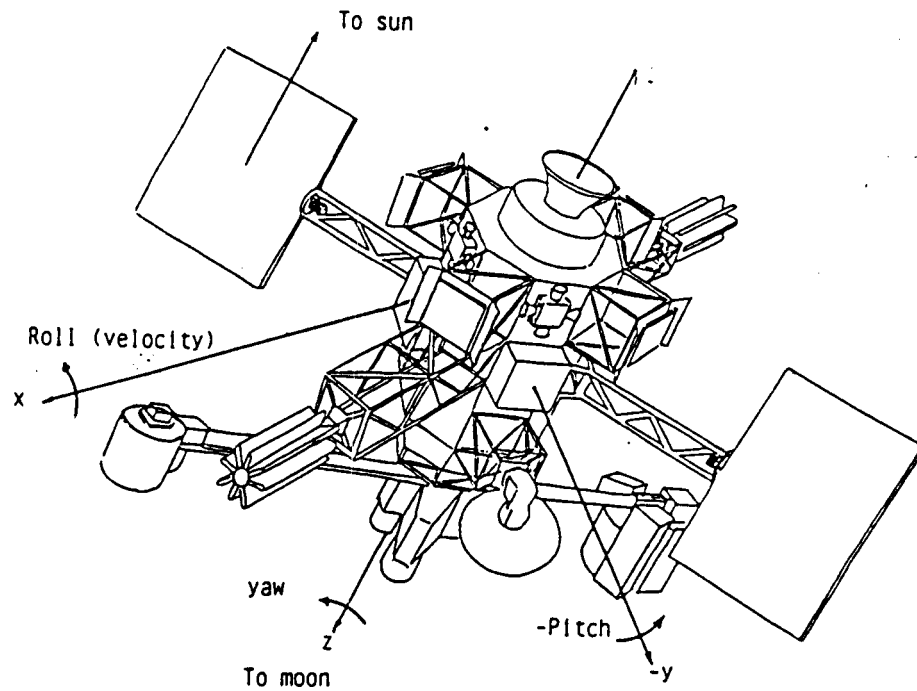


Figure 2. Spacecraft configuration.

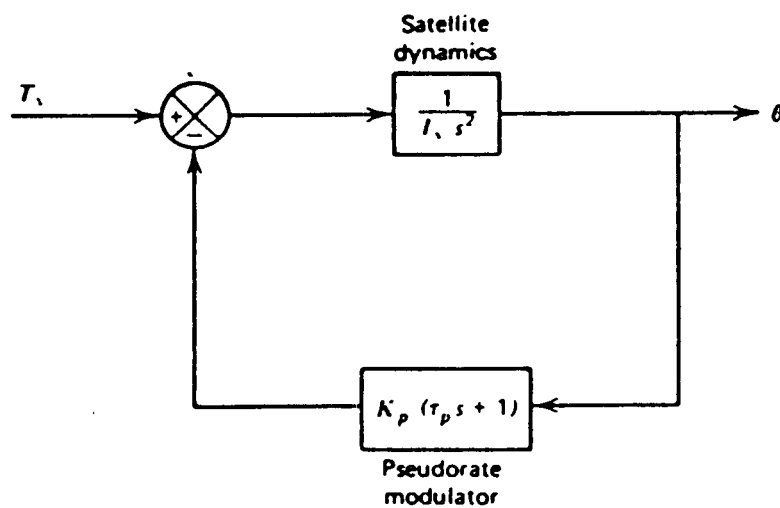


Figure 3. Pitch block diagram².

body in a 100 km circular orbit ($\omega_o = 8.99 \times 10^{-4} \frac{\text{rad}}{\text{sec}}$); (2) the gravitational and solar torques are the only sources of the disturbing torques; (3) the attitude deviations from the equilibrium positions are small, and terms involving products of θ, ϕ, ψ , and their rates are ignored.

Using Euler's moment equations, The attitude motion of a rigid body and the momentum wheel in a circular orbit can be expressed as²

$$\vec{T} + \vec{G} = \frac{d\vec{h}}{dt} = \left[\frac{d\vec{h}}{dt} \right]_{body} + \vec{\omega} \times \vec{h} \quad (1)$$

where \vec{T} is the external disturbing torque due to the solar pressure, \vec{G} is the gravitational torque, $\vec{\omega}$ is the angular velocity of the reference frame, and \vec{h} is the total angular momentum ($h_{vehicle} + h_{wheel}$). Angular momentum of the vehicle (h_v) along the principal axes can be expressed as

$$h_v = I_x \omega_x + I_y \omega_y + I_z \omega_z \quad (2)$$

Assuming small gimbal angles δ (roll), and γ (yaw), the linearized wheel momentum equation can be expressed in matrix form as

$$\begin{pmatrix} h_{wx} \\ h_{wy} \\ h_{wz} \end{pmatrix} = \begin{pmatrix} 1 & -\gamma & 0 \\ \gamma & 1 & -\delta \\ 0 & \delta & 1 \end{pmatrix} \begin{pmatrix} 0 \\ -h_w \\ 0 \end{pmatrix} \quad (3)$$

Deviations from nominal wheel momentum h_n are also assumed small, allowing $\vec{h}_w = \vec{h}_n$. Control components of wheel can be defined using Eq. (3),

$$h_{xc} = \gamma h_n, \quad h_{zc} = -\delta h_n, \quad \dot{h}_{yc} = -\dot{h}_w$$

The attitude rates ($\dot{\theta}, \dot{\phi}, \dot{\psi}$), and body rates ($\omega_x, \omega_y, \omega_z$) are related by

$$\begin{pmatrix} \omega_x \\ \omega_y \\ \omega_z \end{pmatrix} = \begin{pmatrix} 1 & \psi & -\theta \\ -\psi & 1 & \phi \\ \theta & -\phi & 1 \end{pmatrix} \begin{pmatrix} 0 \\ -\omega_o \\ 0 \end{pmatrix} + \begin{pmatrix} \dot{\phi} \\ \dot{\theta} \\ \dot{\psi} \end{pmatrix} \quad (4)$$

From this transformation the body rates can be expressed as

$$\omega_x = \dot{\phi} - \psi\omega_o \quad (5.a)$$

$$\omega_y = \dot{\theta} - \omega_o \quad (5.b)$$

$$\omega_z = \dot{\psi} + \phi\omega_o \quad (5.c)$$

In general the gravitational torque has the following form²

$$\vec{G} = \frac{3\mu}{R^5} \int_b (\vec{r} \cdot \vec{R})(\vec{r} \times \vec{R}) dm \quad (6)$$

where μ is the gravitational constant, R is the radius of the orbit, and \vec{r} is the position of the satellite. After integrating Eq. (6), the gravity components can be expressed as

$$G_x = \frac{\mu}{R^5} (I_z - I_y) R_z R_y \quad (7.a)$$

$$G_y = \frac{\mu}{R^5} (I_x - I_z) R_x R_z \quad (7.b)$$

$$G_z = \frac{\mu}{R^5} (I_y - I_x) R_y R_x \quad (7.c)$$

Using the transformation matrix of Eq. (4), the \vec{R} components in the body frame are

$$\begin{pmatrix} R_x \\ R_y \\ R_z \end{pmatrix} = \begin{pmatrix} 1 & \psi & -\theta \\ -\psi & 1 & \phi \\ \theta & -\phi & 1 \end{pmatrix} \begin{pmatrix} 0 \\ 0 \\ -R \end{pmatrix} = \begin{pmatrix} \theta R \\ -\phi R \\ -R \end{pmatrix} \quad (8)$$

Substitution of Eq. (8) into Set (7) yields

$$G_x = -3\omega_o^2 (I_y - I_z) \phi \quad (9.a)$$

$$G_y = -3\omega_o^2 (I_x - I_z) \theta \quad (9.b)$$

$$G_z = 0 \quad (9.c)$$

where θ , ϕ , and ψ are pitch, roll, and yaw angles, respectively. With the assumption of small δ , γ , and their rates (these terms actively can be controlled to be small) substitution of Eqs. (2), (3), (5), and (9) into (1) will yield

$$T_x = I_x \ddot{\phi} + (4\omega_o^2(I_y - I_z) + \omega_o h_n) \phi + (-\omega_o(I_x - I_y + I_z) + h_n) \dot{\psi} + \dot{h}_{xc} - \omega_o h_{xc} + D_x \quad (10.a)$$

$$T_y = I_y \ddot{\theta} + 3\omega_o^2(I_x - I_z)\theta + \dot{h}_{yc} + D_y \quad (10.b)$$

$$T_z = I_z \ddot{\psi} + (\omega_o^2(I_y - I_x) + \omega_o h_n) \psi - (-\omega_o(I_x - I_y + I_z) + h_n) \dot{\phi} + \dot{h}_{zc} + \omega_o h_{zc} + D_z \quad (10.c)$$

where h_{xc} , h_{yc} , and h_{zc} are control components of the wheel momentum, and

$$\begin{aligned} D_x &= (I_z - I_x) \dot{\theta} \dot{\psi} - \delta \dot{\theta} h_n \\ D_y &= (I_x - I_z) \dot{\psi} \dot{\phi} + (\gamma \dot{\psi} + \delta \dot{\phi}) h_n \\ D_z &= (I_y - I_x) \dot{\theta} \dot{\phi} - \gamma \dot{\theta} h_n \end{aligned}$$

Note that the "D" terms are the only terms that their magnitudes are not assured; other terms contain $\delta\gamma$, $\omega_o\dot{\gamma}$, ..., etc. The latter terms are small and ignored in this analysis. For now the "D" terms are omitted and validity of this assumption will be examined later.

Set (10) represents the complete, linearized motion for roll, pitch, and yaw, respectively. The pitch equation of motion is uncoupled from roll and yaw due to the small angle assumptions. Thus, the problem reduces to pitch control and roll/yaw control. These are now treated separately.

15.2 The Pitch Loop

The linearized pitch equation of motion is presented in Eq. (10.b). This equation is further simplified, since the θ term has a small numerical value ($\omega_o^2(I_x - I_z)\theta \approx 0$). Thus,

$$T_y = I_y \ddot{\theta} + \dot{h}_{yc} \quad (11)$$

This equation indicates that no natural damping is available (no $\dot{\theta}$ in Eq. (11)). The damping can be provided through the control function \dot{h}_{yc} . A satisfactory form of control law is

$$\dot{h}_{yc} = K_p(\tau_p \dot{\theta} + \theta) \quad (12)$$

where K_p is the pitch gain, and τ_p is the time constant. Substitution of Eq. (12) into (11) will yield

$$T_y = I_y \ddot{\theta} + K_p \tau_p \dot{\theta} + K_p \theta \quad (13)$$

Taking the Laplace transfer of the pitch equation, the transfer function (T.F.) is obtained as

$$\frac{\Theta(s)}{T_y(s)} = \frac{1}{I_y s^2 + K_p \tau_p s + K_p} \quad (14)$$

The pitch block diagram associated to the transfer function is illustrated in Fig. 3. The denominator of Eq. (14) is called the characteristic equation (C.E.). Comparison of the C.E. with the general form of the second order C.E. ($s^2 + 2\zeta\omega_n s + \omega_n^2$) will define the natural frequency (ω_p) and the damping factor (ζ_p) as

$$\omega_p = \sqrt{\frac{K_p}{I_y}} \quad (15.a)$$

$$\zeta_p = \frac{\tau_p}{2} \sqrt{\frac{K_p}{I_y}} \quad (15.b)$$

The solar pressure disturbing torques ($t=0$ at 6 A.M. or 6 P.M. orbital position) can be defined as²

$$T_x = 2 \times 10^{-5} (1 - 2 \sin \omega_o t) \quad (16.a)$$

$$T_y = 10^{-4} (\cos \omega_o t) \quad (16.b)$$

$$T_z = -5 \times 10^{-5} (\cos \omega_o t) \quad (16.c)$$

where the dimension of the torques are $N \cdot m$.

It is desirable to have the pitch steady state error not greater than 0.5° (0.009 rad), and a critical damped motion ($\zeta_p = 1$). In order to satisfy the steady state condition, the final value theorem is used³, and the result is

$$\theta_{ss} = \frac{T_{y \cdot max}}{K_p} \quad (17)$$

where $T_{y \cdot max} = 10^{-4} N \cdot m$ due to the solar pressure, and θ_{ss} is in rad . From Eq. (17) the minimum calculated K_p is $0.011 \frac{N \cdot m}{rad}$; values less than 0.011 will cause the motion to be underdamped.

15.2.1 Root Locus of the Pitch Loop

The pitch gain value of $0.15 \frac{N \cdot m}{rad}$ is selected. This value of K_p will give $\omega_p = 0.0109 \frac{rad}{sec}$, $\tau_p = 183 \text{ sec}$, and $\theta_{ss} = 0.038^\circ$. Stability and K_p selection of the pitch loop can be examined by using the root locus diagram. Table 1 contains the summary of guidelines for plotting a root locus³. In this table α and ϕ_l are the asymptotes angle and location, respectively, n and m are the highest order of s in the pole and zero, respectively. Following the steps of Table 1 will yield

- Step 1. It can be seen from Fig. 3 that the system has two open loop poles at $s = 0$ and a single zero on the negative real axis at $s = -0.00545$.
- Step 2. This step is illustrated in Fig. 4.
- Step 3. $n - m = 1$, and $\sum p - \sum z = -0.00545$. So the asymptotes are located at $s = -0.00545$ with associated angles of $\pm 180^\circ$.
- Step 4. The departure angles at $s = 0$ are $\pm 90^\circ$ ($2\theta_{dep} = \pm 180^\circ$)
- Step 5. Using the Routh's criteria for asymptotic stability will yield the positive values of K_p . Substitution of $s = j\omega$ into the C.E. will show that the locus will not cross the imaginary axis. Theoretically any positive K_p value will satisfy the stability criteria, but restriction on the steady state condition will impose a minimum value of 0.011 for K_p .
- Step 6. The equation used in the step 6 (Table 1) is derived from $\frac{d}{ds}(\frac{1}{T.F.}) = 0$. Using this equation gives a break-away point at $s = 0$, and break-in point at $s =$

Table 1. Root locus guideline.

SUMMARY OF GUIDELINES FOR PLOTTING A ROOT LOCUS

STEP 1: Mark poles \times and zeros \circ .

STEP 2: Draw the locus on the real axis to the left of an odd number of real poles plus zeros.

STEP 3: Draw $n - m$ asymptotes, centered at α and leaving at angles ϕ_l , where

$$\alpha = \frac{\sum p_i - \sum z_i}{n - m} = \frac{-a_1 + b_1}{n - m};$$

$$\phi_l = \frac{180^\circ + l360^\circ}{n - m}, \quad l = 0, 1, 2 \dots n - m - 1.$$

STEP 4: Compute loci departure angles from the poles and arrival angles at the zeros.

STEP 5:[†] Assume $s_0 = j\omega_0$ and compute the point(s) where the locus crosses the imaginary axis for positive K .

STEP 6:[†] The equation has multiple roots at points on the locus where

$$b \frac{da}{ds} - a \frac{db}{ds} = 0.$$

If s_0 is on the real axis, these are points of breakaway or break-in. Compute the angles of arrival and the angles of departure for any points of multiple roots.

STEP 7: Complete the locus, using the facts developed in the previous steps and making reference to the illustrative loci for guidance.

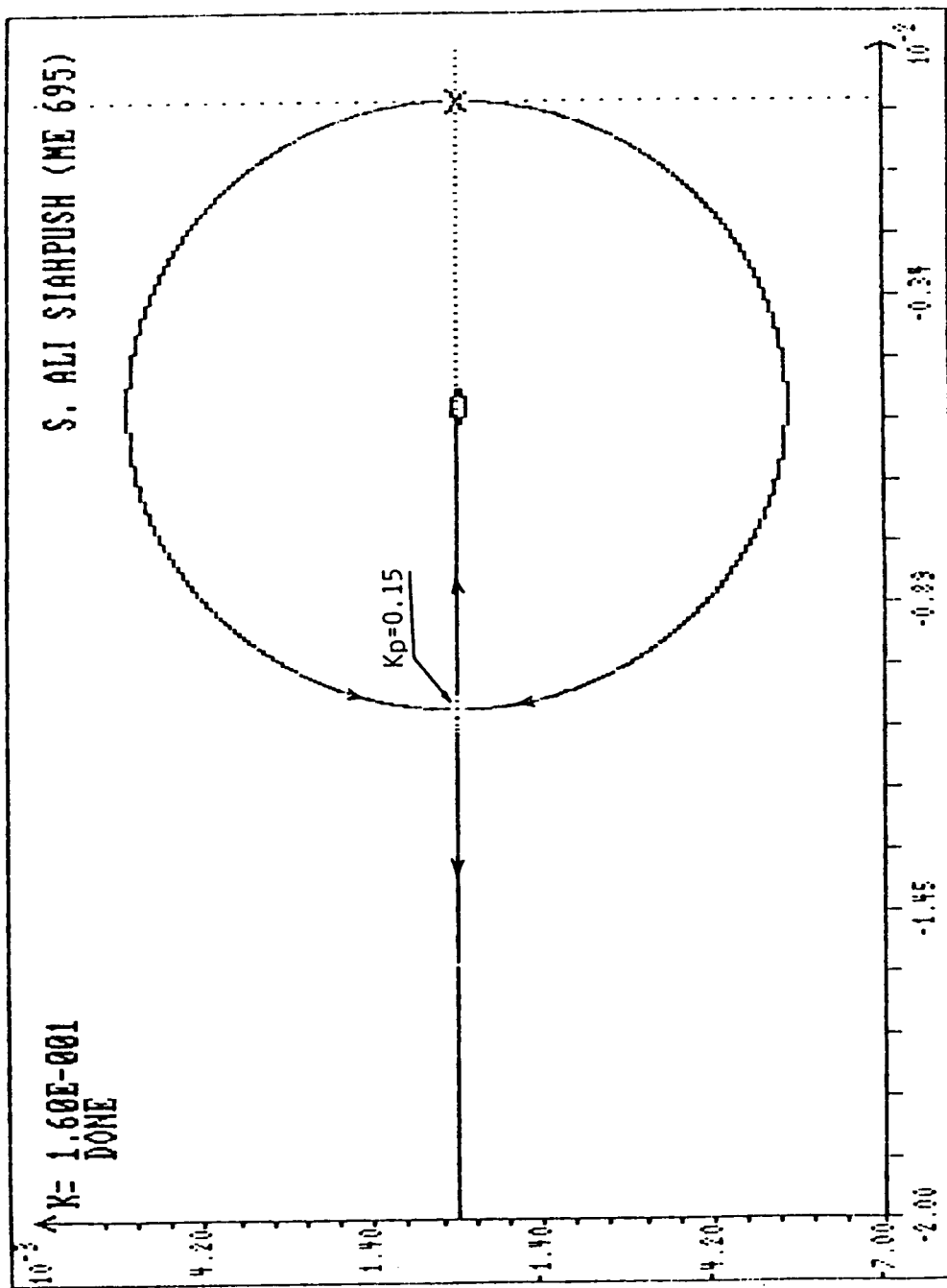


Figure 4. Root locus of the pitch loop.

-0.00545.

Step 7. The completed root locus diagram for the pitch loop is shown in Fig. 4. The design value of $K_p = 0.15 \left(\frac{N \cdot m}{rad} \right)$ is depicted on the real axis.

15.2.2 Computer Simulation of the Pitch Loop

The pitch equation of motion (Eq. (13)) is used in a computer model to simulate the attitude behavior of the pitch axis. The FORTRAN code is presented in Appendix A. The attitude dynamic behavior of the pitch with initial values of $\theta = 0.1$ or 0.2 rad , $\dot{\theta} = 0 \frac{\text{rad}}{\text{sec}}$, and $K_p = 0.15 \frac{N \cdot m}{rad}$ is depicted in Fig. 5. This figure confirm the critical damped assumption (overshoot is not presented). Also, the two cases of Fig. 5 have approximately the same settling time, and reach the steady state stage at $t = 576 \text{ sec}$. This period can be evaluated, analytically through $t = \frac{2\pi}{\omega_p}$.

Figure 6 represents the variation of the θ_{ss} vs. K_p . This figure shows that as K_p increases the θ_{ss} decreases. The slope of the curve rapidly approaches zero for $K_p \geq 0.75$. The lunar orbiter does not need a great deal of accuracy in their attitude control system, and values of $K_p \leq 0.75$ will provide an acceptable steady state error. The steady state error will not reach zero and for $K_p \geq 4.0$, θ_{ss} will be approximately equal to $1. \times 10^{-4} \text{ rad}$. With the assumption of critical damped motion ($\zeta_p = 1$), Equation (15.b) can be used to evaluate the time constant (τ_p). The result is depicted in Fig. 7. From the foregoing discussion on the pitch gain values, it can be seen from this figure that, the slope of the curve will approach zero in the vicinity of the $K_p \approx 0.75$.

For critical damped motion, theoretical minimum value of the pitch gain was evaluated to be $0.011 \frac{N \cdot m}{rad}$. Values of $K_p < 0.011$ will result in underdamped motion. To validate the assumption, Eq. (13) is used to simulate the attitude behavior of the pitch. In this simulation $\zeta_p = 0.4$, and $K_p = 0.003 \frac{N \cdot m}{rad}$ are used. In this case since the damping ratio is not equal to 1, the new time constant is 517 sec . The result of the simulation is depicted in Fig. 8. This figure shows that pitch motion is underdamped, and the system has some overshoot.

Responses produced by the pitch, with the gain and damping value selected above are predicted numerically. Results for cyclic, step, and superposition of cyclic and step disturbance torques are plotted in Fig. 9, 10, and 11, respectively. A cyclic disturbance torque due to the solar pressure causes the periodic response of Fig. 9 with amplitude of about 0.00067 rad . A step input of magnitude $1. \times 10^{-4} \text{ N} \cdot \text{m}$, representing an estimate of thruster misalignment torque about the pitch

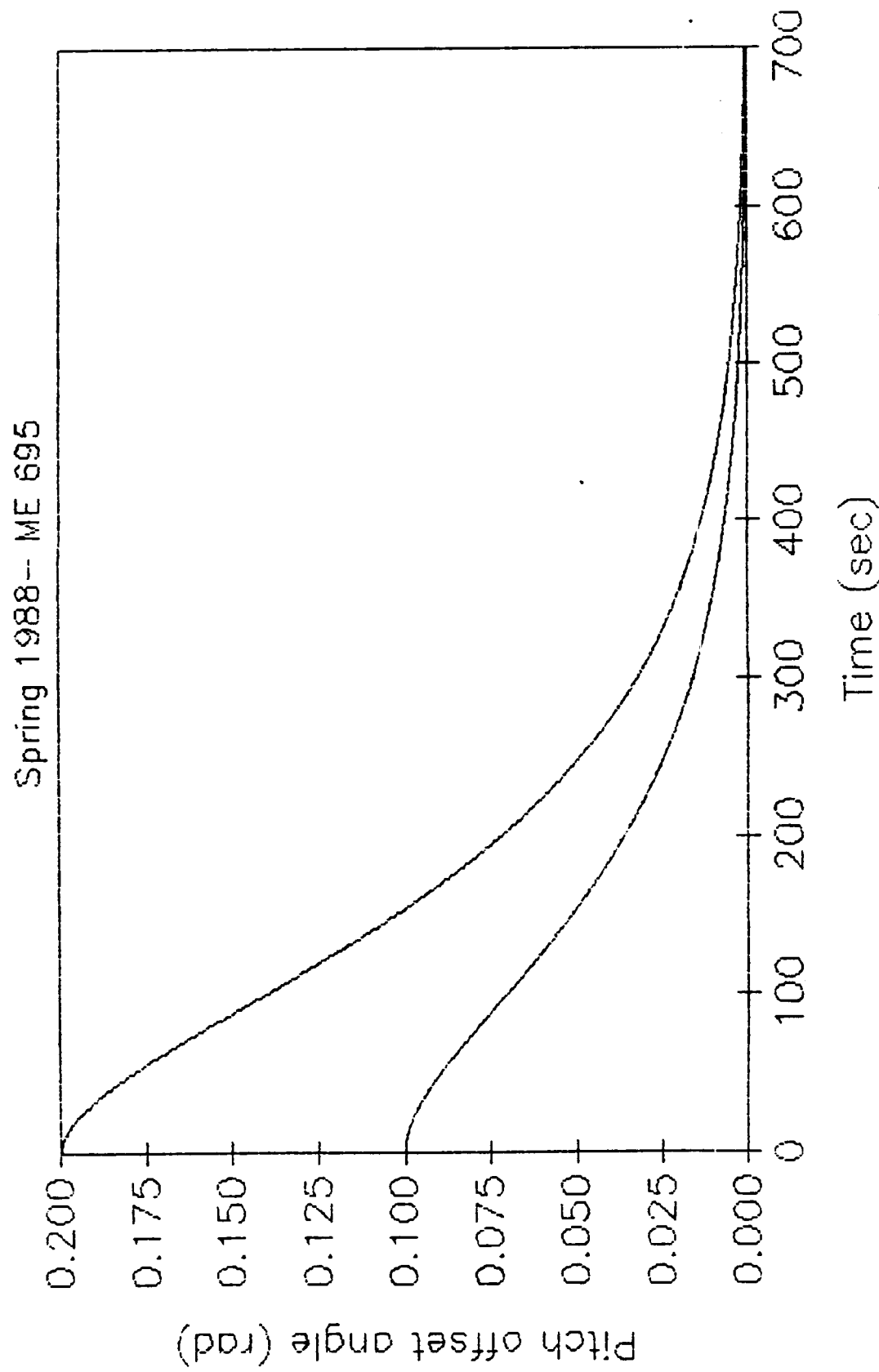


Figure 5. Dynamic behavior of the pitch axis (critical damped).

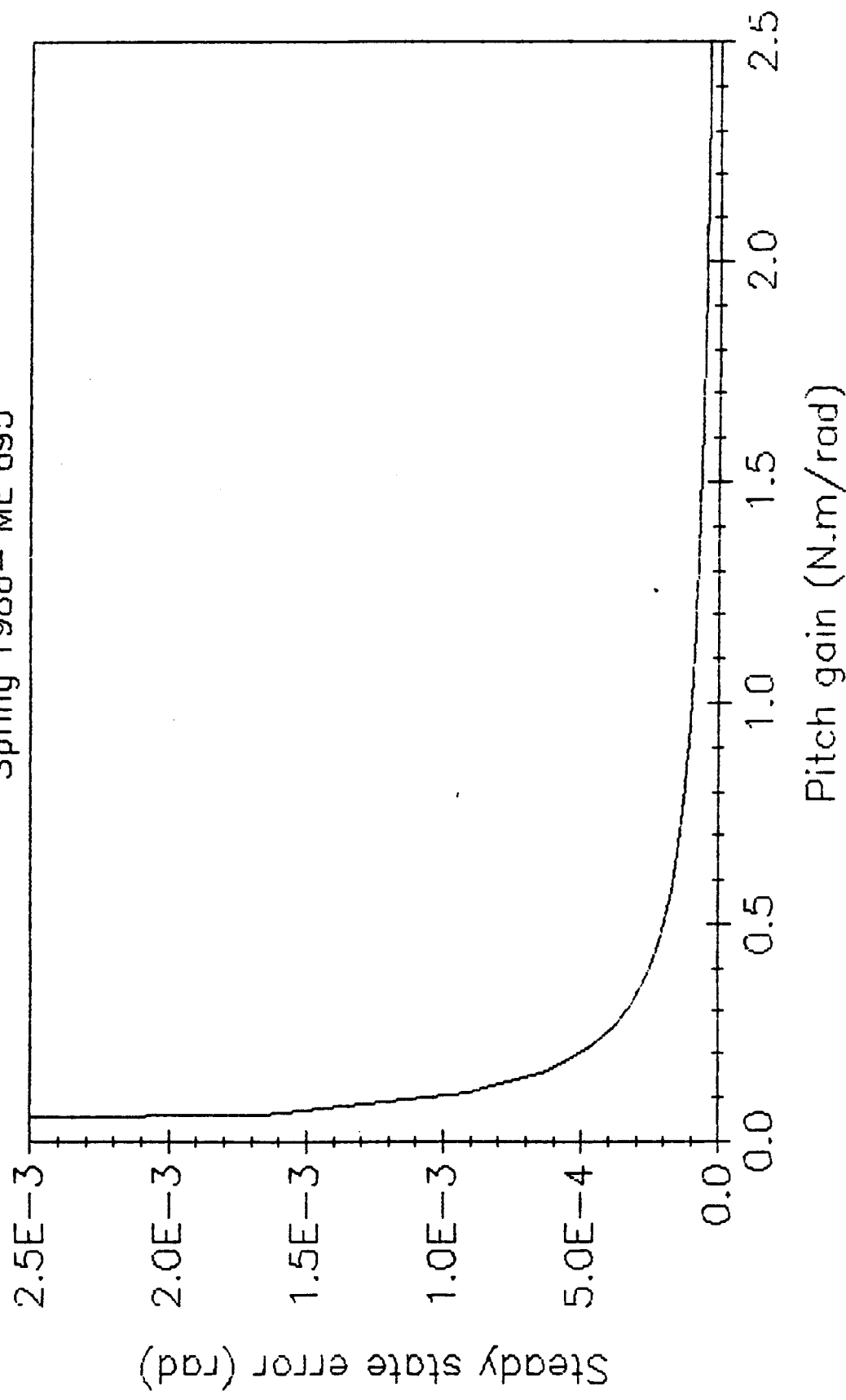
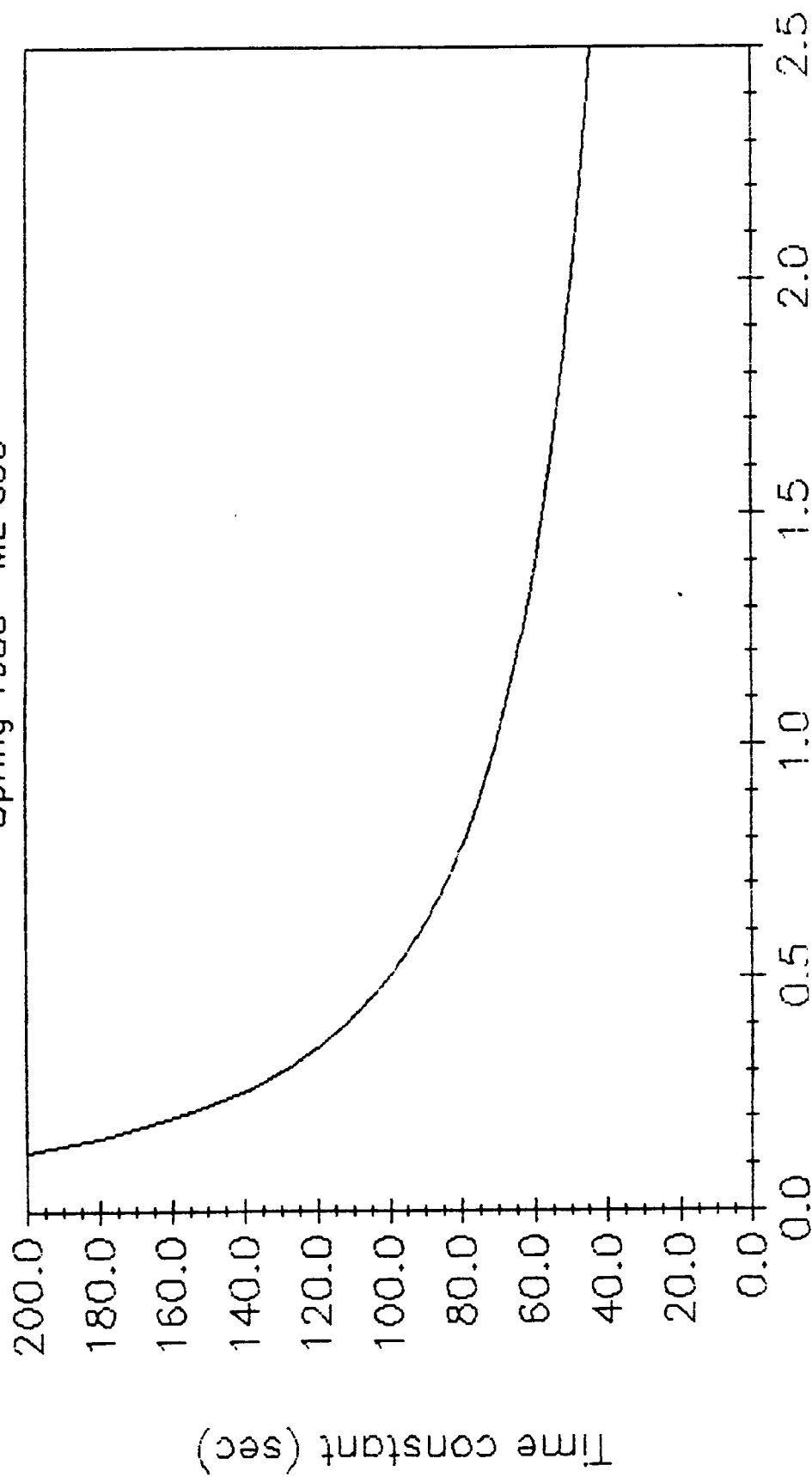


Figure 6. Response of the steady state error to the pitch gain.

Spring 1988— ME 695



Pitch gain (N.m/rad)

Figure 7. Pitch gain vs. time constant.

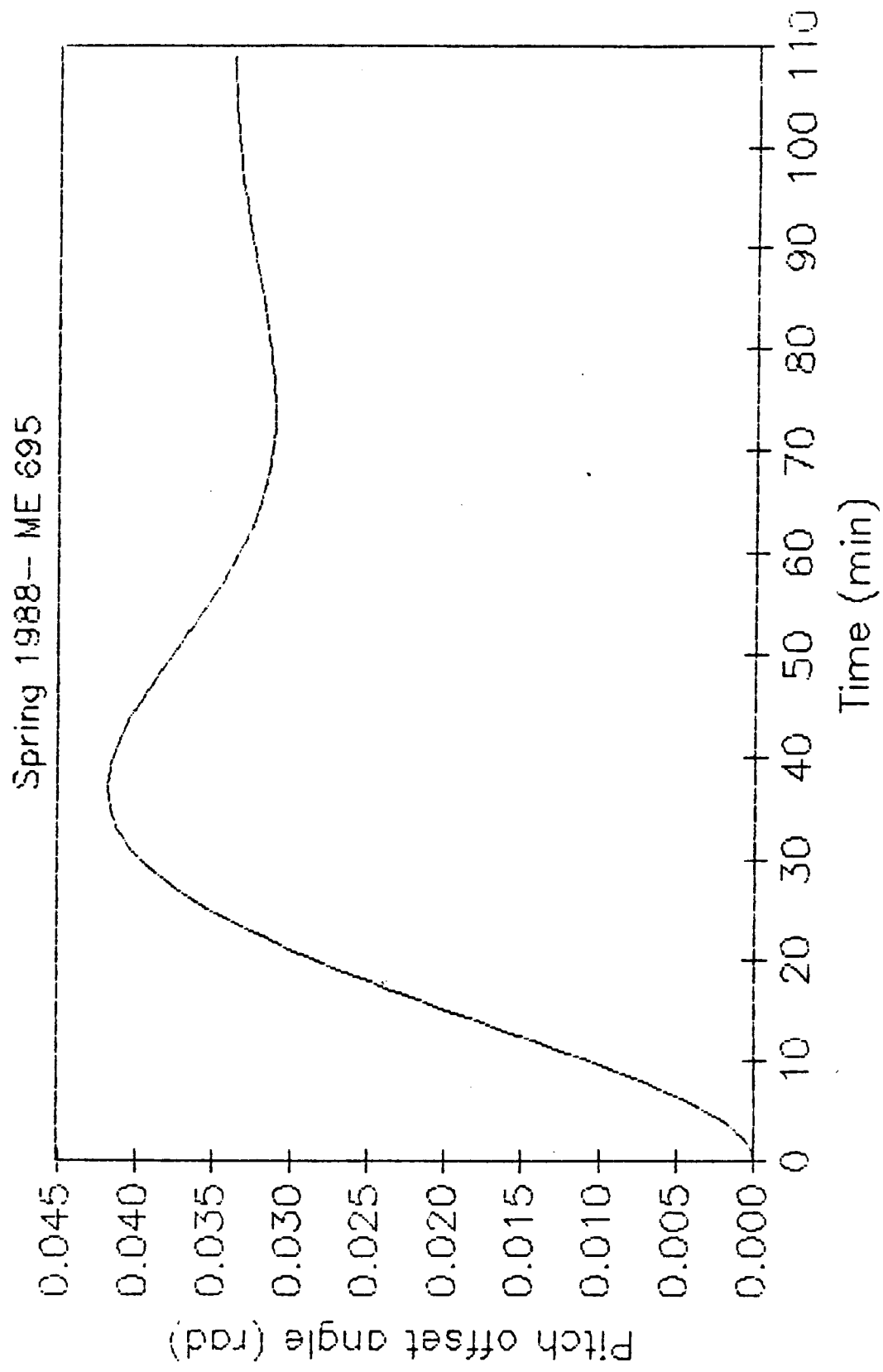


Figure 8. Underdamped motion of the pitch axis.

Spring 1988— ME 695

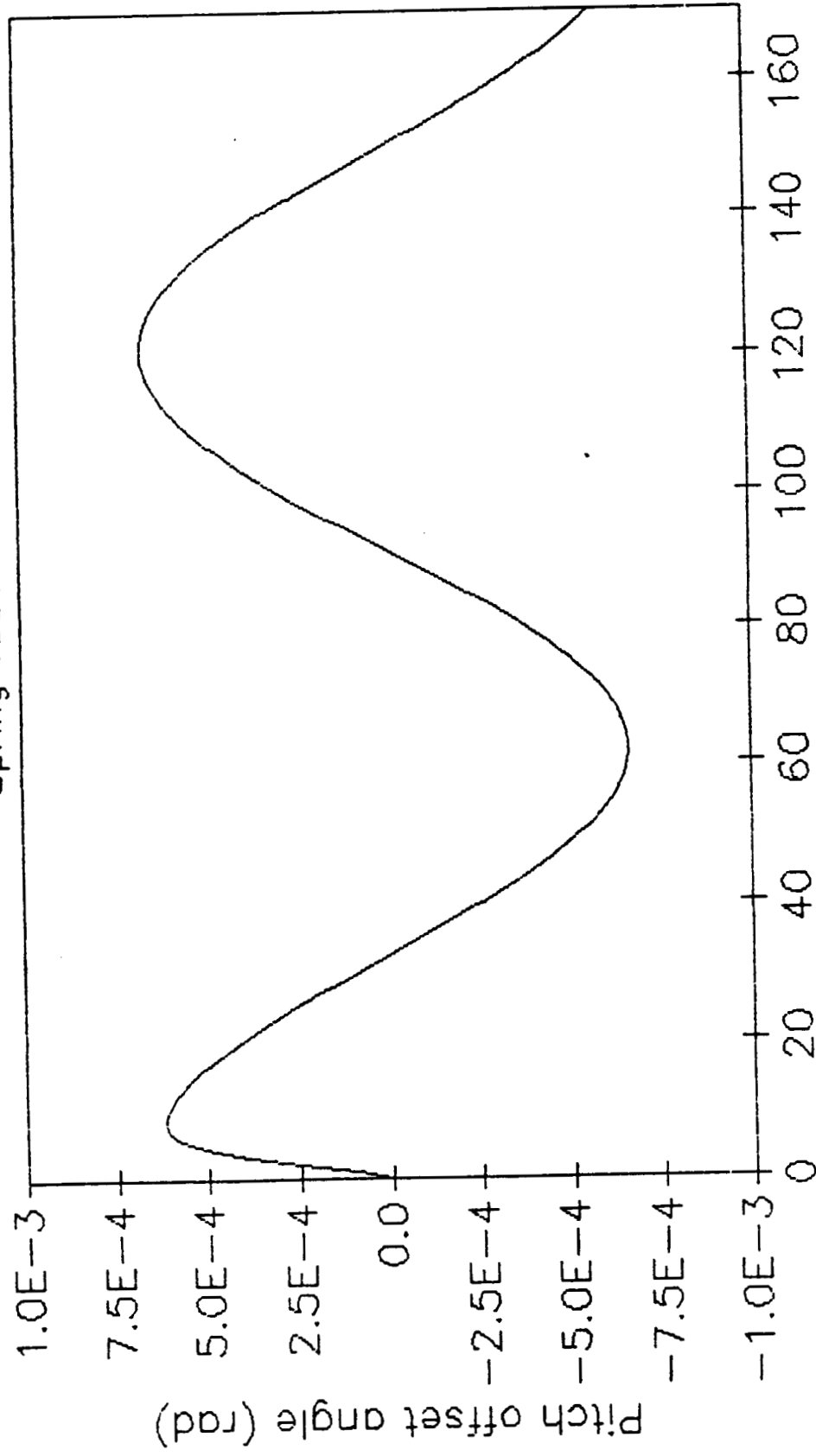


Figure 9. Pitch response to the cyclic solar pressure.

Spring 1988— ME 695

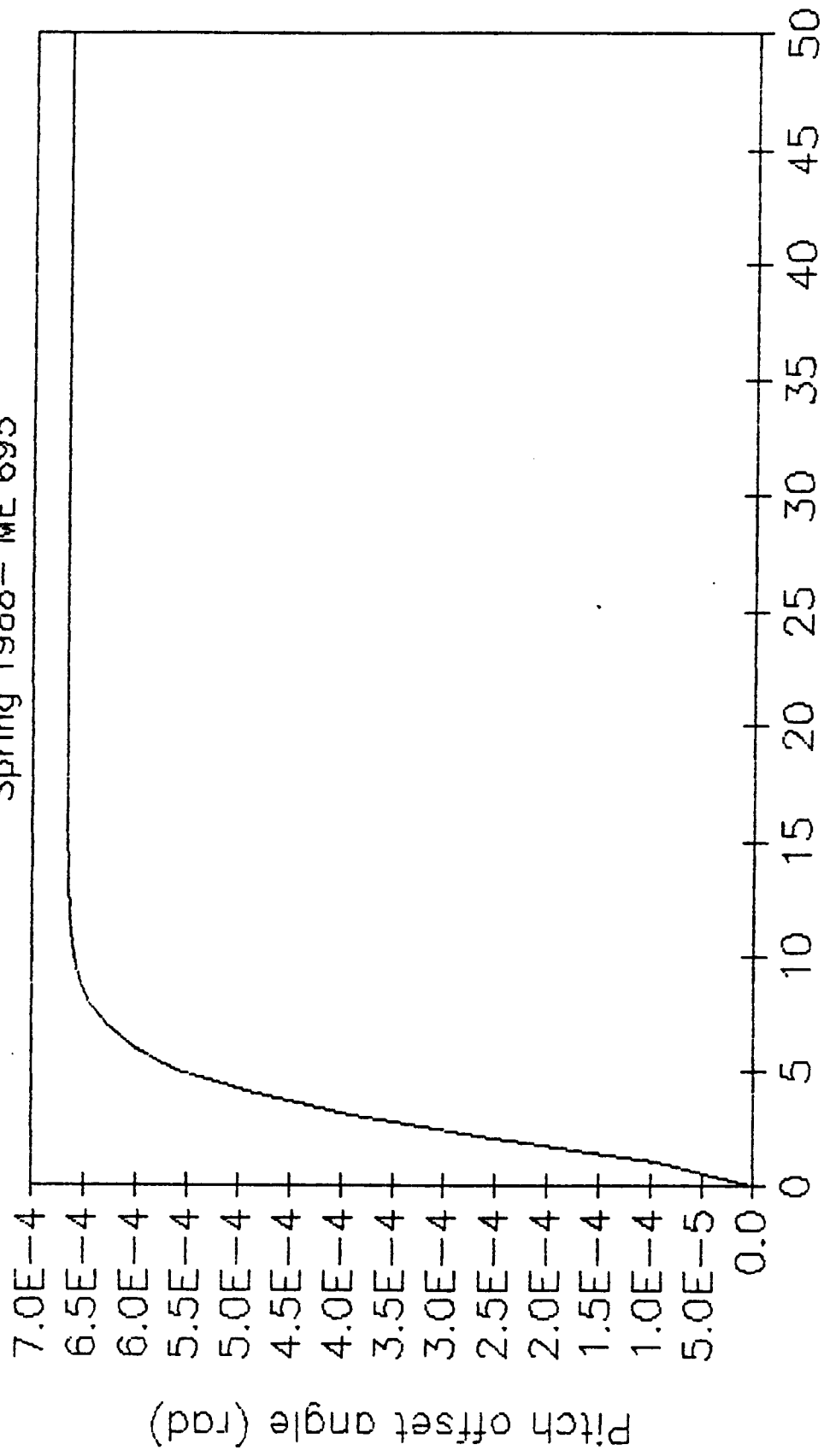


Figure 10. Pitch response to the step disturbing torque.

Spring 1988— ME 695

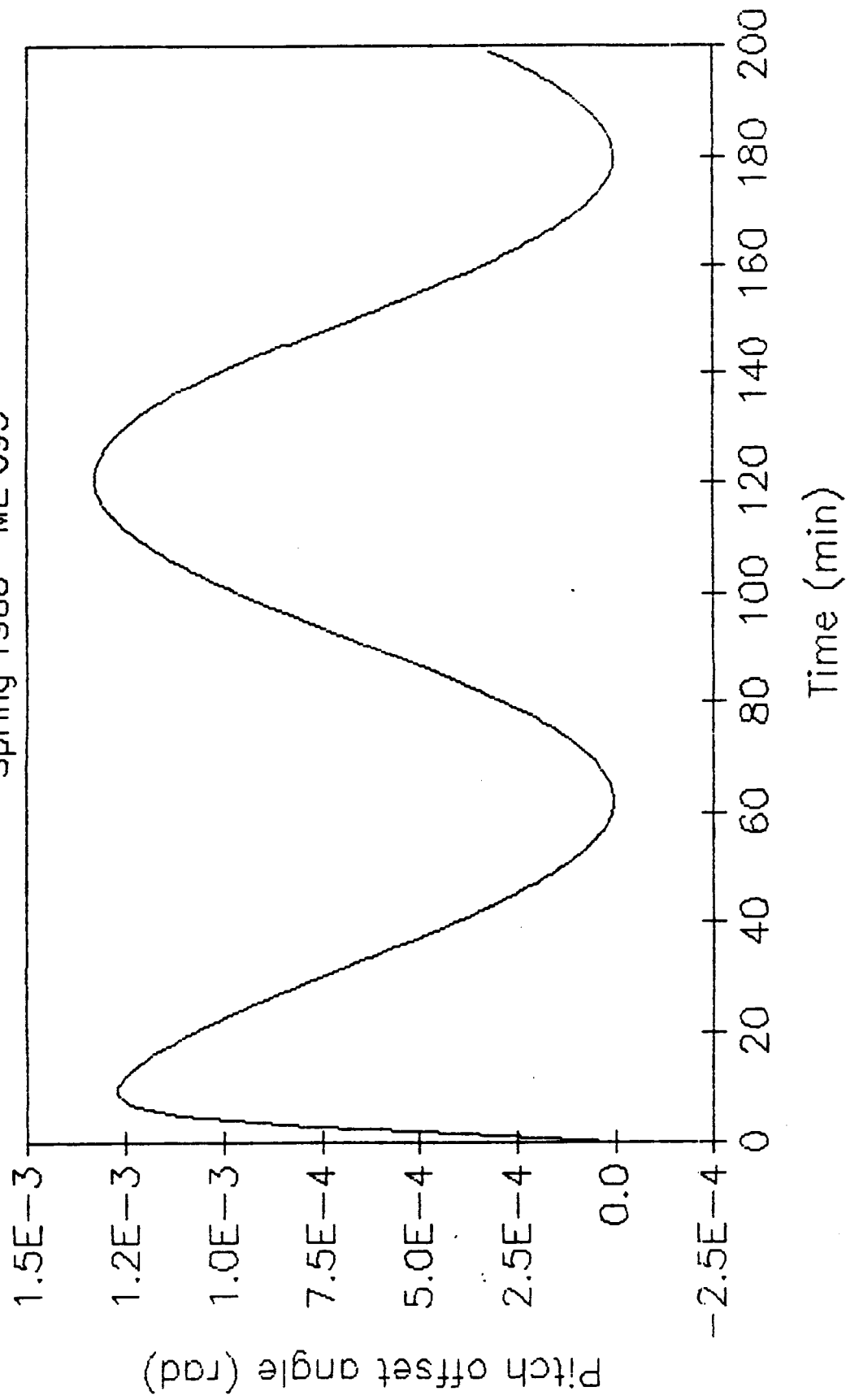


Figure 11. Superposition of the two disturbing torques.

axis, produced the response of Fig. 10. The step disturbance torque result in a steady state error of 0.00067 rad . The result of the superposition is depicted in Fig. 11. The result is a stable periodic response with the amplitude of 0.00134 rad . Note that, the oscillation of the pitch axis (Fig. 11) is about $\theta_p = 0.00067 \text{ rad}$ which corresponds to the steady state error due to the step disturbance torque.

15.3 The Roll/Yaw Loop

Now that the pitch loop design has been completed and the pitch axis is stable, the more sophisticated roll/yaw control system can be attempted. The yaw error is not sensed, but if it is, a control loop could be added for yaw as well. Unfortunately, yaw sensing is a complex proposition, and the development of space-proved yaw sensing hardware has lagged behind Earth sensing. Even though now available, these devices are very expensive, and consequently yaw sensing is avoided unless absolutely necessary. It is often preferable to use a momentum wheel, as in Fig. 1. This couples roll and yaw together, so that stabilization for roll becomes stabilization for yaw also. Control torques, can be produced through variation of gimbal angles (γ , and δ). Through the horizon sensor, direct roll sensing is available and the error of this axis can directly be corrected. Yaw Deviations are sensed indirectly through coupling with the roll axis (since the yaw/roll errors are 90° out of phase, the roll error becomes the yaw error after a quarter of a orbit).

The linearized equations of motion for roll and yaw were given in Set (10). Significant coupling effect are achieved through large values of bias momentum (h_n). Thus, the bias momentum needs to be very much greater than the angular momentum due to the orbital frequency (ω_o).

$$h_n \gg [I_x \omega_o, \quad I_y \omega_o, \quad I_z \omega_o] \quad (18)$$

To investigate active roll/yaw control, rewrite control terms of Set (10),

$$M_{xc} = \dot{h}_{xc} - \omega_o h_{zc}, \quad M_{zc} = \dot{h}_{zc} + \omega_o h_{xc} - h_n \dot{\phi} \quad (19)$$

To simplify the control system and elimininate the $\ddot{\phi}$ terms in the the yaw equation of motion, it is convenient to define *orbital rate decoupled* momentum commands,

$$h_{xd} = h_{xc}, \quad h_{zd} = h_{zc} - h_n \phi \quad (20)$$

where h_{xd} , and h_{zd} are the roll and yaw commands, respectively. The control laws M_{xc} (roll), and M_{zc} (yaw), now written as

$$M_{xc} = \dot{h}_{xd} - \omega_o h_{zd} = K(\tau \dot{\phi} + \phi) \quad (21.a)$$

$$M_{zc} = \dot{h}_{zd} + \omega_o h_{xd} = -kK(\tau \dot{\phi} + \phi) \quad (21.b)$$

where k is the yaw-to-roll gain ratio, K and τ are the roll gain and time constant, respectively. As mentioned elsewhere, in term of the gimbal angle deflection, $h_{xd} = \gamma h_n$, and $h_{zd} = -\delta h_n - h_n \phi$. Substitution of Set (21) into (10) yields the equations of motion for roll/yaw as

$$T_x = I_x \ddot{\phi} + K\tau \dot{\phi} + K\phi + h_n \dot{\psi} \quad (22.a)$$

$$T_z = I_z \ddot{\psi} + \omega_o h_n \dot{\psi} - kK\tau \dot{\phi} - kK\phi \quad (22.b)$$

Take the Laplace transfer of Set (22) and rewrite the equations in a matrix form,

$$\begin{pmatrix} T_x(s) \\ T_z(s) \end{pmatrix} = \begin{pmatrix} I_x s^2 + K\tau s + K & h_n s \\ -kK\tau s - kK & I_z s^2 + \omega_o h_n \end{pmatrix} \begin{pmatrix} \Phi(s) \\ \Psi(s) \end{pmatrix} \quad (23)$$

which yields a fourth-order characteristic equation,

$$\begin{aligned} C.E. = & I_x I_z s^4 + K I_z \tau s^3 + (K I_z + I_x \omega_o h_n + kK\tau h_n) s^2 \\ & + (\omega_o h_n K\tau + kK h_n) s + \omega_o h_n K \end{aligned} \quad (24)$$

The roll and yaw responses are obtained (Cramer's rule), respectively from

$$\Phi(s) = \frac{T_z(s)(I_z s^2 + \omega_o h_n) - T_x(s)h_n s}{C.E.} \quad (25.a)$$

$$\Psi(s) = \frac{T_x(s)(I_x s^2 + K\tau s + K) + kK(\tau s + 1)T_z(s)}{C.E.} \quad (25.b)$$

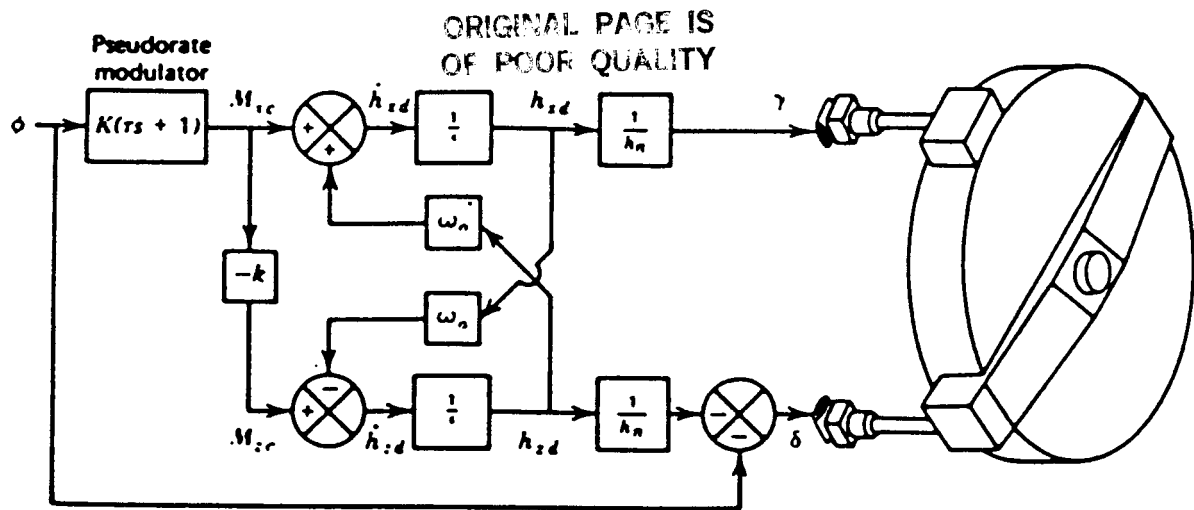


Figure 12. Roll/yaw control system².

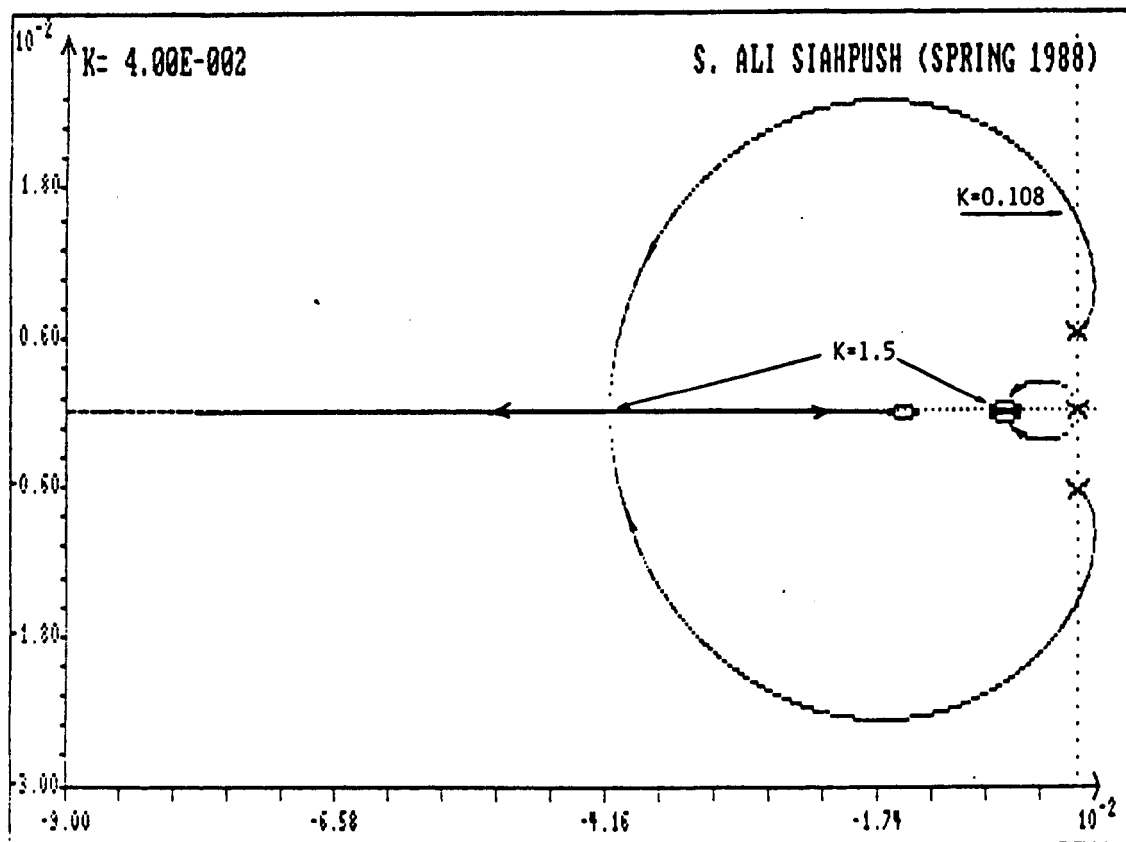


Figure 13. Root locus of the roll/yaw system.

and the block diagram of the roll/yaw control system is presented in Fig. 12.

The present form of the C.E. (Eq. (24)) can not be factored into the product of two quadratics. Assuming,

$$K\tau I_z \gg kh_n I_z \quad (26)$$

and adding this small term to the coefficient of s^3 will yield

$$C.E. \cong (I_x s^2 + K\tau s + K)(I_z s^2 + kh_n s + \omega_o h_n) \quad (27)$$

The roots of this equation will provide the natural frequencies and damping rates of the roll and yaw, respectively.

$$\omega_r = \sqrt{\frac{K}{I_x}}, \quad \zeta_r = \frac{\tau}{2} \sqrt{\frac{K}{I_x}} \quad (28.a)$$

$$\omega_y = \sqrt{\frac{\omega_o h_n}{I_z}}, \quad \zeta_y = \frac{k}{2} \sqrt{\frac{h_n}{\omega_o I_z}} \quad (28.b)$$

To satisfy the steady state condition, the roll gain needs to be evaluated. Applying the final value theorem to Eq. (25.a) will result the steady state roll error produced by a constant roll torque as

$$\phi_{ss} = \frac{T_{x \cdot max}}{K} \quad (29)$$

where $T_{x \cdot max} = 1. \times 10^{-4} \text{ N} \cdot \text{m}$. Based on the allowable steady state roll error of 0.5° , the minimum required value of $K = 0.0114 \frac{\text{N} \cdot \text{m}}{\text{rad}}$ with the corresponding natural frequency of $\omega_r = 0.00334 \frac{\text{rad}}{\text{sec}}$ is obtained.

Smaller steady state error can be obtained through larger value of K . The roll gain of $1.5 \frac{\text{N} \cdot \text{m}}{\text{rad}}$ is selected which result in a very near critical damped motion. This K value corresponds to $\tau = 52 \text{ sec}$, and $\omega_r = 0.0384 \frac{\text{rad}}{\text{sec}}$. It should be noted that, this choice is preliminary and must satisfy condition (26).

The steady state yaw error can be obtained directly from Eq. (25.b). Again, the final value theorem is used, and the result is

$$\psi_{ss} = \frac{T_{z\cdot max} + kT_{x\cdot max}}{\omega_o h_n} \quad (30)$$

The contribution of roll torque to ψ_{ss} can be ignored, since k is selected to be small. So, only yaw disturbance torque needs to be considered. The resulting condition on h_n is

$$h_n \geq \left| \frac{T_{z\cdot max}}{\omega_o \psi_{ss\cdot max}} \right| \quad (31)$$

where $T_{z\cdot max} = 5 \times 10^{-5} \text{ N} \cdot \text{m}$, $\psi_{ss\cdot max} = 0.5^\circ$. This leads to a minimum value of $7 \text{ N} \cdot \text{m} \cdot \text{s}$ for the nominal momentum. Thus, from Eq. (28.b) for $\zeta_y = 1$ and $h_n = 30 \text{ N} \cdot \text{m} \cdot \text{s}$, the yaw-to-roll gain ratio, and ω_y is evaluated as

$$\omega_y = 0.0639 \frac{\text{rad}}{\text{sec}}, \quad k = 0.278$$

Furthermore, parameter selections satisfy condition (18) and (26). Therefore, $h_n = 30 \text{ N} \cdot \text{m} \cdot \text{sec}$ appears to satisfy all criteria for the system.

15.3.1 Root Locus of the Roll/Yaw Loop

As mentioned before, adjustment of parameter values can be made with the aid of the system root locus diagram. Summary of guidelines for plotting a root locus is presented in Table 1. Following the steps of Table 1 yields

Step 1. In order to plot the root locus diagram, it is desired to have the C.E. in a form of $1 + K \frac{b(s)}{a(s)}$. The roots of $b(s) = 0$ are the zeros, while the roots of $a(s)$ are the open loop poles. Equation (24) is transformed to the desired form through dividing the C.E. by $I_x I_z s^4 + I_x \omega_o h_n s^2$. The results are

$$\begin{aligned} b(s) &= I_z \tau s^3 + (I_z + k \tau h_n) s^2 + (\omega_o h_n \tau) s + \omega_o h_n \\ &= 42660.36 s^3 + 1197.6 s^2 + 10.087 s + 0.0267 \end{aligned} \quad (32.a)$$

$$\begin{aligned} a(s) &= I_x I_z s^4 + I_x \omega_o h_n s^2 \\ &= 663084 s^4 + 27.408 s^2 \end{aligned} \quad (32.b)$$

where roots of $b(s)$ (zero) are at $s = -0.00568, -0.00568, -0.0172$ and roots of $a(s)$ (pole) are at $s = 0, 0, \pm j0.00642$.

Step 2. This step is illustrated in Fig. 13.

Step 3. $n - m = 1$, and $\sum p - \sum z = 0.0285$. So asymptotes are located at $s = -0.0285$ with the associated angles of $\pm 180^\circ$.

Step 4. The departure angles at $s = 0$ are $\pm 90^\circ$ ($-2\theta_{dep} = \pm 180^\circ$), and for poles at $s = \pm j0.00642$ are $\pm 7.242^\circ$, respectively ($-(\theta_{dep} + 90 + 90 + 90) + (45 + 45 + 7.242) = \pm 180^\circ$).

Step 5. Using the Routh's criteria for asymptotic stability will impose a minimum value of $K = 0.108$. Values less than 0.108 will be on the right side of the imaginary axis and are unstable. Substitution of $s = j\omega$ into the C.E. shows that the locus crosses the imaginary axis at $s = \pm j0.0156$ which corresponds to the roll gain of 0.108.

Step 6. Utilizing equation of the step 6 (Table 1) shows that the break-away points are at $s = 0, \pm j0.00568$ and break-in points are at $s = -0.00568$, and -0.0505 .

Step 7. The completed root locus diagram for roll/yaw loop is presented in Fig. 13. The design value of $K = 1.5$ and $K = 0.108$ (at this point locus crosses the imaginary axis) is depicted on the diagram.

15.3.2 Computer Simulation of the Roll/Yaw Loop

The same computer model is utilized to simulate the dynamic behavior of the roll/yaw loop. The FORTRAN code is presented in Appendix A. The effect of roll gain variation on the steady state error (ϕ_{ss}) is plotted in Fig. 14. The selected value of K is $1.5 \frac{N \cdot m}{rad}$ which corresponds to $\phi_{ss} = 0.0066 \text{ rad}$. In the vicinity of this K value, the slope of the curve approaches zero, rapidly. After selecting the roll gain, the attention is toward the nominal momentum selection. Equation (28.b) is used to

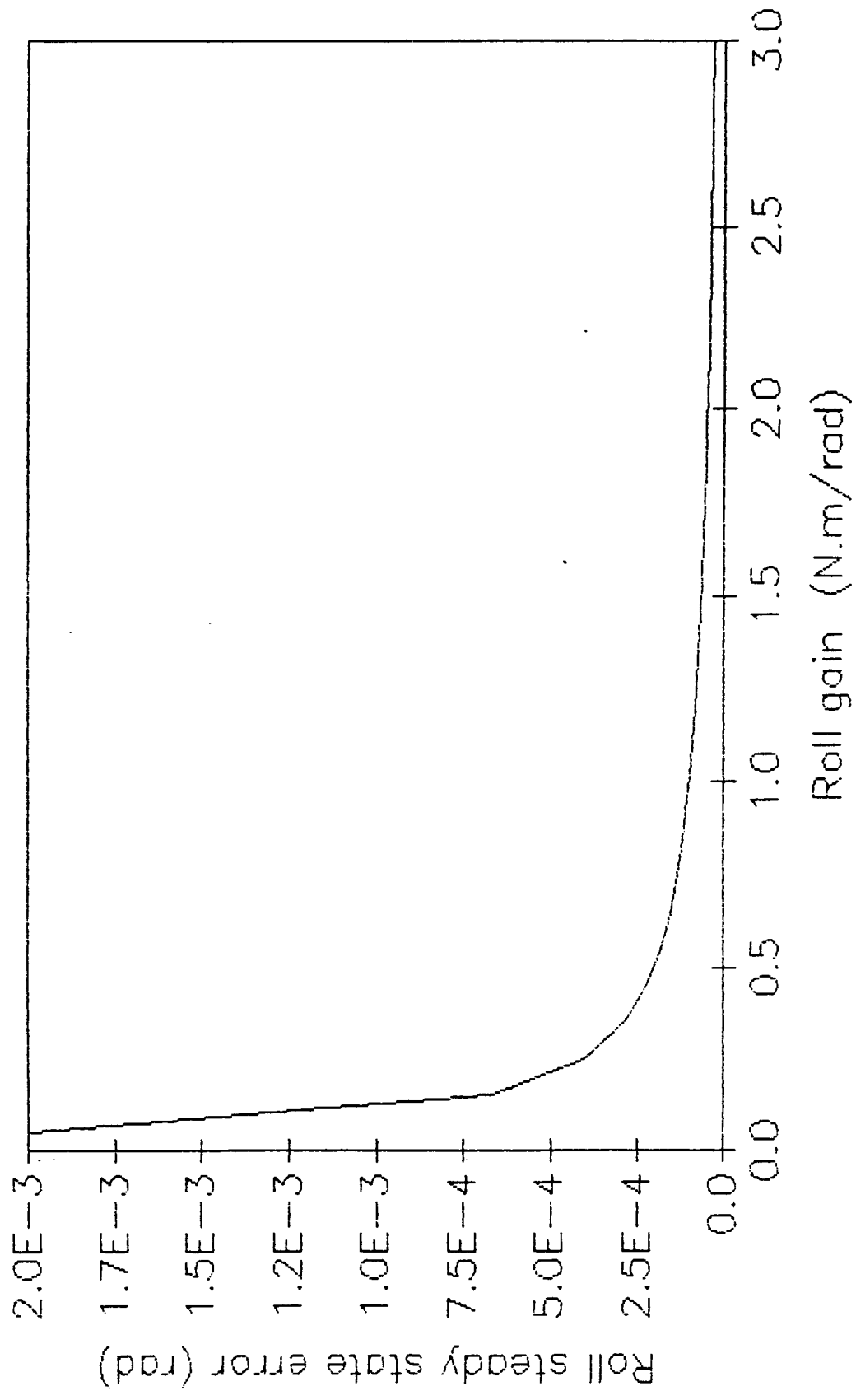


Figure 14. Roll gain vs. steady state error.

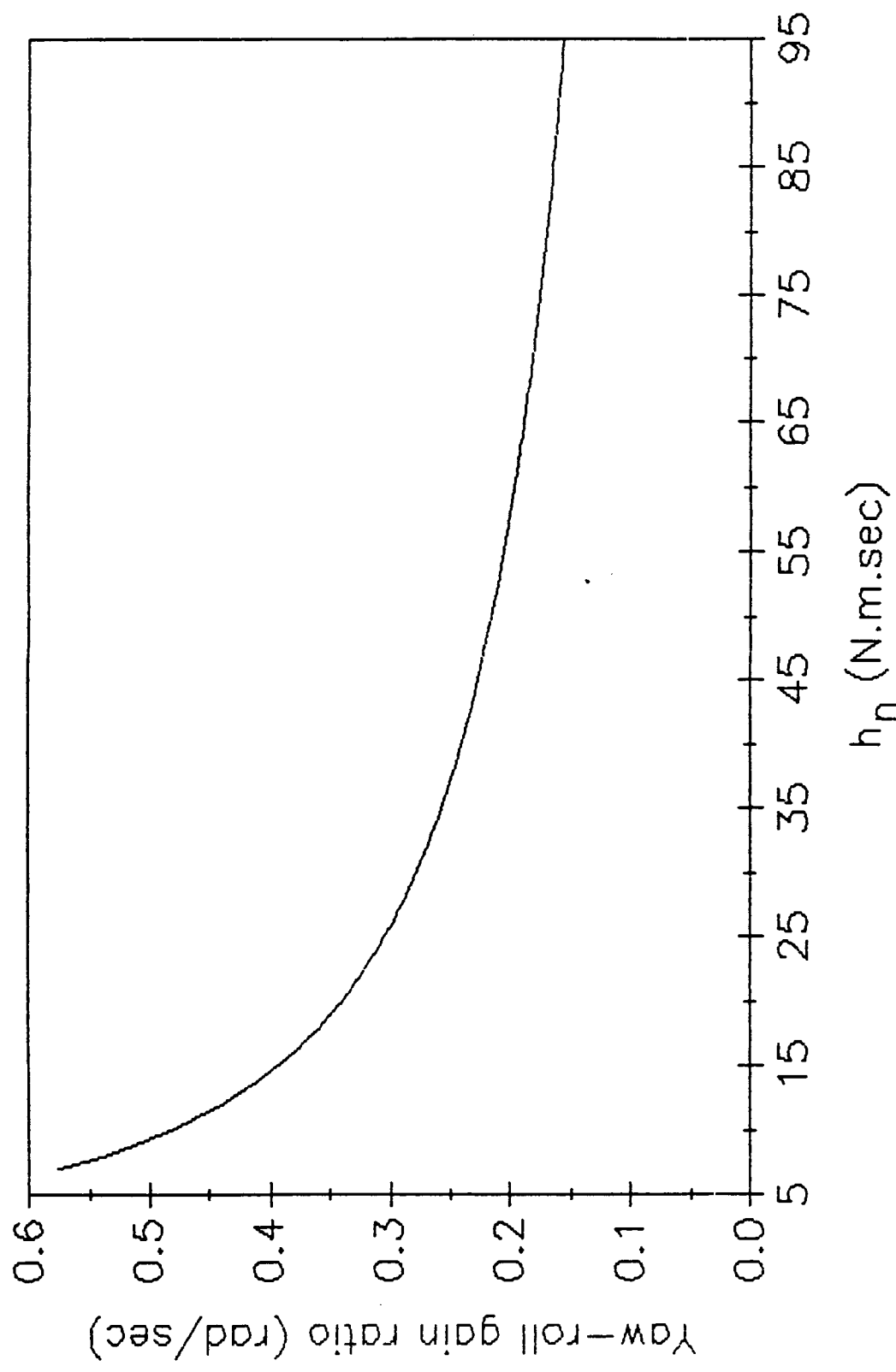


Figure 15. Response of the yaw-to-roll ratio to the nominal momentum.

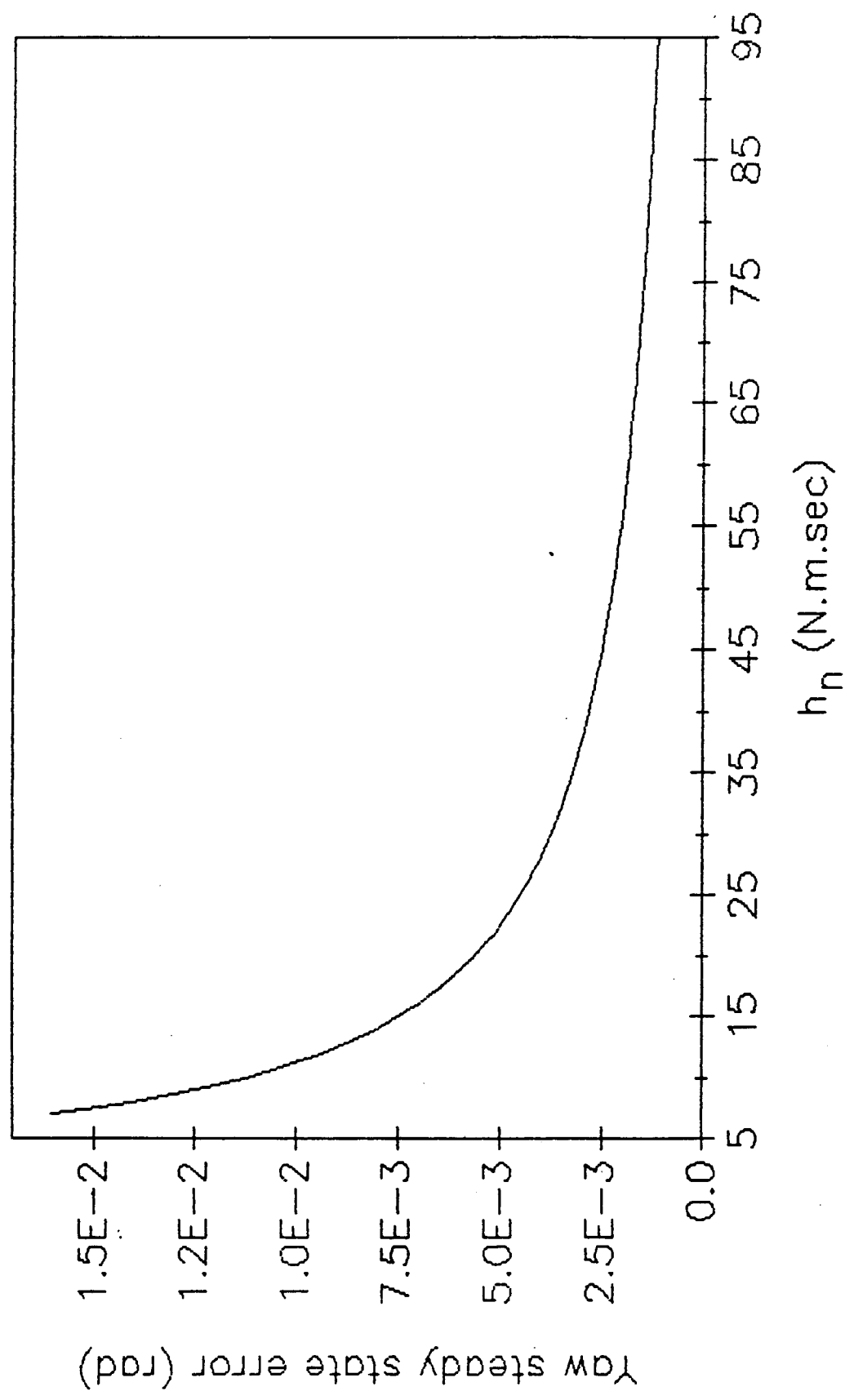


Figure 16. Variation of the yaw steady error vs. the nominal momentum.

simulate the response of the yaw-to-roll ratio to the nominal momentum. The result is plotted in Fig. 15. This figure shows that, the designed value of $h_n = 30 \text{ N} \cdot \text{m} \cdot \text{s}$ satisfies conditions (18) and (26). Also, the corresponded $k = 0.278$ validated the assumption made on the effect of the k value to the yaw steady state error (Eq. 30). Figure 16 illustrates the variation of h_n vs. the yaw steady state error. It can be seen from this figure that the yaw steady state error decreases gradually as the nominal momentum increases.

Set (10) is used to simulate the responses by roll and yaw, with the gain and damping value selected before. The results for cyclic, and step disturbance torques are plotted in Figs 17 and 18, respectively. A cyclic disturbance torques due to solar pressure causes the periodic responses of Figs 17.a and 17.b. The amplitudes of Figs. 17.a and 17.b can be predicted, analytically from Eqs. (29) and (30), respectively. As it can be seen from these figures, neither the yaw nor the roll exceeded the steady state error limitations. Analytically, from Set (25), with $T_z = 0$, $T_x = 1.0 \times 10^{-4} \text{ N} \cdot \text{m}$, through the final value theorem, the steady state errors due to the step disturbance torque is evaluated to be $\phi_{ss} = 0.0000667$ and $\psi_{ss} = 0.000207 \text{ rad}$. Figures 18.a and 18.b present the numerical results of the roll and yaw response to a step disturbance torque in the roll direction. No discrepancy was detected when the numerical and analytical results were compared.

It should be noted that, the axes of libration in Figs. 17.a and 17.b are not zero. As expected, the cause of these shifts are the cyclic torque due to the solar pressure. Figure 19 presents the solar torque effect on the roll and yaw libration, respectively. At time zero, the first term in the roll solar torque ($T_x = 2 \times 10^{-5} - 4 \times 10^{-5} \sin(\omega_o t)$) is a step input disturbing torque which contributes to the shifting of the libration axis.

The final attempt to predict dynamics of the system is to examine the K variation effects on the roll/yaw axis. Theoretically, the minimum calculated value of K is 0.108 (from root locus) and smaller values will result in unstable motion. To verify this assumption, a case was simulated ($K = 0.005$). The response of the roll axis is plotted in Fig. 20. This figure confirm the assumption and shows the response is growing periodically (very slowly).

15.4 Momentum wheel desaturation

Due to the various environmental disturbing torques acting on the spacecraft, the stored angular momentum in the momentum wheel will increase with time. After several orbits this momentum accumulation may exceed the storage capacity of the momentum wheel. Therefore, provision is made for periodic desaturation

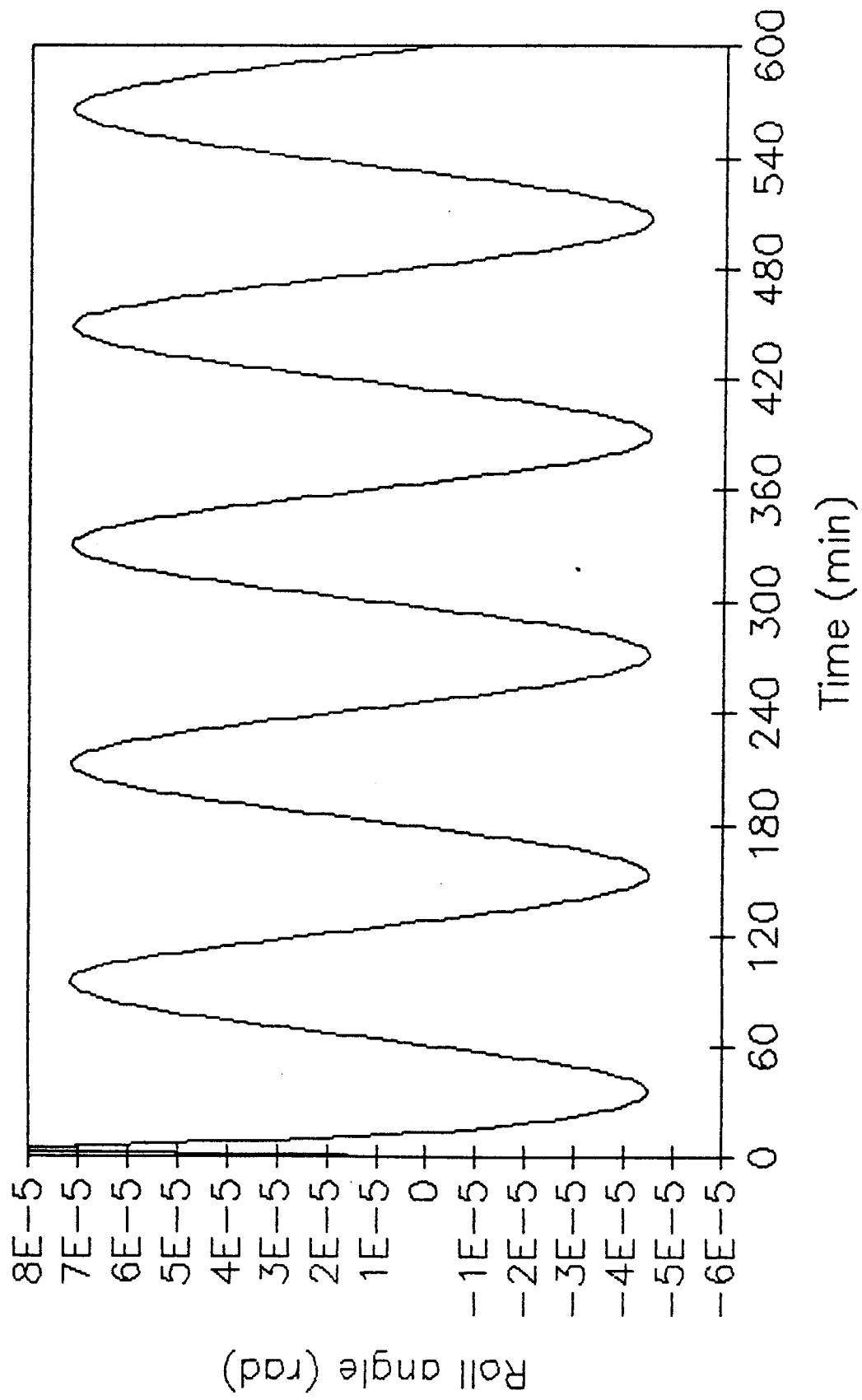


Figure 17.a. Roll response vs. cyclic solar torque.

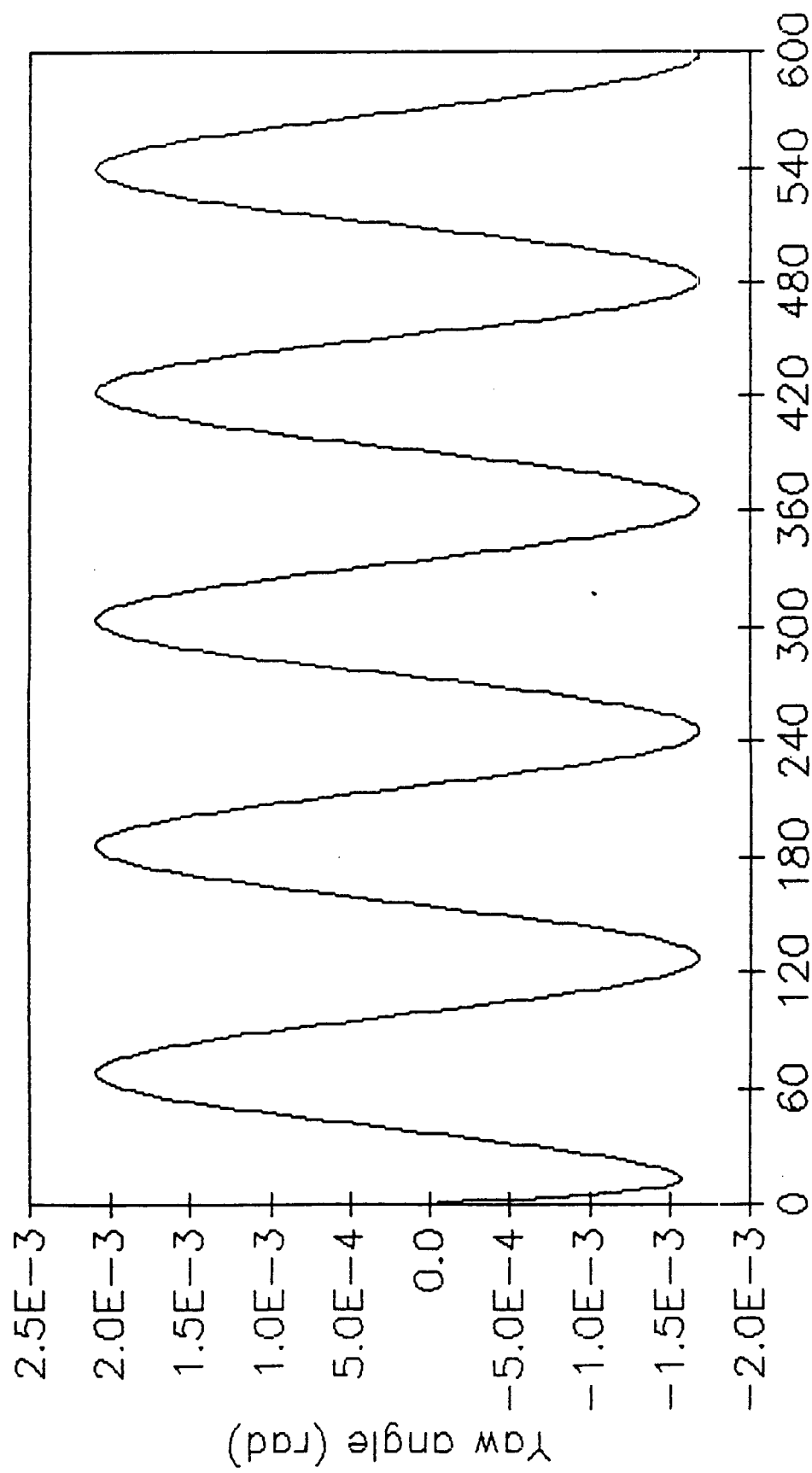


Figure 17.b. Yaw response vs. cyclic solar torque.

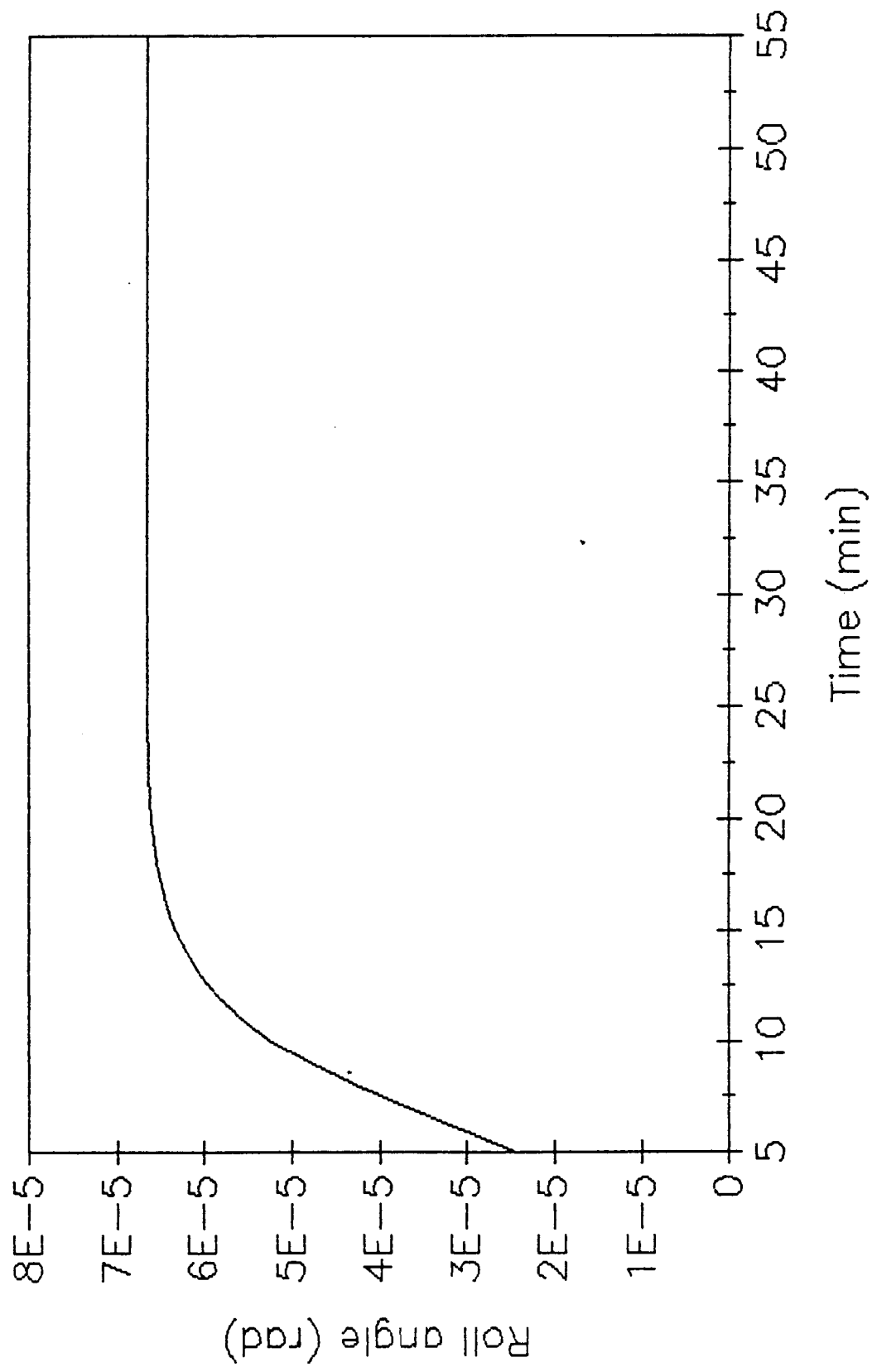


Figure 18.a. Roll response vs. step disturbing torque.

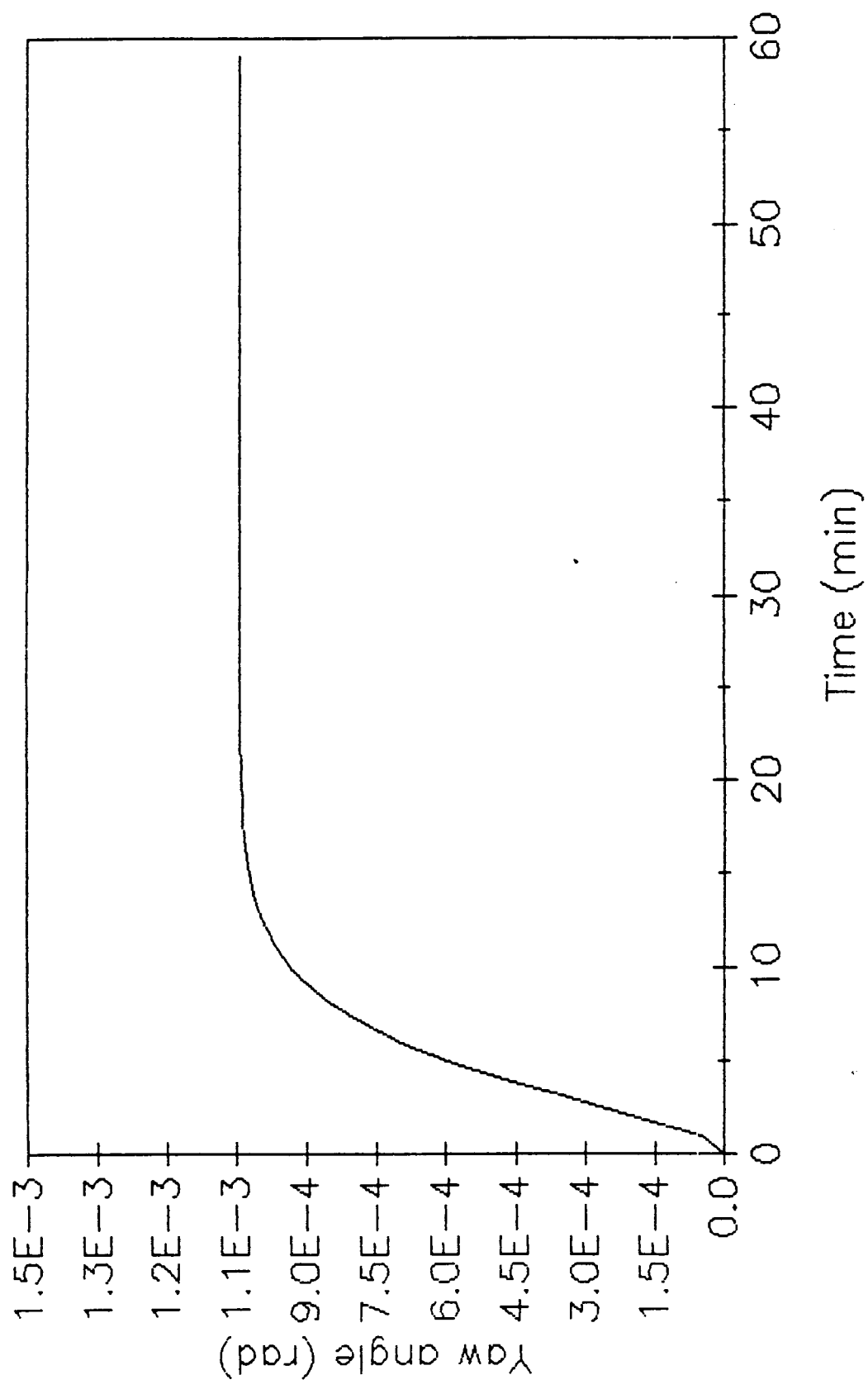


Figure 18.b.b. Yaw response vs. step disturbing torque.

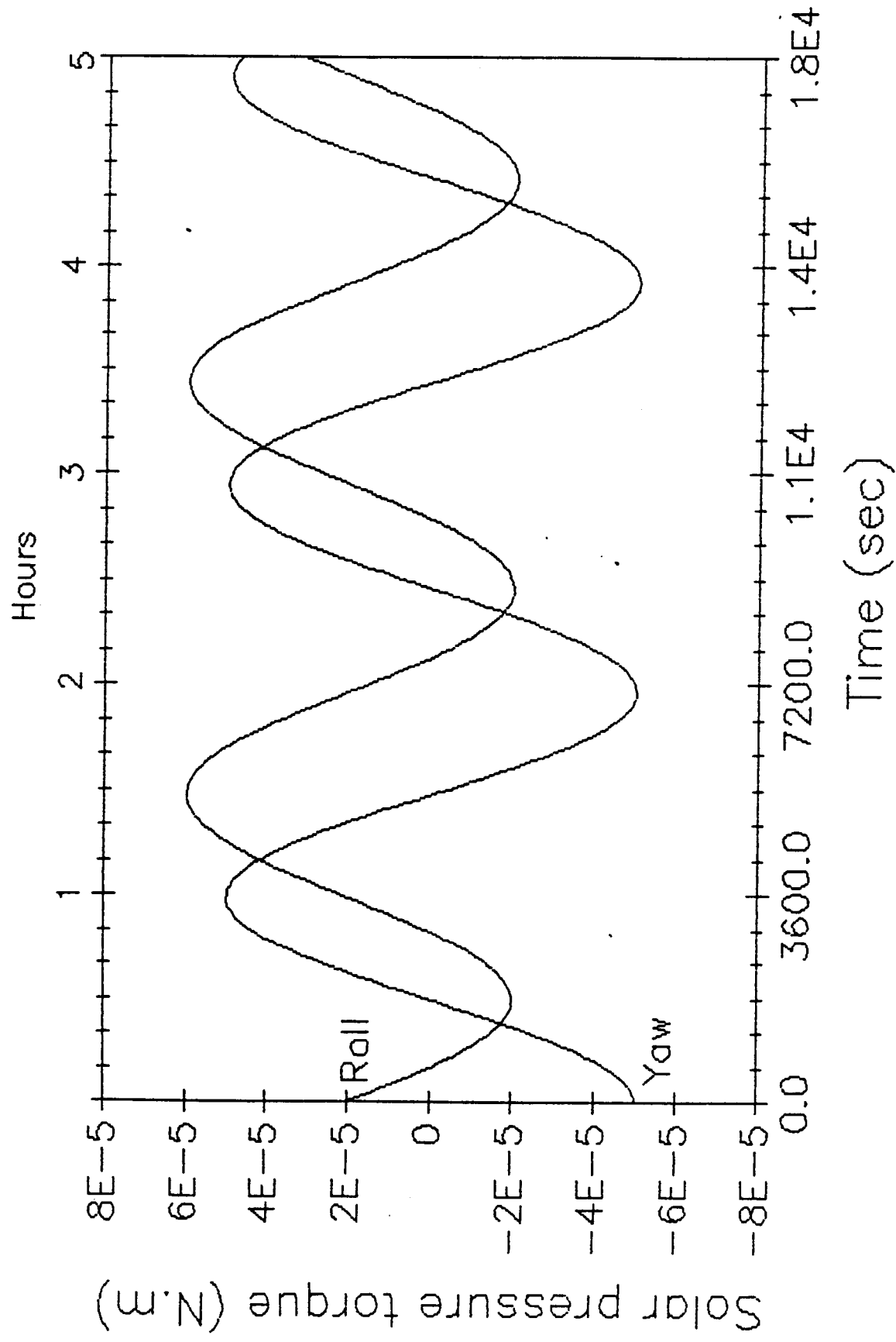


Figure 19. Cyclic solar torques vs. time.

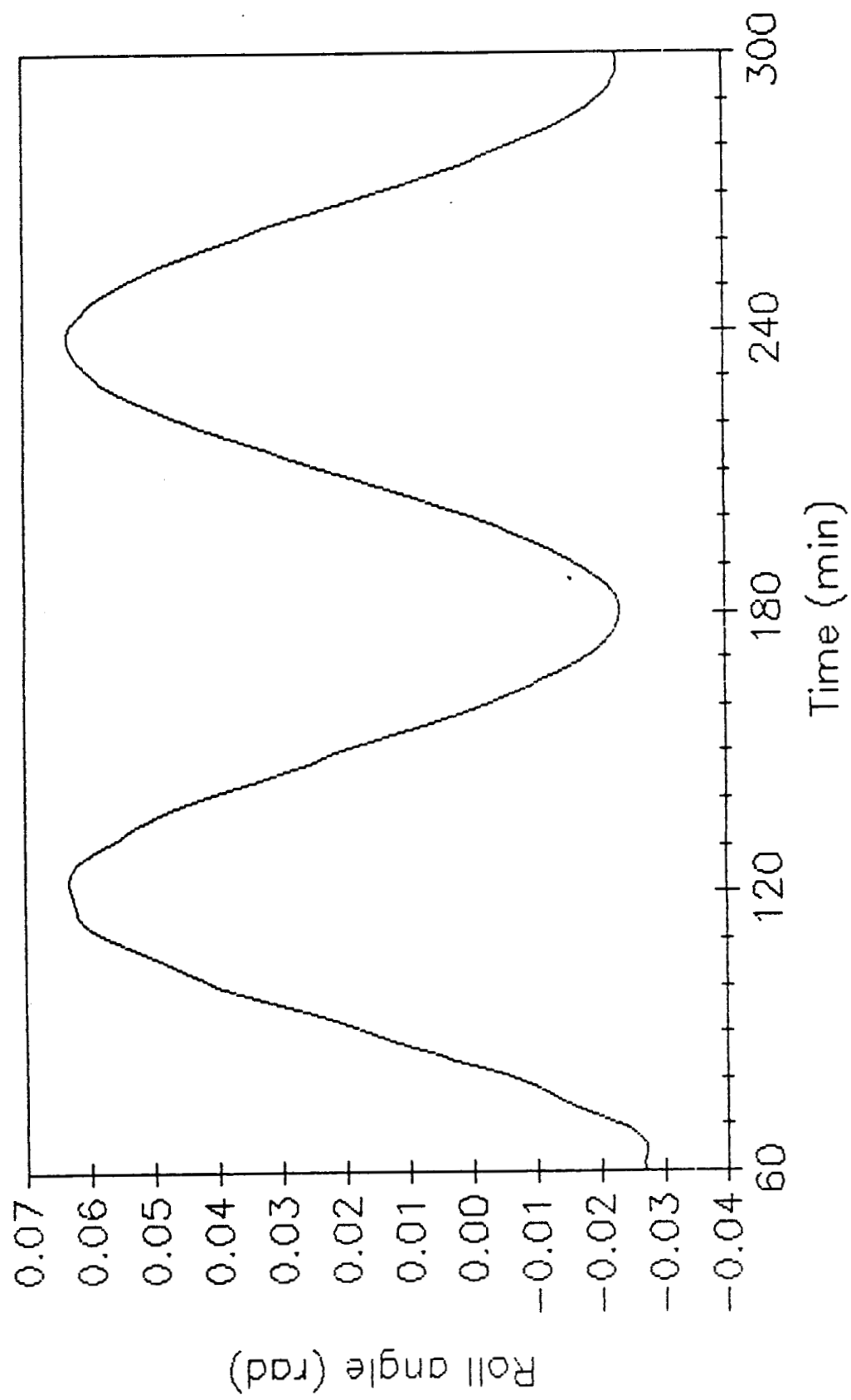


Figure 20. Unstable motion of the roll axis.

through external torques produced by gas jet or magnetic torquers. For the momentum wheel system to be continually effective, the desaturation technique must produce bias torques opposite in direction to the disturbance torques, yielding a net accumulation momentum after each orbit that is less than the storage capacity of the momentum wheel system.

Since the magnetic field of the moon is very weak, the magnetic torquer is not practical, and using a hot gas jet is in favor. Hydrazine thruster (N_2H_4) is selected to perform the momentum wheel desaturation. Hydrazine with catalytic decomposition is the most frequently used hot-gas monopropellant system on spacecraft supported by Goddard Space Flight Center⁴ (NASA).

In a very simplified approach, with a reaction jet desaturation scheme, the desired desaturation torque \vec{T}_D is created by applying the appropriate force \vec{F} associated with its moment arm \vec{d} to the spacecraft center-of-mass ($\vec{T}_D = \vec{d} \times \vec{F}$). Buried in this equation are: (1) the magnitude and direction of the force (torque); (2) size of the thruster tank; (3) time between each thrust; (4) firing period. These questions can be answered easily, if the following fundamental question is answered. What is the maximum angular momentum that the wheel can tolerate (saturation point)?

15.5 Conclusion

The control system presented in this paper is primarily designed to control disturbance torques due to solar pressure which are essentially cyclic; the response to the step input due to thruster misalignment torque is also considered. The numerical results shows that for any stable condition the "D" terms are small and after one orbital period these terms converge to zero.

After comparison of analytical and numerical results, we gain confidence that the simulation computer code provides a correct quantitative representation of the attitude dynamics of the satellite. Thus, the resulting system is capable of maintaining accurate attitude orientation through the use of only a pitch-roll horizon sensor; still further studies in this field are needed to understand the more profound and realistic relations between the different processes defining attitude dynamics of the satellite.

REFERENCES

- [1]. Mingori, D. L., and Kane, T. R., "The Attitude Stabilization of Rotating satellite by Means of Gyroscopic Devices," *Journal of Astronautics Science*, 9 (No. 11), 1967, pp 158-166.
- [2]. Kaplan, M., *Modern Spacecraft Dynamics and Control*, John Wiley, New York, 1976.
- [3]. Franklin G. F., Powell J. D., and Emami-Naeini A., *Feedback Control of dynamic System*, Addison-Wesley, Massachusetts, 1986.
- [4]. Wertz James R., *Spacecraft Attitude Determination and Control*, D. Reidel Publication Company, Boston, 1985.

APPENDIX 4
Instruments

APPENDIX A
LUNAR ORBITING PLATFORM
INSTRUMENT SPECIFICATIONS

INSTRUMENT	VISUAL AND INFRARED MAPPING SPECTROMETER	GAMMA RAY SPECTROMETER
MASS (KG)	30 (electronics and radiator)	15 (electronics & cooler)
POWER (W)	12 ave, 13 peak	10
SIZE (cm)	optics: 40/40/40 elect.: 20/25/13	29/32/50
MOUNTING	bus	boom > one space-craft diameter from space-craft
ORIENTATION	optics: nadir sensor: space	det.: nadir cooler: space
FIELD OF VIEW	optics: 0.5°/6.9° cooler: 150°	det.: 150° cooler: 150°
COOLING	passive radiator (120k) focal plane 80k	passive radiator 100-110 K
RESTRICTIONS	sensitive to gas and particulate contam. on optics and thermal controls	no radioisotopes, mag. fields > 1 G (RTG's potassium paints, etc.)
ENVIRONMENT OUTPUTS	none	weak magnetic field
DUTY CYCLE	daylight side only	continuous
DATA RATE (Kb/s)	1.5, 3, 6, 12 internal command	1.5
DATA VOLUME (bits/day)	up to 15×10^9	1.3×10^8

INSTRUMENT	X-RAY SPECTROMETER	MAGNETOMETER
MASS (KG)	11	3
POWER (W)	10	3
SIZE (cm)	20/20/20	sensor: 8/5/5 elec.: 22/11/15
MOUNTING	body	sensor on boom > 3 space-craft diameters from space-craft body
ORIENTATION	cooler: space solar monitor: anti-nadir	orthogonal sensors
FIELD OF VIEW	solar detector: 20° monitor: 20° cooler: 150°	-
COOLING	TBD (150 K if SiLi detector is used)	-
RESTRICTIONS	no solar reflectance from space-craft components	no space-craft magnetic fields >0.01 nT at sensor location
ENVIRONMENT OUTPUTS	none	weak magnetic (100 nT)
DUTY CYCLE	daylight only	continuous
DATA RATE (Kb/s)	0.3	0.4
DATA VOLUME (bits/day)	3.2×10^7	3×10^7

INSTRUMENT	THERMAL INFRARED MAPPING SPECTROMETER	ELECTRON REFLECTOMETER
MASS (KG)	16	5
POWER (W)	12	
SIZE (cm)	60/50/30	20/20/20
MOUNTING	bus	boom mounted
ORIENTATION	nadir	nadir/zenith
FIELD OF VIEW	30°	5° by 360° in nadir zenith plane
COOLING	100 K passive	none
RESTRICTIONS	no gas or dust contaminants on optics	must fly with magnetometer, no space-craft magnetic fields > 0.01nT, no electrostatic charge.
ENVIRONMENT OUTPUTS	none	none
DUTY CYCLE	continuous	continuous
DATA RATE (Kb/s)	10	0.3
DATA VOLUME (bits/day)	8.6×10^8	2.6×10^7

INSTRUMENT	GEODESIC IMAGER	MICROWAVE RADIOMETER
MASS (KG)	11	10 w/ antenna
POWER (W)	12	5
SIZE (cm)	camera: 10/20/12 electronics: 25/18/5	antenna: 100/60/20 elect.: 10/30/40
MOUNTING	bus	bus
ORIENTATION	nadir and 50° forward	nadir
FIELD OF VIEW	41° by 21° nadir 35° by 11° forward	30°
COOLING	173 K passive	none
RESTRICTIONS	none	none
ENVIRONMENT OUTPUTS	none	none
DUTY CYCLE	daylight side only	minimum 3 data points per lunation. Noon and midnight for each point
DATA RATE (Kb/s)	5	0.2
DATA VOLUME (bits/day)	?	?

INSTRUMENT	HIGH RESOLUTION SOLID STATE IMAGER	ULTRAVIOLET SPECTROMETER
MASS (KG)	15	15
POWER (W)	20	13
SIZE (cm)	optics: 35/20/20 electronics: 40/20/10	TBD
MOUNTING	bus	bus
ORIENTATION	nadir	nadir
FIELD OF VIEW	1°	TBD
COOLING	passive, 250 K	none
RESTRICTIONS	sensitive to gas and particulates on optics	sensitive to gas and particulates on optics
ENVIRONMENT OUTPUTS	none	none
DUTY CYCLE	sunlight side only	sunlight side only
DATA RATE (Kb/s)	100,000 (100 Mb/s)	12
DATA VOLUME (bits/day)	?	15*10 ⁹

INSTRUMENT	RADAR SURFACE AND SUBSURFACE MAPPER
MASS (KG)	50
POWER (W)	200
SIZE (cm)	surface radar dish: 500 subsurface radar - two dipoles: 10.4m ea. transmitter receiver: 10/10/50 optical recorder: 70/70/70
MOUNTING	boom
ORIENTATION	variable w/ respect to nadir
FIELD OF VIEW	10km - 20km swath width @ 50km altitude (circular near polar orbit)
COOLING	heat pipe
RESTRICTIONS	none
ENVIRONMENT OUTPUTS	heat radar frequency: 30GHz (1cm wavelength) 3MHz - 300MHz (100m to 1m wavelength)
DUTY CYCLE	continuous
DATA RATE (Kb/s)	50 - 60
DATA VOLUME (bits/day)	4.3×10^9 to 5.2×10^9

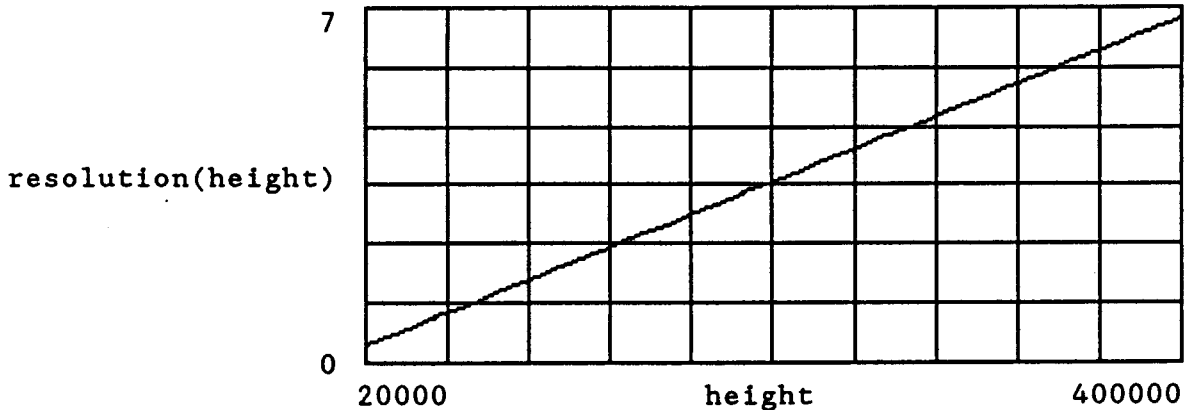
SIZING FOR VHRSSI OPTICS

$\mu\text{m} \equiv 1 \cdot 10^{-6} \cdot \text{m}$ $\text{km} \equiv 1 \cdot 10^3 \cdot \text{m}$ $d \equiv 15 \cdot \mu\text{m}$ distance from center to center of each sensing element in CCD

$\text{field_of_view} := \frac{\pi}{180}$ one degree field of view in radians.

$\text{height} := 20 \cdot \text{km}, 30 \cdot \text{km} \dots 400 \cdot \text{km}$

$\text{resolution}(\text{height}) := 2 \cdot \text{height} \cdot \frac{\tan\left[\frac{\text{field_of_view}}{2}\right]}{1024}$ for 1024 X 1024 pixel CCD sensor



$\text{resolution}(20 \cdot \text{km}) = 0.341 \cdot \text{m}$ $\text{resolution}(40 \cdot \text{km}) = 0.682 \cdot \text{m}$

$\text{resolution}(100 \cdot \text{km}) = 1.704 \cdot \text{m}$ $\text{resolution}(400 \cdot \text{km}) = 6.818 \cdot \text{m}$

set height := 100 km

$\text{focal_length} := \frac{\text{height} \cdot d}{\text{resolution}(\text{height})}$ focal_length = 880.041 mm

for an f5.6:1 system (same as proposed for LG0)

$\text{primary_size} := \frac{\text{focal_length}}{5.6}$ primary_size = 157.15 mm

$\text{secondary_size} := \frac{\text{primary_size}}{3}$ secondary_size = 52.383 mm

$\text{total_mass} := \left[\left[\frac{\text{primary_size}}{2} \right]^2 + \left[\frac{\text{secondary_size}}{2} \right]^2 \right] \cdot \pi \cdot p + 10 \cdot \text{kg}$
10 kg structure mass

total_mass = 13.578 kg

MASS CALCULATION FOR VIMS OPTICS

primary_size := 333·mm

secondary_size = 52.383·mm

$$\text{total_mass} := \left[\left[\frac{\text{primary_size}}{2} \right]^2 + \left[\frac{\text{secondary_size}}{2} \right]^2 \right] \cdot \pi \cdot p + 15 \cdot \text{kg}$$

15 kg structure mass

total_mass = 29.815·kg

primary_size := 333·mm

APPENDIX 7
Raman Spectroscopy

Appendix 7.A Method of Approximating Instrument Resolution and Required Mission Time

Resolution:

Specifications were used from the LGO manual as to the view angle of the instruments, and their resolution. Resolution figures were given in the manual for the instruments at an orbital altitude of 100 Km. The assumption was made that the surface of the Moon was relatively flat over the resolution range of the instruments, and the geometry of figure 1.a was used to estimate the resolution at an altitude of 30 Km.

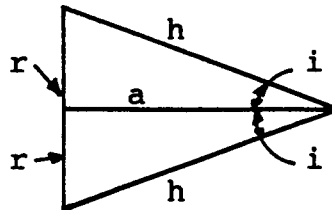


fig. 1.a

The dimension r was found as + the dimension given as the resolution in the manual. The dimension a is known as the altitude. The angle i was found using formula F1 below. The length h was found using formula F2. The resolution r at altitude $a = 30$ Km was then found using formula F3 .

F1	$i = \arctan(r/a)$
F2	$h = a/\cos(i)$
F3	$r = 2(h\sin(i))$
F4	$n = 2cR/2r$
F5	$t = (n \text{ orbits})(2 \text{ hours/orbit})$

Mission Time:

The figures for the view angle of each instrument were taken from the LGO manual. The view angle was taken as 2 times the angle i in figure 1.a above. Using the formulas F2 and F3 above the swath width of each instrument as it orbits the Moon was estimated to be equal to r . Assuming continuous operation of the instruments, the number of orbits n required for complete surface coverage was estimated using formula F4 above. ($2r$ is used for the swath width because the orbiter traces 2 swaths for each orbit). The time for complete coverage of the surface of the Moon was then estimated using formula F5 above. (R is taken to be the mean surface radius of the Moon, 1730 Km).

Appendix 7.B

Surface Coverage and Signal Intensity at the Spacecraft.

Surface Coverage:

At an altitude of 25 km the spacecraft has an orbital velocity of 1.66 km/s. This causes 1.64 km of the lunar surface to pass beneath a static nadir pointing instrument. Diagram B-1 shows the amount of surface covered for a specified sample time of the spectrometer or a specified time for the pulse duration of the laser, depending on the mode of operation. (Raman spectra are gathered on the darkside of the Moon. Light from sources other than the sun have been considered negligible.)

Signal Intensity:

In a first consideration of the expected intensity of the Raman signal at the altitude of the spacecraft, one part per million of the incident light at the surface can be considered to be scattered by the Raman effect, with the light being scattered equally in all directions. Absorption is considered not to occur. In considering levels of detectability specifications projected for the HIRIS spectrometer were used. The detectors efficiency and noise levels are expressed in terms of photon counts. If the incident radiation is expressed in terms of photon numbers, the energy per photon must be considered from the aspect of the laser output power. Diagram B-2 shows the energy/photon for photons of a given wavelength. Utilizing the above considerations it can be shown that if a laser of 10 Watts power output is incident on the lunar surface for 1 second then the satellite will see that the Raman effect has scattered the photon number/square meter that is shown in Diagram B-3 and Table B-1. Using the efficiencies and noise levels projected for the HIRIS satellite an objective diameter of 157mm should be sufficient to detect the Raman effect. From this diagram it can be seen that a laser of longer wavelengths will cause more photons to be received because of the greater number of photons that are incident on the surface.

Normally this would be true but there are two factors that cause more considerations. The amount of light scattered by the Raman effect is dependent on the polarizability of the molecule. Mathematically this may be expressed by the following:

$$\frac{\partial \sigma_i}{\partial \Omega} = \frac{(2\pi)^4 b_j^2 (\nu_0 - \nu_i)^4}{1 - \exp(-hc\nu_i/kT)} g_j (i_j^2 + \frac{7}{45} a_j^2)$$

- $\partial \sigma_i / \partial \Omega$ - Differential Backscattering cross section
 b_j - zero point vibrational amplitude of the j th vibrational mode
 g_i - degeneracy of j th vibrational mode
 i_j - isotropic part of polarizability tensor

α_i - anisotropic part of polarizability tensor
 T - temperature of substance
 ν_0 - assumed to be far different than transition frequency

As it can be seen the intensity is proportional to the fourth power of the exciting frequency and dependent on the temperature of the substance. Table B-2 and diagram B-4 illustrate the relationship of an exciting laser of wavelength X to a laser of wavelength 4800nm. The shown ratio seems overwhelming at shorter wavelengths but the other factors can be extremely small and greatly negating any advantage. However it is evident that the frequency of the exciting laser must be considered carefully and frequencies of absorption haven't even been considered.

The dependence of the temperature of the substance on the intensity causes the intensity of the Stokes lines to increase with decreasing temperature and the opposite for the Anti-stokes lines. As can be seen the denominator of the equation is a result of probability that a molecule at a given temperature will be found in a certain energy state. (A Boltzmann distribution) Naturally at lower temperatures a molecule is more likely to be found in or near the ground state and any incident radiation will more likely induce a change in the molecule that will leave it in a more excited state than in a less excited state. Thus the result is that Stokes lines increase and Anti-stokes lines decrease as temperature drops. Diagrams B-5 through B-9 show how the ratio of the Anti-Stokes/Stokes lines varies with temperature and different exciting frequencies.

$$\frac{I_{\text{ANTI-STOKES}}}{I_{\text{STOKES}}} = \left(\frac{\nu_0 + \Delta\nu}{\nu_0 - \Delta\nu} \right)^4 e^{\left(\frac{-h\Delta\nu}{KT} \right)} \text{ equation from Woodward p267}$$

Notice that a laser of shorter wavelengths causes the ratio to be more pronounced at equivalent temperatures. Diagrams B-7 and B-8 have temperature ranges that are found on the Moon.

SIZING FOR RAMAN SENSING OPTICS

BASE UNITS: $\text{kg} \equiv 1\text{M}$ $\text{m} \equiv 1\text{L}$ $\text{mm} \equiv 1 \cdot 10^{-3} \cdot 1\text{L}$

PRIMARY MIRROR MASS: $p := 166 \cdot \frac{\text{kg}}{2}$ Using 95 kg as maximum mass of system:

$$r := \sqrt{\frac{95 \cdot \text{kg}}{\pi \cdot p}} \quad r = 0.427 \cdot \text{m}$$

If we set: $r \equiv 0.35 \cdot m$

```

      2
mass := r · π · ρ
mass = 63.884 · kg

```

This gives a 0.7 meter diameter primary objective

for an f3:1 system: focal_length := 2·r·3

focal_length = 2.1·m

$$\text{primary_size} := \frac{\text{focal_length}}{3} \quad \text{primary_size} = 700 \cdot \text{mm}$$

Set the length of the system at 1.5 meters with an outside diameter of 0.85 meters.

The secondary mirror is approximately 1/3 the diameter of the primary.

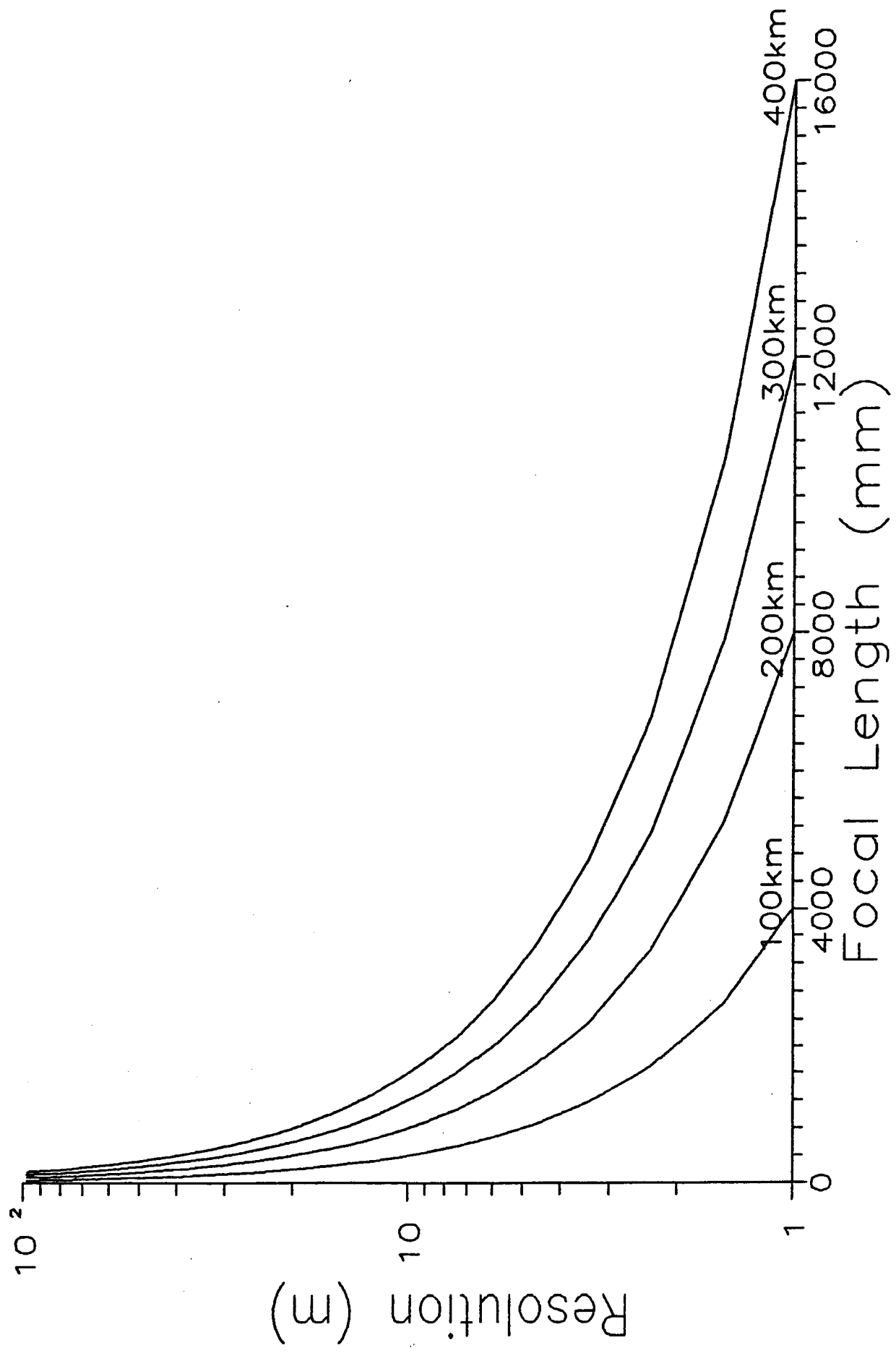
$$\text{secondary_size} := \frac{2 \cdot r}{3} \qquad \text{secondary_size} = 0.233 \cdot m$$

$$\text{sec_mass} := \left[\frac{\text{secondary_size}}{2} \right]^2 \cdot \pi \cdot p \quad \text{sec_mass} = 7.098 \cdot \text{kg}$$

structure mass $\equiv 22 \cdot \text{kg}$

```
total mass := mass + sec mass + structure mass
```

total mass = 92.983 kg



SEVERAL LASERS USED IN REMOTE SENSING

IR Lasers (most common)

UV Lasers (being developed)

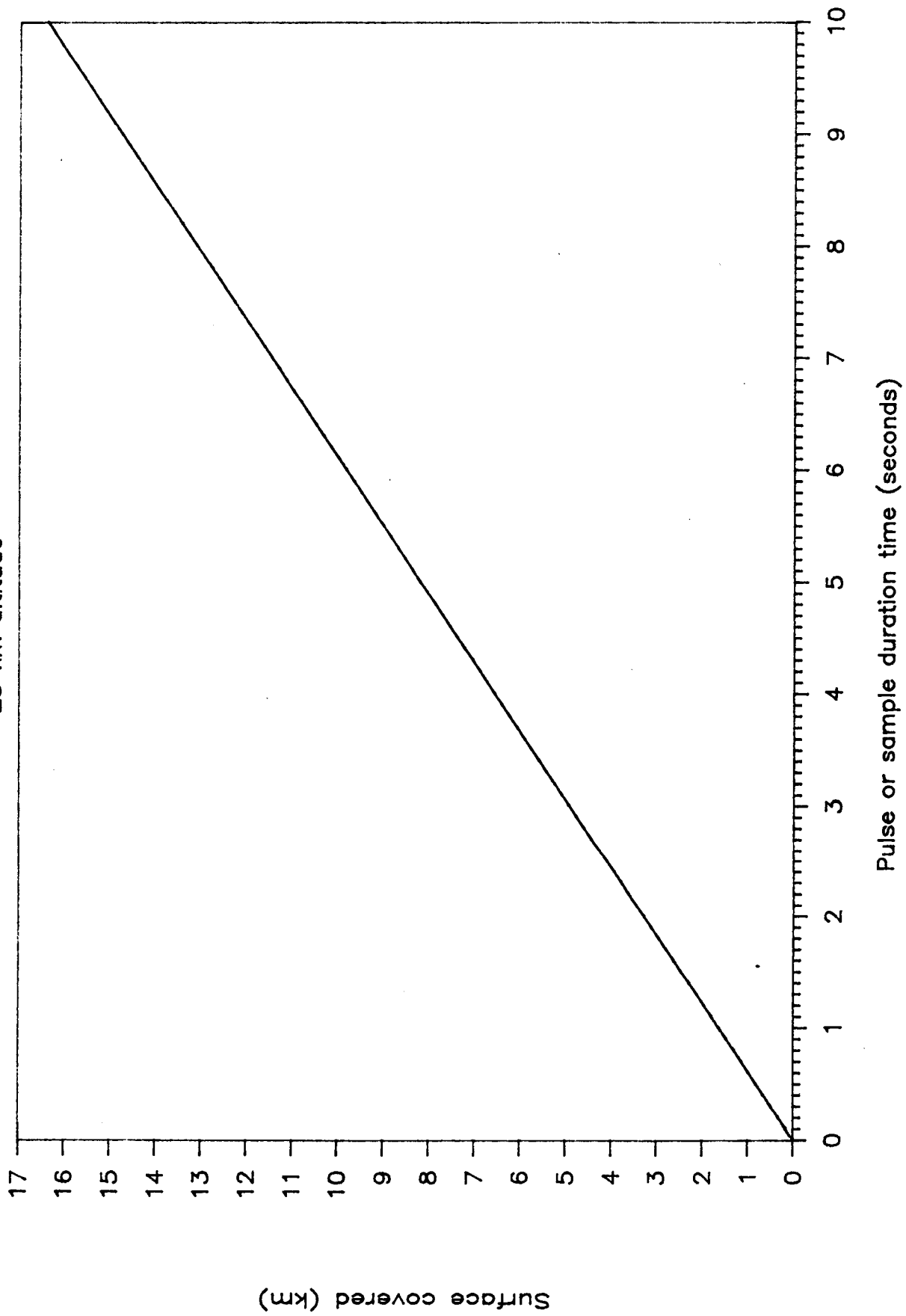
1. Rare gas halide excimer lasers.
2. Pumped dye lasers.
3. Excimer lasers are available in various band centers and are tunable over small ranges. Frequency shifting techniques are projected to cover most of the UV.
4. Some excimer lasers and their central wavelengths:

ArF	193 nm	
KrCl	222 nm	
KrF	249 nm	
XeBr	282 nm	tunable +/- 2 nm
XeCl	308 nm	
XeF	351 nm	
ClF	285 nm	
Cl ₂	256 nm	narrower tuning ranges
F ₂	157 nm	

5. Excimer lasers tend to have finer band coverage but less power than dye lasers whose wavelength band is much larger.
6. Combinations of excimer and dye lasers appear promising for future remote sensing.

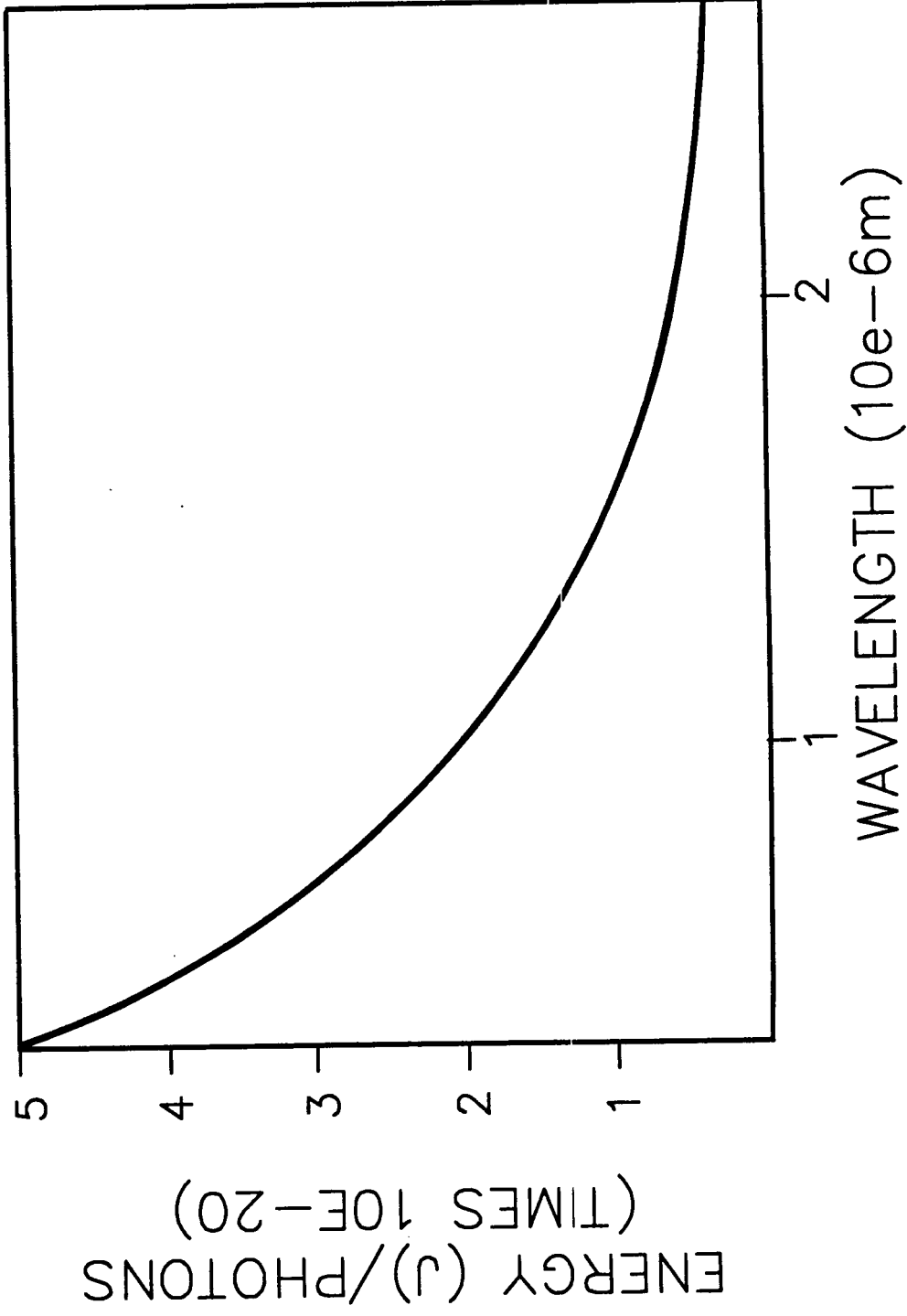
Active Surface Coverage

25 km altitude



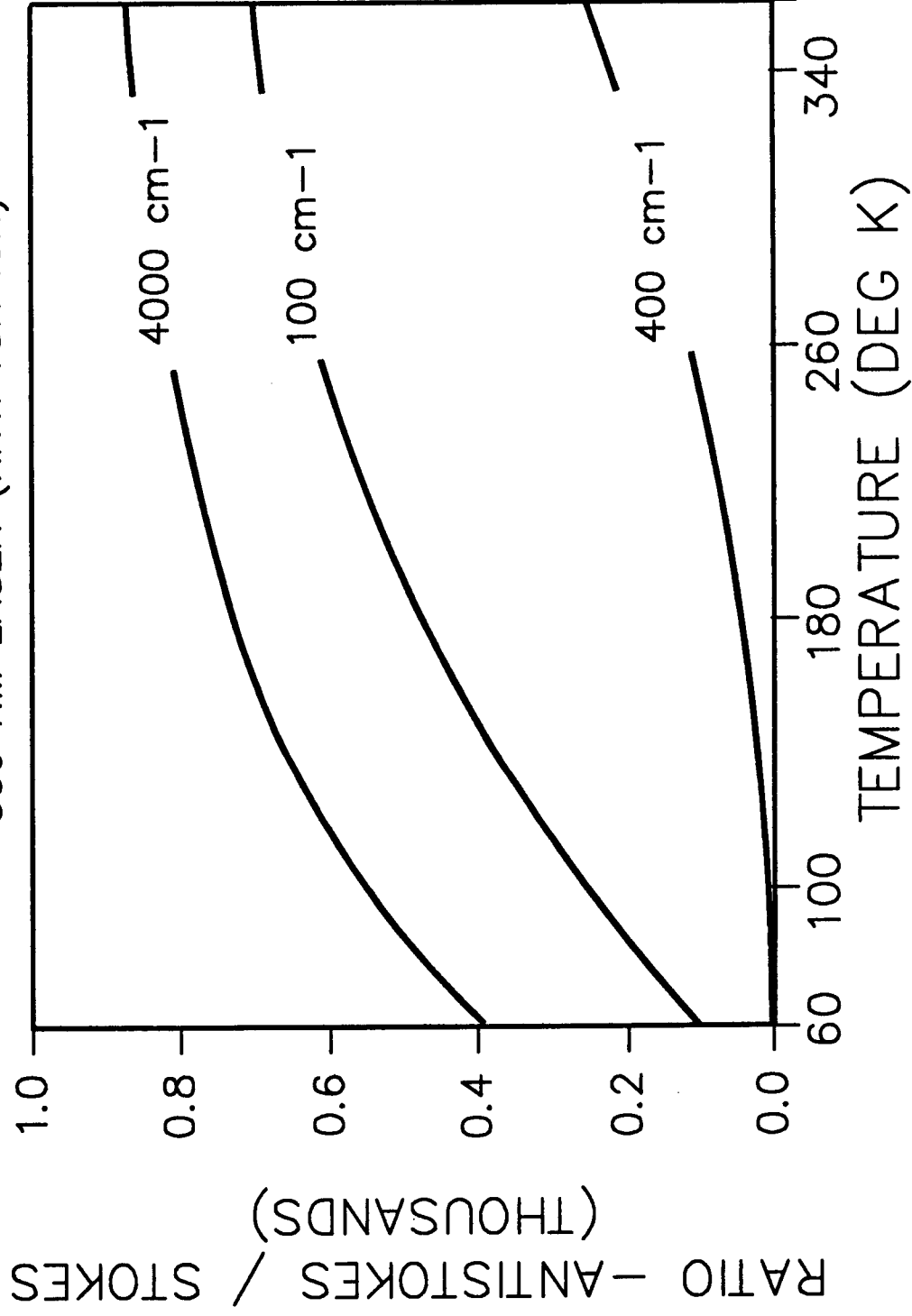
PHOTON ENERGY

PHOTON ENERGY VS PHOTON FREQUENCY



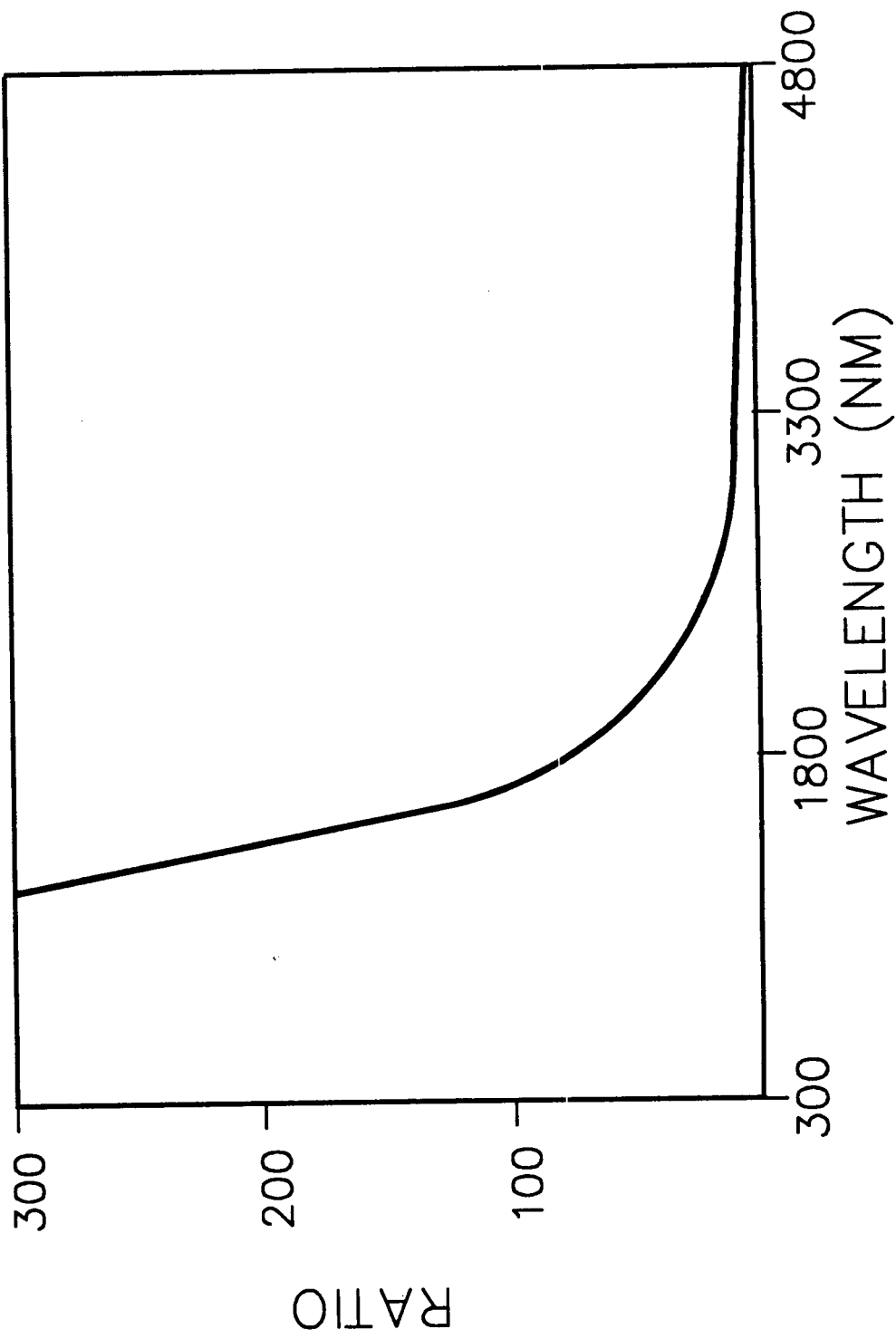
ANTISTOKES / STOKES INTENSITY RATIO

500 NM LASER (KRYPTON ION)



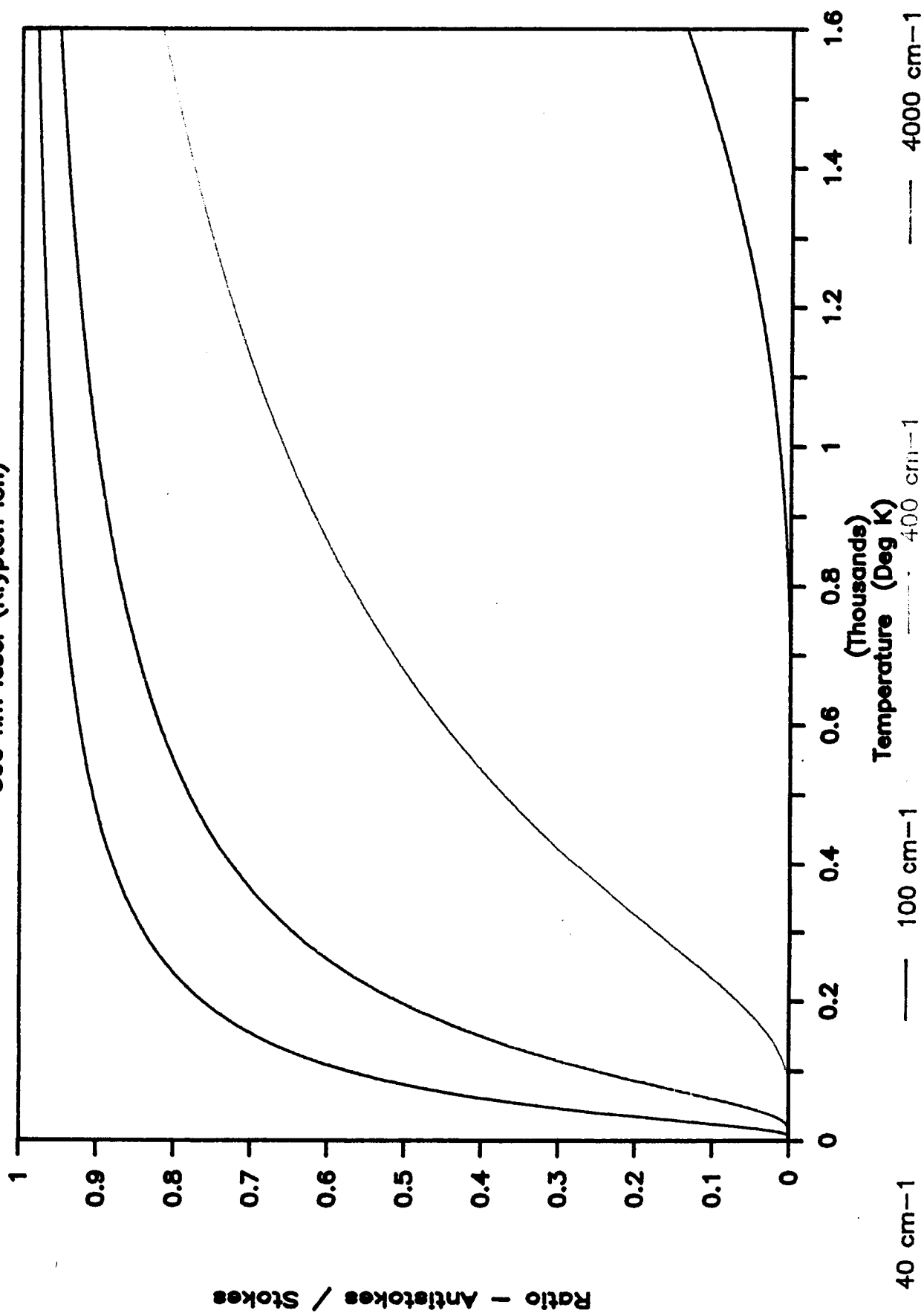
RATIO OF RAMAN INTENSITY

LASER OF X NM / LASER OF 4800 NM



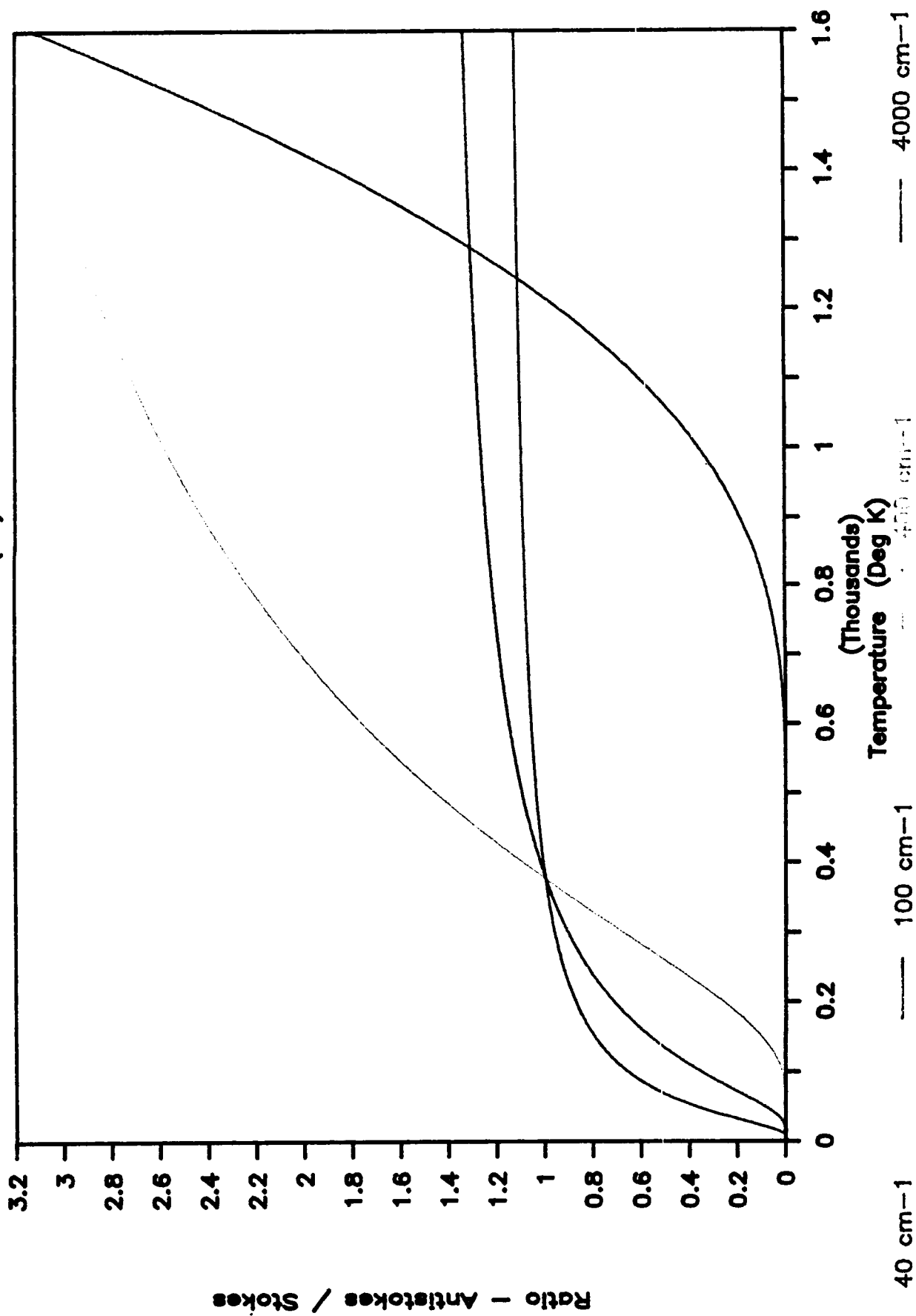
Antistokes / Stokes intensity ratio

500 nm laser (Krypton Ion)



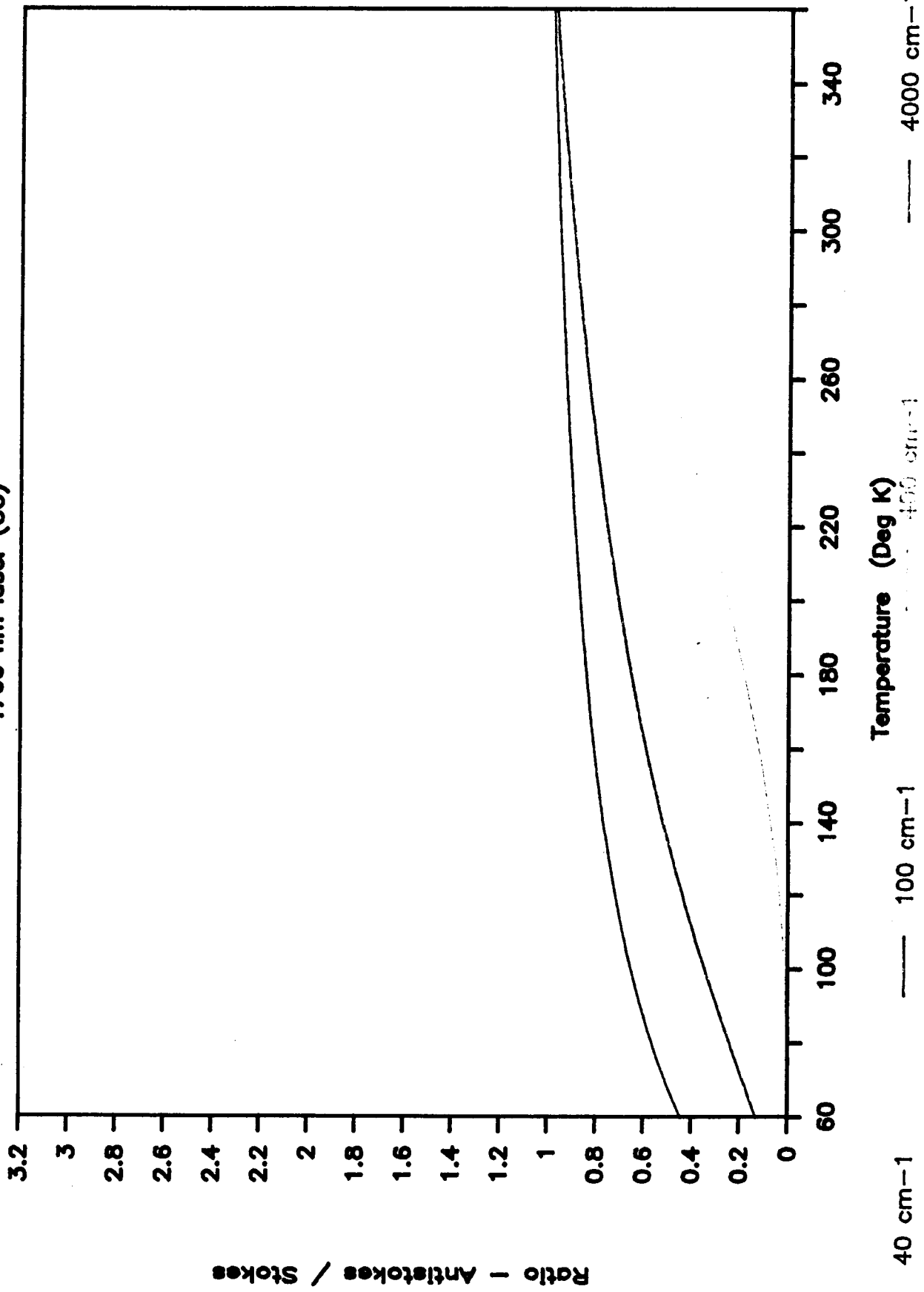
Antistokes / Stokes intensity ratio

4700 nm laser (CO)



Antistokes / Stokes intensity ratio

4700 nm laser (CO)



		1s laser pulse (10 J at surface)			
wavelength	energy	Photons received at 10 km/m2			
(10e-6 m)	(j/photon)	25km	30km	40km	50km
0.4	5.0E-20	2.56E+04	1.78E+04	1.00E+04	6.41E+03
0.5	4.0E-20	3.20E+04	2.22E+04	1.25E+04	8.01E+03
0.6	3.3E-20	3.84E+04	2.67E+04	1.50E+04	9.61E+03
0.7	2.8E-20	4.48E+04	3.11E+04	1.75E+04	1.12E+04
0.8	2.5E-20	5.12E+04	3.56E+04	2.00E+04	1.28E+04
0.9	2.2E-20	5.76E+04	4.00E+04	2.25E+04	1.44E+04
1	2.0E-20	6.40E+04	4.45E+04	2.50E+04	1.60E+04
1.1	1.8E-20	7.04E+04	4.89E+04	2.75E+04	1.76E+04
1.2	1.7E-20	7.68E+04	5.34E+04	3.00E+04	1.92E+04
1.3	1.5E-20	8.33E+04	5.78E+04	3.25E+04	2.08E+04
1.4	1.4E-20	8.97E+04	6.23E+04	3.50E+04	2.24E+04
1.5	1.3E-20	9.61E+04	6.67E+04	3.75E+04	2.40E+04
1.6	1.2E-20	1.02E+05	7.12E+04	4.00E+04	2.56E+04
1.7	1.2E-20	1.09E+05	7.56E+04	4.25E+04	2.72E+04
1.8	1.1E-20	1.15E+05	8.01E+04	4.50E+04	2.88E+04
1.9	1.0E-20	1.22E+05	8.45E+04	4.75E+04	3.04E+04
2	9.9E-21	1.28E+05	8.90E+04	5.00E+04	3.20E+04
2.1	9.5E-21	1.34E+05	9.34E+04	5.25E+04	3.36E+04
2.2	9.0E-21	1.41E+05	9.79E+04	5.50E+04	3.52E+04
2.3	8.6E-21	1.47E+05	1.02E+05	5.76E+04	3.68E+04
2.4	8.3E-21	1.54E+05	1.07E+05	6.01E+04	3.84E+04
2.5	8.0E-21	1.60E+05	1.11E+05	6.26E+04	4.00E+04

ORIGINAL PAGE IS
OF POOR QUALITY

ORIGINAL PAGE IS
OF POOR QUALITY

Intensity of Raman I= λ Exciting Frequency λ^4
Ratio of Wavelength X to 6900 nm

Wavelength (nm)	Frequency (Hz)	Intensity Ratio
--------------------	-------------------	--------------------

300	1.0000E+15	279841.0
400	5.0000E+14	17490.06
500	3.3333E+14	3454.827
1200	2.5000E+14	1093.129
1500	2.0000E+14	447.7456
1800	1.6667E+14	215.9267
2100	1.4286E+14	116.5518
2400	1.2500E+14	68.32057
2700	1.1111E+14	42.65219
3000	1.0000E+14	27.98410
3300	9.0909E+13	19.11352
3600	8.3333E+13	13.49542
3900	7.6923E+13	9.798013
4200	7.1429E+13	7.284492
4500	6.6667E+13	5.527724
4800	6.2500E+13	4.270035
5100	5.8824E+13	3.350547
5400	5.5556E+13	2.645762
5700	5.2632E+13	2.147321
6000	5.0000E+13	1.749006
6300	4.7619E+13	1.438912
6600	4.5455E+13	1.194595
6900	4.3478E+13	1.000000

APPENDIX 9
Orbits

ORBITAL CALCULATIONS

Variable definitions

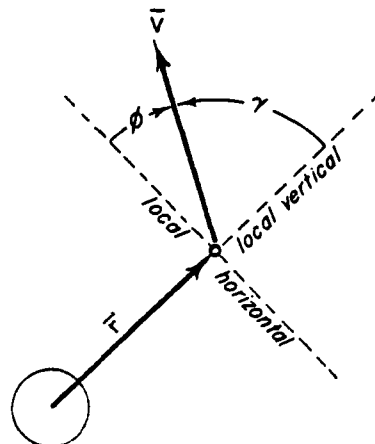
μ	- gravitational parameter
E	- orbital energy
E_t	- orbital energy of the transfer ellipse
h	- specific angular momentum
r	- radius from the focus
R_a	- radius at the periapsis
R_p	- radius at the apoapsis
R_{cs}	- radius of a circular orbit
V_a	- velocity at the apoapsis
V_p	- velocity at the periapsis
V	- velocity at a point in the orbit
V_{esc}	- escape velocity
V_{cs1}	- initial circular orbital velocity
V_1	- velocity at point 1 of the transfer ellipse
V_{cs2}	- final circular orbital velocity
V_2	- velocity at point 2 of the transfer ellipse
Θ	- angle of plane change
ϕ	- flight path angle
ν	- polar angle between the radius vector and the nearest focus
a	- semi-major axis of the orbit
p	- semi-latus rectum
e	- orbital eccentricity
TP_c	- circular orbital period
TP_e	- elliptical orbital period
ToF	- time of flight for a Hohmann Transfer

Equations were taken from:

Bate R, Mueller D, White J. ' Fundamentals of Astrodynamics ',
Dover Publications, Inc., New York, 1971

Determination of fundamental orbital properties

$$\begin{aligned} E &= V^2/2 - \mu/r \\ E &= -\mu/2a \\ h &= r*v*\cos\phi \\ h &= R_p*V_p \\ h &= R_a*V_a \\ p &= a*(1 - e^2) \\ e &= (R_a - R_p)/(R_a + R_p) \\ r &= p/(1 + e*\cos\nu) \\ R_p &= p/(1 + e) \\ R_p &= a*(1 - e) \\ R_a &= p/(1 - e) \\ R_a &= a*(1 + e) \\ a &= (R_p + R_a)/2 \\ TP_c &= 2*\pi*(\mu)^{1/2}*R_{cs} \\ TP_e &= 2*\pi*(\mu)^{1/2}*a^{3/2} \\ V_{esc} &= (2*\mu/r)^{1/2} \end{aligned}$$

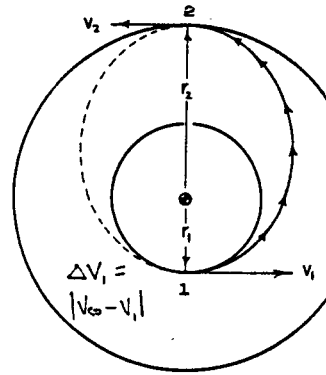


Hohmann Transfer: Concentric orbits

$$\begin{aligned}E_t &= -\mu/(r_1 + r_2) \\V_1 &= (2*(\mu/r_1 + E_t))^{1/2} \\V_{cs1} &= (\mu/r_1)^{1/2} \\V_2 &= (2*(\mu/r_2 + E_t))^{1/2} \\V_{cs2} &= (\mu/r_2)^{1/2}\end{aligned}$$

$$\text{velocity change of transfer} = (V_1 - V_{cs1}) + (V_{cs2} - V_2)$$

$$ToF = \pi * (a^3/\mu) \quad \text{where } a = \text{semi-major axis of the transfer ellipse}$$



Plane Change

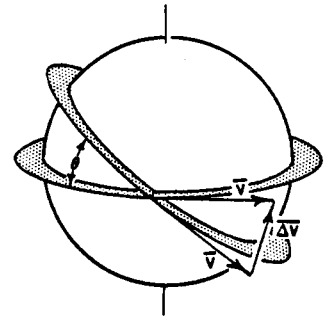
circular orbits:

$$\text{velocity change needed} = 2*V*\sin(\Theta/2)$$

elliptical orbits:

velocity change needed = law of cosines

$$\text{law of cosines} = (V_1^2 + V_{cs1}^2 - 2*V_1*V_{cs1}*\cos\Theta)^{1/2}$$



Mass of Propellant Calculations

M = mass of the propellant

Ms = dry mass of the satellite

Isp = Isp of the fuel

g = acceleration of gravity

$$M = Ms * (\exp(dV/(g*Isp)) - 1)$$

Time of Flight-Eccentric Anomaly

E0 = initial eccentric anomaly

E1 = final eccentric anomaly

t0 = initial time

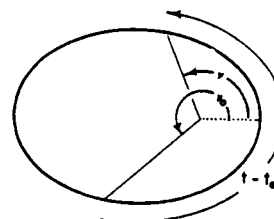
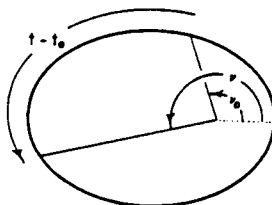
t = final time

k = number of times the object passes through the periapsis enroute from to 0

$$r = a*(1 - e*\cos E)$$

$$E = \arccos((1/e)*1 - r/a)$$

$$t-t_0 = (a^3/\mu)*(2*k*\pi + (E - e*\sin E) - (E_0 - e*\sin E_0))$$



```

C --- PROGRAM CIRCULAR ORBIT
C
C --- THIS PROGRAM CALCULATES THE PERIOD, VEL, AND THE TOTAL ENERGY
C OF A SPACECRAFT IN A CIRCULAR ORBIT OF GIVEN ALTITUDE
C
C --- TP -- PERIOD OF THE ORBIT (MIN)
C --- ALT - ALTITUDE OF THE ORBIT (KM)
C --- RAD - RADIUS OF THE MOON PLUS THE ALTITUDE (M)
C --- RM -- RADIUS OF THE MOON (M)
C --- VEL - VELOCITY OF THE SPACECRAFT (KM/SEC)
C --- ETOT TOTAL ENERGY OF THE SPACECRAFT (KJ)
C --- MU -- G*M(MOON) (M**3)/(SEC**2)
C
REAL TP(500),ALT(500),RAD,RM,VEL(500),ETOT(500),MU,PI
INTEGER I,J
CHARACTER CH1*8,CH2*11,CH3*10,CH4*8
C
CALL CONPDS(9,'STU399.FORTLIB.PRINT$','CIRCORB$', '$')
C
C
PRINT*, ' ALT.(KM)', ' PERIOD(MIN)', ' VEL.(KM/S)', ' ETOT.(J)'
C
CH1 = 'ALT.(KM)'
CH2 = 'PERIOD(MIN)'
CH3 = 'VEL.(KM/S)'
CH4 = 'ETOT.(KJ)'
C
WRITE(9, '(1X,A,3(7X,A))') CH1,CH2,CH3,CH4
WRITE(9,*) ' '
C
PI = ACOS(-1.)
MU = 4.90287E12
RM = 1.73E06
C
J = 1
C
DO 10 I = 25,2000,25
RAD = I*1000 + RM
ALT(J) = I
TP(J) = (2*PI)*(RAD**1.5)/(SQRT(MU))
VEL(J) = SQRT(MU/RAD)
ETOT(J) = ABS(((VEL(J)**2)/2) - (MU/RAD))
C
C --- CHANGE VALUES TO DESIRED UNITS
C
TP(J) = TP(J)/60.
VEL(J) = VEL(J)/1000.
ETOT(J) = ETOT(J)/1000.
C
C
C --- WRITE VALUES TO AN OUTPUT FILE
C
WRITE(9, '(1X,F8.2,3(9X,F8.3))') ALT(J),TP(J),VEL(J),ETOT(J)
C
PRINT*,ALT(J), ' ',TP(J), ' ',VEL(J), ' ',ETOT(J)
C
J = J + 1
C
10 CONTINUE
C

```


NJ - J-1

C

CALL CPLOT(ALT,TP,NJ)
CALL CPLOT(ALT,VEL,NJ)
CALL CPLOT(ALT,ETOT,NJ)

C

STOP
END

```

C --- PROGRAM ELLIPTICAL ORBIT
C
C --- THIS PROGRAM CALCULATES THE PERIOD, VEL, AND THE TOTAL ENERGY
C OF A SPACECRAFT IN A ELLIPTICAL ORBIT OF GIVEN ALTITUDE
C
C --- TP -- PERIOD OF THE ORBIT (MIN)
C --- ALT - ALTITUDE OF THE ORBIT (KM)
C --- RAD - RADIUS OF THE MOON PLUS THE ALTITUDE (M)
C --- RM -- RADIUS OF THE MOON (M)
C --- VEL - VELOCITY OF THE SPACECRAFT (KM/SEC)
C --- ETOT TOTAL ENERGY OF THE SPACECRAFT (KJ)
C --- MU -- G*M(MOON) (M**3)/(SEC**2)
C
      REAL TP(1000),ALT(1000),RM,VEL(1000),ETOT(1000),MU,PI,A
      REAL PER,APO
      INTEGER I,J,APO1,END
      CHARACTER CH6*20
      CHARACTER CH1*8,CH2*11,CH3*10,CH4*8
C
      CALL CONPDS(9,'STU399.FORTLIB.PRINT$', 'ELLORB$', '$')
C
      CH1 = 'APO.(KM)'
      CH2 = 'PERIOD(MIN)'
      CH3 = 'VEL.(KM/S)'
      CH4 = 'ETOT.(KJ)'
      CH6 = 'APO(0) = 25 KM'
C
      WRITE(9,'(1X,A,3(7X,A))')CH1,CH2,CH3,CH4
      WRITE(9,*)' '
C
      PI = ACOS(-1.)
      MU = 4.90287E12
      RM = 1.73E06
C
      PRINT*,' ENTER THE PERIAPSIS '
      READ*,PER
      PRINT*,' ENTER THE INITIAL APOAPSIS '
      READ*,APO1
      PRINT*,' ENTER THE FINAL APOAPSIS '
      READ*,APOF
      PRINT*,' ENTER THE STEP SIZE '
      READ*,NSTEP
C
      END = APOF
C
      J = 1
C
      DO 10 I = APO1,END,NSTEP
        APO = I
        A = .5*(1000*(PER + APO) + 2*RM)
        ALT(J) = APO
        TP(J) = (2*PI)*(A**1.5)/(SQRT(MU))
        ETOT(J) = -(MU/(2*A))
        VEL(J) = SQRT(2*(ETOT(J) + MU/(1000*(APO)+RM)))
C
C --- CHANGE VALUES TO DESIRED UNITS
C
        TP(J) = TP(J)/60.
        VEL(J) = VEL(J)/1000.
        ETOT(J) = -ETOT(J)/1000.

```

```
C
C --- WRITE VALUES TO AN OUTPUT FILE
C
C      WRITE(9,'(1X,F8.2,3(9X,F8.3))')ALT(J),TP(J),VEL(J),ETOT(J)
C
C      J = J + 1
C
C 10  CONTINUE
C
C      NJ = J-1
C
C      CALL ELPLOT(ALT,TP,NJ,CH6)
C      CALL ELPLOT(ALT,VEL,NJ,CH6)
C      CALL ELPLOT(ALT,ETOT,NJ,CH6)
C
C      STOP
C      END
```

```

C --- PROGRAM ELORP
C
C --- THIS PROGRAM CALCULATES THE PERIOD, VEL, AND THE TOTAL ENERGY
C   OF A SPACECRAFT IN A ELLIPTICAL ORBIT OF GIVEN ALTITUDE
C --- THE VEL. OF THE SPACECRAFT IS CALCULATED AT THE PER. & APO.
C
C --- TP -- PERIOD OF THE ORBIT (MIN)
C --- ALT - ALTITUDE OF THE ORBIT (KM)
C --- RAD - RADIUS OF THE MOON PLUS THE ALTITUDE (M)
C --- RM -- RADIUS OF THE MOON (M)
C --- VEL - VELOCITY OF THE SPACECRAFT (KM/SEC)
C --- ETOT  TOTAL ENERGY OF THE SPACECRAFT (KJ)
C --- MU -- G*M(MOON) (M**3)/(SEC**2)
C
  REAL TP(1000),ALT(1000),RM,VEL(1000),ETOT(1000),MU,PI,A
  REAL PER,APO
  INTEGER I,J,APO1,END
  CHARACTER CH6(2)*20,CH7*20
  CHARACTER CH1*8,CH2*11,CH3*10,CH4*10,CH5*8
C
  CALL CONPDS(9,'STU399.FORTLIB.PRINT$','ELORP$','$')
C
  CH1 = 'APO.(KM)'
  CH2 = 'PERIOD(MIN)'
  CH3 = 'VELP(KM/S)'
  CH4 = 'VELA(KM/S)'
  CH5 = 'ETOT.(KJ)'
C
  WRITE(9,'(1X,A,4(5X,A))')CH1,CH2,CH3,CH4,CH5
  WRITE(9,*)' '
C
  PI = ACOS(-1.)
  MU = 4.90287E12
  RM = 1.73E06
C
  PRINT*,' ENTER THE PERISELENE '
  READ*,PER
  PRINT*,' ENTER THE INITIAL APOSELENE '
  READ*,APO1
  PRINT*,' ENTER THE FINAL APOSELENE '
  READ*,APOF
  PRINT*,' ENTER THE STEP SIZE '
  READ*,NSTEP
C
  END = APOF
  NS = (END - APO1)/NSTEP
C
  J = 1
C
  DO 10 I = APO1,END,NSTEP
    APO = I
    A = .5*(1000*(PER + APO) + 2*RM)
    ALT(J) = APO
    TP(J) = (2*PI)*(A**1.5)/(SQRT(MU))
    ETOT(J) = -(MU/(2*A))
    VEL(J) = SQRT(2*(ETOT(J) + MU/(1000*(PER)+RM)))
    VEL(J+NS) = SQRT(2*(ETOT(J) + MU/(1000*(APO)+RM)))
C
C --- CHANGE VALUES TO DESIRED UNITS
C

```

```

      TP(J) = TP(J)/60.
      VEL(J) = VEL(J)/1000.
      VEL(J+NS) = VEL(J+NS)/1000.
      ETOT(J) = -ETOT(J)/1000.
C
C --- WRITE VALUES TO AN OUTPUT FILE
C
  99  FORMAT(1X,F8.2,4(6X,F8.3))
      WRITE(9,99)ALT(J),TP(J),VEL(J),VEL(J+NS),ETOT(J)
C
      J = J + 1
C
  10  CONTINUE
C
      NJ = J-1
C
      CH6(1) = 'VEL AT PER.'
      CH6(2) = 'VEL AT APO.'
      CH7 = 'APO INIT = 25 KM'
      N6 = 13
      N7 = 17
C
      CALL ELPLOT(ALT,TP,NJ,1,CH7,N7)
      CALL ELPLOT(ALT,VEL,NJ,2,CH6,N6)
      CALL ELPLOT(ALT,ETOT,NJ,1,CH7,N7)
C
      STOP
      END

```

```

C --- PROGRAM HOHMANN
C
C --- THIS PROGRAM CALCULATES THE DELTA VEL. AND MASS OF THE PROPELLANT
C      NEEDED FOR A HOHMAN TRANSFER BETWEEN TWO CONCENTRIC CIRCULAR
C      ORBITS FOR A GIVEN ISP.
C --- PLOTS THE DELV. VS. ORBIT CHANGE; CIRC TO CIRC, CIRC TO ELLIPT.
C
      REAL R1,R2,RM,V1,VCS1,V2,VCS2,DELV1,DELV2,DELVT1,DELVT2
      REAL MP1,MP2,ISPG,RAD1,RAD2,ETOT
      REAL MU,PI,MF1,ISP
      INTEGER I,J
C
      PARAMETER(MU=4.90287E12,RM=1.73E06)
C
      OPEN(8,FILE='HVCIRC.DAT',STATUS='UNKNOWN')
      OPEN(9,FILE='HVELLP.DAT',STATUS='UNKNOWN')
      OPEN(10,FILE='HMPCIR.DAT',STATUS='UNKNOWN')
      OPEN(11,FILE='HMPELP.DAT',STATUS='UNKNOWN')
      OPEN(12,FILE='HOHMANN.DAT',STATUS='UNKNOWN')
C
      PRINT*,' ENTER THE TOTAL DRY MASS OF THE SYSTEM '
      READ*,MF1
      PRINT*,' ENTER THE ISP VALUE '
      READ*,ISP
      PRINT*,' ENTER THE INITIAL & FINAL ALTITUDES (KM) '
      READ*,R1,R2
C
      RAD1 = R1*1000 + RM
      ISPG = ISP*9.81
      PI = ACOS(-1.)
C
      WRITE(12,*)' MASS (KG)          - ',MF1
      WRITE(12,*)' ISP (/S)           - ',ISP
      WRITE(12,*)' PERIAPSIS (KM) - ',R1
      WRITE(12,*)' APOAPSIS (KM) - ',R2
C
      DO 10 I = R1,R2,25
C
          RAD2 = I*1000 + RM
          ETOT = (-MU/(RAD1 + RAD2))
          V1 = SQRT(2*(MU/RAD1 + ETOT))
          VCS1 = SQRT(MU/RAD1)
          DELV1 = V1 - VCS1
          V2 = SQRT(2*(MU/RAD2 + ETOT))
          VCS2 = SQRT(MU/RAD2)
          DELV2 = VCS2 - V2
C
          DELVT1 = (DELV1 + DELV2)/1000
          DELVT2 = (DELV1)/1000
          MP1 = MF1*(EXP((DELV1+DELV2)/ISPG) - 1)
          MP2 = MF1*(EXP(DELV1/ISPG) - 1)
C
          WRITE(8,*)I,DELVT1
          WRITE(9,*)I,DELVT2
          WRITE(10,*)I,MP1
          WRITE(11,*)I,MP2
C
10  CONTINUE
      STOP
      END

```

```

C
C --- PROGRAM PLANE
C
C --- THIS PROGRAM CALCULATES THE DELTA VELOCITY AND THE MASS OF THE
C PROPELLANT NEEDED FOR A PLANE CHANGE. ISP = VARIABLE AND THE
C INITIAL AND FINAL ORBITS ARE CIRCULAR.
C
REAL R,RM,V,DELV,DELVL,THETA,THRAD
REAL MF,MP,ISP,ISPG,RAD
REAL MU,PI
INTEGER I,J
CHARACTER*14 OUTF1,OUTF2

C
PARAMETER(MU=4.90287E12,RM=1.73E06)

C
PRINT*,' ENTER THE NAME OF VEL VS. ANGLE OUTPUT FILE '
READ*,'(A')OUTF1
PRINT*,' ENTER THE NAME OF MP VS. ANGLE OUTPUT FILE '
READ*,'(A')OUTF2

C
OPEN(10,FILE=OUTF1,STATUS='UNKNOWN')
OPEN(11,FILE=OUTF2,STATUS='UNKNOWN')
OPEN(12,FILE='PLANE.DAT',STATUS='UNKNOWN')

C
PI = ACOS(-1.)

C
PRINT*,' ENTER THE TOTAL DRY MASS OF THE SYSTEM '
READ*,MF
PRINT*,' ENTER THE ISP '
READ*,ISP

C
ISPG = ISP*9.81

C
PRINT*,' ENTER THE ALTITUDE OF THE SATELLITE '
READ*,R

C
RAD = R*1000. + RM
A = .5*((25000 + RM) + RAD)
ETOT = -(MU/(2*A))
V = SQRT(2*(ETOT + MU/(RAD)))

C
WRITE(12,*)'
WRITE(12,*)' DRY MASS (KG) = ',MF
WRITE(12,*)' ISP = ',ISP
WRITE(12,*)' CIRC. ORBIT ALT = ',R
WRITE(12,*)'

C
DO 10 I = 0,90,1
  THETA = I
  THRAD = 2*PI*THETA/360.
  DELV = (2 * V*SIN(THRAD/2))/1000.
  MP = MF*(EXP(DELV*1000/ISPG)-1)

C
  WRITE(10,*)THETA,DELV
  WRITE(11,*)THETA,MP

C
10  CONTINUE

C
STOP
END

```

```

C
C --- PROGRAM HMAN
C
C --- THIS PROGRAM CALCULATES THE DELTA VEL. AND MASS OF THE PROPELLANT
C      NEEDED FOR A HOHMAN TRANSFER BETWEEN TWO CONCENTRIC CIRCULAR
C      ORBITS FOR A GIVEN ISP.
C --- TWO OR MORE SPACECRAFT MASSES MAY BE ENTERED IN ORDER TO COMPARE THE
C      DIFFERENCE IN PROPELLANT MASS NEEDED AS A FUNCTION OF THE INITIAL MASS
C
      REAL R1,R2(500),RM,V1,VCS1,V2,VCS2,DELV1,DELV2,DELVTT(500)
      REAL MP(2000),ISPG,RAD1,RAD2,ETOT,EGTV,VGTV1,VGTCS,DELV25,DELV
      REAL MU,PI,MF(500),MP1,MP2,MGTV,MPGTV,ISP
      INTEGER I,J,NMF,P
      CHARACTER*9 CH1,CH2,CH3*12,CH4,CH5,KEYS1*20,KEYS2(2)*29
C
      PARAMETER(MU=4.90287E12,RM=1.73E06)
C
      CALL CONPDS(8,'STU399.FORTLIB.PRINT$','HMAN$','$')
C
      CH1 = 'ALT1 (KM)'
      CH2 = 'ALT2 (KM)'
      CH3 = 'DELV (KM/S)'
      CH4 = 'MP1 (KG)'
      CH5 = 'MP2 (KG)'
C
      PI = ACOS(-1.)
      R1 = 25.
      RAD1 = R1*1000. + RM
C
      PRINT*,' ENTER THE NUMBER OF MASSES TO BE EVALUATED,(2 MASSES)'
      READ*,NMF
C
      PRINT*,' THE FIRST MASS TO BE ENTERED SHOULD BE THE MASS OF THE '
      PRINT*,' PLATFORM ONLY. THE SECOND MASS SHOULD BE THE MASS OF '
      PRINT*,' PLATFORM AND THE MASS OF THE GTV COMBINED. '
      PRINT*,' '
C
      DO 5 I = 1,NMF
C
C        PRINT*,' ENTER THE TOTAL DRY MASS OF THE SYSTEM '
C        READ*,MF(I)
C
C      5 CONTINUE
C
      MGTV = ABS(MF(2) - MF(1))
C
      PRINT*,' ENTER THE ISP VALUE '
      READ*,ISP
C
      ISPG = ISP*9.81
C
      WRITE(8,*)'
      WRITE(8,*)' THE GTV IS USED TO MOVE THE PLATFORM. '
      WRITE(8,*)'
      WRITE(8,*)' THE MASS OF THE PROPELLANT IS THE TOTAL MASS NEEDED '
      WRITE(8,*)' TO BE CARRIED UP FROM THE MOON SURFACE, THIS ACCOUNTS '
      WRITE(8,*)' FOR THE TOTAL PROPELLANT NEEDED FOR THE GTV AND THE '
      WRITE(8,*)' PLATFORM. THE LAUNCH FROM THE MOON AND THE RETURN '
      WRITE(8,*)' TRIP FOR THE GTV ARE TAKEN INTO ACCOUNT.'
      WRITE(8,*)' THE MASS OF THE GTV IS TAKEN TO BE 450 KG '

```



```

C      WRITE(8,*)'
C
C      DO 7 I = 1,NMF
C        WRITE(8,*)' MF',I,' (KG) = ',MF(I)
7      CONTINUE
C
C      WRITE(8,*)' MASS OF GTV = ',MGTV
C      WRITE(8,*)' ISP = ',ISP
C
C      J = 1
C
C      DO 10 I = 25,2000,25
C        R2(J) = I
C        RAD2 = R2(J)*1000 + RM
C        ETOT = (-MU/(RAD1 + RAD2))
C        V1 = SQRT(2*(MU/RAD1 + ETOT))
C        VCS1 = SQRT(MU/RAD1)
C        DELV1 = V1 - VCS1
C        V2 = SQRT(2*(MU/RAD2 + ETOT))
C        VCS2 = SQRT(MU/RAD2)
C        DELV2 = VCS2 - V2
C
C        DELVTT(J) = (DELV1 + DELV2)/1000
C
C        J = J + 1
C
C      10 CONTINUE
C
C      NJ = J - 1
C
C      KEYS1 = 'INITIAL ALT. = 25 KM'
C      K1C = 20
C      N1 = 1
C
C      CALL ICPlot(R2,DELVTT,NJ,KEYS1,K1C,N1)
C
C      --- MASS OF PROPELLANT CALCULATIONS
C
C      --- CHECK TO SEE IF THE PLATFORM OR THE PLATFORM AND THE GTV WILL
C      BE MOVED. IF THE GTV WILL BE MOVED WITH THE PLATFORM CALCULATE
C      THE DELTA VEL. REQUIRED TO BRING IT BACK TO THE MOON FROM THE
C      NEW ORBIT USING A HOHMAN TRANSFER.
C
C      --- THE MASS OF THE PROPELLANT IS THE TOTAL AMOUNT NEEDED TO EXECUTE
C      THE TRANSFER AND BRING THE GTV BACK TO THE SURFACE OF THE MOON.
C
C      DELV25 = 0.0
C
C      MF1 = MF(1)
C      MF2 = MF(2)
C
C      IF (MF1.GT.600.) THEN
C        EGTV = -MU/(RM + 1000.*25)
C        VGTV1 = SQRT(2*(MU/RM + EGTV))
C        VGTVCS = SQRT(MU/(RM + 1000.*25))
C        DELV25 = VGTV1 + VGTVCS
C      END IF
C
C      IF (MF2.GT.600.) THEN
C        EGTV = -MU/(RM + 1000.*25)

```

```

      VGTV1 = SQRT(2*(MU/RM + EGTV))
      VGTVCS = SQRT(MU/(RM + 1000.*25))
      DELV25 = VGTV1 + VGTVCS
C
      WRITE(8,*)' DELV25 FOR GTV = ',DELV25
C
      END IF
C
      MPGTV = 2*MGTV*(EXP(DELV25/ISPG) - 1)
C
      DO 20 I = 1,NJ,1
C
        IF (MF1.GT.600) THEN
          DELV1 = 2*1000.*DELVTT(I)
        ELSE
          DELV1 = 1000.*DELVTT(I)
        END IF
C
        IF (MF2.GT.600) THEN
          DELV2 = 2*1000.*DELVTT(I)
        ELSE
          DELV2 = 1000.*DELVTT(I)
        END IF
C
        MP(I) = MF1*(EXP(DELV1/ISPG) - 1)
        MP(I+100) = MF2*(EXP(DELV2/ISPG) - 1) + MPGTV
C
      20  CONTINUE
C
C --- PLOT THE MASS OF THE PROPELLANT VS. THE CHANGE IN ALTITUDE
C      THE INITIAL ALTITUDE IS 25 KM
C
      KEYS2(1)='MASS = 560KG'
      KEYS2(2)='MASS = 1010KG'
      K2C = 15
C
      CALL ICPlot(R2,MP,NJ,KEYS2,K2C,NMF)
C
C --- WRITE VALUES TO AN OUTPUT FILE
C
      WRITE(8,*)'
      WRITE(8, '(1X,A,4(6X,A))')CH1,CH2,CH3,CH4,CH5
      WRITE(8,*)'
C
      DO 30 L = 1,NJ
        LL = L + 100
        WRITE(8,*)'
        WRITE(8, '(1X,F6.2,4(6X,G12.7))')R1,R2(L),DELVTT(L),MP(L),MP(LL)
        PRINT*,' ',R1,' ',R2(L),' ',DELVTT(L),' ',MP(L),' ',MP(LL)
C
      30  CONTINUE
C
      STOP
      END

```

APPENDIX 10

Propulsion

APPENDIX A - TABLES

ORIGINAL PAGE IS
OF POOR QUALITYTable 1 - Rates of Production of Various Materials

(Units - Kg/person*day)

O ₂ intake	0.806	Resupplied (5)
Food intake	0.641	Resupplied (5)
Total water	3.216	Resupplied (5)
Drink rate	1.3	Resupplied (2)
Trash production	0.818	50% Cellulose, 50% Ethylene (2)
Feces	0.2	75% Water (5)
Sweat rate	0.918	Water (assume 60% recovery) (2)
Urine	1.5	60% Urea (2)
CO ₂	0.943	Metabolic byproduct (5)

Table 2 - Human Waste Produced in 360 Days

(Units = Kg)

Crew = 25

<u>Trash</u>	<u>=</u>	<u>7362</u>	(<u>Stored</u>)
<u>Feces</u>	<u>=</u>	<u>1800</u>	(<u>1350 Water</u>)
<u>Sweat</u>	<u>=</u>	<u>4957</u>	(<u>Water recovered physically</u>)
<u>Urine</u>	<u>=</u>	<u>13500</u>	(<u>8100 Urea</u>)
<u>CO₂</u>	<u>=</u>	<u>8487</u>	

Crew = 100

<u>Trash</u>	<u>=</u>	<u>29448</u>	(<u>TBD</u>)
<u>Feces</u>	<u>=</u>	<u>7200</u>	(<u>5400 Water</u>)
<u>Sweat</u>	<u>=</u>	<u>19828</u>	(<u>Water</u>)
<u>Urine</u>	<u>=</u>	<u>54000</u>	(<u>32400 Urea</u>)
<u>CO₂</u>	<u>=</u>	<u>33948</u>	

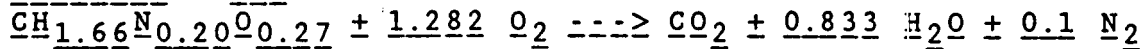
Crew = 500

<u>Trash</u>	<u>=</u>	<u>147240</u>	(<u>TBD</u>)
<u>Feces</u>	<u>=</u>	<u>36000</u>	(<u>27000 Water</u>)
<u>Sweat</u>	<u>=</u>	<u>99144</u>	(<u>Water</u>)
<u>Urine</u>	<u>=</u>	<u>270000</u>	(<u>162000 Urea</u>)
<u>CO₂</u>	<u>=</u>	<u>169740</u>	

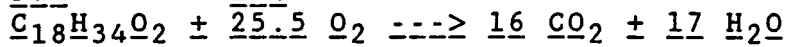
Table 3 - Waste Combustor Reaction Equations (2)

1) Fecal Composition:

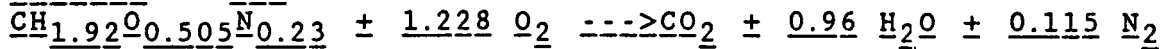
Bacteria 28%



Fat 20%



Protein 20%



Fiber 30%



Salts 2%

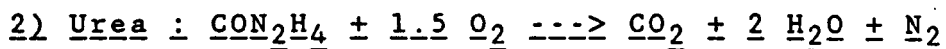


Table 4 - Masses of Hydrogen and Oxygen Produced from Human Wastes Using the (a) Water Electrolysis and (b) Waste Combustor Modules (Unit - Kg)

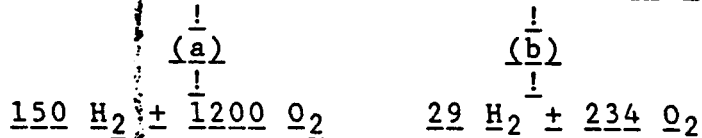
Input: Crew = 25, 360 days, 41967 O₂/Food/Water Resupply
Cost = \$ 420 million

Output:

1) Trash	=	7362	(Stored)
2) Feces	=	1800	(1350 Water)
3) Sweat	=	4231	(Water 50% recovery)
4) Urine	=	13500	(8100 Urea)
5) CO ₂	=	15719	(Metabolic and combustor)

1) Trash was assumed to be stored during the 1st year if no extra oxygen was to be imported into the base. Trash will not be burned in the combustor unless the oxygen produced is not needed for fuel production

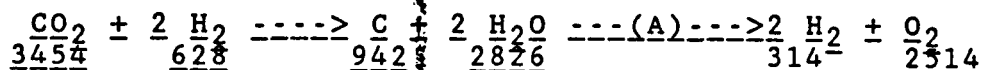
2) 1800 Feces:--> evaporate 1350 water ----> 450 solids



3) 4957 Sweat -----(a) ----> 551 H₂ + 4410 O₂

4) 8100 Urea -----(b) -----> 5325 H₂O ---> 590 H₂ + 4725 O₂
4125 N₂

5) If more O₂ is needed then excess H₂, that amount that exceeds 105 kg/maintenance-event, can be used in a Bosch reactor:



The overall efficiency of recovery is reduced to 53.4 % when the Bosch reactor is used to shift the balance towards increased O₂ production.

ORIGINAL PAGE IS
 OF POOR QUALITY

Table 5 - Total Amounts of Gases Recovered by Physico-chemical Processing of Human Wastes Produced by a 25 Man Crew in 360 Days (Unit - Kg)

Net H_2 produced	=	1320 (w/ Bosch: 1006)	
Net O_2 produced	=	$\frac{10569}{2564}$ O_2 produced - $\frac{8005}{5035}$ O_2 required	
	=	(w/ Bosch: 5035)	oxidant
Net N_2 produced	=	4125	
Net CO_2 produced	=	15719 (w/ Bosch: 12265)	
Overall efficiency	=	$\frac{\text{Total material recovered}}{\text{Total } O_2/\text{Food/Water supplied}}$	$\frac{23728}{41967} = 56.5 \%$

Table 6 - Biomass Production Rates Due to Lunar Agriculture

Minimum size of lunar base estimated from (6) assuming:

Growing area/person	-->	12 m^2 Crop/person (wheat)
Light energy	-->	6.8 kW/person
Biomass production	-->	0.090 $Kg/m^2 \cdot day$
Harvest Index		
= edible/total	-->	40 % Edible biomass

Table 7 - Biogas (50% CH_4) Production Rates from Different Biomasses

$$\frac{\text{liter Biogas/Kg Dung}}{\text{Density } CH_4} = \frac{0.0005 \text{ } m^3 \text{ } CH_4 / kg \text{ Dung}}{0.672 \text{ } kg/m^3}$$

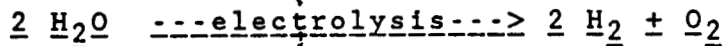
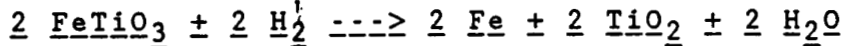
Human feces	=	20-28 liter/Kg = 0.007-0.009	Kg CH_4 /Kg Dung
Pretreated Crop waste	=	34-40 liter/Kg = 0.012-0.014	Kg CH_4 /Kg Dung
Chicken dung	=	66-115 liter/Kg = 0.022-0.039	Kg CH_4 /Kg Dung

ORIGINAL PAGE IS
OF POOR QUALITY

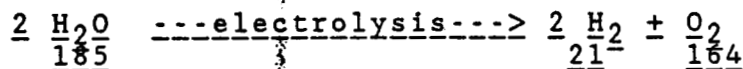
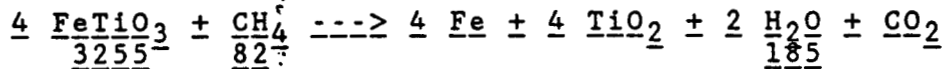
Table 8 - 3 Rocket Fuel Production Schemes From Lunar Soil

1) Ilmenite (FeTiO₃) reduction:

- a) - LOX from H₂ reduction at high temperatures
- Requires H₂ resupply or lunar derived
- Requires cryogenic storage if resupplied
- H₂ produced is recycled (4)



- b) - LO₂, LH₂ from CH₄ reduction at 1100 deg C
- Requires CH₄ resupply or lunar derived
- 80% yield when ground to 0.3 mm particles
- No cryogenic storage needed if resupplied (3)

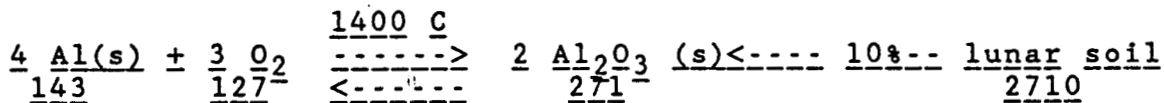


2) Pyroxene carbothermal reduction (SEE Section 1.3 Perry)

3) Vacuum Reduction of Metal Oxides(10): Aluminum production

- Metal extraction from metal oxides in a ultra-high vacuum and at high temperatures.
- Moon has ultra-high vacuum since it lacks an atmosphere.
- Requires no additional chemical reducing agents such as H₂, CH₄ or the supporting equipment.
- Requires high temperatures ie. solar concentrator or electric arc
- All metals (Ti, Fe, Ca, Si, Mg, Al) are separated at once since the lunar soil contains a mixture of the metal oxides.

The decomposition:



- 143 Kg of Al are needed for 1 LOP mission
- Assuming a soil density of 1.3 g/cm³ then 2.08 m³ of soil should contain

Table 9 - Methane, LOX, and LH₂ Production From Ilmenite Using Biogas Produced from Agricultural Wastes in 360 Days.

Crew = 25

<u>Area of base</u>	=	<u>300</u> m ²
<u>Total Biomass</u>	=	<u>9720</u> Kg
<u>Waste</u>	=	<u>5832</u> Kg
<u>CH₄ produced</u>	=	<u>82</u> Kg
<u>H₂ produced</u>	=	<u>21</u> Kg
<u>O₂ produced</u>	=	<u>165</u> Kg

Crew = 100

<u>Area of base</u>	=	<u>1200</u> m ²
<u>Total Biomass</u>	=	<u>38880</u> Kg
<u>Waste</u>	=	<u>23328</u> Kg
<u>CH₄ produced</u>	=	<u>326</u> Kg
<u>H₂ produced</u>	=	<u>84</u> Kg
<u>O₂ produced</u>	=	<u>660</u> Kg

Crew = 500

<u>Area of base</u>	=	<u>6000</u> m ²
<u>Total Biomass</u>	=	<u>194400</u> Kg
<u>Waste</u>	=	<u>116640</u> Kg
<u>CH₄ produced</u>	=	<u>1632</u> Kg
<u>H₂ produced</u>	=	<u>420</u> Kg
<u>O₂ produced</u>	=	<u>3300</u> Kg

ORIGINAL PAGE IS
OF POOR QUALITY

Table 10 - List of Equipment Needed for Utilization of Lunar Materials

waste recycling equipment
 waste combustor
 water electrolyzer
 water condensation units
 biogas bioreactor
 Bosch reactor
 gas storage tanks
mining equipment
 drilling units
 rock crusher
 transport system
metal extraction equipment
 vacuum reduction unit
 ball mill unit
 solar concentrator/furnace
 zone refining unit
 vacuum distillation
 slag separator

PROPULSION APPENDIX

Digging Rate (Kg/Day)=[Digging Rate (m³/Day)][33% Error][Lunar Soil Density (Kg/m³)]
 =(20)(.33)(1300 to 1800)=8580 - 11880 Kg/Day

1% Oxygen Yield=85.8 - 118.8 Kg O₂/Day

5% Hydrogen Conversion:

H₂O --> H₂ + 0.5O₂
 (.05)(85.8 to 118.8)[(2 kg H₂)/(16 kg O₂)]=
 0.540 - 0.743 Kg H₂/Day

100% Efficient Hydrogen Process:

(Digging Rate)(Hydrogen Concentration)=
 0.429 - 0.594 Kg H₂/Day

100% Efficient Aluminum Process:

(Digging Rate)(1.0% Yield of O₂)(6.97% Al Conc.)=
 5.98 - 8.28 Kg Al/Day

100% Efficient Silicon Process:

(Digging Rate)(1.0% Yield of O₂)(21.0% Si Conc.)=
 18 - 25 Kg Si/Day

100% Efficient MgO Process:

(Digging Rate)(1.0% Yield of O₂)(2.04% MgO Conc.)=
 1.75 - 2.42 Kg MgO/Day

Silane Process Equations: (From Ref. 1)

2MgO electrolysis→ 2Mg + O₂
 lunar derived
 e.g. carbothermal
 process
 2Mg + Si --> Mg₂Si
 lunar
 derived
 e.g. carbothermal
 process
 Mg₂Si + 4HCl --> 2MgCl₂ + SiH₄
 terrestrially
 supplied

NOTE: 2.5 Kg MgO/Kg SiH₄, 4.56 Kg HCL/Kg SiH₄

Propellant Quantity Equations:

M_p/M_o =Ratio of Propellant Mass to Total Mass (Vehicle Mass plus Propellant Mass)= $1-\text{EXP}[-DV/c]$
 DV =Change in Velocity (m/s)
 c =Nozzle Exhaust Velocity (m/s)= $I_{sp}g_o$
 I_{sp} =Specific Impulse per Thrust Force
 g_o =Acceleration rate of earth=9.80 m/s²
 $m_{platform}$ =560 kg
 m_{GTV} =460 kg
 $DV_{platform}$ =1500 m/s
 DV_{GTV} =4000 m/s
 T =Thrust (N)=(mass) g_o
Oxygen Density=1140 Kg/m³
Hydrogen Density=71 Kg/m³
Silane Density=680 Kg/m³
Aluminum Density=2699 Kg/m³
Boiloff mass (From Ref. 12)=5% of Volume
 MFR =Mass Flow Rate (Kg/s)= T/c
 $OMFR$ =Oxidizer Mass Flow Rate (Kg/s)=[$r(MFR)$]/($r+1$)
 $FMFR$ =Fuel Mass Flow Rate (Kg/s)= $MFR/(r+1)$
 tp =Propellant Burn Time (s)=(propellant mass)/ MFR
 m =mass (Kg)=(tp) MFR
 V =Volume (m³)=mass/density
 r =Mass Ratio=Mass of Oxidizer per Mass of Fuel
 A_b =propellant fuel burn area

SEE NEXT 3 PAGES FOR DETAILS

Thrust Chamber Dimensions

From Eq. 10-8 of Ref. 9:
 $A_b=168A_t=1035 \text{ cm}^2$

With the Thrust Chamber Length=15 cm
 $R_i=6 \text{ cm}$
 $R_o=31.6 \text{ cm}$

Pressure-Fed System

Diameter of Spherical Liquid Oxygen Tank=0.804 m
From Eq. 9-14 of Ref. 9:
Assume Argon Pressure=6 times the Oxygen Pressure
 $m_{Ar}=36 \text{ Kg}$
Diameter of Spherical Tank of Argon=0.558 m
Assume Neon Pressure=6 times the Oxygen Pressure
 $m_{Ne}=18.2 \text{ Kg}$
Diameter of Spherical Tank of Neon=0.558 m

PLATFORM MASS = 560 Kg GTV MASS = 460 Kg
 Al/LOX $I_{spv} = 275$ s $LSiH_4/LOX$ $I_{spv} = 345$ s
 LH₂/LOX $I_{spv} = 480$ s ONE PLATFORM $\Delta V = 1500$ m/s
 TWO GTV $\Delta V's = 4000$ m/s (TOTAL) 52 BOILOFF RATE

Al/LOX

LH₂/LOX

PLATFORM GTV

PLATFORM

GTV

$M_{O_2} = 294.3$ Kg

$M_{O_2} = 1108$ Kg

$M_{O_2} = 624.2$ Kg

$M_{H_2} = 122.6$ Kg

$M_{H_2} = 462$ Kg

$M_{H_2} = 104.3$ Kg

$V_{O_2} = 0.271$ m³

$V_{O_2} = 1.021$ m³

$V_{O_2} = 0.575$ Kg

$V_{H_2} = 0.045$ m³

$V_{H_2} = 0.171$ m³

$V_{H_2} = 1.542$ Kg

MAX. PROD. TIME:
41.0 DAYS

MAX. PROD. TIME:
154.5 DAYS

MAX. PROD. TIME:
443.7 DAYS

MAX. PROD. TIME:
485.1 DAYS

LSiH₄/LOX

PLATFORM

GTV

$M_{O_2} = 228$ Kg

$M_{O_2} = 835$ Kg

$M_{SiH_4} = 136.8$ Kg

$M_{SiH_4} = 464$ Kg

$V_{O_2} = 0.210$ m³

$V_{O_2} = 0.769$ m³

$V_{SiH_4} = 0.211$ m³

$V_{SiH_4} = 0.716$ m³

MAX. PROD. TIME:
390.9 DAYS

MAX. PROD. TIME:
1326 DAYS

ORIGINAL PAGE IS
OF POOR QUALITY

NOZZLE THRUSTER PARAMETERS: (FOR PLATFORM ONLY)

ASSUMPTIONS

ORIGINAL PAGE IS
OF POOR QUALITY

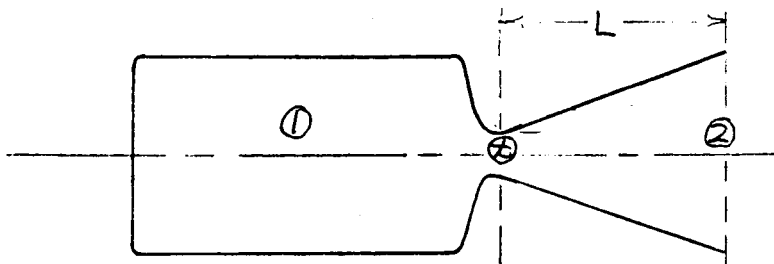
PERFECT GAS

$\dot{m} = \text{CONSTANT}$

CHEMICAL EQUILIBRIUM THROUGHOUT = Al_2O_3

0.5g ACCELERATION RATE

CHOKED FLOW AT THROAT - $M_x = 1.0$



$$\begin{aligned} T_2 &= 3000 \text{ K} & T_1 &= 4500 \text{ K} & P_1 &= 400 \text{ psi} = 2.76 \times 10^6 \text{ Pa} \\ I_{sp \text{ vacuum}} &= 245 \text{ s} & r &= 2.4 & C_{p \text{ Al}} &= 765 \text{ J/kg K} \\ C &= 2401 \text{ m/s} & \Delta V &= 1500 \text{ m/s} & P_2 &= .0404 \text{ atm} = 4094 \text{ Pa} \\ m_{\text{platform}} &= 560 \text{ Kg} & m_0 &= 1093.5 \text{ Kg} & T_c &= 4350 \text{ K} \end{aligned}$$

$$R = \frac{R}{M_w} = \frac{8314 \text{ Nm/Kg K}}{2(26.98) + 3(16)} = 81.54 \text{ J/Kg K}$$

$$C_p = \frac{kR}{k-1} \Rightarrow k = \frac{C_p}{C_p - R} = 1.119$$

$$C_v = \frac{C_p}{k} = 683.6 \text{ J/Kg K}$$

$$M_2 = \frac{C}{a_2} = \frac{C}{\sqrt{kRT_2}} = 4.589$$

$$n_1 = \frac{RT_1}{P_1} = 0.1329 \text{ m}^3/\text{kg}$$

$$n_c = n_1 \left(\frac{k+1}{2} \right)^{\frac{1}{k-1}} = 0.216 \text{ m}^3/\text{kg}$$

$$n_2 = n_1 \left(\frac{P_1}{P_2} \right)^{\frac{1}{k}} = 44.82 \text{ m}^3/\text{kg}$$

$$\dot{m} = \frac{T}{C} = \frac{m_0 g_0 (\text{ACCELERATION RATE})}{C} = 1.776 \text{ Kg/s}$$

$$V_c = \sqrt{\frac{2k}{k+1} RT_1} = 622.5 \text{ m/s}$$

$$V_2 = \sqrt{\frac{2k}{k-1} RT_1} \eta = 2118 \text{ m/s} \quad \eta = 0.65$$

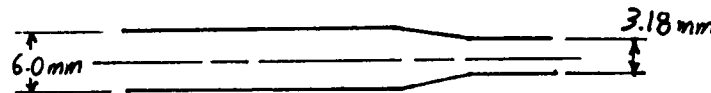
$$A_c = \frac{\dot{m} n_c}{V_c} = 6.16 \text{ cm}^2 \Rightarrow r_c = 1.40 \text{ cm}$$

$$A_2 = \frac{\dot{m} n_2}{V_2} = 358. \text{ cm}^2 \Rightarrow r_2 = 10.7 \text{ cm}$$

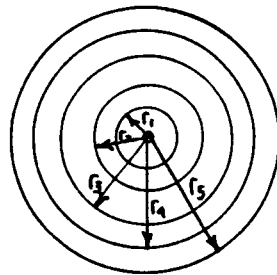
$$L = 12 D_c (\text{FROM REF. 12}) = 33.61 \text{ cm}$$

Injector Design

Use a short tube with conical entrance orifice type



Assume 93 holes with 3 mm of space between each making concentric circles around the center would make the diameter approx. 0.12 m diameter.



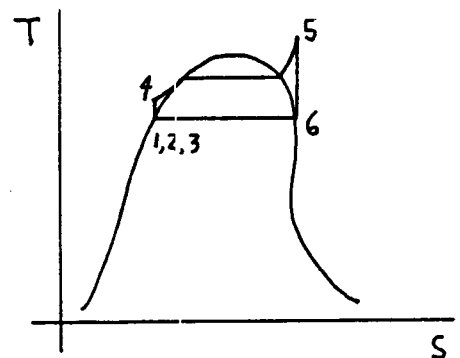
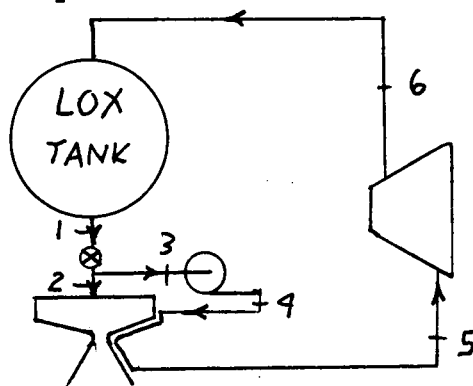
$$\begin{aligned}
 r_0 &= 1 \text{ hole} \\
 r_1 &= 6 \text{ holes (1.2 cm)} \\
 r_2 &= 12 \text{ holes (2.4 cm)} \\
 r_3 &= 18 \text{ holes (3.6 cm)} \\
 r_4 &= 25 \text{ holes (4.8 cm)} \\
 r_5 &= 31 \text{ holes (6 cm)}
 \end{aligned}$$

93 holes total

12 cm diameter

Turbopump System

The process schematic is drawn below:



STATE	T , K	P , MPa	h , kJ/Kg	s , kJ/Kg-K	NOTES
1	149	4.0	182.29	1.8292	Quality=0.0
2	149	4.0	182.29	1.8292	MFR=1.25 Kg/s
3	149	4.0	182.29	1.8292	Quality=0.0
4	149.7	4.5	184.10	1.8292	Subcooled
5	350	37	425	2.4157	Quality=1.0
6	149	4.0	269.25	2.4157	Quality=1.0

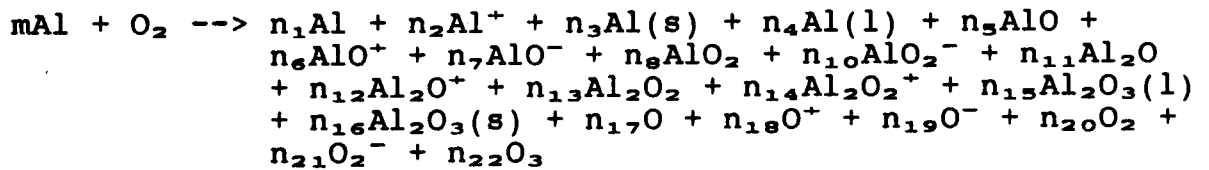
Setting the mass flow rate at each state=0.1 Kg/s

$$\begin{aligned}
Q_6 &= \text{MFR}(h_1 - h_6) = -8.7 \text{ kW} \\
W_{56} &= \text{MFR}(h_5 - h_6)(\text{turbine efficiency}) = 4.7 \text{ kW} \\
Q_{45} &= \text{MFR}(h_5 - h_4) = 24.1 \text{ kW} \\
W_{34} &= \text{MFR}(h_3 - h_4)(\text{pump efficiency}) = -0.15 \text{ kW} \\
\text{So mass flow rate at state 1} &= 1.35 \text{ Kg/s}
\end{aligned}$$

Amount of Oxygen left in tank after a complete propellant burn

$$\begin{aligned}
\text{Propellant burn time} &= 235 \text{ s} \\
\text{Mass remaining} &= \text{MFR}(\text{propellant burn time}) = 23.5 \text{ Kg}
\end{aligned}$$

Equilibrium Constants



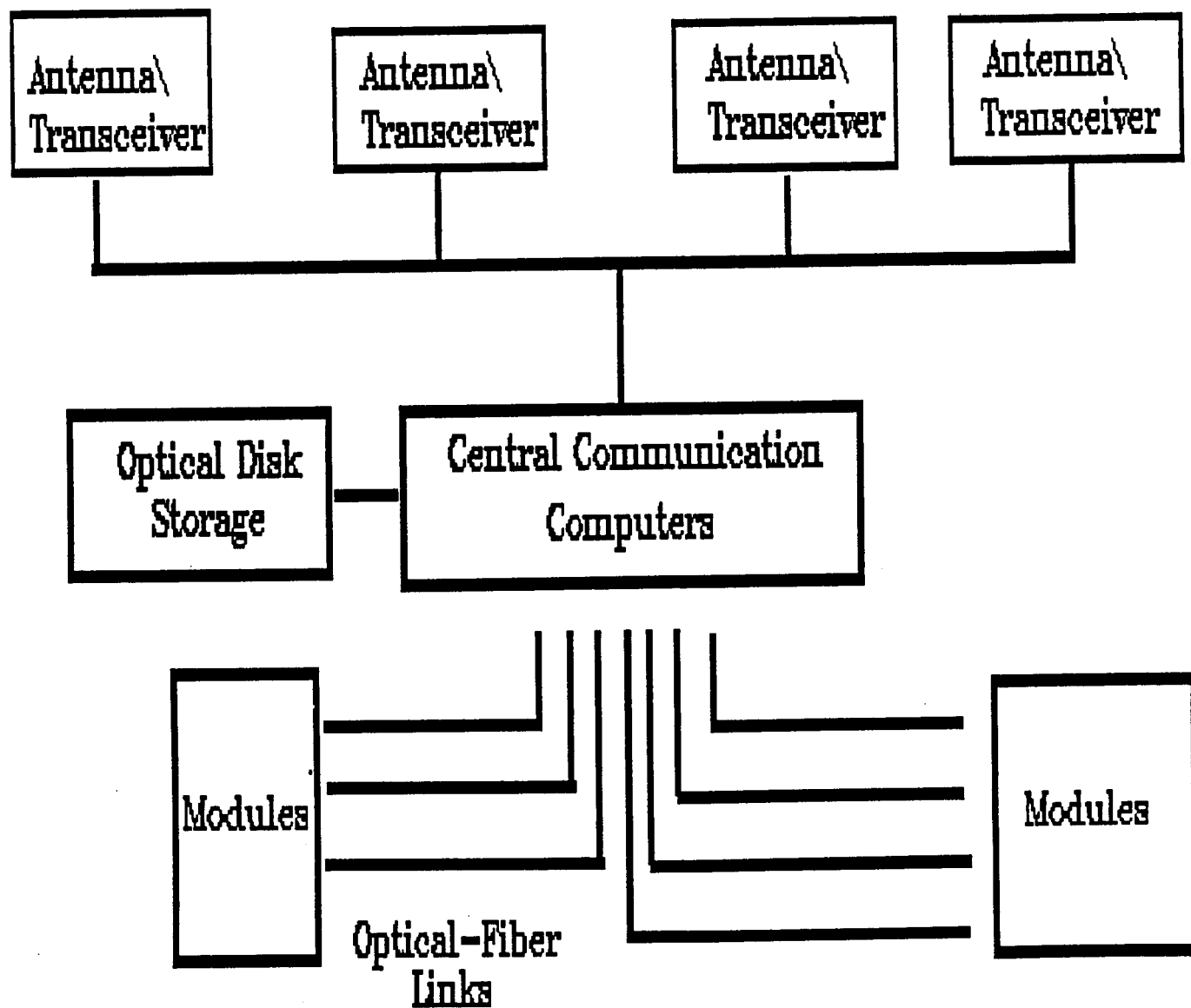
From Ref. 8 and the theory of equilibrium constants some of the equilibrium constants can be determined:

AlO	Kp=27.57
AlO ⁺	Kp=1.106
AlO ⁻	Kp=3.319
AlO ₂ ⁻	Kp=13.27
Al ₂ O ⁺	Kp=1.224
Al ₂ O ₃ (l)	Kp=7.896

APPENDIX 11
Communications

Appendix A

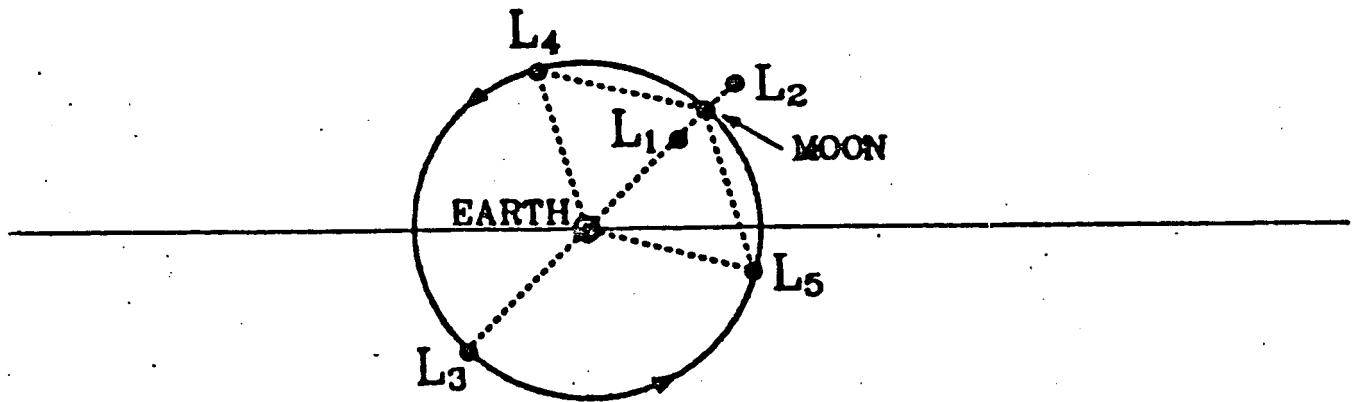
Internal Diagram of the LOP Communications System



Appendix B

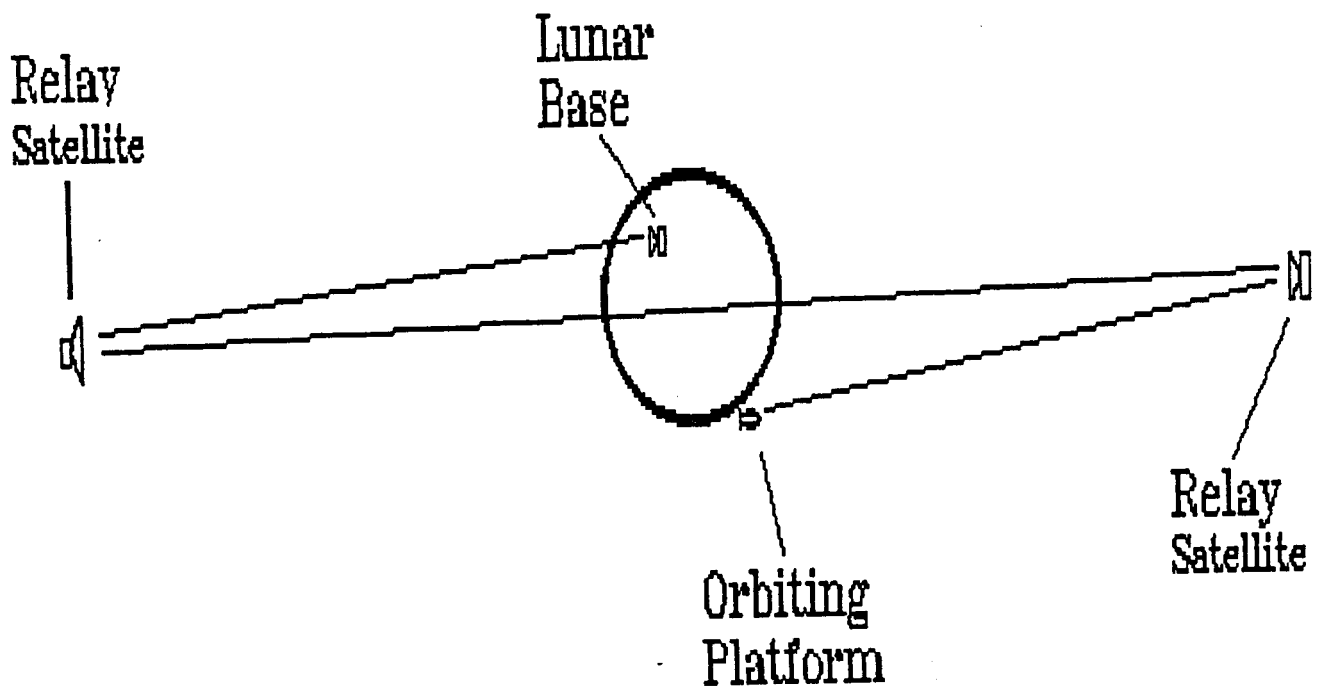
Moon's LaGrange Points

EARTH-MOON SYSTEM



Appendix C

Worst Case Platform to Lunar Base Communication Scenario



Appendix D

Breakdown of Communication System Component Masses and Power

	Mass KG	Power WATTS
Antenna/Transceiver Module		
Phased Array Antenna	2	
Transceiver	5	50

Total for four Units	28	50
Computer Modules		
Computer (1 of 3)	3	10

Total for three Units	10	30
Data Storage Modules		
Optical Storage	5	10

Total for one unit	5	10
Optical Fiber Bus		
Infrared source and detectors	1	5
Fiber	4	

Total for Bus system	5	5
Grand Total	48	95
		K G s
Watts		

APPENDIX 12
Power System

FIG. 4a

```

PROGRAM COMPUTE_OPTIMAL_MASS_MAX_INST.
IMPLICIT NONE
INTEGER PRTG
REAL LOADBAT, PDARK/623.0/, TDARK/1.12/, CAPBAT, DOD
REAL TLIGHT/2.456/, PLIGHT/638.0/, MSOLAR, MRTG, MBAT, MASS
REAL RATEREQ, PSOLAR, OLDMASS/10000.0/
OPEN (3, FILE = 'GOODSIZE.OUT', STATUS = 'NEW')
OPEN (4, FILE = 'PRTG.OUT', STATUS = 'NEW' )
WRITE (3,*) '          POWER SYSTEM FOR 3 INSTRUMENT MODULES'
WRITE (3,*) '          POWER IS IN WATTS, MASS IS IN KG'
WRITE (3,*)
WRITE (3,*)
WRITE(3,10)'POWER RTG', 'MASS RTG','MASS ARRAY','MASS BATTERY',
1  'DOD', 'TOTAL MASS'
FORMAT (11X, A9, 2X, A8, 2X, A10, 2X,A12, 2X, A3, 2X, A10)
DO PRTG = 0,640,20
SIZE BATTERY BY AMOUNT OF ENERGY IT WILL NEED TO PRODUCE ON DARK SIDE
COMPUTE ENERGY REQUIRED OF BATTERY *
    LOADBAT = (PDARK - PRTG)*TDARK
    IF (LOADBAT .LE. 0.0) LOADBAT = 0.0
    COMPUTE RATE REQUIRED FOR BATTERY TO COMPLETELY RECHARGE *
    RATEREQ = LOADBAT/TLIGHT
    CAPBAT = RATEREQ * 15
    SIZE MASSES OF SYSTEM *
        PSOLAR = RATEREQ +PLIGHT -PRTG
        IF(PSOLAR .LE. 0.0) PSOLAR = 0
        MSOLAR = PSOLAR/220.0
        MRTG = PRTG/7.5
        MBAT = CAPBAT/60.0
        MASS = MSOLAR + MRTG + MBAT
        OLDMASS = MIN (OLDMASS,MASS)
        COMPUTE DEPTH OF DISCHARGE
        IF(CAPBAT .GT. 0.0) THEN
            DOD = LOADBAT/CAPBAT
        ELSE
            DOD = 0.0
        END IF
        WRITE (3,20) PRTG, MRTG, MSOLAR, MBAT,DOD, MASS
FORMAT(14X,I3,6X, F6.2, 5X, F6.2, 7X, F6.2, 4X, F5.3, 3X, F6.2)
        WRITE (4,*) PRTG, MASS
END DO
WRITE (3,*)
WRITE (3,*)
WRITE (3,*) 'THE MINIMUM TOTAL MASS IS', OLDMASS
CLOSE (3)
CLOSE (4)
END

```

FIG. 4b

```

PROGRAM COMPUTE_OPTIMAL_MASS_RAMEN
IMPLICIT NONE
INTEGER PRTG
REAL LOADBAT, PDARK/403.0/, TDARK/1.12/, CAPBAT, DOD
REAL TLIGHT/2.456/, PLIGHT/403.0/, MSOLAR, MRTG, MBAT, MASS
REAL RATEREQ, PSOLAR, OLDMASS/10000.0/
OPEN (3, FILE = 'GOODSIZER.OUT', STATUS = 'NEW')
OPEN (4, FILE = 'PRTG.OUTR', STATUS = 'NEW')
WRITE (3,*) '          POWER SYSTEM FOR RAMAN MODULE'
WRITE (3,*) '          POWER IS IN WATTS, MASS IS IN KG'
WRITE (3,*)
WRITE (3,*)
WRITE(3,10)'POWER RTG', 'MASS RTG', 'MASS ARRAY',
1  'MASS BATTERY', 'DOD', 'TOTAL MASS'
10  FORMAT(11X, A9, 2X, A8, 2X, A10, 2X, A12, 2X, A3, 2X, A10)
DO PRTG = 0,1900,20
*   SIZE BATTERY BY AMOUNT OF ENERGY IT WILL NEED TO PRODUCE ON DARK SIDE
*   COMPUTE ENERGY REQUIRED OF BATTERY FIGURING RAMEN WILL ONLY GO FOR45 MIN *
      LOADBAT = (PDARK - PRTG)*TDARK + 1500.0* .75
      IF (LOADBAT .LE. 0.0) LOADBAT = 0.0
*   COMPUTE RATE REQUIRED FOR BATTERY TO COMPLETELY RECHARGE *
      RATEREQ = LOADBAT/TLIGHT
      CAPBAT = RATEREQ * 15
*   SIZE MASSES OF SYSTEM *
      PSOLAR = RATEREQ +PLIGHT -PRTG
      IF(PSOLAR .LE. 0.0) PSOLAR = 0
      MSOLAR = PSOLAR/220.0
      MRTG = PRTG/7.5
      MBAT = CAPBAT/60.0
      MASS = MSOLAR + MRTG + MBAT
      OLDMASS = MIN (OLDMASS,MASS)
*   COMPUTE DEPTH OF DISCHARGE
      IF(CAPBAT .GT. 0.0) THEN
          DOD = LOADBAT/CAPBAT
      ELSE
          DOD = 0.0
      END IF
      WRITE (3,20) PRTG, MRTG, MSOLAR, MBAT,DOD, MASS
20  FORMAT(14X, I4, 6X,F6.2,5X, F6.2, 7X, F6.2, 4X, F5.3, 3X, F6.2)
      WRITE (4,*) PRTG, MASS
END DO
WRITE (3,*)
WRITE (3,*)
WRITE (3,*) 'THE MINIMUM TOTAL MASS IS', OLDMASS
CLOSE (3)
CLOSE (4)
END

```


Fig. 4 C

LEGEND

PRTG - Power supplied continuously by RTGs
LOADBAT - Energy (W-Hrs) that the battery will need to supply in the shadow
PDARK - Total amount of power that will be required in the shadow (w)
TDARK - Total time will be in shadow (Hrs)
CAPBAT - Capacity that the battery will need to have in order to be able to recharge completely while in the light (W-Hrs)
RATEREQ - Rate of energy acceptance that the battery needs in order to become fully recharged while in the light (W)
PSOLAR - Amount of power the solar cells must produce (W)
PLIGHT - Amount of power that will be required in the light (W)
TLIGHT - Total time will be in light (Hrs)
MSOLAR - Mass of solar array, using 220 W/KG as specific power density (EOL)
MBAT - Mass of battery, using 60 W-Hr/Kg as specific energy density
MRTG - Mass RTG, using 7.5 W/Kg as specific power density
Mass - Total mass of power system
OLDMASS - Dummy variable used in MIN function to find the minimum total mass
DOD - depth of discharge

Fig. 5a

POWER SYSTEM FOR 3 INSTRUMENT MODULES

POWER IS IN WATTS, MASS IS IN KG

POWER RTG	MASS RTG	MASS ARRAY	MASS BATTERY	DOD	TOTAL MASS
0	0.00	4.19	71.03	0.164	75.22
20	2.67	4.06	68.75	0.164	75.47
40	5.33	3.93	66.47	0.164	75.73
60	8.00	3.79	64.19	0.164	75.98
80	10.67	3.66	61.91	0.164	76.23
100	13.33	3.53	59.63	0.164	76.49
120	16.00	3.40	57.35	0.164	76.74
140	18.67	3.26	55.07	0.164	77.00
160	21.33	3.13	52.79	0.164	77.25
180	24.00	3.00	50.50	0.164	77.50
200	26.67	2.87	48.22	0.164	77.76
220	29.33	2.74	45.94	0.164	78.01
240	32.00	2.60	43.66	0.164	78.27
260	34.67	2.47	41.38	0.164	78.52
280	37.33	2.34	39.10	0.164	78.78
300	40.00	2.21	36.82	0.164	79.03
320	42.67	2.07	34.54	0.164	79.28
340	45.33	1.94	32.26	0.164	79.54
360	48.00	1.81	29.98	0.164	79.79
380	50.67	1.68	27.70	0.164	80.05
400	53.33	1.54	25.42	0.164	80.30
420	56.00	1.41	23.14	0.164	80.56
440	58.67	1.28	20.86	0.164	80.81
460	61.33	1.15	18.58	0.164	81.06
480	64.00	1.01	16.30	0.164	81.32
500	66.67	0.88	14.02	0.164	81.57
520	69.33	0.75	11.74	0.164	81.83
540	72.00	0.62	9.46	0.164	82.08
560	74.67	0.49	7.18	0.164	82.33
580	77.33	0.35	4.90	0.164	82.59
600	80.00	0.22	2.62	0.164	82.84
620	82.67	0.09	0.34	0.164	83.10
640	85.33	0.00	0.00	0.000	85.33

THE MINIMUM TOTAL MASS IS 75.21744

Fig. 5b
POWER SYSTEM FOR RAMAN MODULE
POWER IS IN WATTS, MASS IS IN KG

POWER RTG	MASS RTG	MASS ARRAY	MASS BATTERY	DOD	TOTAL MASS
0	0.00	4.75	160.46	0.164	165.21
20	2.67	4.62	158.18	0.164	165.46
40	5.33	4.48	155.90	0.164	165.72
60	8.00	4.35	153.62	0.164	165.97
80	10.67	4.22	151.34	0.164	166.23
100	13.33	4.09	149.06	0.164	166.48
120	16.00	3.96	146.78	0.164	166.73
140	18.67	3.82	144.50	0.164	166.99
160	21.33	3.69	142.22	0.164	167.24
180	24.00	3.56	139.94	0.164	167.50
200	26.67	3.43	137.66	0.164	167.75
220	29.33	3.29	135.38	0.164	168.01
240	32.00	3.16	133.10	0.164	168.26
260	34.67	3.03	130.82	0.164	168.51
280	37.33	2.90	128.54	0.164	168.77
300	40.00	2.76	126.26	0.164	169.02
320	42.67	2.63	123.98	0.164	169.28
340	45.33	2.50	121.70	0.164	169.53
360	48.00	2.37	119.42	0.164	169.78
380	50.67	2.23	117.14	0.164	170.04
400	53.33	2.10	114.86	0.164	170.29
420	56.00	1.97	112.58	0.164	170.55
440	58.67	1.84	110.30	0.164	170.80
460	61.33	1.70	108.02	0.164	171.06
480	64.00	1.57	105.74	0.164	171.31
500	66.67	1.44	103.46	0.164	171.56
520	69.33	1.31	101.18	0.164	171.82
540	72.00	1.18	98.90	0.164	172.07
560	74.67	1.04	96.62	0.164	172.33
580	77.33	0.91	94.34	0.164	172.58
600	80.00	0.78	92.06	0.164	172.83
620	82.67	0.65	89.78	0.164	173.09
640	85.33	0.51	87.50	0.164	173.34
660	88.00	0.38	85.22	0.164	173.60
680	90.67	0.25	82.94	0.164	173.85
700	93.33	0.12	80.66	0.164	174.11
720	96.00	0.00	78.38	0.164	174.38
740	98.67	0.00	76.10	0.164	174.76
760	101.33	0.00	73.82	0.164	175.15
780	104.00	0.00	71.54	0.164	175.54
800	106.67	0.00	69.25	0.164	175.92
820	109.33	0.00	66.97	0.164	176.31
840	112.00	0.00	64.69	0.164	176.69
860	114.67	0.00	62.41	0.164	177.08
880	117.33	0.00	60.13	0.164	177.47
900	120.00	0.00	57.85	0.164	177.85
920	122.67	0.00	55.57	0.164	178.24
940	125.33	0.00	53.29	0.164	178.63
960	128.00	0.00	51.01	0.164	179.01
980	130.67	0.00	48.73	0.164	179.40
1000	133.33	0.00	46.45	0.164	179.79
1020	136.00	0.00	44.17	0.164	180.17
1040	138.67	0.00	41.89	0.164	180.56
1060	141.33	0.00	39.61	0.164	180.95
1080	144.00	0.00	37.33	0.164	181.33

1100	146.67	0.00	35.05	0.164	181.72
1120	149.33	0.00	32.77	0.164	182.11
1140	152.00	0.00	30.49	0.164	182.49
1160	154.67	0.00	28.21	0.164	182.88
1180	157.33	0.00	25.93	0.164	183.27
1200	160.00	0.00	23.65	0.164	183.65
1220	162.67	0.00	21.37	0.164	184.04
1240	165.33	0.00	19.09	0.164	184.43
1260	168.00	0.00	16.81	0.164	184.81
1280	170.67	0.00	14.53	0.164	185.20
1300	173.33	0.00	12.25	0.164	185.58
1320	176.00	0.00	9.97	0.164	185.97
1340	178.67	0.00	7.69	0.164	186.36
1360	181.33	0.00	5.41	0.164	186.74
1380	184.00	0.00	3.13	0.164	187.13
1400	186.67	0.00	0.85	0.164	187.52
1420	189.33	0.00	0.00	0.000	189.33
1440	192.00	0.00	0.00	0.000	192.00
1460	194.67	0.00	0.00	0.000	194.67
1480	197.33	0.00	0.00	0.000	197.33
1500	200.00	0.00	0.00	0.000	200.00
1520	202.67	0.00	0.00	0.000	202.67
1540	205.33	0.00	0.00	0.000	205.33
1560	208.00	0.00	0.00	0.000	208.00
1580	210.67	0.00	0.00	0.000	210.67
1600	213.33	0.00	0.00	0.000	213.33
1620	216.00	0.00	0.00	0.000	216.00
1640	218.67	0.00	0.00	0.000	218.67
1660	221.33	0.00	0.00	0.000	221.33
1680	224.00	0.00	0.00	0.000	224.00
1700	226.67	0.00	0.00	0.000	226.67
1720	229.33	0.00	0.00	0.000	229.33
1740	232.00	0.00	0.00	0.000	232.00
1760	234.67	0.00	0.00	0.000	234.67
1780	237.33	0.00	0.00	0.000	237.33
1800	240.00	0.00	0.00	0.000	240.00
1820	242.67	0.00	0.00	0.000	242.67
1840	245.33	0.00	0.00	0.000	245.33
1860	248.00	0.00	0.00	0.000	248.00
1880	250.67	0.00	0.00	0.000	250.67
1900	253.33	0.00	0.00	0.000	253.33

THE MINIMUM TOTAL MASS IS 165.2094

Fig. 6a

POWER RTG VS. TOTAL MASS

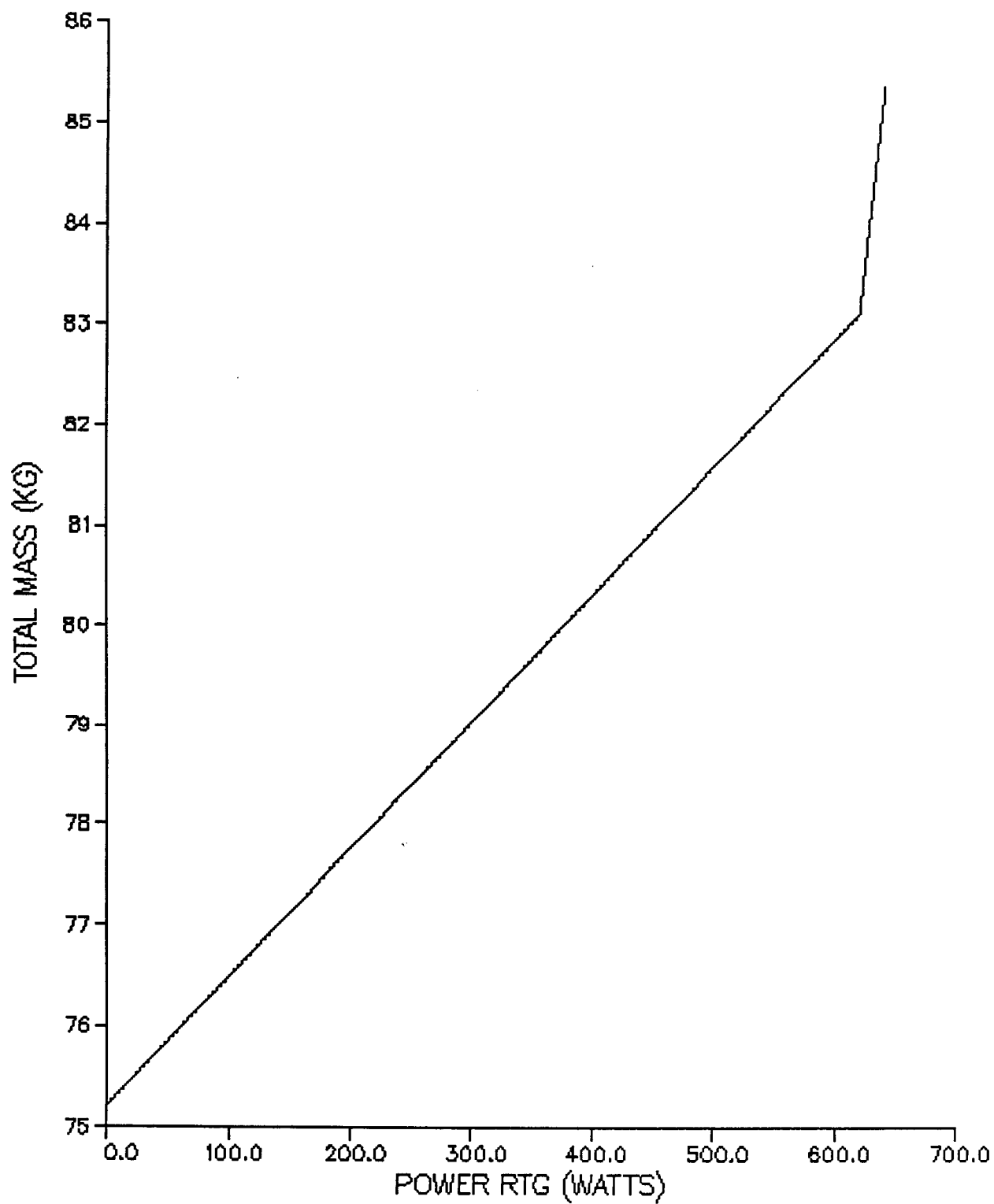


Fig. 6b

POWER RTG VS. TOTAL MASS, RAMEN

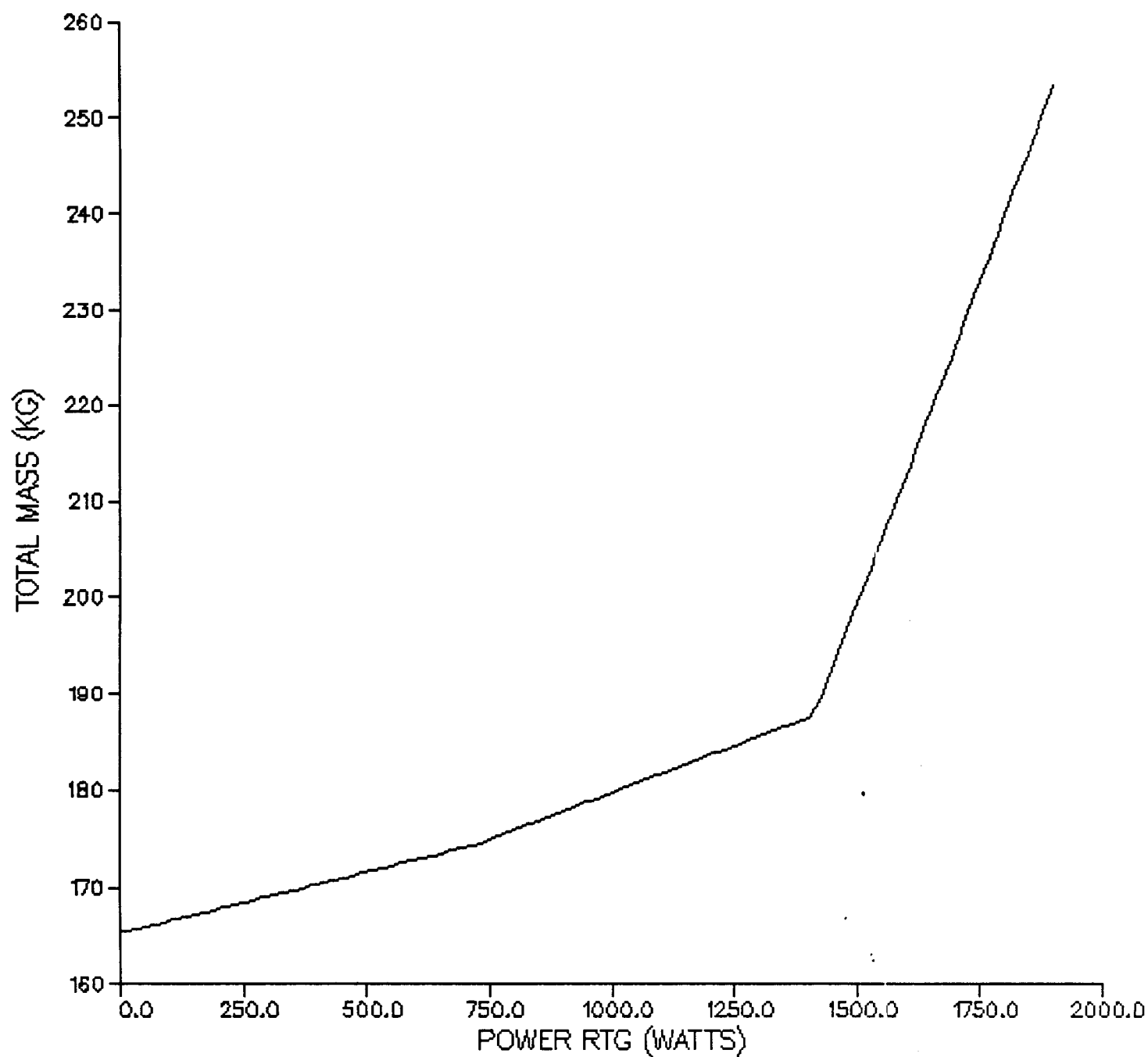


Fig. 7

Computing DOD and Battery Mass

Load battery = (Power dark req. - Power RTG) * Time dark
Rate recharge req. = Load battery/ time light
Capacity battery = Rate recharge req * 15
Mass battery = Capacity battery/ 60
Depth of discharge = Load battery/ capacity battery
= (Rate recharge req. * time light)/ (Rate recharge req. * 15)
= Time light/ 15
= 2.456 hr/ 15
= .164

Computations with Power RTG = 100 W and 3 Instrument modules
power requirements

Load battery = (640 W - 100 W) * 1.12 Hr = 604.8 W Hr
Rate Recharge req. = 604.8 W Hr / 2.456 Hr = 246 W
Capacity battery = 246 W * 15 = 3693.8 W Hr
Mass battery = 3693.8 W / 60 W/Kg = 61.5 kg

Fig. 8

SIZING THE SOLAR ARRAY CALCULATIONS

Total Power (EOL) = $220 \text{ W/Kg} * 4.087 \text{ Kg} = 899.23 \text{ W}$
Temperature effect = $(50 - 28) * 0.005$ (used 50 degrees Celsius)
Array Capacity (BOL) = $899.23 \text{ W} / (.7 * \cos(6.5 \text{ degrees})) * (1 - .11) * .9 = 1652 \text{ W}$
Array size = $1652 \text{ W} / (1350 \text{ W/m}^2 * .2) = 6.12 \text{ m}^2$
Number of cells = $(6.12 \text{ m}^2 * .9) / .0012 \text{ m}^2 = 4590 \text{ cells}$

cell size

cell size = $2 \text{ cm} * 6 \text{ cm}$
cell voltage = $.5 \text{ V/cell}$
power/cell (EOL) = $899.23 \text{ W} / 4590 \text{ cells} = .196 \text{ W/cell}$
power/cell (BOL) = $1652 \text{ W} / 4590 \text{ cells} = .360 \text{ W/cell}$
current/cell (EOL) = $.196 \text{ W} / .5 \text{ V} = .392 \text{ amps}$
current/cell (BOL) = $.360 \text{ W} / .5 \text{ V} = .72 \text{ amps}$

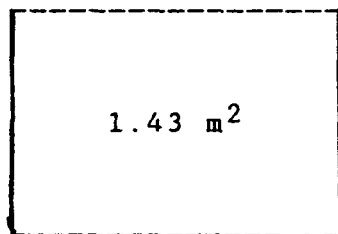
array dimensions

array voltage required = 33 V
number of cells per column = $33 \text{ V} / (.5 \text{ V/cell}) = 66 \text{ cells}$
total number of cells in each row = $66 / 4590 = 70 \text{ cells}$

divide row into four arrays 18 cells each
dimensions of each array

18 cells, 1.08 m

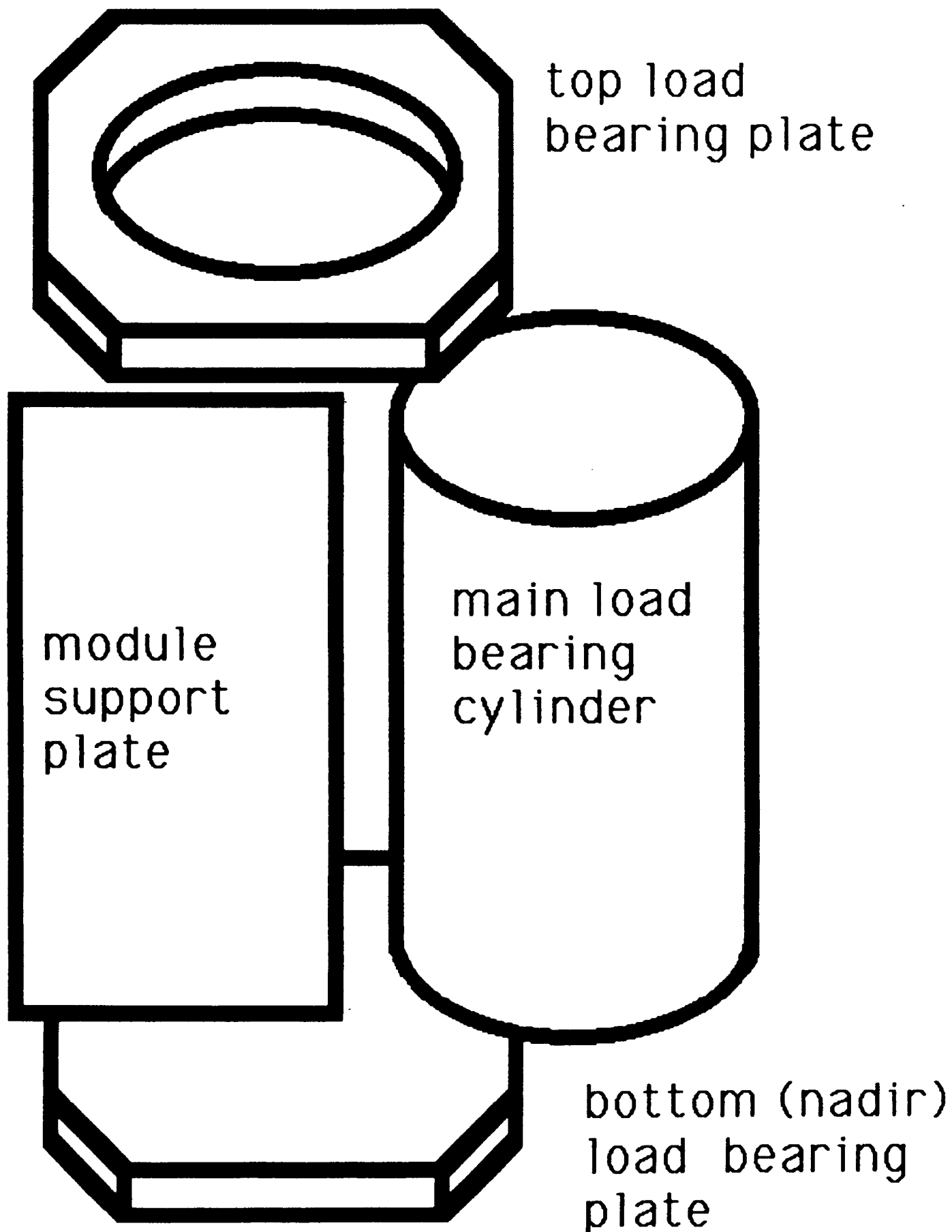
66 cells
1.32 m



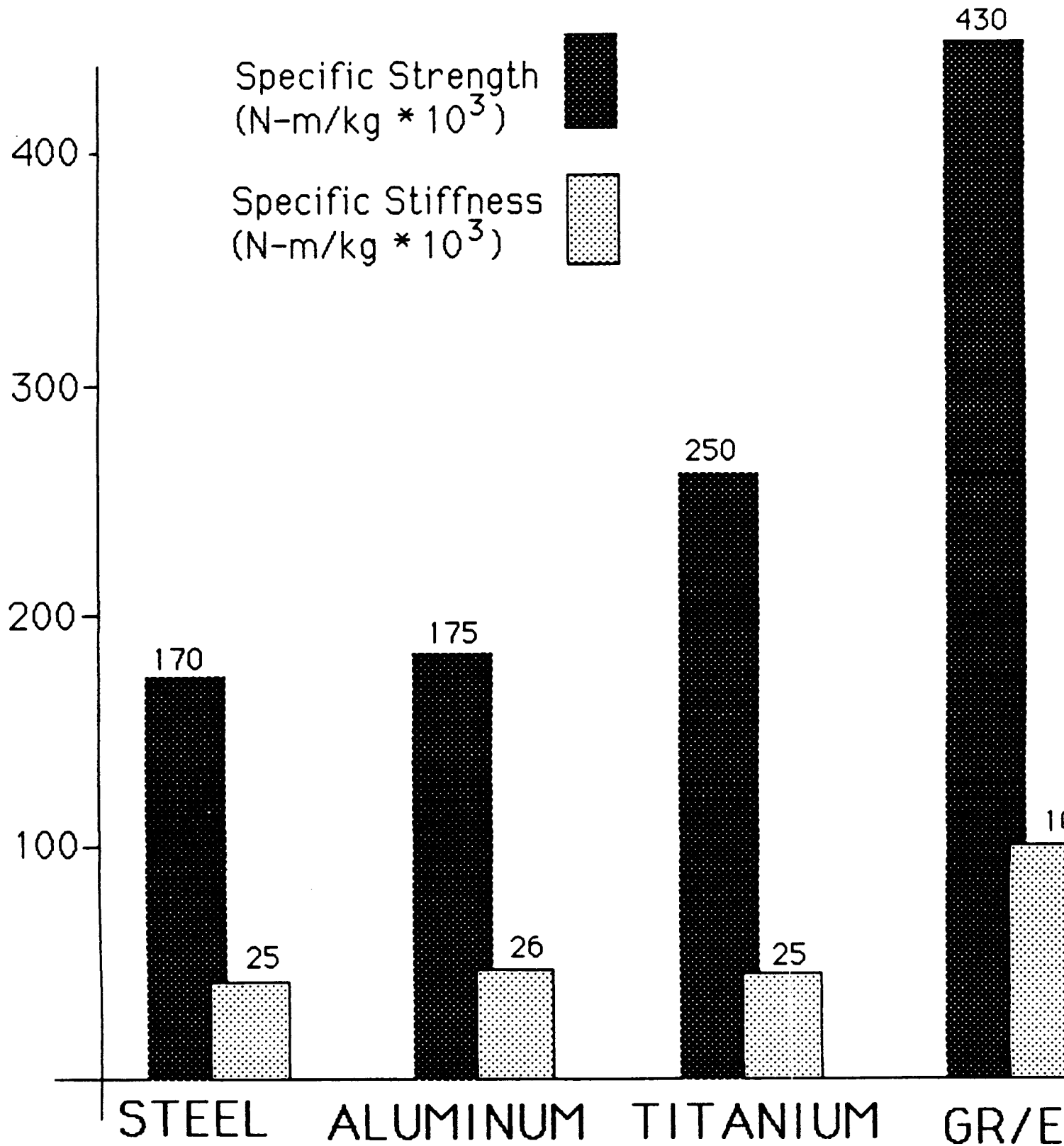
plus 10 % packing factor (spacing between cells)
Array Area = $1.45 \text{ m} * 1.19 \text{ m} = 1.73 \text{ m}^2$

APPENDIX 13
Configuration and Structure

Appendix 1. Load bearing portion of lunar orbital prospector.



SPACECRAFT MATERIALS



Appendix 3. Calculations for the sizing of the main load bearing cylinder.

The following equations were used to calculate the tabulated data below. Note, that finding the thickness is an iterative solution.

$$P = \text{Critical load} = 1.2[1 - 0.9(1 - e^{((1/16)*(r/t)^{1/2}))}] \pi E t^2$$

[From B. N. Agrawal, *Design of Geosynchronous Spacecraft*, Prentice-Hall, Inc. Englewood Cliffs, N. J., 1986, pp. 213.]

$$V = \text{Volume} = \pi D L t$$

$$m = \text{mass} = \text{density} * \text{volume}$$

r is the mean radius of the cylinder, D is the mean diameter of the cylinder, L is the length of the cylinder, and t is the thickness of the cylinder.

For this case r = .5m, L = 1m.

Factor of Safety = 1

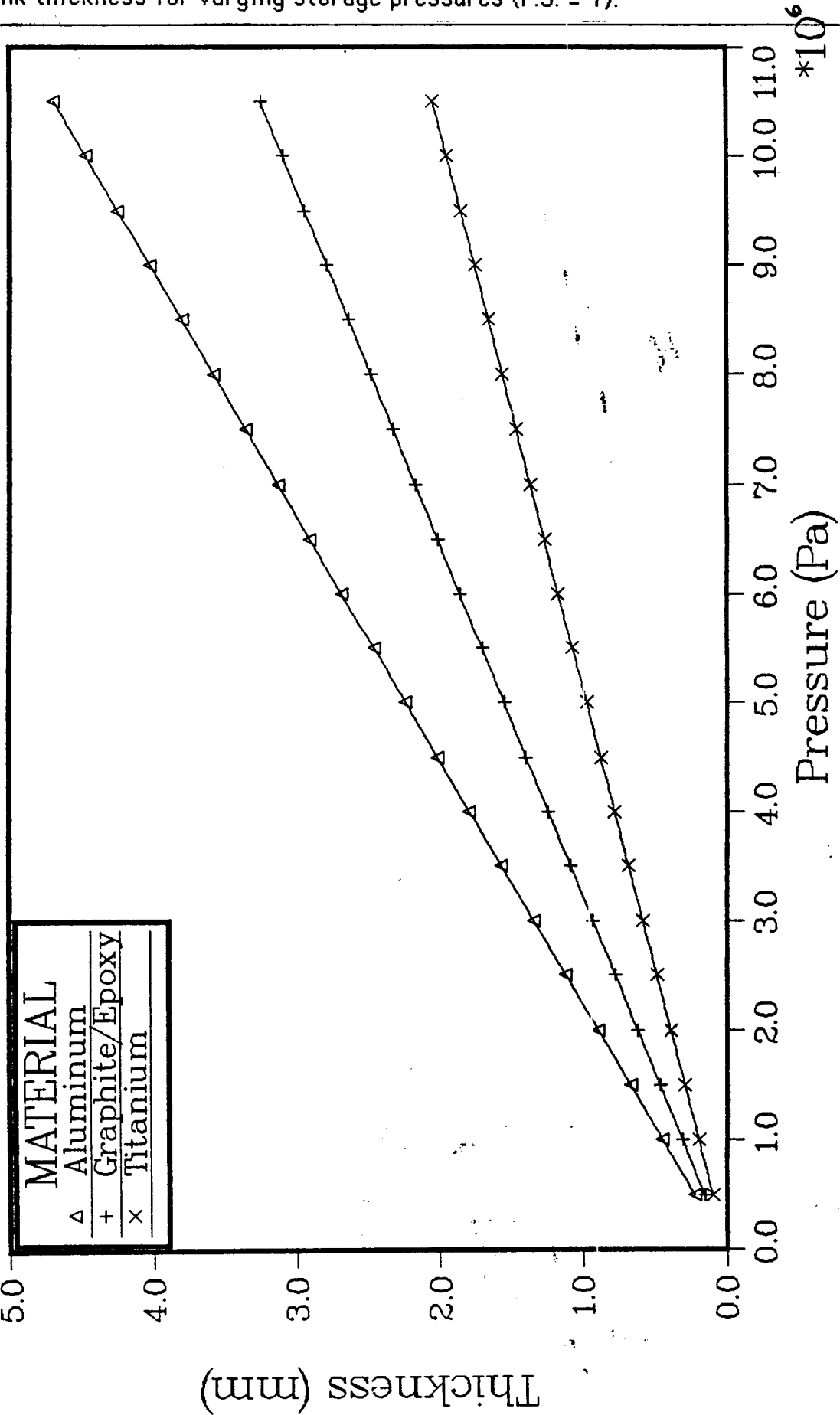
	<u>den.(kg/m**3)10</u>	<u>E.(Pa)10⁹</u>	<u>P(kN)</u>	<u>t(mm)</u>	<u>V(m**3)</u>	<u>m(kg)</u>
Gr/Ep	1.61	186.	27.	.43	.0014	2.17
Aluminum	2.71	67.	27.	.64	.0020	5.44
Titanium	4.43	110.	27.	.53	.0017	7.38
Steel	7.9	186.	27.	.43	.0014	10.67

Factor of Safety = 2

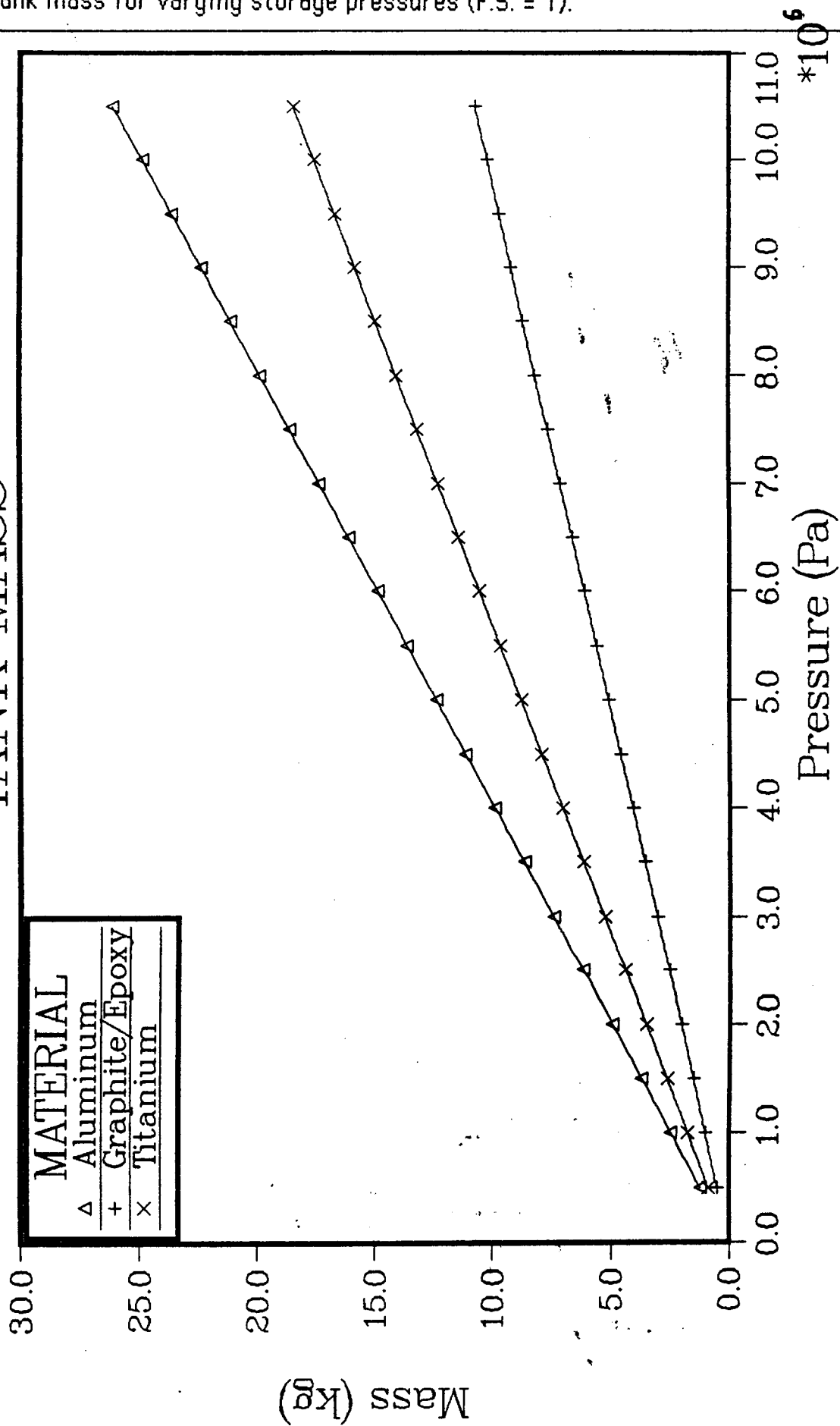
Gr/Ep	1.61	186.	54.	.56	.0018	2.86
Aluminum	2.71	67.	54.	.84	.0026	8.13
Titanium	4.43	110.	54.	.69	.0022	9.60
Steel	7.9	186.	54.	.56	.0018	13.90

Conclusion: Graphite/epoxy is the lightest material to take the biggest axial load on the main load bearing cylinder.

TANK THICKNESS



TANK MASS



Appendix 6

```

C --- A program to generate a plot of thickness versus pressure, and
C      mass versus pressure for a spherical pressure vessel that has a
C      Diameter = .804 m and is made of various materials. In particular
C      Aluminum and Graphite/Epoxy.
C
C --- This program was written on 8 May 1988 for design purposes for
C      ME 595. Signed R.J. Schmid.
C
C --- Dictionary of Variables
C
C      DIAM    = Diameter of sphere (m)
C      T       = Thickness of pressure vessel (mm)
C      SIGMAA  = Sigma sub a which is the axial stress in pressure vessel
C               this is the maximum allowed for aluminum (Pa)
C      SIGMAG  = Sigma as above but for graphite epoxy (Pa)
C      SIGMAT  = Sigma as above but for titanium
C      PIN     = Pressure on the inside of the pressure vessel (Pa)
C               Pressure on the outside is zero in space
C      DENS    = Density of material container is made of (kg/m**3)
C      MASS    = Mass of the container itself (not what it contains) (kg)
C      PI      = A rather obvious term wouldn't you say?
C
PROGRAM PRES
IMPLICIT REAL(A-Z)
INTEGER I,J,K
OPEN(UNIT=13, NAME='PRES.DAT', STATUS='UNKNOWN')
PI = 2.*ASIN(1.)
PIN = 0.0
DIAM = .804
SIGMAA = 450.E6
SIGMAG = 650.E6
SIGMAT = 1034.E6
DENSEA = 2.71E3
DENSEG = 1.61E3
DENST = 4.43E3
DO WHILE(PIN .LE. 10000000.)
    PIN = PIN + 500000.
    TA = PIN*DIAM/4./SIGMAA
    MASSA = DENSEA*PI/6.*((DIAM+2.*TA)**3 - (DIAM)**3)
    TG = PIN*DIAM/4./SIGMAG
    MASSG = DENSEG*PI/6.*((DIAM+2.*TG)**3 - (DIAM)**3)
    TT = PIN*DIAM/4./SIGMAT
    MASST = DENST*PI/6.*((DIAM+2.*TT)**3 - (DIAM)**3)
C
C --- First convert the standard SI units to more convenient units
C      before printout: T in mm, MASS in kg, PIN in PA
C
    TA = TA*1000.
    TG = TG*1000.
    TT = TT*1000.
    WRITE(13,20)PIN,TA,MASSA,TG,MASSG,TT,MASST
END DO
20 FORMAT(1X,F12.1,F12.10,F12.8,F12.10,F12.8,F12.10,F12.8)
STOP
END

```

```
C --- *****
C --- ***** KYLE ADAMS *****
C --- *****
C --- ***** ME595 *****
C --- *****
C --- ***** MASS ANALYSIS *****
C --- *****
C --- *****
C --- THIS PROGRAM IS WRITTEN TO SOLVE FOR THE MAXIMUM MOMENT ON A
C --- CANTILEVER BEAM CAUSED BY A FORCE AT THE END OF THE BEAM DUE TO
C --- ACCELERATION AND A TIP MASS (RTG, SOLAR PANAL, ALTIMETER, ETC.)
C --- THE OUTSIDE DIAMETER OF THE BEAM IS VARIED IN ORDER TO DESIGN
C --- AN OPTIMAL SIZE OF BEAM FOR A TRUSS. THE MASS OF THE BEAM IS
C --- THEN CALCULATED.
C ---
REAL M,DO,DI,MASS,LENGTH,X(10),Y(10),RHO,SIGMA,SHEAR
INTEGER K
OPEN(UNIT=10,FILE='ME595.OUT',STATUS='UNKNOWN')
C ---
C --- DEFINE KNOWN VALUES
SHEAR = 29E06
SIGMA=675E06
RHO = 1610
PI = ACOS(-1.)
WRITE(10,*)'THE VALUE FOR THE ULTIMATE TENSILE STRENGTH IS',
&SIGMA,'N/M**2'
WRITE(10,*)'THE DENSITY USED IS',RHO,'KG/M**3'
WRITE(10,*)' '
PRINT*, 'SHEAR,SIGMA,RHO,PI=',SHEAR,SIGMA,RHO,PI
C ---
C --- ENTER THE TRUSS CHARACTERISTICS
51 PRINT*, 'ENTER THE MASS OF THE OBJECT ON THE END OF THE TRUSS'
PRINT*, 'IN KG'
READ*,XMASS
PRINT*, 'ENTER THE DISTANCE AT WHICH THE FORCE OCCURS IN METERS'
PRINT*, 'FROM THE FIXED POINT'
READ*,DISTNC
PRINT*, 'ENTER THE LENGTH OF THE BEAM IN QUESTION IN METERS'
READ*,LENGTH
C ---
C --- BEGIN LOOP TO OBTAIN THE NECESARY INFORMATION.
C ---
FORCE = XMASS/4.0*(.5*9.81)
M = FORCE * DISTNC
WRITE(10, '(1X,130(' '*'))')
WRITE(10,61)'THE MASS OF THE OBJECT IS',XMASS,'KG'
WRITE(10,*)' THE DISTANCE FROM THE FIXED POINT'
WRITE(10,61)'AT WHICH THE FORCE ACTS IS',DISTNC,'METERS'
WRITE(10,61)'THE LENGTH OF THE BEAM IS',LENGTH,'METERS'
WRITE(10,*)' USING AN ACCELERATION OF .5G THE '
WRITE(10,61)'FORCE OF THE TIP MASS IS',FORCE,'NEWTONS'
WRITE(10,61)'THE MOMENT CAUSED BY THE OBJECT IS',M,'N-M'
WRITE(10, '(1X,130(' '*'))')
WRITE(10,63)'OUTSIDE INSIDE BEAM
& BEAM '
WRITE(10,63)'DIAMETER DIAMETER MASS
& MOMENT'
WRITE(10,63)' IN CM IN CM KG
```



```

&          N-M '
WRITE(10,'(1X,130(''***'))')
WRITE(10,'(1X,130(''***'))')
TEMP = 0.0
K=0
DO 10 DO = .02,0.10,.01
    C=DO/2
5      DI=(DO**4-(64*M*C)/(PI*SIGMA))**.25
      PDO = DO*100
      PDI = DI*100
      VOLUME=(PI/4)*(DO**2-DI**2)*LENGTH
      MASS=RHO*VOLUME
      K=K+1
      IF(K.GT.100)THEN
          STOP
      END IF
      F2 = (.5*9.81)*MASS
      M = FORCE*DISTNC + F2*(LENGTH/2.)
      IF (ABS(TEMP - M).GE.(.001)) THEN
          TEMP = M
          GO TO 5
      END IF
      PRINT*,'THE O.D.,ID,MASS,MOMENT ARE'
      WRITE(10,64)PDO,PDI,MASS,M
      WRITE(6,*)PDO,PDI,MASS,M
      X(K)=DO
      Y(K)=DI
      PRINT*,'THE NUMBER OF TIMES THROUGH THE LOOP IS',K
C ---      X(K+8)=DO
C ---      Y(K+8)=DI
10 CONTINUE
PRINT*,'DO YOU WANT TO RUN AGAIN?'
PRINT*,'IF YES ENTER A 1 IF NO ENTER A 2'
READ*,III
IF (III.EQ.1)THEN
    WRITE(10,65)'
    GO TO 51
ELSE
    STOP
END IF

C ---
C ---
61 FORMAT(1X,A34,1X,F10.3,1X,A10)
62 FORMAT(1X,A5)
63 FORMAT(1X,A51)
64 FORMAT(1X,2X,F6.2,7X,F8.4,7X,G11.4,4X,F8.3)
65 FORMAT('1',A10)
END

```

THE VALUE FOR THE ULTIMATE TENSILE STRENGTH IS 6.7500000E+08N/M**2
 THE DENSITY USED IS 1610.000 KG/M**3

 THE MASS OF THE OBJECT IS 17.000 KG
 THE DISTANCE FROM THE FIXED POINT
 AT WHICH THE FORCE ACTS IS 1.000 METERS
 THE LENGTH OF THE BEAM IS 1.000 METERS
 USING AN ACCELERATION OF .5G THE
 FORCE OF THE TIP MASS IS 20.846 NEWTONS
 THE MOMENT CAUSED BY THE OBJECT IS 20.846 N-M

OUTSIDE DIAMETER IN CM	INSIDE DIAMETER IN CM	BEAM MASS KG	BEAM MOMENT N-M
2.00	1.9800	0.1006E-01	20.871
3.00	2.9912	0.6654E-02	20.863
4.00	3.9951	0.4981E-02	20.858
5.00	4.9969	0.3982E-02	20.856
6.00	5.9978	0.3317E-02	20.854
7.00	6.9984	0.2843E-02	20.853
8.00	7.9988	0.2487E-02	20.852
9.00	8.9990	0.2212E-02	20.852
10.00	9.9992	0.1990E-02	20.851

THE MASS OF THE OBJECT IS 6.650 KG
THE DISTANCE FROM THE FIXED POINT
AT WHICH THE FORCE ACTS IS 2.200 METERS
THE LENGTH OF THE BEAM IS 2.000 METERS
USING AN ACCELERATION OF .5G THE
FORCE OF THE TIP MASS IS 8.155 NEWTONS
THE MOMENT CAUSED BY THE OBJECT IS 17.940 N-M

OUTSIDE DIAMETER IN CM	INSIDE DIAMETER IN CM	BEAM MASS KG	BEAM MOMENT N-M
------------------------------	-----------------------------	--------------------	-----------------------

2.00	1.9828	0.1735E-01	18.025
3.00	2.9924	0.1148E-01	17.996
4.00	3.9958	0.8588E-02	17.982
5.00	4.9973	0.6863E-02	17.974
6.00	5.9981	0.5716E-02	17.968
7.00	6.9986	0.4898E-02	17.964
8.00	7.9989	0.4284E-02	17.961
9.00	8.9992	0.3809E-02	17.959
10.00	9.9993	0.3425E-02	17.957

```

*****
THE MASS OF THE OBJECT IS      20.000      KG
THE DISTANCE FROM THE FIXED POINT
AT WHICH THE FORCE ACTS IS      0.850      METERS
THE LENGTH OF THE BEAM IS      0.700      METERS
USING AN ACCELERATION OF .5G THE
FORCE OF THE TIP MASS IS      24.525      NEWTONS
THE MOMENT CAUSED BY THE OBJECT IS 20.846      N-M
*****

```

```

*****
OUTSIDE      INSIDE      BEAM      BEAM
DIAMETER      DIAMETER      MASS      MOMENT
IN CM      IN CM      KG      N-M
*****
2.00      1.9800      0.7035E-02      20.858
3.00      2.9912      0.4656E-02      20.854
4.00      3.9951      0.3486E-02      20.852
5.00      4.9969      0.2787E-02      20.851
6.00      5.9978      0.2322E-02      20.850
7.00      6.9984      0.1990E-02      20.850
8.00      7.9988      0.1741E-02      20.849
9.00      8.9990      0.1548E-02      20.849
10.00     9.9992      0.1393E-02      20.849
*****

```

5-4

THE MASS OF THE OBJECT IS 4.000 KG
THE DISTANCE FROM THE FIXED POINT
AT WHICH THE FORCE ACTS IS 0.500 METERS
THE LENGTH OF THE BEAM IS 0.080 METERS
USING AN ACCELERATION OF .5G THE
FORCE OF THE TIP MASS IS 4.905 NEWTONS
THE MOMENT CAUSED BY THE OBJECT IS 2.453 N-M

OUTSIDE	INSIDE	BEAM	BEAM
DIAMETER	DIAMETER	MASS	MOMENT
IN CM	IN CM	KG	N-M

2.00	1.9977	0.9371E-04	2.453
3.00	2.9990	0.6242E-04	2.453
4.00	3.9994	0.4682E-04	2.453
5.00	4.9996	0.3743E-04	2.453
6.00	5.9997	0.3118E-04	2.453
7.00	6.9998	0.2671E-04	2.453
8.00	7.9999	0.2341E-04	2.453
9.00	8.9999	0.2073E-04	2.453
10.00	9.9999	0.1865E-04	2.453

THE MASS OF THE OBJECT IS 5.000 KG
THE DISTANCE FROM THE FIXED POINT
AT WHICH THE FORCE ACTS IS 0.280 METERS
THE LENGTH OF THE BEAM IS 0.080 METERS
USING AN ACCELERATION OF .5G THE
FORCE OF THE TIP MASS IS 6.131 NEWTONS
THE MOMENT CAUSED BY THE OBJECT IS 1.717 N-M

OUTSIDE DIAMETER IN CM	INSIDE DIAMETER IN CM	BEAM MASS KG	BEAM MOMENT N-M
------------------------------	-----------------------------	--------------------	-----------------------

2.00	1.9984	0.6557E-04	1.717
3.00	2.9993	0.4369E-04	1.717
4.00	3.9996	0.3277E-04	1.717
5.00	4.9997	0.2619E-04	1.717
6.00	5.9998	0.2183E-04	1.717
7.00	6.9999	0.1870E-04	1.717
8.00	7.9999	0.1639E-04	1.717
9.00	8.9999	0.1451E-04	1.717
10.00	9.9999	0.1310E-04	1.717

THE MASS OF THE OBJECT IS 2.040 KG
THE DISTANCE FROM THE FIXED POINT
AT WHICH THE FORCE ACTS IS 2.310 METERS
THE LENGTH OF THE BEAM IS 1.770 METERS
USING AN ACCELERATION OF .5G THE
FORCE OF THE TIP MASS IS 2.502 NEWTONS
THE MOMENT CAUSED BY THE OBJECT IS 5.779 N-M

OUTSIDE	INSIDE	BEAM	BEAM
DIAMETER	DIAMETER	MASS	MOMENT
IN CM	IN CM	KG	N-M

2.00	1.9945	0.4911E-02	5.800
3.00	2.9976	0.3263E-02	5.793
4.00	3.9986	0.2445E-02	5.789
5.00	4.9991	0.1955E-02	5.787
6.00	5.9994	0.1628E-02	5.786
7.00	6.9996	0.1397E-02	5.785
8.00	7.9997	0.1223E-02	5.784
9.00	8.9997	0.1086E-02	5.783
10.00	9.9998	0.9776E-03	5.783

```

*****
THE MASS OF THE OBJECT IS      0.500      KG
THE DISTANCE FROM THE FIXED POINT
AT WHICH THE FORCE ACTS IS      0.755      METERS
THE LENGTH OF THE BEAM IS      0.680      METERS
USING AN ACCELERATION OF .5G THE
FORCE OF THE TIP MASS IS      0.613      NEWTONS
THE MOMENT CAUSED BY THE OBJECT IS 0.463      N-M
*****

```

```

*****
OUTSIDE      INSIDE      BEAM      BEAM
DIAMETER      DIAMETER      MASS      MOMENT
IN CM      IN CM      KG      N-M
*****
2.00      1.9996      0.1503E-03      0.463
3.00      2.9998      0.1002E-03      0.463
4.00      3.9999      0.7508E-04      0.463
5.00      4.9999      0.6006E-04      0.463
6.00      6.0000      0.5025E-04      0.463
7.00      7.0000      0.4324E-04      0.463
8.00      8.0000      0.3804E-04      0.463
9.00      9.0000      0.3363E-04      0.463
10.00     10.0000     0.2963E-04      0.463
*****

```

THE MASS OF THE OBJECT IS	10.000	KG
THE DISTANCE FROM THE FIXED POINT		
AT WHICH THE FORCE ACTS IS	1.000	METERS
THE LENGTH OF THE BEAM IS	1.000	METERS
USING AN ACCELERATION OF .5G THE		
FORCE OF THE TIP MASS IS	12.263	NEWTONS
THE MOMENT CAUSED BY THE OBJECT IS	12.263	N-M

OUTSIDE	INSIDE	BEAM	BEAM
DIAMETER	DIAMETER	MASS	MOMENT
IN CM	IN CM	KG	N-M

2.00	1.9883	0.5891E-02	12.277
3.00	2.9948	0.3910E-02	12.272
4.00	3.9971	0.2929E-02	12.270
5.00	4.9981	0.2342E-02	12.268
6.00	5.9987	0.1951E-02	12.267
7.00	6.9991	0.1672E-02	12.267
8.00	7.9993	0.1464E-02	12.266
9.00	8.9994	0.1300E-02	12.266
10.00	9.9995	0.1171E-02	12.265

ORIGINAL PAGE IS
OF POOR QUALITY

PROPERTIES OF SATURATED OXYGEN

T K	P MPa	volume, m ³ /kg		enthalpy, kJ/kg			entropy, kJ/(kg·K)		
		v _f	v _g	h _f	h _{fg}	h _g	s _f	s _{fg}	s _g
54.34	0.0001453	0.000764	97.12	0.0	242.37	242.37	0.0	4.4602	4.4602
60	0.0007249	0.000780	21.49	9.23	238.26	247.49	0.1615	3.9710	4.1325
65	0.002331	0.000794	7.229	17.54	234.43	251.97	0.2945	3.6066	3.9011
70	0.006253	0.000808	2.896	25.88	230.50	256.38	0.4182	3.2928	3.7110
75	0.01453	0.000824	1.331	34.22	226.47	260.69	0.5331	3.0196	3.5527
80	0.03009	0.000840	0.6813	42.56	222.30	264.86	0.6405	2.7788	3.4193
85	0.05679	0.000857	0.3805	50.92	217.92	268.84	0.7417	2.5637	3.3054
90	0.09932	0.000876	0.2279	59.36	213.23	272.59	0.8377	2.3692	3.2069
90.19	0.101325	0.000877	0.2237	59.69	213.03	272.72	0.8413	2.3621	3.2034
95	0.1631	0.000896	0.1444	67.91	208.14	276.05	0.9296	2.1909	3.1205
100	0.2540	0.000917	0.09590	76.61	202.57	279.18	1.0179	2.0258	3.0437
105	0.3785	0.000940	0.06612	85.47	196.45	281.92	1.1033	1.8709	2.9742
110	0.5434	0.000966	0.04701	94.52	189.69	284.21	1.1860	1.7244	2.9104
115	0.7554	0.000994	0.03426	103.79	182.17	285.96	1.2666	1.5840	2.8506
120	1.022	0.001027	0.02546	113.34	173.75	287.09	1.3455	1.4480	2.7935
125	1.351	0.001064	0.01921	123.24	164.24	287.48	1.4236	1.3139	2.7375
130	1.749	0.001108	0.01463	133.65	153.30	286.95	1.5018	1.1793	2.6811
135	2.225	0.001161	0.01120	144.77	140.50	285.27	1.5817	1.0407	2.6224
140	2.788	0.001230	0.008562	156.91	125.11	282.02	1.6650	0.8937	2.5587
145	3.448	0.001324	0.006458	170.52	105.93	276.45	1.7547	0.7305	2.4852
150	4.216	0.001479	0.004671	186.90	79.53	266.43	1.8583	0.5302	2.3885
154.58	5.043	0.002293	0.002293	226.53	0.0	226.53	2.1080	0.0	2.1080

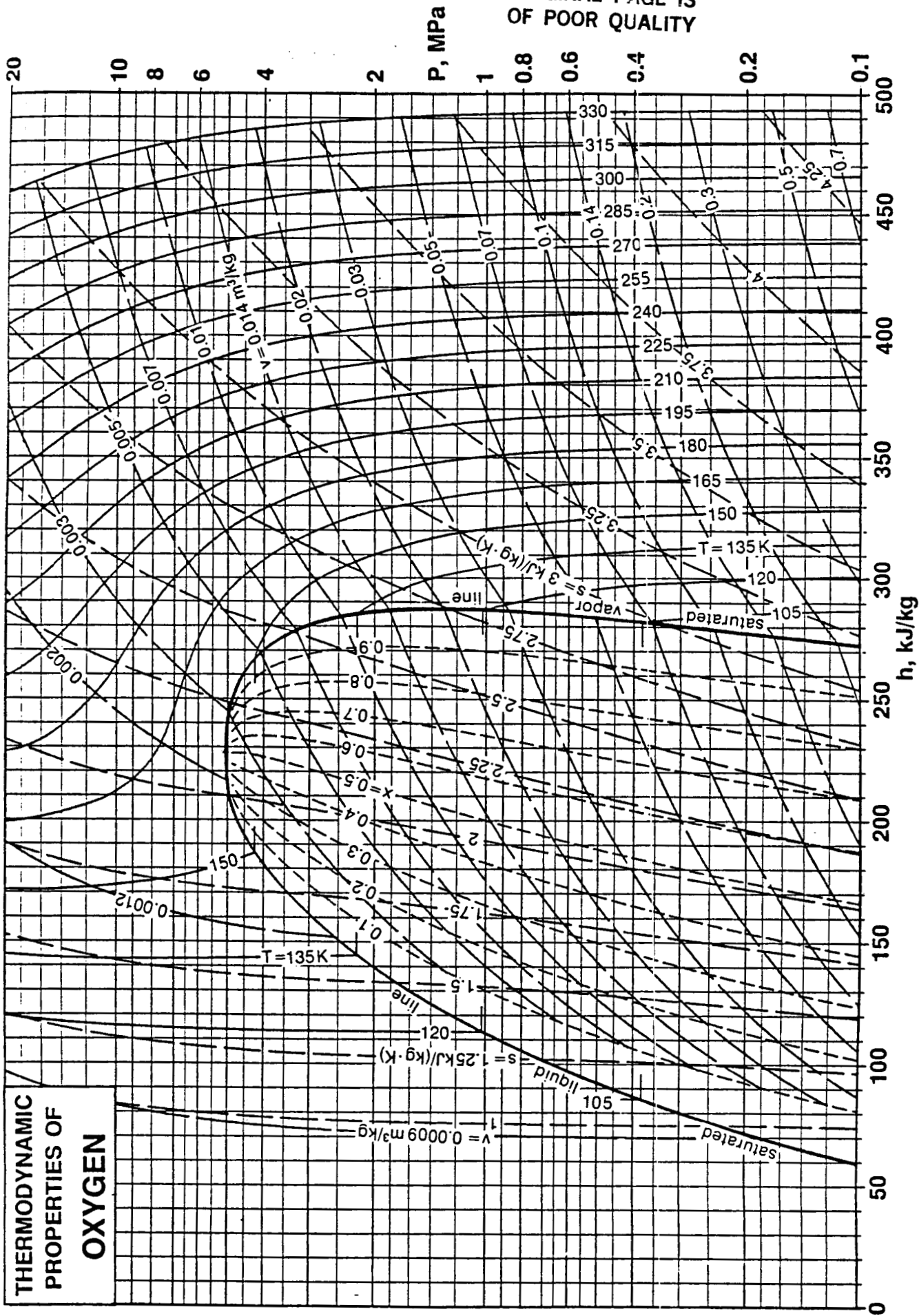
PROPERTIES OF GASEOUS OXYGEN

P, MPa (T _{sat} , K)		T, K								
		sat	200	300	400	500	600	700	800	1000
0.020	v, m ³ /kg	0.9916	2.597	3.897	5.196	6.496	7.795	9.094	10.39	12.99
(77.11)	h, kJ/kg	262.47	374.80	466.17	559.04	654.65	753.40	855.13	959.42	1174.07
	s, kJ/(kg·K)	3.4938	4.3661	4.7365	5.0035	5.2167	5.3967	5.5534	5.6926	5.9320
0.050	v, m ³ /kg	0.4276	1.038	1.558	2.079	2.598	3.118	3.638	4.158	5.197
(83.94)	h, kJ/kg	268.02	374.65	466.10	559.00	654.63	753.40	855.13	959.43	1174.09
	s, kJ/(kg·K)	3.3281	4.1275	4.4982	4.7653	4.9786	5.1586	5.3153	5.4546	5.6939
0.101325	v, m ³ /kg	0.2237	0.5113	0.7688	1.026	1.282	1.539	1.795	2.052	2.565
(90.19)	h, kJ/kg	272.72	374.39	465.97	558.94	654.60	753.39	855.14	959.45	1174.11
	s, kJ/(kg·K)	3.2034	3.9431	4.3143	4.5816	4.7950	4.9750	5.1318	5.2710	5.5104
0.20	v, m ³ /kg	0.1196	0.2583	0.3893	0.5197	0.6498	0.7798	0.9098	1.040	1.300
(97.24)	h, kJ/kg	277.50	373.89	465.73	558.82	654.54	753.38	855.15	959.48	1174.17
	s, kJ/(kg·K)	3.0851	3.7647	4.1370	4.4047	4.6181	4.7982	4.9551	5.0944	5.3337
0.50	v, m ³ /kg	0.05087	0.1024	0.1554	0.2079	0.2601	0.3122	0.3642	0.4162	0.5201
(108.8)	h, kJ/kg	283.71	372.35	464.99	558.44	654.37	753.33	855.19	959.57	1174.33
	s, kJ/(kg·K)	2.9252	3.5212	3.8969	4.1656	4.3796	4.5599	4.7169	4.8562	5.0957
1.0	v, m ³ /kg	0.02602	0.05039	0.07749	0.1039	0.1302	0.1563	0.1823	0.2083	0.2603
(119.6)	h, kJ/kg	287.03	369.73	463.76	557.81	654.09	753.25	855.25	959.73	1174.59
	s, kJ/(kg·K)	2.7977	3.3320	3.7135	3.9840	4.1987	4.3794	4.5366	4.6760	4.9156
2.0	v, m ³ /kg	0.01264	0.02439	0.03853	0.05198	0.06520	0.07832	0.09137	0.1044	0.1304
(132.7)	h, kJ/kg	286.19	364.33	461.29	556.57	653.52	753.11	855.38	960.04	1175.13
	s, kJ/(kg·K)	2.6493	3.1328	3.5266	3.8007	4.0169	4.1984	4.3560	4.4958	4.7356
5.0	v, m ³ /kg	0.00276	0.00876	0.01516	0.02082	0.02624	0.03156	0.03681	0.04204	0.05244
(154.4)	h, kJ/kg	239.04	346.74	453.93	552.90	651.86	752.69	855.78	961.00	1176.75
	s, kJ/(kg·K)	2.1897	2.8310	3.2684	3.5533	3.7740	3.9578	4.1167	4.2571	4.4977
10.	v, m ³ /kg	0.00361	0.00743	0.01046	0.01327	0.01598	0.01864	0.02126	0.02647	
	h, kJ/kg	313.19	442.21	547.14	649.30	752.12	856.53	962.66	1179.50	
	s, kJ/(kg·K)	2.5239	3.0559	3.3582	3.5861	3.7736	3.9345	4.0762	4.3180	
20.	v, m ³ /kg	0.00173	0.00370	0.00534	0.00682	0.00822	0.00957	0.01089	0.01350	
	h, kJ/kg	268.46	422.72	537.55	645.22	751.58	858.40	966.22	1185.16	
	s, kJ/(kg·K)	2.1834	2.8202	3.1515	3.3919	3.5858	3.7505	3.8944	4.1386	

ORIGINAL PAGE IS
OF POOR QUALITY

© Department of Mechanical Engineering, Stanford University

THERMODYNAMIC PROPERTIES OF OXYGEN



APPENDIX 14
Thermal Control

CALCULATION

The following data was used for the absorptivity and the emissivity of the different materials (Spacecraft Design, 1988).

Table 14.1

<u>Surface</u>	<u>Absorptance</u>		<u>Emittance</u>	
	<u>BOL</u>	<u>EOL</u>	<u>BOL</u>	<u>EOL</u>
White Paint	0.20	0.60	0.90	0.90
Anodized Al.	0.20	0.60	0.80	0.80
Graphite Epoxy	0.84	0.84	0.85	0.85
Gold	0.20	0.30	0.03	0.60

BOL = Beginning of life

EOL = End of life

Life = 7 years

Equations for Calculation of the Skin Temperature

Qr = radiation	Es = emissivity of satellite
Qi = internal	Em = emissivity of Moon
Qs = sun	a = absorptivity
Qref = reflected	alb = Moon albedo
Qm = moon	sigma = Stefan-Boltzman

Is = solar flux
 Fpm = view factor: satellite to Moon
 Fpsm = view factor: satellite to sunlit Moon
 Fps = view factor: satellite to space
 An = projected area normal to the Sun's rays
 As = total area of the satellite
 Tmn = night time temperature of the Moon
 Tmd = day time temperature of the Moon
 Tp = steady state temperature of the satellite
 Tsp = temperature of space

Qr = $\sigma \cdot Es \cdot Fps \cdot As (Tp^4 - Tsp^4)$
 Qs = $a \cdot An \cdot Is$
 Qref = $alb \cdot a \cdot Fpsm \cdot As \cdot Is$
 Qm = $\sigma \cdot Em \cdot Es \cdot Fpm \cdot As (Tm^4 - Tp^4)$
 Qi = 1100 W

let $Fps + Fpm = 1.0$
 $Em = 1.0$
 $Ts = 0.0 \text{ K}$

$Qr = Qs + Qref + Qm + Qi$ and $Qr - Qm = Qs + Qref + Qi$

Through substitution and manipulation:

$$Tp = (1/\sigma \cdot Es \cdot As) \cdot (Qs + Qref + Qi + \sigma \cdot Es \cdot Fpm \cdot As \cdot Tm^4)$$

APPENDIX 15
Attitude Control

APPENDIX A: Attitude Control System Program.

C.....4-20-88.....

C PROGRAM GIMBL1.FOR ; BY S. ALI SIAHPUSH

C

C X---> YAW AXIS, Y---> ROLL AXIS, Z---> PITCH AXIS.

C C ALL UNITS ARE IN METRIC.

C NOTE THAT, DOT MEAN TIME DERI. (EXAMPLE YAW-DOT IS TIME DERI. OF
C THE YAW ANGLE; ANGULAR VELOCITY OF THE THE YAW)

C

program lunar1

REAL IP,IR,IY,KP,U(6)

CHARACTER*1 ANS,OUT*10,ANSR*1

C open(13,file='pax.out')

OPEN(14,FILE='RAX.OUT')

OPEN(15,FILE='YAX.OUT')

C WRITE(*,*)'ENTER OUTPUT FILE NAME (LESS THAN 10 CH.)'

C READ(*,'(A)')OUT

C OPEN(12,FILE=OUT)

WRITE(*,*) 'ENTER INITIAL YAW,YAW-DOT,ROLL,ROLL-DOT,PITCH,PIT
+-DOT (RAD. & RAD/SEC)'

READ(*,*) (U(I),I=1,6)

IP=1253.

IR=1017.

IY=652.

ALTI=100.

RADIUS=ALTI+1737.63

THRUST=0.0

WRITE(*,*)'MISALIGNMENT TORQUE IN EFFECT (Y/N)?'

READ(*,'(A)')ANSR

IF(ANSR.EQ.'Y'.OR.ANSR.EQ.'y')THRUST=1.0E-4

C

C AMUE=G*M WHERE G IS THE UNIVERSAL CONST., AND M MASS OF THE MOON

C W IS ORBITAL FREQUENCY

C NPER IS INT. PERIOD OF THE ORBIT (USED IN THE DO LOOP)

C WP IS THE ANGULAR VELOCITY OF THE PITCH (RAD/SEC).

C KP=PITCH GAIN, CK=Y/R GAIN, HN= NOMINAL ANGULAR MOMENTUM.

C SK=YAW-TO-ROLL GAIN RATIO.

C TYR=TIME CONSTANT OF YAW/ROLL, TP=TIME CONSTANT OF PITCH.

C

C WRITE(*,*)'ENTER CK'

C READ(*,*)CK

KP=0.15

CK=1.5

HN=30.0

GM=4902.78

W=SQRT(GM/(RADIUS**3))

WP=SQRT(KP/IP)

WR=SQRT(CK/IR)

WY=SQRT(W*HN/IY)

SK=2./SQRT(HN/(IY*W))


```

TYR=2./WR
TP=2./WP
PI2=8.*ATAN(1.)
C PERIOD=PI2/(W*60.)
C WRITE(*,*)'ORB. PER.(MIN), FREQ. (RAD/SEC)',PERIOD,W
DT=1.
T=0.
WRITE(*,130) WP,WR,WY
WRITE(*,140)TYR,TP,SK
130 FORMAT(1X,'WP=',F8.5,2X,'WR=',F8.5,2X,'WY=',2X,F8.5,2X,'(RAD/S)'
140 FORMAT(1X,'TIME-CON. ROL, PIT (S)=' ,2(F9.3,2X),'GAIN Y/R=' ,F8.5)
WRITE(*,120)
120 FORMAT(1X,'TIME(S),Y,YD,R,RD,P,PD IN RAD, AND RAD/SEC')
WRITE(*,*)'ENTER THE SIMULATION TIME (SEC IN INTEGER)?'
READ(*,*)NVAL

DO 65 I=1,NVAL
  IF(AMOD(T,60.) .EQ. 0. .OR. T .EQ. 0.) THEN
    WRITE(*,100) T/60.,(U(J),J=1,6)
    C WRITE(12,100) T,(U(J),J=1,6)
    C WRITE(13,*)T/60.,U(5)
    WRITE(14,*)T/60.,U(3)
    WRITE(15,*)T/60.,U(1)
  ENDIF
  CALL RUNG(IP,IR,IY,W,SK,CK,HN,TYR,TP,KP,DT,T,U,THRUST)
65 CONTINUE
C WRITE(12,100)T,(U(I),I=1,6)
100 FORMAT(1X,F9.1,1X,6(F8.5,1X))
C30 WRITE(*,*) 'DO YOU WANT TO RUN THE PROGRAM ONE MORE TIME Y/N'
C READ(*,'(A)')ANS
C IF(ANS .EQ. 'Y') GO TO 20
STOP
END

```

```

SUBROUTINE RUNG(IP,IR,IY,W,SK,CK,HN,TYR,TP,KP,H,T,U,THRUST)
REAL F(6),U(6),UTMP(6),SUMK(6),K1,K2,K3,K4,KP,IP,IR,IY
NEQ=6
  CALL DERIV(IP,IR,IY,W,SK,CK,HN,TYR,TP,KP,T,u,f,THRUST)
  DO 10 I=1,NEQ
    UTMP(I)=U(I)
    K1=F(I)*H
    SUMK(I)=K1
    U(I)=UTMP(I)+0.5*K1
10 CONTINUE
  t=t+0.5*H
  CALL DERIV(IP,IR,IY,W,SK,CK,HN,TYR,TP,KP,T,u,f,THRUST)
  DO 20 I=1,NEQ
    K2=H*F(I)
    SUMK(I)=SUMK(I)+2.*K2
    U(I)=UTMP(I)+0.5*K2
20 CONTINUE
  CALL DERIV(IP,IR,IY,W,SK,CK,HN,TYR,TP,KP,T,u,f,THRUST)
  DO 30 I=1,NEQ

```

```

        K3=H*F(I)
        SUMK(I)=SUMK(I)+2.*K3
        U(I)=UTMP(I)+K3
30      CONTINUE
        t=t+0.5*H
        CALL DERIV(IP,IR,IY,W,SK,CK,HN,TYR,TP,KP,T,u,f,THRUST)
        DO 40 I=1,NEQ
            K4=H*F(I)
            SUMK(I)=SUMK(I)+K4
            U(I)=UTMP(I)+SUMK(I)/6.
40      CONTINUE
        RETURN
        END

C
C
        SUBROUTINE DERIV(IP,IR,IY,W,SK,CK,HN,TYR,TP,KP,T,u,f,THRUST)
        REAL U(6),F(6),KP,IP,IR,IY

C TRQY,TRQR, AND TRQP ARE EXTERNAL PERTURBING TORQUES DUE TO SOLAR PR.
C U(1)=YAW,      U(2)=YAW-DOT
C U(3)=ROLL,     U(4)=ROLL-DOT
C U(5)=PITCH,    U(6)=PITCH-DOT

        CONY=-5.E-5
        TRQY=CONY*COS(W*T)
        CONR=2.E-5
        TRQR=CONR*(1.-2.*SIN(W*T))
        CONP=1E-4
        TRQP=CONP*COS(W*T)
        F(1)=U(2)
        F(2)=(SK*CK*(TYR*U(4)+U(3))+TRQY-W*HN*U(1))/IY
        F(3)=U(4)
        F(4)=(-CK*(TYR*U(4)+U(3))-HN*U(2)+TRQR+THRUST)/IR
        F(5)=U(6)
        F(6)=(-KP*(TP*U(6)+U(5))+TRQP+THRUST)/IP
        RETURN
        END

```